Acta Universitatis Szegediensis

Acta Biologica Szegediensis

Volume 64,
Number 2,
2020

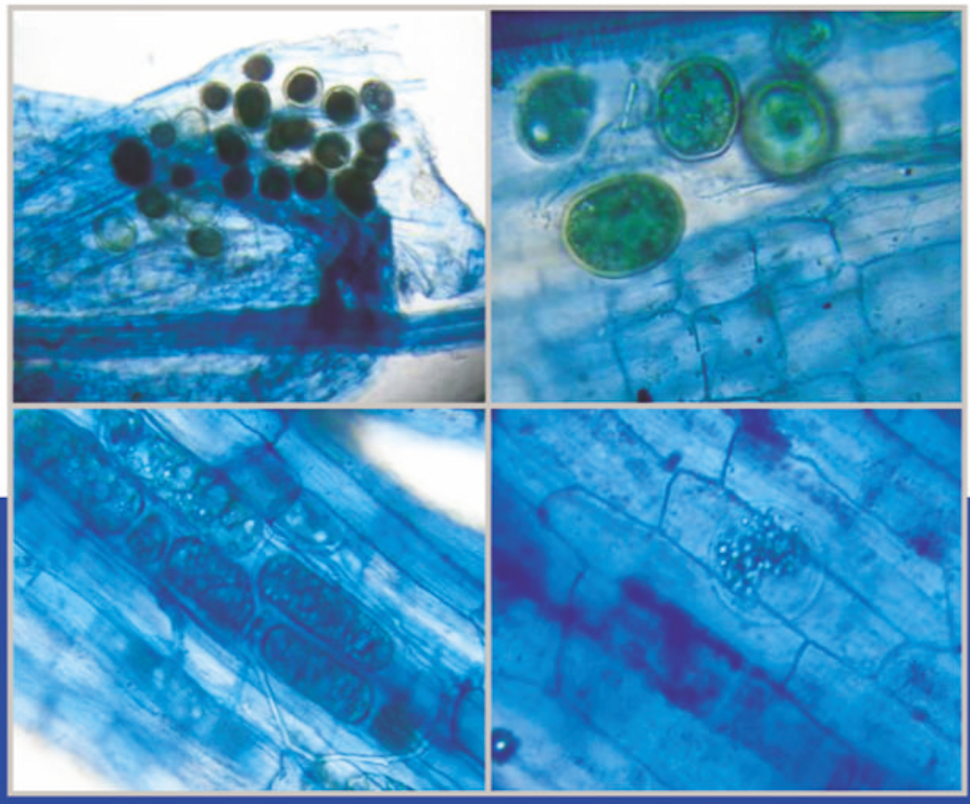

University of Szeged, Szeged, Hungary

http://abs.bibl.u-szeged.hu/index.php/abs

Acta Biologica Szegediensis

Volume 64(2):91-98, 2020
Acta Biologica Szegediensis
http://abs.bibl.u-szeged.hu/index.php/abs
DOI:10.14232/abs.2020.2.91-98

ARTICLE

Agreement and bias in the estimation of fat free mass using bioelectrical impedance analysis and a resistance and reactance-based formula for the Mexican adults: A study from Merida, Yucatan

Sudip Datta Banik

Department of Human Ecology, Cinvestav del IPN, Merida, Yucatan, Mexico

ABSTRACT Bioelectrical impedance analysis (BIA) is used to estimate body composition characteristics. The values of body fat and fat free mass (FFM) are obtained as per algorithms of the device that are often unknown to the researchers. Some models of the analyzer provide resistance and reactance values that may be useful to estimate FFM. Objective of the present study was to test the agreement and proportional bias in the estimation of FFM obtained through BIA and that derived from the resistance and reactance values using a formula for Mexican adults. A cross-sectional study was carried out in 2019 selected 60 university male students aged 21 to 23 years from Merida, Yucatan. A multifrequency whole body bioelectrical impedance analyzer Tanita MC 180 MA (Tanita Corporation, Tokyo-Japan) was used to evaluate body composition characteristics. The device gives estimates of FFM in kg (based on algorithm) and the resistance and reactance values (ohms). There is an existing formula for Mexican adults to estimate FFM (FFM_FOR) from the resistance and reactance values obtained through BIA. An agreement between the two estimates of FFM has been tested using Bland-Altman plot and linear regression analysis. Mean value of age of the participants was 21.88 years. FFM estimated by BIA (FFM_BIA = 41.44 kg) and that derived from FFM_FOR (41.36 kg) had significant intraclass correlation coefficient (ICC) (Cronbach's alpha = 0.99, p<0.0001). One sample t-test estimating the difference of mean values between FFM_BIA and FFM_FOR was not significant (t = 1.37, mean difference -0.02, p = 0.18). The Bland-Altman plot shows almost all data points lie within 95% confidence interval limits. A linear regression analysis using the difference of FFM values as dependent variable and the average of the measurements as the independent variable showed no significant interrelationships. In conclusion, the formula to estimate FFM using the resistance and reactance values of BIA has been found to be useful in the present study.
Acta Biol Szeged 64(2):91-98 (2020)

KEY WORDS
bioelectrical impedance analysis
Bland-Altman
intraclass correlation
reactance
regression
resistance

ARTICLE INFORMATION
Submitted
11 October 2020.
Accepted
02 November 2020.
***Corresponding author**
E-mail: dattabanik@cinvestav.mx

Introduction

Evaluation of body composition characteristics is important in public health nutrition research. The last National Health and Nutrition Survey, 2012 (ENSANUT in Spanish acronym) reported high prevalence of obesity and related disorders in Mexican populations, particularly among adults (Gutiérrez et al. 2013). Remarkably high prevalence of overweight (39.6%) and obesity (31.6%) among adults from the southern region of the country have been reported in the survey. Yucatan is one of the Southern Peninsular States of Mexico where prevalence of excess weight (overweight and obesity) was very high (80%) among adults that exceeded the national average (71.3%). Prevalence of obesity was higher in the urban regions (34%) than in the rural areas (26.5%) of Yucatan (Gutiérrez et al. 2013).

Nutritional status assessment procedures are summarized by the mnemonic ABCD: anthropometric measurements, biochemical parameters, clinical diagnosis, and dietary habits (Dwyer et al. 1993). In anthropometric evaluation of nutritional status and body fatness using skinfold caliper, measurement errors could be high among excess weight individuals, particularly among centrally obese people (Sebo et al. 2017). Despite some limitations on the assumption of hydration factor and body geometry of severely obese individuals, bioelectrical impedance analysis (BIA) is reliable to evaluate body composition characteristics (body fat and fat free mass) with less intra-observer error than anthropometry (Coppini et al. 2005; Macias et al. 2007; Yamashita et al. 2012). The BIA is a

simple and non-invasive technique; the portable equipment is relatively non expensive and provides accurate results (Bohm and Heitmann 2013; Ricciardi and Talbot 2007). The bioelectrical impedance (BI) instruments are different in number of electrodes and the models have in-built software programs (specific algorithm of the device that are unknown to the researcher) to estimate body composition characteristics by age, sex, and activity patterns etc. Several models of BI instruments are available in the market and quality assessment and validation are very important (Macias et al. 2007; Ramírez et al. 2012). The results obtained using BIA are also required to be validated with reference to the results obtained through dual-energy X-ray absorptiometry (DEXA or DXA) that is often considered as a gold standard for the evaluation of body composition characteristics (Khalil et al. 2014; Scafoglieri and Clarys 2018).

In this background, instead of using the direct values of body composition characteristics obtained from the BIA, Macias et al. (2007) developed a prediction equation to estimate fat free mass (FFM) for the Mexican adults using the resistance and reactance (ohms) values obtained through BIA and cross-validated the proposed equation with reference to the results obtained through air displacement plethysmography (ADP). In that study, the participants were 20 to 50-year-old men and women from Sonora, a northern State in Mexico. The authors reported that the equation, based on two-compartment model was accurate, precise, and free of bias. They also reviewed the literature to justify that ADP was a reliable and valid method and as good as hydrostatic weighing for the evaluation of body composition characteristics. Till date, the prediction formula developed by Macias et al. (2007) is a reliable one that is available in Mexico to estimate FFM of adult individuals from the resistance and reactance values obtained through BIA and the article has been cited by many authors stating the usefulness of the formula (Balas-Nakash et al. 2010; Caicedo-Eraso et al. 2019; Lu et al. 2016; Mbada et al. 2015; Schifferli et al. 2011; Schifferli Castro and Zuniga 2017; Wada and Tekin 2007). This raised my interest to use the same formula for Mexican adults (Macias et al. 2007) and to find the agreement and bias between the estimated values of FFM (BIA-based and resistance and reactance-based) in a sample of adults from Merida, Yucatan, Mexico.

The objectives of the present study were to estimate body composition characteristics (body fat mass and fat free mass) of young adult men using the BIA, and to test the agreement and proportional bias in the estimation of fat free mass (FFM) obtained through BIA and that derived from the resistance and reactance values using in a formula for Mexican adults.

Participants and Methods

The present cross-sectional study recruited 60 male students aged 21 to 23 years from the *Universidad Modelo*, a private University in Merida, Yucatan. The participants were selected through non-probability sampling (convenience sample) from a group of students of the Faculty of Medicine. Ethical clearance was obtained from the institutional committee and the participants signed the informed consent form as per guideline.

Anthropometric measurements were recorded by the author, following international protocol (Lohman et al. 1988). Height (cm) was measured to the nearest tenth of a centimeter using a standard stadiometer with platform (Seca, Germany). Body weight (kg) was recorded to the nearest 0.05 kg using an electronic scale (Tanita Co., Tokyo-Japan). Data of age (years), sex, and the anthropometric measurements were necessary for bioelectrical impedance analysis (BIA).

Body composition characteristics (body fat mass or FM and fat free mass or FFM) were estimated using a multifrequency whole body bioelectrical impedance (BI) analyzer Tanita MC 180 MA (Tanita Co., Tokyo-Japan), following a standard protocol (BIA 1994) and manufacturer's instruction. The equipment had eight pairs of tactile electrodes for foot pad and hand grips. Previous studies reported reliability of the obtained results using a similar model of Tanita (number 305) that mentioned best-fit algorithm of the device (Jebb et al. 2000). Participants were in light clothing, without jewelry and metal objects in the body. They were asked to abstain from foods (fasting for last 12 hours), moderate or vigorous exercise, alcohol consumption and any medicine intake in 24 hours prior to the evaluation. Assessment was done in the morning, between 7 and 8 A.M. Data collection was done in the University with prior appointments. The participants were apparently healthy and did not report any health complications at least in three months prior to the evaluation.

The FFM was also estimated using a formula for Mexican adults (Macias et al. 2007). FFM (kg) = 0.7374 * (Height^2 / Resistance in ohms) + 0.1763 * (Body weight) - 0.1773 * (Age) + 0.1198 * (Reactance in ohms) - 2.4658. The dimensions for age, height, and weight were years, cm, and kg respectively. The resistance and reactance values obtained from the Tanita MC 180 MA (Tanita Co., Tokyo-Japan) have been used in the formula to estimate FFM. Body mass index (BMI) might be an interest for the readers that has been calculated as weight (kg) divided by height in meter square. Evaluation of BMI-based nutritional status of adult men followed standard guideline (WHO 1995). Fat mass (FM) (kg and %) was obtained from BIA and was also calculated from FFM and body

weight. Fat mass index (FMI) was calculated as FM (kg) divided by height (m^2).

The SPSS® statistical software (version 15.00) was used for data analysis. Mean and standard deviation values of age, anthropometric (height, body weight, BMI) and body composition characteristics (FM and FFM) were calculated. Normality in the distribution of variables followed the principle of Shapiro-Wilk test ($p > 0.05$). The values of FFM, obtained directly from the BIA and that derived from the formula (Macias et al. 2007) were compared and statistical tests to find agreement between the estimates and proportional bias were run. Intraclass correlation coefficient, t-test (one sample and paired), linear regression analysis, and Bland-Altman plots (Bland and Altman 1986) were used to estimate the agreement and bias. Level of significance was set at $\alpha = 0.05$ in all analyses.

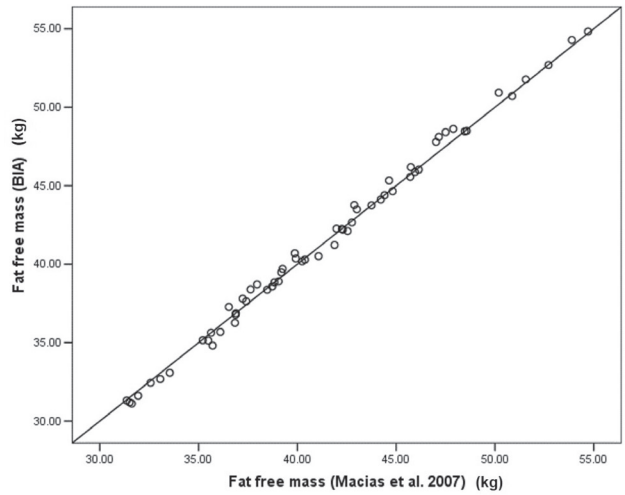

Figure 1. Scatter plot of linear regression model predicting BIA-based fat free mass (FFM) by the formula-based FFM (Macias et al. 2007).

Results

The participants were young adult men (age 21.88 ± 0.85 years). Mean value of height (167.63 cm) ranged between 159.0 cm and 188.0 cm. Mean value of body weight (62.65 kg) also had wide ranging minimum (48.10 kg) and maximum (80.70 kg) values. The participants had moderate BMI (22.59 ± 2.69 kg/m^2) and 23.33% of them were overweight. No participant was obese. Mean values of fat free mass (FFM) obtained directly from BIA (41.44 ± 6.08 kg) was marginally different from that derived using formula (Macias et al. 2007) (41.36 ± 5.91 kg). Estimated values of fat mass (FM) (BIA-based = 22.21 ± 4.89 kg, formula-based = 21.29 ± 4.59 kg) and fat mass index (FMI) (both BIA and formula-based = 0.13) were marginally different or similar, respectively that were obtained using the two methods. Estimated mean values of percentage body fat (PBF) using BIA (33.37 ± 5.83%) and that derived from the FFM value obtained using formula (33.87 ± 5.18%) were also marginally different (Table 1).

Table 1. Descriptive statistics of age, anthropometric and body composition characteristics of young adult male university students (n = 60)

Variables	Mean (SD)	Minimum	Maximum
Age (years)	21.88 (0.85)	21.45	23.87
Height (cm)	167.63 (7.17)	159.00	188.00
Weight (kg)	62.65 (8.33)	48.10	80.70
BMI (kg/m^2)	22.59 (2.69)	19.85	28.81
FM_BIA (kg)	22.21 (4.89)	11.71	33.09
FM-FOR (kg)	21.29 (4.59)	12.47	32.53
FMI_BIA (kg/m^2)	0.13 (0.03)	0.07	0.19
FMI_FOR (kg/m^2)	0.13 (0.03)	0.08	0.19
FFM_BIA (kg)	41.44 (6.08)	31.12	54.82
FFM_FOR (kg)	41.36 (5.91)	31.36	54.71
PBF_BIA (%)	33.37 (5.83)	23.37	45.45
PBF_FOR (%)	33.87 (5.18)	24.90	44.80
Resistance (BIA) (ohms)	524.82 (45.99)	405.00	645.00
Reactance (BIA) (ohms)	59.79 (6.68)	45.60	71.40

SD: Standard deviation; BMI: Body mass index; FM_BIA: Fat mass (BIA-based); FM_FOR: Fat mass (formula-based) (Macias et al. 2007); FMI_BIA: Fat mass index (BIA-based); FMI_FOR (FMI formula-based) (Macias et al. 2007); FFM_BIA: Fat free mass (BIA-based); FFM_FOR: Fat free mass (formula-based) (Macias et al. 2007); PBF_BIA: Percentage Body fat (BIA-based); PBF_FOR: Body fat (%) (formula-based) (Macias et al. 2007)

Paired t-tests between BIA-based and formula-based estimates, e.g., FFM ($t = 1.37$, $p = 0.18$) and PBF ($t = 1.43$, $p = 0.16$) did not show significant differences of mean values. Intraclass correlation coefficient (ICC) between the two estimates of FFM was significant (Cronbach's alpha = 0.99, $p<0.0001$). ICC of the estimated PBF using two methods also showed similar value that was calculated in case of FFM. The difference in the values of two estimates of FFM (BIA-based and formula-based) was normally distributed (p-value = 0.63). One sample t-test for the difference of FFM values (BIA and formula-based) was not significant ($t = 1.37$, mean difference -0.02, $p = 0.18$). A simple linear regression model predicting BIA-based FFM from the formula-based FFM after adjusting for age and sex was significant (regression coefficient = 1.03, standard error = 0.009, $t = 110.79$, $p< 0.0001$, R^2 and adjusted $R^2 = 0.99$), showing interrelationships between the variables (Fig. 1).

In addition, BMI showed significant correlation ($p< 0.001$) with both BIA-based and formula-based FM ($r = 0.52$), FFM ($r = 0.60$), and FMI ($r = 0.60$). However, correlation between BMI and PBF (either BIA-based or

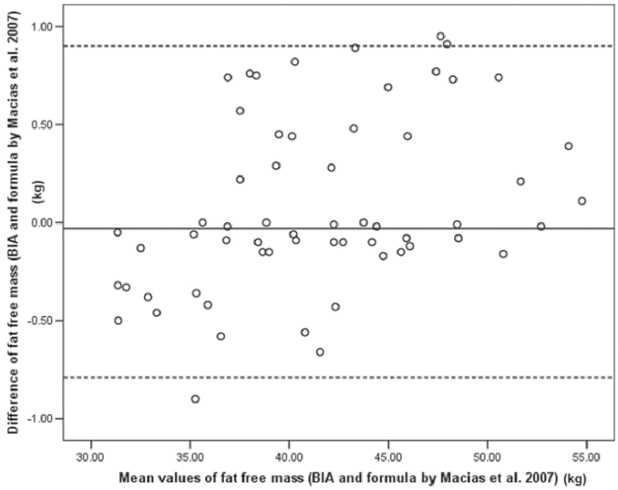

Figure 2. Bland-Altman plot of BIA-based and formula-based (Macias et al. 2007) fat free mass.

formula-based) was not significant (p-value = 0.40).

The result of Bland–Altman test for agreement or proportional bias between the estimated FFM using two methods (BIA and formula-based) is presented in Fig. 2. In the resulting scatter plot, Y axis shows the difference of two paired FFM estimates (BIA and formula-based) and X axis presents the average of the measures. Mean value of the difference of paired estimates of FFM (BIA and formula-based) (Y axis) was -0.02 that had minimum (-0.90) and maximum (0.95) values, standard error of estimate 0.06, and standard deviation 0.44. The average of the measures (BIA and formula-based FFM) in the X axis had mean (41.40 kg), minimum (31.34 kg), maximum (54.77 kg) values, standard error of estimate (0.77), and standard deviation (5.99). The Bland-Altman plot shows almost all data points lie within 95% confidence interval limits and the points were equally distributed above and below the line of mean difference (upper limit = 0.90, lower limit = -0.89) (Fig. 2) that indicates no proportional bias in the estimates of FFM using two methods.

A linear regression analysis using the difference of FFM values as dependent variable and the average of the measurements as the independent variable showed no significant interrelationship (t = 1.52, p-value 0.14, and standard error 0.002) that accepted the null hypothesis. Age was adjusted in the model and regression coefficient was close to zero (0.003) with 95% confidence interval limits (lower -0.001, upper 0.008) that indicated no proportional bias and appeared to have an agreement between the measures (estimated FFM using BIA and that derived from formula, proposed by Macias et al. 2007).

Discussion

It is evident from the present study that the prediction formula proposed by Macias et al. (2007) to estimate FFM using the resistance and reactance values of BIA is reproducible and that has been successfully used in the present study. No significant difference between the BIA-based and formula-based FFM values was observed in the present study. A consistent agreement between the estimates was clear from correlation coefficients, regression models, and Bland-Altman plot. These results confirm the reliability of the use of resistance and reactance values to estimate body composition characteristics when the in-built algorithm of the BIA device to estimate the same is not known. The participants were young adults and values of their body composition characteristics were wide ranging: FFM (31 to 55 kg) and PBF (23 to 45%). Interestingly, BMI of the participants was not very high in the sample (mean value 22.59 kg/m^2). In addition, BMI showed significant correlation with FM, FFM, and FMI (height adjusted FM) but not with PBF. The results indicate body fat in kilogram (FM) and height adjusted values (FMI) are more important indicators of adiposity than a generalized value of PBF in relation to BMI. Considering high prevalence of BMI-based overweight and obesity in Mexican adults as reported earlier (Gutiérrez et al. 2013), the present sample of young adults (n= 60) showed relatively low frequency of overweight (23%) and nobody was obese. This result may be due to a non-probability sample that neither represent the population of this age-group from Merida, nor the State of Yucatan. In the previous study from Sonora, a northern Mexican State, mean values of BMI were also not very high (men 26.2 kg/m^2, women 25.4 kg/m^2) in the sample of 20 to 50-year-old adults (Macias et al. 2007).

Mexico is a country with huge ethnic and genetic diversity (Moreno-Estrada et al. 2014). We understand that human biology of the populations in the north of the country is different from that in the Southern Peninsular Mexico. Mean values of BIA-based PBF (25.8%) and FFM (57.9 kg) among adult male participants in the previous report (Macias et al. 2007) were different from that recorded in the present study (PBF 33.37%, FFM 41.44 kg). The adult men in the present study showed higher PBF and lower FFM in comparison with that reported in the previous study (Macias et al. 2007). This may be interpreted as differences in body composition characteristics between the two sub-populations of Mexico.

A standard multifrequency whole body bioelectrical impedance (BI) analyzer Tanita MC 180 MA (Tanita Co. Tokyo-Japan) was used in the present study that was reported to be similar in the reliability of another model

(Tanita 305) used in a previous study (Jebb et al. 2000). Body composition characteristics were evaluated using a different equipment (Model BIA-103, RJL Systems Detroit, MI) in the previous study by Macias et al. (2007). When the in-built software programs for body composition assessment are not known, it seems that the resistance and reactance values obtained from the equipment used in the present study worked satisfactorily. The resistance and reactance-based prediction formula to estimate FFM for adults (Macias et al. 2007) is pioneering of its kind in Mexico. In their study, the authors cross-validated the results obtained using the equation with reference to results from the air displacement plethysmography (ADP). Mean values of BIA-based and ADP-based FFM were same (57.9 kg) among men in that study. In the present study, mean value of BIA-based FFM (41.44 kg) was marginally different from the derived one obtained using the resistance and reactance values applied in the prediction equation (41.36 kg) proposed earlier (Macias et al. 2007). However, the difference in the mean values was not significant ($p > 0.05$) as evaluated using paired t-test.

Dual-energy X-ray absorptiometry (DEXA or DXA) is considered as a gold standard for the evaluation of body composition characteristics (Laskey 1996; Scafoglieri and Clarys 2018). Magnetic resonance imaging and DXA are highly precise methods to estimate body composition characteristics (Taing et al. 2017). However, the instruments are expensive, invasive, not portable, and time consuming for the evaluation process. In large-scale surveys, BIA provides satisfactory results and advanced models are capable of segmental analysis of body composition: whole body and regional (extremities). Studies reported higher reliability of the results from whole body BIA than segmental BIA when the values were compared with the results obtained using DXA (Bracco et al. 1996; Demura et al. 2004; Erselcan et al. 2000; Ricciardi and Talbot 2007). In this background, BIA-based prediction formula for FFM on a two-compartment model was reported to be accurate, precise, and free of bias (Macias et al. 2007).

A study from Mexico among 86 postmenopausal women aged 42 to 74 years with metabolic syndrome (Balas-Nakash et al. 2010), estimated body fat using DXA and compared the results with the derived values using the formulas proposed in a study based on the data of National Health and Nutrition Examination Survey III (NHANES III) (Sun et al. 2005) of the U.S.A and by another study from Mexico (Macias et al. 2007). The DXA-based PBF (44.54%) had different levels of agreement (Bland-Altman plot) with the values derived from the formula proposed in a NHANES III-based study (41.93%) (Sun et al. 2005) and that estimated using the equation proposed by Macias et al. 2007 (43.32%). The NHANES III-based formula and prediction equation by Macias et al. 2007 underestimated PBF. However, the report (Balas-Nakash et al. 2010) raised doubt about the use of prediction equation to estimate FFM that was proposed by Macias et al. 2007 because age of many women participants in that study was higher than 50 years. In the reference study (Macias et al. 2007), age of women participants was between 22 and 48 years.

A study from China, developed BIA-based prediction equations to estimate FFM for adult men and women using two different BI instruments (hand-to-hand and hand-to-foot) and DXA was the criterion method (Lu et al. 2016). Both types of BIA-based prediction equations demonstrated similar reliability and the hand-to-hand BIA model was found to be more practical for the assessment of body composition characteristics. The study suggested importance of separate prediction equations for men and women. Another study among indigenous Australian adults aged 36 to 60 years developed prediction equation to estimate FFM and the reference method was DXA (Hughes et al. 2015).

A study from Brazil reported that mean values of BIA-based PBF (38.0%) and formula-based PBF (38.7%) were similar; BIA overestimated PBF in overweight and underestimated the same among obese adult women (Pimentel et al. 2010). The formula was developed in an earlier study (Segal et al. 1988). Low sensitivity of BIA to identify individuals with high BMI and body fat was reported by several authors (Macias et al. 2007; Pimentel et al. 2010). Another study among adults of 18 to 64 years of age from Chile (Schifferli Castro and Zuniga 2017) compared BIA-based estimate of FFM with that derived from a prediction formula for FFM reported earlier (Schifferli et al. 2011). The previous study (Schifferli et al. 2011) developed prediction equation for BIA-based FFM, taking DEXA as the criterion or reference method. BIA overestimated PBF in men and underestimated in women compared to the corresponding values obtained using the prediction formula (Schifferli Castro and Zuniga 2017). Therefore, it is evident that BIA-based estimates of FFM may be different in men and women and vary with the levels of BMI and body fatness. This raised concern for separate formulas for men and women and selection of a precise criterion method like DXA. In addition, this issue reflects the limitation of the use of the BIA-based estimates where the in-built algorithm of the device (that varies with the models also) is not known.

A cross-sectional study among university students aged 18 to 24 years from Colombia developed single-frequency BIA-based prediction equations for total body water and FFM, where BI spectroscopy for three compartment model was used as the criterion method (Caicedo-Eraso et al. 2019). In both methods, resistance and reactance values were used. Estimated values of total body water and FFM that were obtained using the two methods did not show

significant differences. The results of regression models showing low standard error of estimates and increase in R^2 were like that reported in Macias et al. 2007.

A study from the U.S. (Wada and Tekin 2007) used BIA-based FFM data from NHANES III and applied the prediction equations reported earlier from the same country for men and women to derive FFM (Sun et al. 2003). The study reported huge number of prediction formulas for FFM and lean body mass (LBM). The authors (Wada and Tekin 2007) also cited articles to show the conversion of LBM to FFM using formulas. Therefore, prediction formulas for FFM had received better technical precision.

The prediction formula by Macias et al. 2007 is common for adult men and women. Another study also reported single prediction equation to estimate FFM for adult men and women aged 20 to 94 years of age (Kyle et al. 2001). Separate prediction formulas for men and women were reported from the U.S. (Sun et al. 2003); validation and cross-validation samples of whites and blacks were taken into consideration. A report from China also reported separate equations for adult men and women (Lu et al. 2016). Higher adiposity in women compared to men was reported in previous studies from Nigeria (Mbada et al. 2015) and Mexico (Macias et al. 2007). High correlation between BIA-based PBF and skinfold-based values was observed instead of overestimation of PBF by the former method (Mbada et al. 2015).

Accuracy of the results obtained using BIA depends on the specific algorithm of the device (Jaffrin and Bousbiat 2014). Therefore, validation and cross-validation of the results obtained from an equipment are important before use. Comparison of the results with that obtained through more precise method like DXA is important. In spite of several limitations of the use of BIA as mentioned before (Coppini et al. 2005), the advantages include portability, safety, non-invasive nature of application, less intra-observer error in the estimation of body composition characteristics, segmental analysis of body fat and fat free mass, relatively moderate cost, and reliable results etc. However, care should be taken for the hydration factor and body geometry of severely obese individuals, variation of body water during menstruation and other health conditions. Another important issue will be the use of the terms FFM and LBM that are not interchangeable. The LBM consists of FFM and essential body fat that may vary between 2% and 10% (Scafoglieri and Clarys 2018; Segal et al. 1988).

In this background, it is justified to mention the limitations of the present study and new call for improved research. In the present study, the term FFM has been used to maintain uniformity with the reference study (Macias et al. 2007). Previous reports on the use of BIA, authors mentioned LBM prediction instead of FFM (Tagliabue et al. 2001). Another report also cited articles on how to convert prediction formulas for LBM to FFM (Wada and Tekin 2007). This issue should be considered in future research. Other limitations of the present study were non-probability sampling, relatively small sample size from a short age-range of 21 to 23-year-old adult men. Neither of the two samples (Macias et al. 2007 and the present study) were probabilistic. The present report shows the results of male participants. Therefore, sample size and age might be the other important factors that call for future research to explore the results in wider age-group and in the representative samples of the populations from different regions of Mexico where individuals with BMI-based nutritional status of normal, overweight, and obesity will be present. It is also important to estimate the differential agreement and bias of the obtained values of FFM using two methods at the levels of BMI. Perhaps in future research, separate formulas for men and women will give more precise results as reported in other studies that were also compared with the results obtained through DXA (Sun et al. 2003). Separate prediction equations for men and women may show differential degree of agreement between the BIA-based FFM and the corresponding value derived from the resistance and reactance-based equations.

Despite such limitations, the present study showed significant concordance of the estimated values of FFM using BIA with that estimated one using the prediction formula (resistance and reactance value-based). The results further established the reproducibility of the prediction formula for Mexican adults proposed earlier (Macias et al. 2007).

From the above discussion, it seems that the estimation of FFM using the BIA has certain limitations because the in-built algorithm of the device is not known and that also may vary in different models. Moreover, the formulas used in the program of the device may differ by age, sex, activity patterns, and population backgrounds. On the other hand, the prediction formulas to estimate FFM using the resistance and reactance values obtained from BIA has several advantages over the problems of unknown algorithm of the device. Studies reported agreement of the results obtained using such formulas with those obtained using a gold standard method like DXA. However, some reports are also available on the disagreement of results (over and underestimation of FFM) at the levels of high BMI (overweight and obesity) and body fat. Differential agreements were also found in men and women.

In conclusion, the present study has shown significant agreement of the estimated FFM using the bioelectrical impedance analyzer (Tanita MC 180 MA, Tanita Corporation, Tokyo, Japan) with the estimated FFM using the resistance and reactance values obtained from the BIA that has been used in a prediction formula proposed

earlier for Mexican adults (Macias et al. 2007).

Acknowledgements

The author thankfully acknowledges help and cooperation of the colleagues and participants from the Faculty of Medicine of the *Universidad Modelo* in Merida, Yucatan. The author is also thankful to a colleague of the Autonomous University of Yucatan (UADY) for lending the bioelectrical impedance analyzer during field work. The author declares no conflict of interest.

References

Balas-Nakash M, Legorreta-Legorreta J, Rodríguez-Cano A, Aguilera-Pérez R, Perichart-Perera O (2010) Validación del uso de ecuaciones para estimar la composición corporal por análisis de impedancia bioeléctrica en mujeres postmenopáusicas con síndrome metabólico. Rev Invest Clín 62(6):538-545

BIA (No author listed) (1994) Bioelectrical impedance analysis in body composition measurement. Proceedings of a National Institutes of Health Technology Assessment Conference. Bethesda, Maryland, December 12-14, 1994. Am J Clin Nutr 64:387S-532S.

Bland JM, Altman DG (1986) Statistical methods for assessing agreement between two methods of clinical measurement. Lancet 1:307-310.

Bohm A, Heitmann BL (2013) The use of bioelectrical impedance analysis for body composition in epidemiological studies. Eur J Clin Nutr 67:S79-S85.

Bracco D, Thiebaud D, Chiolero RL, Landry M, Burckhardt P, Schutz Y (1996) Segmental body composition assessed by bioelectrical impedance analysis and DEXA in humans. J Appl Physiol 81(6):2580-2587.

Caicedo-Eraso JC, Gonzalez-Correa CH, Gonzalez-Correa CA, Gallagher D (2019) Bioelectrical impedance analysis, hydrometry and hydrodensitometry for body composition assessment in adult Colombian women. J Phys Conf Ser (3rd Latin-American Conference on Bioimpedance) 1272:012002.

Coppini LZ, Waitzberg DL, Campos ACL (2005) Limitations and validation of bioelectrical impedance analysis in morbidly obese patients. Curr Opin Clin Nutr 8(3):329-332.

Demura S, Sato S, Kitabayashi T (2004) Percentage of total body fat as estimated by three automatic bioelectrical impedance analyzers. J Physiol Anthropol Appl Human Sci 23(3):93-99.

Dwyer JT, Gallo JJ, Reichel W (1993) Assessing nutritional status in elderly patients. Am Fam Physician 47(3):613-620.

Erselcan T, Candan F, Saruhan S, Ayca T (2000) Comparison of body composition analysis methods in clinical routine. Ann Nutr Metab 44(5-6):243-248.

Gutiérrez JP, Rivera-Dommarc, J, Shamah-Levy T, Villalpando-Hernández S, Franco A, Cuevas-Nasu L, Romero-Martínez M, Hernández-Ávila M (2013) Encuesta Nacional de Salud y Nutrición 2012. Resultados nacionales (2a ed.) Cuernavaca, México: Instituto Nacional de Salud Pública.

Hughes, JT, Maple-Brown LJ, Piers LS, Meerkin J, O'Dea K, Ward LC (2015) Development of a single-frequency bioimpedance prediction equation for fat-free mass in an adult Indigenous Australian population. Eur J Clin Nutr 69(1):28-33.

Jaffrin MY, Bousbiat S (2014) Accuracy of plantar electrodes compared with hand and foot electrodes in fat-free-mass measurement. J Healthc Eng 5(2):123-144.

Jebb SA, Cole TJ, Doman D, Murgatroyd PR, Prentice AM (2000) Evaluation of the novel Tanita body-fat analyser to measure body composition by comparison with a four-compartment model. Br J Nutr 83(2):115-22.

Khalil SF, Mohktar MS, Ibrahim F (2014) The theory and fundamentals of bioimpedance analysis in clinical status monitoring and diagnosis of diseases. Sensors 14:10895-10928.

Kyle UG, Genton L, Karsegard L, Slosman DO, Pichard C (2001) Single prediction equation for bioelectrical impedance analysis in adults aged 20-94 yrs. Nutrition 17:248-283.

Laskey MA (1996) Dual-energy X-ray absorptiometry and body composition. Nutrition 12(1):45-51.

Lohman TG, Roche AF, Martorell R (1988) Anthropometric Standardization Reference Manual. Champagne, IL.

Lu HK, Chiang LM, Chen YY, Chuang CL, Chen KT, Dwyer GB, Hsu YL, Chen CH, Hsieh KC (2016) Hand-to-hand model for bioelectrical impedance analysis to estimate fat free mass in a healthy population. Nutrients 8(10):654.

Macias N, Alemán-Mateo H, Esparza-Romero J, Valencia ME (2007) Body fat measurement by bioelectrical impedance and air displacement plethysmography: a cross-validation study to design bioelectrical impedance equations in Mexican adults. Nutr J 6:18.

Mbada CE, Akintayo ND, Johnson OE, Dada OO (2015) Correlates, predictors, reference ranges and agreement between percent body fat measured using bioelectric impedance analysis and skinfold-thickness measurements in young Nigerian adults. Arch Physiother Glob Res 19(4):7-20.

Moreno-Estrada A, Gignoux CR, Fernández-López JC, Zakharia F, Sikora M, Contreras AV, Acuña-Alonzo V, Sandoval K, Eng C, Romero-Hidalgo S, Ortiz Tello P, Robles V, et al. (2014) The Genetics of Mexico recapitu-

lates Native American substructure and affects biomedical traits. Science 344(6189):1280-1285.

Pimentel GD, Bernhard AB, Frezza MP, Rinaldi AM, Burini RC (2010) Bioelectric impedance overestimates the body fat in overweight and underestimates in Brazilian obese women: a comparation with Segal equation 1. Nutr Hosp 25(5):741-745.

Ramírez E, Valencia ME, Bourges H, Espinosa T, Moya-Camarena SY, Salazar G, Aléman-Mateo H (2012) Body composition prediction equations based on deuterium oxide dilution method in Mexican children: a national study. Eur J Clin Nutr 66(10):1099-1103.

Ricciardi R, Talbot LA (2007) Use of bioelectrical impedance analysis in the evaluation, treatment, and prevention of overweight and obesity. J Am Acad Nurse Pract 19(5):235-241.

Scafoglieri A, Clarys JP (2018) Dual energy X-ray absorptiometry: gold standard for muscle mass? Letter to the Editor. J Cachexia Sarcopeni Muscle 9:786-787.

Schifferli I, Carrasco F, Inostroza J (2011) Formulación de una ecuación para predecir la masa grasa corporal a partir de bioimpedanciometría en adultos en un amplio rango de edad e índice de masa corporal. Rev Med Chile 139:1534-1543.

Schifferli Castro I, Zuniga ML (2017) Behavior of a new equation using bio-impedancemetry to predict body fat in Chilean adults. Obes Control Ther 4(2):1-7.

Sebo P, Herrmann FR, Haller DM (2017) Accuracy of anthropometric measurements by general practitioners in overweight and obese patients. BMC Obes 4:23.

Segal KR, Van Loan M, Fitzgerald PI, Hodgdon JA, Van Itallie TB (1988) Lean body mass estimation by bioelectrical impedance analysis: a four-site cross-validation study. Am J Clin Nutr 47(1):7-14.

Sun SS, Chumlea WC, Heymsfield SB, Lukaski HC, Schoeller D, Friedl K, Kuczmarski RJ, Flegal KM, Johnson CL, Hubbard VS (2003) Development of bioelectrical impedance prediction equations from body composition with the use of a multicomponent model for use in epidemiologic surveys. Am J Clin Nutr 77:331-340.

Sun G, French CR, Martin GR, Younghusband B, Green RC, Xie YG, Mathews M, Barron JR, Fitzpatrick DG, Gulliver W, Zhang H (2005) Comparison of multifrequency bioelectrical impedance analysis with dual-energy X-ray absorptiometry for assessment of percentage body fat in a large, healthy population. Am J Clin Nutr 81:74-78.

Tagliabue A, Andreoli A, Comelli M, Bertoli S, Testolin G, Oriani G, De Lorenzo A (2001) Prediction of lean body mass from multifrequency segmental impedance: influence of adiposity. Acta Diabetol 38:93-97

Taing KY, Farkuoh ME, Moineddin R, Tu JV, Jha P (2017) Comparative associations between anthropometric and bioelectric impedance analysis derived adiposity measures with blood pressure and hypertension in India: a cross-sectional analysis. BMC Obes 4:37.

Wada R, Tekin E (2007) Body Composition and Wages. NBER Working Paper No. 13595. National Bureau of Economic Research. Cambridge, MA.

WHO (1995) Physical status: the use and interpretation of anthropometry. Report of a WHO expert committee. Technical report series no. 854. Geneva: World Health Organization. From: <http://whqlibdoc.who.int/trs/WHO_TRS_854.pdf> (Retrieved on 5th October 2020).

Yamashita K, Kondo T, Osugi S, Shimokata K, Maeda K, Okumura N, Matsudaira K, Shintani S, Muramatsu T, Matsushita K, Murohara T (2012) The significance of measuring body fat percentage determined by bioelectrical impedance analysis for detecting subjects with cardiovascular disease risk factors. Circ J 76(10):2435-2442.

Acta Biologica Szegediensis

Volume 64(2):99-109, 2020
Acta Biologica Szegediensis
http://abs.bibl.u-szeged.hu/index.php/abs

DOI:10.14232/abs.2020.2.99-109

ARTICLE

Lipid biomarker-based verification of TB infection in mother's and daughter's mummified human remains (Vác Mummy Collection, 18th century, CE, Hungary)

Orsolya A. Váradi[1,2]*, Ildikó Szikossy[1,3], Olga Spekker[1], Dávid Rakk[2], Gabriella Terhes[4], Edit Urbán[5,6], William Berthon[1], Ildikó Pap[1,3,7], Frank Maixner[8], Albert Zink[8], Csaba Vágvölgyi[2], Helen D. Donoghue[9], David E. Minnikin[10], György Pálfi[1#], András Szekeres[2#]

[1]Department of Biological Anthropology, Faculty of Science and Informatics, University of Szeged, Hungary.
[2]Department of Microbiology, Faculty of Science and Informatics, University of Szeged, Hungary.
[3]Department of Anthropology, Hungarian Natural History Museum, Budapest, Hungary.
[4]Institute of Clinical Microbiology, Faculty of Medicine, University of Szeged, Szeged, Hungary.
[5]Department of Medical Microbiology and Immunology, Medical School, University of Pécs, Pécs, Hungary.
[6]Institute of Translational Medicine, Medical School, University of Pécs, Pécs, Hungary.
[7]Department of Biological Anthropology, Eötvös Loránd University, Budapest, Hungary.
[8]Institute for Mummy Studies, Eurac Research, Bolzano, Italy.
[9]Centre for Clinical Microbiology, University College London, London, UK.
[10]Institute of Microbiology and Infection, School of Biosciences, University of Birmingham, UK.

ABSTRACT The perpetual burden of tuberculosis (TB) keeps drawing the focus of research on this disease. Among other risk factors (e.g., poor living conditions, malnutrition, smoking, HIV infection, etc.), being in close contact with a TB infected person requires special attention. For a better understanding of the disease, paleopathological investigations concerning TB have been carried out with various techniques for a long a time; nevertheless, analysis of incidence among family members is hardly possible in past populations. An exceptional group of naturally mummified individuals, the collection of the Vác mummies (Hungary, 18th century CE), is known about the large TB incidence rate, which has been revealed by aDNA analysis. Besides the high rate of TB infection, another interesting aspect of the collection is that in some cases, the family connections could be reconstructed. In this paper, we present the mycocerosic acid profiles gained by HPLC-HESI-MS measurements of two Vác mummies, who were mother and daughter according to the personal records. Earlier metagenomic analysis already revealed mixed *M. tuberculosis* infection with the same bacterial strains in both individuals; moreover, the same bacterial strains were recorded in both cases.

Acta Biol Szeged 64(2):99-109 (2020)

KEY WORDS
high-performance liquid chromatography
lipid biomarkers
mass spectrometry
mummies
mycocerosates
tuberculosis

ARTICLE INFORMATION
Submitted
15 December 2020.
Accepted
29 December 2020.
***Corresponding author**
E-mail: varadi.orsolya.90@gmail.com

Introduction

Tuberculosis (TB) is a well-known infectious disease, which can be caused by members of *Mycobacterium tuberculosis* complex (MTBC), in humans, and also several animal species (Brites et al. 2018; WHO 2020). The 12 species/varieties, included in the complex, are genetically closely related, presenting 99.9% similarity in the nucleotide level (Brosch et al. 2002; Brites and Gagneux 2017; Brites et al. 2018; Riojas et al. 2018). Up to now, the following species are considered as members of the complex: *M. tuberculosis, M. africanum, "M. canettii", M. bovis, M. microti, M. pinnipedii, M. orygis, M. mungi, M. suricattae, M. caprae,* "chimpanzee bacillus", and "dassie bacillus" (Brites et al. 2018; Riojas et al. 2018), but only the first three are specifically human pathogens (Castets et al. 1968; Brosch et al. 2002; Niemann et al. 2004; Bañuls et al. 2015). In human infections, the most common scenario is when transmission occurs via inhalation of bacilli-filled droplets, which are projected in the air while coughing, sneezing or even talking (Flynn and Chan 2001; Bañuls et al. 2015; Getahun et al. 2015).

Several risk factors contribute to the spread of TB: some of them affect the transmission itself (e.g. poor living and working condition, household overcrowding, etc.), and some increase the host's susceptibility (e.g., HIV infection, malnutrition, smoking, diabetes) (Lönnroth et al. 2009; WHO 2020). To reduce TB burden, the prevention of new infections is crucial, and a key factor is

#The two last authors contributed equally.

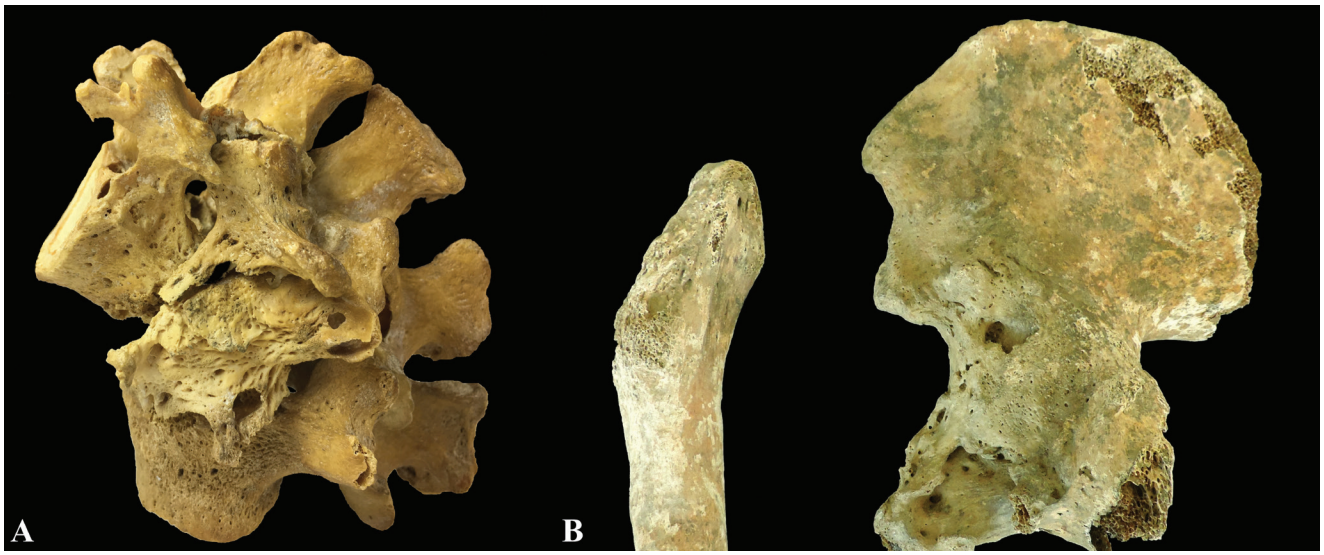

Figure 1. Examples of osteoarticular TB associated lesions. **A:** Pott's gibbus (Robert J. Terry Anatomical Skeletal Collection, Terry No. 1124R). **B:** *Coxitis tuberculosa* (Bélmegyer–Csömöki domb, Grave No. 90).

providing TB preventive treatment for high-risk groups (WHO 2020). Being in close contact with a person who has active TB – especially in newly diagnosed TB patients – means a high risk for transmission; thus, close family members, principally those from the same household, need particular attention (Vidal et al. 1997; Wang and Lin 2000; Horsburgh and Rubin 2011; Augustynowicz-Kopeć et al. 2012; Acuña-Villaorduña et al. 2018; WHO 2020).

According to WHO estimates, approximately 1.2 million HIV-negative and an additional 208000 HIV-positive people died of TB and about 10 million people fell ill with the disease globally in 2019 (WHO 2020). The relatively high incidence, the appearing rifampicin- and multidrug-resistant TB (MDR-TB) strains and the co-infection cases (especially with HIV) highlight the necessity of extensive TB research. This disease is mainly remembered due to its devastating effects during the 18th - 19th century, when it was highly spread in Europe, implying an extraordinary burden (Bello et al. 1999; Vuorinen 1999, Glaziou et al. 2018; Loddenkemper et al. 2018; Roberts 2020), but has been a recognised threat for thousands of years (Gutierrez et al. 2005; Daniel 2006; Baker et al. 2015; Barberies et

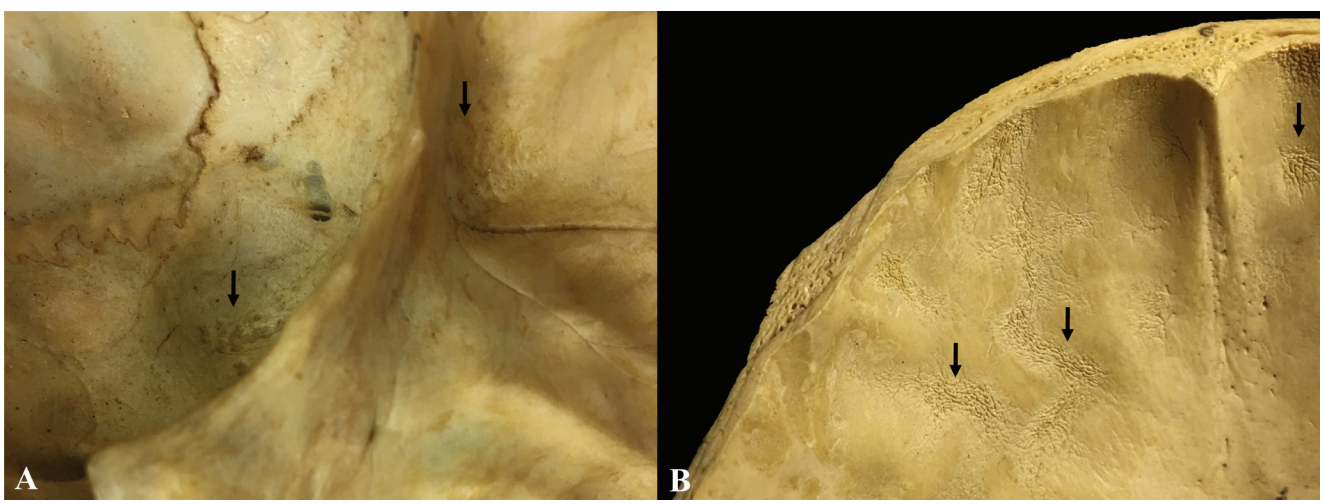

Figure 2. Examples of TBM associated lesions. **A:** Granular impressions on the greater wing of the sphenoid bone (Robert J. Terry Anatomical Skeletal Collection, Terry No. 566). **B:** Abnormal blood vessel impressions on the endocranial surface of the frontal bone (Robert J. Terry Anatomical Skeletal Collection, Terry No. 254).

al. 2017). To achieve a better understanding of the evolution of the infectious agent, paleopathological research investigating the epidemiology of TB in past populations is highly important.

The paleopathological signs of TB include Pott's gibbus (Fig. 1A) and *coxitis tuberculosa* (Fig. 1B), traces of cold abscess, and endocranial lesions caused by tuberculous meningitis (TBM) e.g. granular impressions (Fig. 2A), and abnormal blood vessel impressions (Fig. 2B) (Schultz 1993, 1999, 2001, 2003; Aufderheide and Rodríguez-Martín 1998; Marcsik et al., 1999; Pálfi and Marcsik 1999; Hershkovitz et al. 2002; Maczel 2003; Ortner 2003; Pálfi and Molnár 2009; Pálfi et al. 2012, 2015; Spekker et al. 2012; Kajdocsi Lovász 2015; Masson et al. 2015; Molnár et al. 2015; Paja et al. 2015; Schultz and Schmidt-Schultz 2015; Spekker 2018; Spekker et al. 2020a, 2020b). Moreover, new bone formation on the long bones and on the visceral surface of ribs are used as TB-related markers (Roberts et al. 1994; Marcsik et al. 2009; Santos and Roberts 2001, 2006; Hershkovitz et al. 2002; Maczel 2003; Matos and Santos 2006; Pálfi and Molnár 2009; Pálfi et al. 2012, 2015; Kajdocsi Lovász 2015; Masson et al. 2015; Molnár et al. 2015). Since skeletal TB and CNS TB develop in only a few cases (Golden and Vikram 2005; Rock et al. 2008; Spekker et al. 2018; Rodriguez-Takeuchi et al. 2019; Spekker et al. 2020a; Spekker et al. 2020b), the simultaneous application of molecular biological and analytical techniques are useful tools to draw a clearer picture about the paleoepidemiology of TB (Molnár et al. 2015; Pálfi et al. 2015; Donoghue et al. 2017). Since the 1990s, two approaches are commonly applied to supplement the morphological TB-related paleopathological investigations, namely aDNA based and lipid biomarker-based methods (Spigelman and Lemma 1993; Donoghue et al. 1998; Gernaey et al. 1998; Hershkovitz et al. 2008; Redman et al. 2009; Chan et al. 2013; Kay et al. 2015; Donoghue et al. 2017).

The lipid biomarker-based methods benefit from the lipid-rich cell wall, characteristic of mycobacteria (Minnikin and Goodfellow 1980; Minnikin 1982; Daffé and Lanéelle 1988; Minnikin et al. 1993; Hershkovitz et al. 2008; Redman et al. 2009; Lee et al. 2012; Minnikin et al. 2015a; Donoghue et al. 2017). Most commonly, the mycolic acid (MA) and mycocerosic acid (MC) components, and the C27 mycolipenic acid are used. MAs, MCs, and mycolipenic acids can be found in the so-called Mycobacterial Outer Membrane (MOM) (Minnikin et al. 2015b). MAs are long chain α-alkyl-β-hydroxy fatty acids, which are covalently bound to the mycoloylarabinogalactan-peptidoglycan macromolecules (Watanabe et al. 2001; Minnikin et al. 2015b; Abrahams and Besra 2016; Batt et al. 2020; Dulberger et al. 2020). MCs are long-chain multimethyl-branched-chain fatty acids esterified mainly with phthiocerol and phenolphthiocerol long-chain diols (Minnikin 1982; Daffé and Lanéelle 1988; Redman et al. 2009; Minnikin et al. 2015b; Batt et al. 2020). In contrast with MAs, MCs can be found only in a smaller group of mycobacteria, namely in *M. tuberculosis*, *M. bovis*, *M. gastri*, *M. haemophilum*, *M. kansasii*, *M. leprae*, *M. marinum,* and *M. ulcerans* (Draper et al. 1983; Minnikin et al. 1985; Daffé and Lanéelle 1988; Hartmann and Minnikin, 1992; Minnikin et al. 1993; Redman et al. 2009). MCs have been detected for paleopathological investigations traditionally via NICI-GCMS (Redman et al. 2009) and a HPLC-MS method has been newly introduced (Váradi et al. 2021).

Figure 3. Dominican Church of Vác. Photo taken by András Thumbasz.

In 1994, a group of naturally mummified individuals were found in a long-forgotten crypt during the renovation of the Dominical Church of Vác (1994–1995) (Fig. 3) (Pap et al. 1999). The discovered Vác mummy collection is well-documented, with many available individual data (Szikossy et al. 1997). The mummies are curated in the Department of Anthropology, Hungarian Natural History Museum, Budapest, Hungary. The collection is known for the high presence of TB infected cases, that drew the focus of several studies on this group (Szikossy et al. 1997; Pap et al. 1999; Fletcher et al. 2003; Donoghue et al. 2011; Chan et al. 2013; Kay et al. 2015; Pap et al. 2017). Most of these individuals lived in the 18th century CE, which is from the pre-antibiotic era; therefore, they represent a well-characterised link between recent and archaeological samples. Besides the broad pathological investigations, demographical analysis and exploration of family connections were carried out, as well as attempts to reconstruct individual life stories (Kustár et al. 2011a, 2011b; Szikossy et al. 2015; Szikossy 2020).

The aim of this study is to present and compare the results of mycocerosic acid profiling of two TB infected Vác mummies, a mother (Fig. 4A) and her daughter (Fig.

4B). Earlier both individuals were proved to have mixed infection with the same *M. tuberculosis* strains via aDNA analysis (Kay et al. 2015), and samples taken from the daughter presented positive MC profiles in previous HPLC-MS measurements (Váradi et al. 2021).

Materials and Methods

MTBC strains and mummy samples used in this study

For reference, in an earlier study, we used five MTBC strains (laboratory IDs of the isolated strains MTBC-1/2015; MTBC-254/2000; MTBC-3910/2014; MTBC-242/2000; and MTBC-1/8508/2014), isolated from patients, who had been diagnosed with pulmonary tuberculosis. The average distribution of the reference strains has been evaluated and published in our earlier report (Váradi et al. 2021). The isolation of the reference strains was carried out in the Institute of Clinical Microbiology, University of Szeged, Szeged, Hungary and the National Korányi Institute of TB and Pulmonology, Budapest, Hungary, according to the national recommendations (EMMI, State Secretariat for Healthcare, 2018). The identification and growing conditions followed a previously described protocol (Váradi et al. 2021). The harvested bacterial samples were stored in freeze-dried form at -20 °C.

The examined human sample was taken from the chest region of the late Anna Schőner (body number: #28, inventory number: 2009.19.28., age at death: 55 years). The rib sample was removed by sanitized tweezers and stored in a tightly closed bag at room temperature. The bone was powdered in the clean laboratory of the Institute for Mummy Studies, EURAC Research, Bolzano, Italy.

Sample preparation and instrumental analysis

In the case of the sample pre-treatment and measurement of the MTBC strains, 20 mg of bacterial material was utilized and the previously described method was applied (Váradi et al. 2021). For the lipid analysis of the mummy sample, 434 mg of bone powder was used. The sample pre-treatment was carried out briefly as follows: the samples were heated at 100 °C overnight with the addition of 20% KOH in MeOH (2 mL; m/V) and toluene (1 mL) in PTFE capped glass tubes. Samples were acidified to pH 1 with the addition of 10% HCl and 37% HCl solutions. Thereafter, the samples were extracted with the addition of toluene (1 mL) three times, and one more time with the addition of hexane isomer mixture (1 mL). The removed and combined organic layers were evaporated to dryness in vacuum with a Savant SC250EXP SpeedVac concentrator (Thermo Scientific, Waltham, Massachusetts, USA). The mummy sample was dissolved in 1000 µl and the bacterial samples were dissolved in 200 µL of the following mixture: isopropanol (IPA):heptane:acetonitrile (MeCN) (4:1:5). The sample solutions were filtered by PTFE syringe filters (pore size: 2.0 µm; diameter: 13 mm).

The measurements were carried out on a Dionex Ultimate 3000 UHPLC system (Thermo Scientific, Waltham, Massachusetts, USA), which was coupled with a Q-Exactive Plus (Thermo Scientific, Waltham, Massachusetts, USA) mass spectrometer (MS). For the separation, a Gemini – NX C18 (3 µm, 110A, 50 mm x 2 mm) column (Phenomenex, Torrance, California, USA) was used at 30 °C.

The separation was carried out with gradient elution

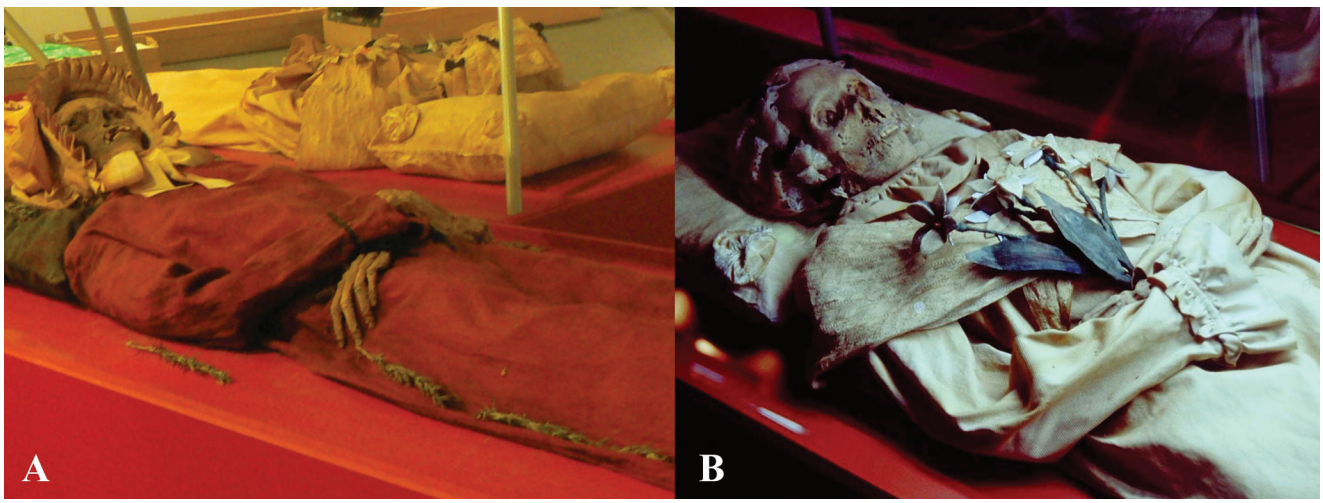

Figure 4. Sources of the mummy samples. **A:** Anna Schőner (Body No: 28, Inv. No: 2009.19.28.). **B:** The late Terézia Hausmann (Body No: 68, Inv. No: 2009.19.68.). Photos were taken on the exhibition of the Hungarian Natural History Museum.

Table 1. Gradient elution program applied for the HPLC separation of mycocerosic acids.

Time (min)	Eluent A (%): MeCN + 0.1% acetic acid	Eluent B (%): IPA:heptane (8:2) + 0.1% acetic acid
0	90	10
5	85	15
15	30	70
16	10	90
18	10	90
18.5	80	20
19.5	80	20
20	10	90
23	10	90
24	90	10
28	90	10

(see details in Table 1), and 200 µL/min flow rate was applied. The injection needle was thoroughly washed before and after injection, with 150 µL IPA:heptane (8:2). Solvent blank injections were made between each sample investigation.

Regarding the MS parameters, the following settings were applied: the sheath gas flow and the auxiliary gas rates were set to 35 L/min and 10 L/min, respectively, the capillary and the auxiliary gas was heated to 350 °C, the spray voltage was set to 4 kV, while the S-lens voltage was 70 V. The targeted MCs (Fig. 5) were monitored in negative Selected Ion Monitoring (SIM) mode: 409.40510 (C27, $C_{27}H_{53}O_2$), 437.43640 (C29, $C_{29}H_{57}O_2$), 451.45205 (C30, $C_{30}H_{59}O_2$), 479.48335 (C32, $C_{32}H_{63}O_2$), and 493.49900 (C33, $C_{33}H_{65}O_2$), with 0.4 *m/z* isolation window. The area values of the MC peaks were calculated with TraceFinder 4.0 General Quan Software (Thermo Scientific, Waltham, Massachusetts, USA). The maximum mass deviation from the calculated $[M\text{-}H]^-$ ion mass was 5 ppm for peak identification. The detected MC peaks were normalised to the peak with the highest area value.

Results and Discussion

Three members of the Hausmann family were identified in the Vác Mummy Collection of the Hungarian Natural History Museum. The mother, Anna Schőner (1738-1793) and her two daughters, Terézia (1769-1797) and Barbara Hausmann (1780-1795). Their father, János Hausmann is not in the collection. According to the aDNA examinations (Fletcher et al. 2003; Chan et al. 2013; Kay et al. 2015), all three female members of the Hausmann family were infected by tuberculosis. First, Anna Schőner died at the age of 55 in 1793, December 16. Two years later, she was followed by her younger daughter, Barbara Hausmann, who died at the age of 15, on March 2, 1975. In another two years, the elder daughter, Terézia Hausmann passed away at the age of 28, on December 25, 1797 (Exploration documentation of the Dominican Church of Vác, 1994-1995, Tragor Ignác Múzeum.). Both girls were emaciated, suggesting a long-lasting illness. It is possible that the thirteen-year-older Terézia took care of her sister before the illness made her too weak (Cseplák et al. 2015, Donoghue et al. 2021). In this study, we present the mycocerosate profiles observed by the analysis of samples taken from Anna Schőner (#28) and Terézia Hausmann (#68).

The lipid profile observed for the extract of the rib sample taken from the #28 individual is shown in Fig. 6A and Fig. 7. The *M. tuberculosis* C27 MC minor component was not detected in the extract. In the MC profile, the main peak was the C32 (100), and it was accompanied by a relatively high peak of C30 (49). The C29 MC was presented in a relatively high ratio (25), as well. The C33 MC was also detectable but was a minor component in the extract (3). The first eluting component was the C29 MC with the retention time of 8.20 min, followed by the C30 and C32 MCs at 8.75 and 10.64 min, respectively. The retention time of the C33 MC peak was 10.97. The general distribution of the detected MCs was in accord with others from the same group of mummies, and with the average profile gained by the analysis of clinical samples (e.g., Fig. 5B, Fig. 6B), and with the MTB profiles published using different approaches (Minnikin et al. 1993; Redman et al. 2009; Váradi et al. 2021). Based on our previous results, the observed lipid profile fulfills the requirement to be identified as a positive case, as the three most presented MCs were the C32, C30, and C29, with a principal amount of the C32 component (Fig. 6C, Fig. 7). The samples belonging to the daughter (#68) of this individual were found earlier to be positive with HPLC-MS analysis (Váradi et al. 2021). In that case, both soft tissue and rib samples were included in the investigation. The MC profile of the soft tissue presented provided clean peaks for C32, C29, C30 and C33 MCs. The main peak was the C32 (100), which was accompanied by major C29 (38) and C30 (97) peaks and with C33 MC (5) as minor

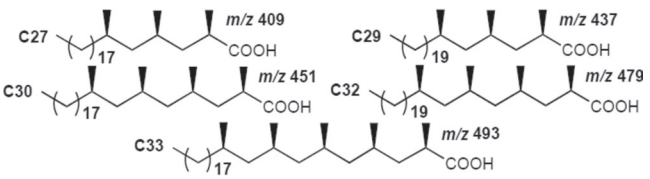

Figure 5. Structures of mycocerosic acids. The mass spectral *m/z* values correspond to carboxylate anions ($M - H^+$).

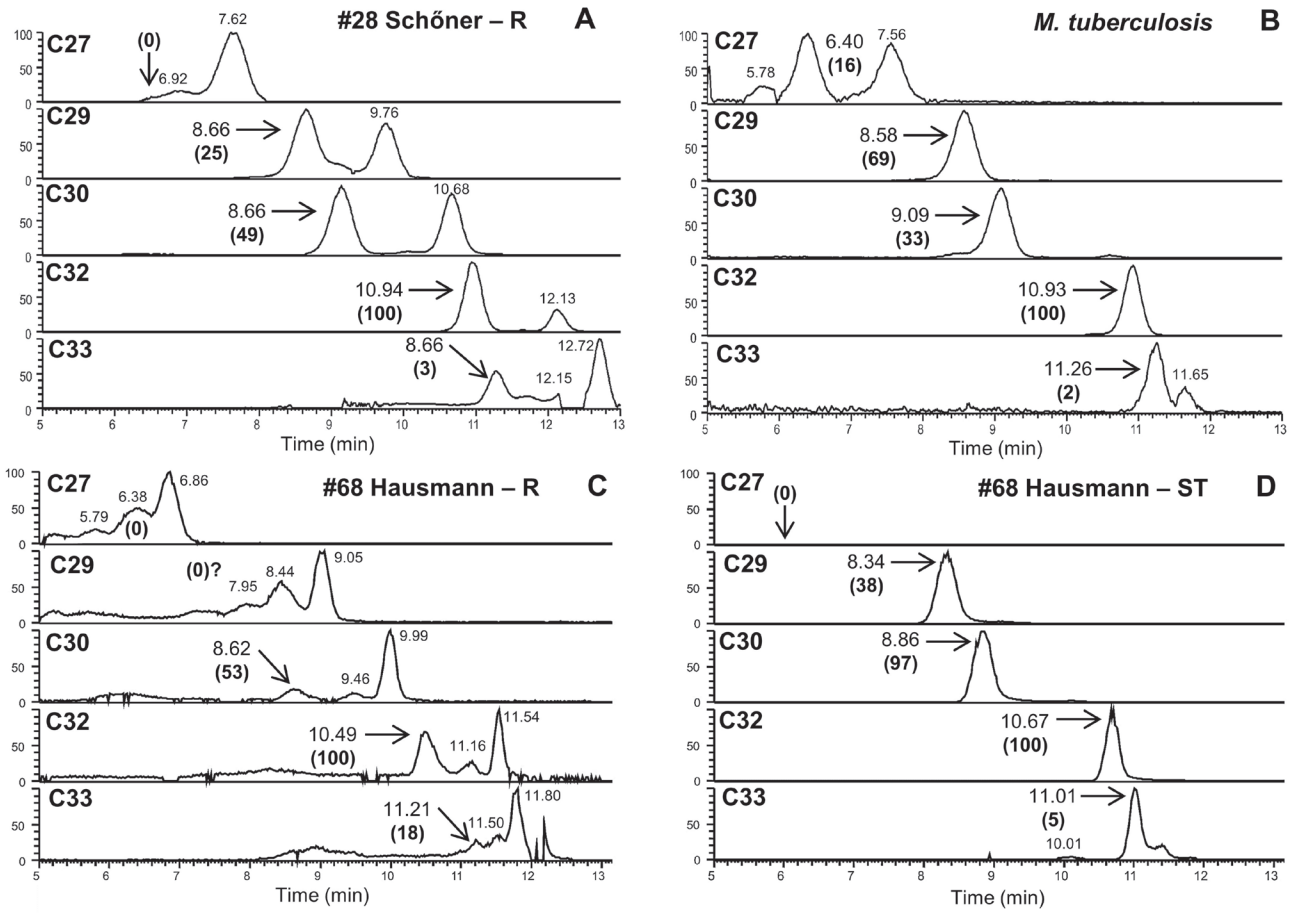

Figure 6. Mycocerosic acid profile of M. tuberculosis and positive mycocerosate (MC) profiles from mummy samples #28 and #68. **A:** Rib (R) sample from Anna Schőner (#28). **B:** Mycocerosate profile of M. tuberculosis 254-2000. **C** and **D:** Rib (R) and Soft Tissue (ST) samples from Terézia Hausmann (#68). MC distributions are shown normalised to the main component (100).

component (Fig. 6D, Fig. 7). The extract of the rib sample of #68 individual had clear main C32 (100) and major C30 components (53), but the minor C33 was indistinct (~18) and the area for the expected C29 was obscured.

Samples taken from the same individuals were earlier analysed with two different aDNA techniques. Firstly, as part of an extensive study, the examination of over 350 samples covering 168 individuals were screened for the 123-bp region of the IS*6110* insertion sequence (Fletcher et al. 2003). The positive samples were investigated for silent point mutations of the *gyrA* 95 and *katG* 463 genes; for the differentiation of the infectious agents into three genotypes, following the work of Sreevatsan et al. (1997). Our positive MC profile matched the result of the DNA-based analysis; traits of *gyrA* 95 and *katG* 463 genes were found in the abdomen, with the silent point mutations characteristic to the group 2 genotype of *M. tuberculosis* (Fletcher et al. 2003). In the case of the same study, during the analysis of the samples taken from the #68 individual's left chest, the silent point mutations of the *gyrA* 95 and *katG* 463 genes were characteristic of the group 3 genotype of *M. tuberculosis*. Metagenomic analysis carried out on the samples taken from the abdomen region of the #28 individual and on the samples taken from the left chest region of the #68 individual presented similar results (Kay et al. 2015). In both cases, a mixed MTB infection was revealed, but although the detected genotypes were the same, they were detected in different proportions. One of the *M. tuberculosis* strains belonged to sublineage 4.1.2.1, also known as the Haarlem lineage (Kay et al. 2015; Stucki et al. 2016), and the other was assigned by Kay et al. (2015) to sublineage 4.7, which is currently part of sublineage 4.10 according to Stucki et al. (2016). The metagenomic results suggest a transmission between mother and child or infection from the same source (Kay et al. 2015).

Although in this case the applied MC profiling method cannot provide the same resolution regarding the *M.*

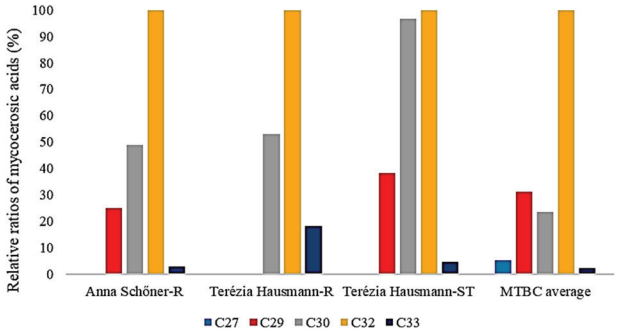

Figure 7. The normalised distribution of positive mycocerosate profiles from mummy rib (R) and soft tissue (ST) samples. Also shown is an "MTB average", calculated in previous examinations of clinical samples.

tuberculosis strains, it demonstrates the widespread occurrence of TB infection among the Vác mummies. The combined application of morphology, aDNA and lipid biomarker analysis is important to gain a clearer picture in paleopathological practice as the results can support each other, and help to reveal positive cases, which would possibly remain hidden if only one method was applied (Hershkovitz et al. 2008; Lee et al. 2012; Baker et al. 2015; Masson et al. 2015; Molnár et al. 2015; Donoghue et al. 2017; Luna et al. 2020). The examination of mummified human remains with a variety of different approaches is especially useful and provides a unique insight to TB research (Salo et al. 1994; Zink et al. 2003; Donoghue et al. 2004; Donoghue et al. 2009; Minnikin et al. 2011; Chan et al. 2013; Lalremruata et al. 2013; Kay et al. 2015; Piombino-Mascali et al. 2015; Szikossy et al. 2015).

Acknowledgements

David E. Minnikin acknowledges Leverhulme Trust Project Grant F/00 094/BL and UK Medical Research Council Programme Grant MR/S000542/1. We acknowledge the support of the National Research, Development and Innovation Office (Hungary) (grant number: K 125561). We also acknowledge the support for establishing the infrastructural background (grant number: GINOP-2.3.3-15-2016-00006).

References

Abrahams KE, Besra GS (2016) Mycobacterial cell wall biosynthesis: a multifaceted antibiotic target. Parasitology 145(2):116-133.

Acuña-Villaorduña C, Jones-López EC, Fregona G, Marques-Rodrigues P, Gaeddert M, Geadas C, Hadad DJ, White LF, Molina LPD, Vinhas S, Ribeiro-Rodrigues R, Salgame P, Palaci M, Alland D, Ellner JJ, Dietze R (2018) Intensity of exposure to pulmonary tuberculosis determines risk of tuberculosis infection and disease. Eur Respir J 51:1701578.

Aufderheide AC, Rodríguez-Martín C (1998) The Cambridge encyclopedia of human paleopathology. Cambridge University Press, Cambridge, UK; 118-141.

Augustynowicz-Kopeć E, Jagielski T, Kozińska M, Kremer K, van Sooligen D, Bielecki J, Zwolska Z (2012) Transmission of tuberculosis within family-households. J Infect 64: 596-608.

Baker O, Lee OY-C, Wu HHT, Besra GS, Minnikin DE, Llewellyn G, Williams CM, Maixner F, O'Sullivan N, Zink A, Chamel B, Khawam R, Coqueugniout E, Helmer D, Le Mort F, Perrin P, Gourichon L, Dutailly, Pálfi Gy, Coqueugniot H, Dutour O (2015) Human tuberculosis predates domestication in ancient Syria. Tuberculosis 95(Suppl.1):S4-S19.

Bañuls A-L, Sanou A, Nguyen TVA, Godreuil S (2015) *Mycobacterium tuberculosis*: ecology and evolution of human bacterium. J Med Microbiol. 64(11):1261-1269.

Barberis I, Bragazzi NL, Galluzzo L, Martini M (2017) The history of tuberculosis: from the first historical records to the isolation of Koch's bacillus. J Prev Med Hyg 58:E9-E12.

Batt SM, Minnikin DE, Besra GS (2020) The thick waxy coat of mycobacteria, a protective layer against antibiotics and the host's immune system. Biochem J 477(10):1983-2006.

Bello S, Signoli M, Maczel M, Dutour O (1999) Evolution of mortality due to tuberculosis in France (18-20th centuries). In Pálfi Gy, Dutour O, Deák J, Hutás I, Eds., Tuberculosis Past and Present. TB Foundation: Szeged, Hungary & Golden Book Publisher, Budapest, Hungary, 95-104.

Brites D, Gagneux S (2017) The nature and evolution of genomic diversity in the *Mycobacterium tuberculosis* complex. In Gagneux S, Ed., Strain Variation in the *Mycobacterium tuberculosis* Complex: Its Role in Biology, Epidemiology and Control. Advances in Experimental Medicine and Biology 1019. Springer International Publishing, Cham, Switzerland, 1-26.

Brites D, Loiseau C, Menardo F, Borrell S, Boniotti MB, Warren R, Dippenaar A, Parsons SDC, Beisel C, Behr MA, Fyfe JA, Coscolla M, Gagneux S (2018) A new phylogenetic framework for the animal-adapted *Mycobacterium tuberculosis* complex. Front Microbiol 9:2820.

Brosch R, Gordon SV, Marmiesse M, Brodin P, Buchrieser C, Eiglmeier K, Garnier T, Gutierrez C, Hewinson G, Kremer K, Parsons LM, Pym AS, Samper S, van Soolingen D, Cole ST (2002) A new evolutionary scenario for the *Mycobacterium tuberculosis* complex. PNAS 99(6):3684-3689.

Castets M, Boisvert H, Grumbach F, Brunel M, Rist N (1968)

Tuberculosis bacilli of the African type: preliminary note. Rev Tuberc Pneumol 32:179-184.
Chan JZ-M, Sergeant MJ, Lee OY-C, Minnikin DE, Besra GS, Pap I, Spigelman M, Donoghue HD, Pallen MJ (2013) Metagenomic analysis of tuberculosis in a mummy. N Engl J Med 369:289-290.
Cseplák Gy, Szikossy I, Pap I (2015) A váci múmiákról. Antropo-medicinális tanulmányok 52 váci múmia vizsgálatáról egy bőrgyógyász fényképes jegyzeteivel. Semmelweis Kiadó és Multimédia Stúdió Kft., Budapest.
Daffé M, Lanéelle MA (1988) Distribution of phthiocerol diester, phenolic mycosides and related compounds in mycobacteria. J Gen Microbiol 134(7):2049-2055.
Daniel TM (2006) The history of tuberculosis. Respir Med 100:1862-1870.
Donoghue HD, Lee OY-C, Minnikin DE, Besra GS, Taylor JH, Spigelman M (2009) Tuberculosis in Dr Granville's mummy: a molecular re-examination of the earliest known Egyptian mummy to be scientifically examined and given a medical diagnosis. Proc R Soc B 27751-2776.
Donoghue HD, Pap I, Szikossy I, Spigelman M (2011) Detection and characterization of *Mycobacterium tuberculosis* DNA in 18th century Hungarians with pulmonary and extra-pulmonary tuberculosis. In Gill-Frerking H, Rosendahl W, Zink A, Piombino-Mascali D, Eds., Yearbook of Mummy Studies, Verlag Dr. Friedrich Pfeil, München, Germany, 1:51-56.
Donoghue HD, Spigelman M, Greenblatt CL, Lev-Maor G, Bar-Gal GK, Matheson C, Vernon K, Nerlich AG, Zink AR (2004) Tuberculosis: from prehistory to Robert Koch, as revealed by ancient DNA. Lancet Infect Dis 4(9):584-592.
Donoghue HD, Spigelman M, Zias J, Gernaey-Child AM, Minnikin DE (1998) *Mycobacterium tuberculosis* complex DNA in calcified pleura from remains 1400 years old. Lett Appl Microbiol 27:265-269.
Donoghue HD, Taylor MG, Stewart GR, Lee OY-C, Wu HHT, Besra GS, Minnikin DE (2017) Positive diagnosis of ancient leprosy and tuberculosis using ancient DNA and lipid biomarkers. Diversity 9(4):46.
Donoghue HD, Pap I, Szikossy I, Spigelman M (2021) The Vác Mummy Project: Investigation of 265 eighteenth-century mummified remains from the TB pandemic era. In Shin DH, Bianucci R, Eds., The Handbook of Mummy Studies. Springer, Singapore.
Draper P, Payne SN, Dobson G, Minnikin DE (1983) Isolation of a characteristic phthiocerol dimycocerosate from *Mycobacterium leprae*. J Gen Microbiol 129(3):859-863.
Dulberger CL, Rubin EJ, Boutte CC (2020) The mycobacterial cell envelope – a moving target. Nat Rev Microbiol 18:47-59.
EMMI, State Secretariat for Healthcare (2018) Egészségügyi szakmai irányelv – A tuberkulózis prevenciójáról, diagnosztikájáról, terápiájáról és gondozásáról. Available: https://www.hbcs.hu/uploads/jogszabaly/2838/fajlok/EMMI_szakmai_iranyelve_tuberkulozis.pdf; 2014. Accessed 01 August 2020.
Exploration documentation of the Dominican Church of Vác, 1994-1995, Tragor Ignác Múzeum. (TIM ND.95.3.1. Munkanapló; ND.95.3.2. 1-262. Feltárási adatlapok).
Fletcher HA, Donoghue HD, Holton J, Pap I, Spigelman M (2003) Widespread occurrence of *Mycobacterium tuberculosis* DNA from 18th-19th century Hungarians. AJPA 120(2):144-152.
Flynn JL, Chan J (2001) Tuberculosis: latency and reactivation. Infect Immun 69(7):4195-4201.
Gernaey AM, Minnikin DE, Copley MS, Power JJ, Ahmed AMS, Dixon RA, Roberts CA, Robertson JD, Nolan J, Chamberlain A (1998) Detecting ancient tuberculosis. Internet Archaeol Available: http://intarch.ac.uk/journal/issue5/gernaey_index.html. Accessed: 03 August 2020.
Getahun H, Matteelli A, Chaisson RE, Raviglione M (2015) Latent *Mycobacterium tuberculosis* infection. N Engl J Med 372:2127-2135.
Glaziou P, Floyd, K, Raviglione M (2018) Trends in tuberculosis in the UK. Thorax 73:702-703.
Golden MP, Vikram HR (2005) Extrapulmonary tuberculosis: an overview. Am Fam Physician 72(9):1761-1768.
Gutierrez MC, Brisse S, Brosch R, Fabre M, Omaïs B, Marmiesse M, Supply P, Vincent V (2005) Ancient origin and gene mosaicism of the progenitor of *Mycobacterium tuberculosis*. PloS Pathog 1(1):e5.
Hartmann S, Minnikin DE (1992) Mycobacterial phenolic glycolipids. In Tyman JHP, Ed., Surfactants in Lipid Chemistry: Recent Synthetic, Physical and Biodegradative Studies. Royal Society of Chemistry, Cambridge, UK, 135-158.
Hershkovitz I, Donoghue HD, Minnikin DE, Besra GS, Lee OY-C, Gernaey, AM, Galili E, Eshed V, Greenblatt CL, Lemma E, Bar-Gal GK, Spigelman M (2008) Detection and molecular characterization of 9000-year-old *Mycobacterium tuberculosis* from a Neolithic settlement in the Eastern Mediterranean. PLOS ONE 3(10):e3426..
Hershkovitz I, Greenwald CM, Latimer B, Jellema LM, Wish-Baratz S, Eshed V, Dutour O, Rothschild BM (2002) Serpens endocrania symmetrica (SES): a new term and a possible clue for identifying intrathoracic disease in skeletal populations. AJPA 118(3):201-216.
Horsburgh CR, Rubin RJ (2011) Latent tuberculosis infection in the United States. N Engl J Med 364:1441-1448.
Kajdocsi Lovász G (2015) A török hódoltság kori idegen etnikumok összehasonlító embertani vizsgálata. PhD Thesis, University of Szeged, Szeged, Hungary.
Kay GL, Sergeant MJ, Zhou Z, Chan JZ-M, Millard A, Quick J, Szikossy I, Pap I, Spigelman M, Loman NJ, Achtman M, Donoghue HD, Pallen MJ (2015) Eighteenth-century ge-

nomes show that mixed infections were common at time of peak tuberculosis in Europe. Nat Commun 6:6717.

Kustár Á, Pap I, Végvári Zs, Kristóf LA, Pálfi Gy, Karlinger K, Kovács KB, Szikossy I (2011a) Using of 3D virtual reconstruction for pathological investigation and facial reconstruction of an 18th century mummified nun from Hungary. In Gill-Frerking H, Rosendahl W, Zink A, Piombino-Mascali D, Eds., Yearbook of Mummy Studies. Verlag Dr. Friedrich Pfeil, München, Germany, 1:83-93.

Kustár Á, Pap I, Végvári Zs, Kristóf LA, Pálfi Gy, Karlinger K, Kovács B, Szikossy I (2011b) Tauber Antónia, 18. századi váci apáca múmiájának patológiai vizsgálata és arcrekonstrukciója 3D rekonstrukciós módszerek alkalmazásával. Anthropol Közl 52:5-15.

Lalremruata A, Ball M, Bianucci R, Welte B, Nerlich AG, Kun JFJ, Pusch CM (2013) Molecular identification of *Falciparum malaria* and human tuberculosis co-infection in mummies from the Fayum Depression (Lower Egypt). PLOS ONE 8(4):e60307.

Lee OY-C, Wu HHT, Donoghue HD, Spigelman M, Greenblatt CL, Bull ID, Rothschild BM, Martin LD, Minnikin DE, Besra GS (2012) *Mycobacterium tuberculosis* complex lipid virulence factors preserved in the 17,000-year-old skeleton of an extinct bison, *Bison antiquus*. PLOS ONE 7:e41923.

Loddenkemper R, Murray JF, Gradmann C, Hopewell PC, Kato-Maeda M (2018) History of tuberculosis. In Migliori GB, Bothamley G, Duarte R, Rendon A, Eds., Tuberculosis. Charlesworth Press, Wakefield, UK, 8-27.

Lönnroth K, Jaramillo E, Williams BG, Dye C, Raviglione M (2009) Drivers of tuberculosis epidemics: The role of risk factors and social determinants. Soc Sci Med 68:2240-2246.

Luna LH, Aranda CM, Santos AL, Donoghue HD, Lee OY-C, Wu HHT, Besra GS, Minnikin DE, Llewellyn G, Williams CM, Ratto N (2020) Oldest evidence of tuberculosis in Argentina: A multidisciplinary investigation in an adult male skeleton from Saujil, Tinogasta, Catamarca (905-1030 CE). Tuberculosis 125:101995.

Maczel M. (2003) "On the traces of tuberculosis" Diagnostic criteria of tuberculosis affection of the human skeleton and their application in Hungarian and French anthropological series. PhD Thesis, University of La Méditerranée, Marseille, France, University of Szeged, Szeged, Hungary.

Marcsik A, Molnár E, Ősz B, Donoghue HD, Zink A, Pálfi Gy (2009) Adatok a lepra, tuberculosis és syphilis magyarországi paleopatológiájához. Folia Anthropologica 8:5-34.

Marcsik A, Szentgyörgyi R, Gyetvai A, Finnegan M, Pálfi Gy (1999) Probable Pott's paraplegia from the 7th-8th century AD. In Pálfi Gy, Dutour O, Deák J, Hutás I, Eds., Tuberculosis: Past and Present. TB Foundation: Szeged, Hungary & Golden Book Publisher: Budapest, Hungary, 331-336.

Masson M, Bereczki Zs, Molnár E, Donoghue HD, Minnikin DE, Lee OY-C, Wu HHT, Besra GS, Bull ID, Pálfi Gy (2015) 7000-year-old tuberculosis cases from Hungary – Osteological and biomolecular evidence. Tuberculosis 95(Suppl. 1):S13-S17.

Matos V, Santos AL (2006) On the trail of pulmonary tuberculosis based on rib lesions: results from the human identified skeletal collection from the Museu Bocage (Lisbon, Portugal). AJPA 130(2):190-200.

Minnikin DE, Besra GS, Lee OY-C, Spigelman M, Donoghue HD (2011) The interplay of DNA and lipid biomarkers in the detection of tuberculosis and leprosy in mummies and other skeletal remains. In Gill-Frerking H, Rosendahl W, Zink A, Piombino-Mascali D, eds., Yearbook of Mummy Studies. Verlag Dr. Friedrich Pfeil, München, Germany, 1:109-114.

Minnikin DE, Bolton RC, Hartmann S, Besra GS, Jenkins PA, Mallet AI, Wilkins E, Lawson AM, Ridell M (1993) An integrated procedure for the direct detection of characteristic lipids in tuberculosis patients. Ann Soc Belg Med Trop 73(Suppl. 1):13-24.

Minnikin DE, Dobson G, Goodfellow M, Magnusson M, Ridell M (1985) Distribution of some mycobacterial waxes based on the phthiocerol family. J Gen Microbiol 131(6):1375-1381.

Minnikin DE, Goodfellow M (1980) Lipid composition in the classification and identification of acid-fast bacteria. In Goodfellow M, Board RG, Eds., Microbiological Classification and Identification. Academic Press, London, UK, 189-256.

Minnikin DE, Lee OY-C, Wu HHT, Besra GS, Bhatt A, Nataraj V, Rothschild BM, Spigelman M, Donoghue HD (2015a) Ancient mycobacterial lipids: Key reference biomarkers in charting the evolution of tuberculosis. Tuberculosis 95(Suppl. 1):S133-139.

Minnikin DE, Lee OY-C, Wu HHT, Nataraj V, Donoghue HD, Ridell M, Watanabe M, Alderwick L, Bhatt A, Besra GS (2015b) Pathophysiological implications of cell envelope structure of *Mycobacterium tuberculosis* and related taxa. In Ribon W, Ed., Tuberculosis – Expanding Knowledge. InTech - Open Access Publisher. 145-75.

Minnikin, DE (1982) Lipids: complex lipids, their chemistry, biosynthesis and role. In Ratledge C, Stanford J, Eds., The Biology of Mycobacteria. Academic Press, London, UK, 95-184.

Molnár E, Donoghue HD, Lee OY-C, Wu HHT, Besra GS, Minnikin DE, Bull ID, Llewellyn G, Williams CM, Spekker O, Pálfi Gy (2015) Morphological and biomolecular evidence for tuberculosis in 8th century AD skeletons from Bélmegyer-Csömöki domb, Hungary. Tuberculosis 95(Suppl. 1):S35-S41.

Niemann S, Kubica T, Bange FC, Adjei O, Browne EN, Chinbuah MA, Diel R, Gyapong J, Horstmann RD, Joloba ML, Meyer CG, Mugerwa RD, Okwera A, Osei I, Owusu-Darbo E, Schwander SK, Rüsh-Gerdes S (2004) The species *Mycobacterium africanum* in the light of new molecular markers. J Clin Microbiol 42(9):3958-3962.

Ortner DJ (2003) Infectious diseases: tuberculosis and leprosy. In Ortner DJ, Ed., Identification of pathological conditions in human skeletal remains. Academic Press, San Diego, CA, USA, 227-271.

Paja L, Coqueugniot H, Dutour O, Willmon R, Farkas GyL, Palkó A, Pálfi Gy (2015) Knee ankyloses associated with tuberculosis from the Medieval Hungary – Differential diagnosis based on medical imaging techniques. Int J Osteoarchaeol 25(3):352-360.

Pálfi Gy, Bereczki Zs, Ortner DJ, Dutour O (2012) Juvenile cases of skeletal tuberculosis from the Terry Anatomical Collection (Smithsonian Institution, Washington, D.C., USA). Acta Biol Szeged 56(1):1-12.

Pálfi Gy, Dutour O, Perrin P, Sola C, Zink A (2015) Tuberculosis in evolution. Tuberculosis 95(Suppl. 1):S1-S3.

Pálfi Gy, Marcsik A (1999) Palaeoepidemiological data of tuberculosis in Hungary. In Pálfi Gy, Dutour O, Deák J, Hutás I, Eds., Tuberculosis: Past and Present. TB Foundation: Szeged, Hungary & Golden Book Publisher: Budapest, Hungary, 531-540.

Pálfi Gy, Molnár E (2009) The paleopathology of specific infectious diseases from Southeastern Hungary: a brief overview. Acta Biol Szeged 53(2):111-116.

Pap I, Józsa L, Repa I, Bajzik G, Lakhani SR, Donoghue HD, Spigelman M. (1999) 18-19th century tuberculosis in naturally mummified individuals (Vác, Hungary). In Pálfi Gy, Dutour O, Deák J, Hutás I, Eds., Tuberculosis: Past and Present. TB Foundation: Szeged, Hungary & Golden Book Publisher: Budapest, Hungary, 419-428.

Pap I, Pálfi Gy, Molnár E, Karlinger K, Kovács KB, Korom Cs, Schultz M, Schmidt-Schultz TH, Spigelman M, Donoghue HD, Kustár Á, Szikossy I (2017) A tuberkulózis előfordulása egy XVIII. századi váci családban. Anthropol Közlem 58:37-47.

Piombino-Mascali D, Jankauskas R, Tamošiūnas A, Valančius R, Gill-Frerking H, Spigelman M, Panzer S (2015) Evidence of probable tuberculosis in Lithuanian mummies. HOMO 66(5):420-431.

Redman JE, Shaw MJ, Mallet AI, Santos AL, Roberts CA, Gernaey AM, Minnikin DE (2009) Mycocerosic acid biomarkers for the diagnosis of tuberculosis in the Coimbra skeletal collection. Tuberculosis 89(4):267-277.

Riojas MA, McGough KJ, Rider-Riojas C, Rastogi N, Hazbón MH (2018) Phylogenomic analysis of the species of the *Mycobacterium tuberculosis* complex demonstrates that *Mycobacterium africanum, Mycobacterium bovis, Mycobacterium caprae, Mycobacterium microti* and *Mycobacterium pinnipedii* are later heterotypic synonyms of *Mycobacterium tuberculosis*. Int J Syst Evol Microbiol 68(1):324-332.

Roberts C (2020) Fashionable but debilitating diseases: Tuberculosis past and present. In Sheridan SG, Gregoricka LA, Eds., Purposeful Pain: The Bioarchaeology of Intentional Suffering. Springer Nature Switzerland AG, Cham, Switzerland, 21-38.

Roberts CA, Lucy D, Manchester K (1994) Inflammatory lesions of ribs: an analysis of the Terry Collection. AJPA 95(2):169-182.

Rock RB, Olin M, Baker CA, Molitor TW, Peterson PK (2008) Central nervous system tuberculosis: pathogenesis and clinical aspects. Clin Microbiol Rev 21(2):243-261.

Rodriguez-Takeuchi SK, Renjifo ME, Medina FJ (2019) Extrapulmonary tuberculosis: pathophysiology and imaging findings. RadioGraphics 39(7):2023-2037.

Salo WL, Aufderheide AC, Buikstra J, Holcomb TA (1994) Identification of *Mycobacterium tuberculosis* DNA in a pre-Columbian Peruvian mummy. Proc Natl Acad Sci 91:2091-2094.

Santos AL, Roberts CA (2001) A picture of tuberculosis in young Portuguese people in the early 20th century: a multidisciplinary study of the skeletal and historical evidence. AJPA 115(1):38-49.

Santos AL, Roberts CA (2006) Anatomy of a serial killer: differential diagnosis of tuberculosis based on rib lesions of adult individuals from the Coimbra Identified Skeletal Collection, Portugal. AJPA 130(1):38-49.

Schultz M (1993) Spuren unspezifischer Entzündungen an prähistorischen und historischen Schädeln. Ein Beitrag zur Paläopathologie. Anthropologisches Forschungsinstitut, Aesch, Switzerland & Anthropologische Gesellschaft, Basel, Switzerland.

Schultz M (1999) The role of tuberculosis in infancy and childhood in prehistoric and historic populations. In Pálfi Gy, Dutour O, Deák J, Hutás I, Eds., Tuberculosis: Past and Present. TB Foundation: Szeged, Hungary & Golden Book Publisher: Budapest, Hungary, 503-507.

Schultz M (2001) Paleohistopathology of bone: a new approach to the study of ancient diseases. AJPA 116(Suppl. 33):106-147.

Schultz M (2003) Light microscopic analysis in skeletal paleopathology. In Ortner DJ, Ed., Identification of Pathological Conditions in Human Skeletal Remains. Academic Press, San Diego, CA, USA, 73-107.

Schultz M, Schmidt-Schultz TH (2015) Is it possible to diagnose TB in ancient bone using microscopy? Tuberculosis 95(Suppl. 1):S80-S86.

Spekker O (2018) Evaluation of endocranial bony changes in relation to tuberculosis in the Robert J. Terry Anatomical Skeletal Collection (Washington, DC, USA). PhD Thesis. University of Szeged, Szeged, Hungary.

Spekker O, Hunt DR, Paja L, Molnár E, Pálfi G, Schultz

M (2020a) Tracking down the white plague: The skeletal evidence of tuberculous meningitis in the Robert J. Terry Anatomical Skeletal Collection. PLOS ONE 15(3):e0230418.

Spekker O, Hunt DR, Váradi OA, Berthon W, Molnár E, Pálfi Gy (2018) Rare manifestations of spinal tuberculosis in the Robert J. Terry Anatomical Skeletal Collection (National Museum of Natural History, Smithsonian Institution, Washington, DC, USA). Int J Osteoarchaeol 28:343-353.

Spekker O, Pálfi Gy, Kozocsay G, Pósa A, Bereczki Zs, Molnár E (2012) New cases of probable skeletal tuberculosis from the Neolithic period of Hungary – A morphological study. Acta Biol Szeged 56(2):115-123.

Spekker O, Schultz M, Paja L, Váradi OA, Molnár E, Pálfi G, Hunt DR (2020b) Tracking down the White Plague. Chapter two: The role of endocranial abnormal blood vessel impressions and periosteal appositions in the paleopathological diagnosis of tuberculous meningitis. PLOS ONE 15(9):e0238444.

Spigelman M, Lemma E (1993) The use of the polymerase chain reaction (PCR) to detect *Mycobacterium tuberculosis* in ancient skeletons. Int J Osteoarchaeol 3(2):137-143.

Sreevatsan S, Pan X, Stockbauer KE, Conell ND, Kreiswirth BN, Whittam TS, Musser JM (1997) Restricted structural gene polymorphism in the *Mycobacterium tuberculosis* complex indicates evolutionarily recent global dissemination. PNAS 94(18):9869-9874.

Stucki D, Brites D, Jeljeli L, Coscolla M, Liu Q, Trauner A, Fenner L, Rutaihwa L, Borrell S, Luo T, Gao Q, Kato-Maeda M, Ballif M, Egger M, Macedo R, Mardassi H, Moreno M, Vilanove GV, Fyfe J, Globan M, Thomas J, Jamieson F, Guthrie JL, Asante-Poku A, Yeboah-Manu D, Wampande E, Ssengooba W, Joloba M, Boom WH, Basu I, Bower J, Saraiva M, Vaconcellos SEG, Suffys P, Koch A, Wilkinson R, Gail-Bekker L, Malla B, Ley SD, Beck H-P, de Jong BC, Toit K, Sancher-Padilla E, Bonnet M, Gil-Brusola A, Frank M, Beng VNP, Eisenack K, Alani E, Ndung'u PW, Revathi G, Gehre F, Akter S, Ntoumi F, Stewart-Ischerwood L, Ntinginya NE, Rachow A, Hoelscher M, Cirillo DM, Skenders G, Hoffner S, Bakonyte D, Stakenas P, Diel R, Crudu V, Moldovan O, Al-Hajoj S, Otero L, Barletta D, Carter EJ, Diero L, Supply P, Comas I, Niemann S, Gagneux S (2016) *Mycobacterium tuberculosis* lineage 4 comprises globally distributed and geographically restricted sublineages. Nat Genet 48(12):1535-1543.

Szikossy I (2020) Sebészeti beavatkozások nyomai a XVIII. századi váci múmiákon. PhD Thesis. University of Szeged, Szeged, Hungary.

Szikossy I, Bernert Zs, Pap I (1997) Anthropological investigation of the 18th-19th century ossuary of the Dominican Church, Vác, Hungary. Acta Biol Szeged 42:145-150.

Szikossy I, Pálfi Gy, Molnár E, Karlinger K, Balázs K, Kovács KB, Korom Cs, Schultz M, Tyede HS-S, Spigelman M, Donoghue HD, Kustár Á, Pap I (2015) Two positive tuberculosis cases in the late Nigrovits family, 18th century, Vác, Hungary. Tuberculosis 95(Suppl. 1):S69-72.

Váradi OA, Rakk D, Spekker O, Terhes G, Urbán E, Berthon W, Pap I, Szikossy I, Maixner F, Zink A, Vágvölgyi Cs, Donoghue HD, Minnikin DE, Szekeres A, Pálfi Gy (2021) Verification of tuberculosis infection among Vác mummies (18th century CE, Hungary) based on lipid biomarker profiling with a new HPLC-HESI-MS approach. Tuberculosis 126:102037.

Vidal R, Miravitlles M, Caylà JA, Torella M, de Gracia J, Morell F (1997) Increased risk of tuberculosis transmission in families with microepidemics. Eur Respir J 10:1327-1331.

Vuorinen HS (1999) The tuberculosis epidemic in Finland from the 18th to the 20th century. In Pálfi Gy, Dutour O, Deák J, Hutás I, Eds., Tuberculosis: Past and Present. TB Foundation: Szeged, Hungary & Golden Book Publisher: Budapest, Hungary, 105-112.

Wang PD, Lin RS (2000) Tuberculosis transmission in the family. J Infect 41:249-251.

Watanabe M, Aoyagi Y, Ridell M, Minnikin DE (2001) Separation and characterization of individual mycolic acids in representative mycobacteria. Microbiology 147:1825-1837.

World Health Organization. (2020) TB disease burden. In Global Tuberculosis Report 2020. WHO, Geneva, Italy, 23-70.

Zink AR, Sola C, Reischl U, Grabner W, Rastogi N, Wolf H, Nerlich AG (2003) Characterization of *Mycobacterium tuberculosis* complex DNAs from Egyptian mummies by spoligotyping. J Clin Microbiol 41(1):359-367.

Acta Biologica Szegediensis

Volume 64(2):111-119, 2020
Acta Biologica Szegediensis
http://abs.bibl.u-szeged.hu/index.php/abs

DOI:10.14232/abs.2020.2.111-119

ARTICLE

Revealing of biodiversity and antimicrobial effects of *Artemisia asiatica* endophytes

Aruna Vigneshwari[1], Saruul Erdenebileg[1], Kata Fujkin[1], Dezső Csupor[3], Judit Hohmann[3], Tamás Papp[1,2], Csaba Vágvölgyi[1], András Szekeres[1]*

[1]Department of Microbiology, Faculty of Science and Informatics, University of Szeged, Szeged, Hungary
[2]MTA-SZTE Fungal Pathogenicity Mechanisms Research Group, Hungarian Academy of Sciences - University of Szeged, Szeged, Hungary
[3]Department of Pharmacognosy, Faculty of Pharmacy, University of Szeged, Szeged, Hungary

ABSTRACT Endophytic fungi produce a plethora of secondary metabolites, which may open new avenues to study their applicability in pharmaceuticals. Therefore, the present study focuses on the fungal endophytic community of *Artemisia asiatica*. During our work, fungal endophytes were isolated from a medicinal plant, *A. asiatica*. The culturable endophytic fungi were identified using molecular techniques and biodiversity, richness and tissue specificity were examined. As these microorganisms have been generally identified as an abundant reservoir of novel antimicrobial compounds, the antimicrobial (i.e. antibacterial and antifungal) activities of the metabolites produced by the isolated fungi were studied. Numerous extracts containing the endophytic metabolites proved to be active against the applied test microorganisms including Gram-positive and Gram-negative bacteria, as well as yeasts and filamentous fungi, which can be examined in detail in the future and, based on the the chemical nature of these active metabolites, allow to discover novel bioactive metabolites. **Acta Biol Szeged 64(2):111-119 (2020)**

KEY WORDS
antimicrobial effect
Artemissia asiatica
endophytic fungi
fungal biodiversity

ARTICLE INFORMATION
Submitted
26 November 2020.
Accepted
28 December 2020.
***Corresponding author**
E-mail: andras.j.szekeres@gmail.com

Introduction

Endophytic fungi can be defined as an ecological group of fungi colonizing the inner tissues of plants without any recognizable features of their presence (Wani et al. 2016). The plant's endophytic fungi spend their lifecycle colonizing inter- and/or intra-cellularly the healthy tissues of the host plants, without causing any apparent indication of disease.

For agriculture, pharmaceutical and food industry, plant-associated endophytic fungi have been observed as important and novel sources of natural bioactive products (Zhao et al. 2010; Yo and Ting 2017). Until now tens of thousands of natural products have been identified in the world, but still a vast number of unknown compounds are waiting for discovery and to be utilized for the benefits of mankind (Sarker 2012). The comprehensive review by Newman and Cragg (2016), provides detailed information about the natural compounds discovered between 1981-2014. Of the 1562 new chemical entities discovered in this period, 73% belongs to natural products and their derivatives and only 27% of the drugs were of synthetic origin. Furthermore, the increasing prevalence of new diseases results in the continuous need of exploiting natural products for drugs (Cragg and Newman 2013). Especially, the emergence of multidrug-resistant microbes increases the urge to find novel therapeutic leads (Talebi et al. 2019). Demain and Sanchez (2009) estimate that currently more than 1 million natural compounds have been isolated, from which 50-60% have plant and 5% have microbial origins. In recent decades, endophytes have been recognized as a source of several bioactive compounds and are studied as potential sources of novel natural products for the health sector and for drug discovery (Jalgaonwala et al. 2011; Lam 2007; Strobel and Daisy 2003; Shukla et al. 2014; Vigneshwari et al. 2019). However, it could provide an important alternative to overcome the increasing levels of drugs resistance to various pathogenic microorganisms, only a few plant species have been investigated for their endophytic diversity and their bioactive secondary metabolites until now (Shukla et al. 2014).

The medicinal plants are potential sources of fungal endophytes producing novel bioactive compounds (Kaul et al. 2012), plant hormones (Khan et al. 2017; Turbat et al. 2020), and plant associated therapeutic metabolites (Huang et al. 2007; Vigneshwari et al. 2019). The plant genus *Artemisia* consists of around 400 species and these are one of the most important sources of medicinal compounds (Koul et al. 2018). Among the *Artemisia* species, *A.*

annua is the best known due to its artemisinin content, which is an important antimalarial drug (Weathers et al. 2011). Liu et al. (2001) identified 14 fungal endophytes, which produced antagonistic compounds against four phytopathogens, in *A. annua*. Another study showed the bioactive potential of endophytic fungi isolated from *A. annua*, including *Aspergillus* sp. and *Cephalosporium* sp., which showed the highest antibacterial activity (Zhang et al. 2014).

A. asiatica Nakai is also the member of the *Artemisia* (mugwort) genus. This is a perennial plant and abundantly found in the northern temperate regions of Asia, Europe and North America. This species is widely known for its medicinal properties and their essential oil is commonly used in medicine and food products (Oh et al. 2005; Ryu et al. 1998; Ahuja et al. 2018). Characteristic secondary metabolites of *A. asiatica* include flavonoids, coumarins, terpenes, sesquiterpene lactones, monoterpenes, guaianolidem secoguianolide, lignans, phenylpropanoids and steroids (Hajdú et al. 2014). Despite the broad-spectrum bioactivity of *A. asiatica,* its endophytic fungal community and their bioactive compounds has not been investigated. Therefore, in our study, isolation and identification of endophytic fungi from *A. asiatica* were carried out and their biodiversity parameters were evaluated. Furthermore, antimicrobial activities of metabolites extracted using different organic solvents from both the ferment broth and the mycelia of the isolated endophytic fungi were also determined.

Materials and Methods

Collection of A. asiatica samples and isolation of the endophytes

The *A. asiatica* Nakai plants were provided by the Department of Pharmacognosy, University of Szeged (Szeged, Hungary). The samples were collected in 2016 and the plant specimens have been identified and authenticated by experts. Collected specimen was placed in a sealed plastic bag and was labelled with the number and date of collection and stored at 4 °C until processing.

Isolation of endophytic fungi from plant parts was done based on the method described by Gariyali (2013) with minor modifications. The plant materials were rinsed in running tap water to remove contaminations and the specimens were cut via a sterile blade into small segments of about 0.5 to 1 cm in length. The leaf and stem parts were separated, and these parts were examined for their fungal endophyte content. The plant segments were firstly surface sterilized by sequentially immersing the plant material in 70% (60 sec) ethanol, washing with sterile distilled water and then, steeping in 0.01% (30 sec) mercuric chloride (VWR International, Hungary). Finally, the specimens were washed again 2-3 times with sterile distilled water and then dried on a sterile blotting paper. After the surface sterilisation, each segment was placed onto the surface of PDA medium (VWR International, Hungary) supplemented with 50 μg/mL ampicillin (Merck, Hungary) in a Petri dish. Then, the plates were incubated at 25 °C and the growth of fungal colonies were checked daily for 5-10 days. Pure isolates were collected by picking up individual colonies from the plates and transferring them onto a fresh PDA medium, which were incubated at 25 °C for 10 days. Each fungal culture was checked again for purity and transferred separately to PDA slants. These colonies were maintained at 4 °C and were deposited into the Szeged Microbiological Collection (SZMC, Hungary; http://www.wfcc.info/ccinfo/collection/by_id/987).

Molecular identification of isolates

For DNA isolation, fungal isolates were grown in PDB (VWR International, Hungary) at 25 °C for 5 days. Isolation of the genomic DNA from the mycelia was performed using the E.Z.N.A. Fungal DNA Mini Kit (Omega Bio-tek, Norcross, USA) based on the manufacturer's instructions. The internal transcribed spacer (ITS) region of the rDNA was amplified using the primers ITS1 and ITS4 as described previously (White et al. 1990). Sequencing was performed commercially by BaseClear B.V. (Leiden, The Netherlands). Sequences were first analyzed by BLAST similarity search at the website of the National Center for Biotechnology Information (http://www.ncbi.nlm.nih.gov/BLAST) and the species were identified based on their identity values (>97%).

Screening of bioactive metabolite producing endophytic fungi

Secondary metabolite extraction

Endophytic isolates were cultivated in 50 mL PDB medium at 25 °C, 120 rpm for 7 days. At the end of the incubation period mycelia was filtered through a cotton wool. The ferment broths were extracted three times sequentially with 50-50 mL of hexane, ethyl acetate and chloroform, respectively, and the extracts containing same solvents were pooled. The mycelial samples were overnight dried in an oven until constant weight and 25 mL distilled water was added to each. Then, the mixtures were sonicated for 20 min after the addition of an aliquot of liquid nitrogen to maintain the chilled condition. After that, the extraction of the aqueous samples was done three times with the mixture of 25 mL of chloroform and methanol (4:1, V/V). Both the ferment broth and the mycelial extracts were evaporated by a rotary evaporator (IKA HB10 basic, VWR International, Hungary) in vacuum at 30 °C. The

resulted four dry samples per each isolate were stored at -20 °C and resuspended in 1 mL of HPLC grade methanol (VWR International, Hungary) prior to use.

Microdilution based antimicrobial assay

To test the antibacterial effects of the metabolites, 400 µL of the methanolic solution of all extracts were transferred into Eppendorf tubes and after the evaporation were dissolved in 1 mL 10% methanol. These solutions were tested against two Gram-negative bacteria, *E. coli* (SZMC 6271) and *P. aeruoginosa* (SZMC 23290), two Gram-positive bacteria, *S. aureus* (SZMC 14611) and *B. subtilis* (SZMC 0209) and two yeasts, *C. albicans* (SZMC 1533) and *C. krusei* (SZMC 1352) according to the M07-A10 CLSI guideline (Weinstein 2018), all of which were obtained from the SZMC, Szeged, Hungary. For the test, the suspensions of the microbes were prepared from overnight cultures, which were cultivated in Luria-Bertani broth (10 g tryptone, 5 g yeast extract and 5 g NaCl in 1 L distilled water) and yeast extract peptone dextrose broth (20 g peptone, 10 g yeast extract and 20 g glucose in1 L distilled water) for the bacteria and yeasts, respectively, at 37 °C. The concentrations of the suspensions were set to 4×10^5 cells/mL with sterile media and 100 µL of this suspension were transfered into the wells of 96-well plates. Then, 100 µL of the extract was added into each well, and the plates were then incubated for 24 h at 37 °C. The mixture of 100 µL of ferment broth and 100 µL of 10% methanol was used as the blank sample for background correction, while 100 µL of the microbial suspension supplemented with 100 µL of 10% methanol was applied as the negative control. The positive control contained ampicillin (100 µg/mL, Merck, Hungary) for bacteria and nystatin (10 µg/mL, Merck, Hungary) for yeasts. The inhibitory effects of the extracts were spectrophotometrically (SPECTROstar Nano, BMG LABTECH, Ordenberg, Germany) determined at 620 nm after incubation, and the inhibition rate was calculated as the percentage of the positive control after blank correction.

Agar diffusion test

To determine the potential antifungal activity of the fungal extracts against plant pathogenic fungi four holes with a diameter of 8 mm were bored into PDA plates, at the 2.5-cm distances around the centre of the plate. Then precultured (25 °C, 7 days) *Fusarium culmorum* (SZMC 11039) and *Rhizoctonia solani* (SZMC 21048) strains were placed in the centre of plates with agar plugs and 100 µL of the 10% methanolic extracts prepared for the microdilution assay were applied into the wells. As a solvent control, 10% methanol was used and a mycelial plug inoculated without any extracts was applied as a growing control. Antifungal activities of the samples were determined by the detection of the inhibition zone.

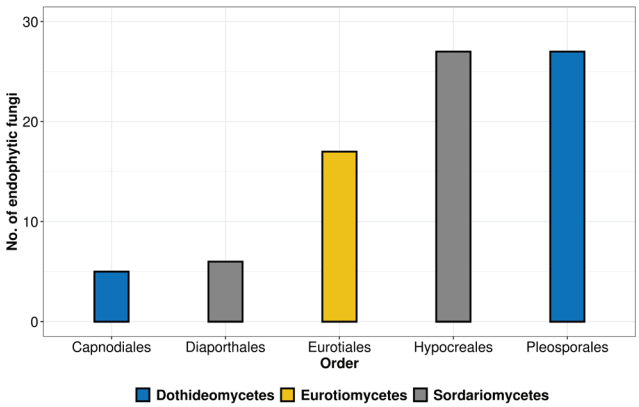

Figure 1. Distribution of endophytic fungi isolated from *A. asiatica* into classes and orders.

Biodiversity mapping of endophytic fungi of A. asiatica

Calculating isolation rate and diversity parameters

The isolation rate of the endophytic fungi was calculated as the total number of tissue segments infected by fungi divided by the total number of tissue segments incubated (Kumar and Hyde 2004).

The diversity of endophytic fungi were evaluated using the Shannon-Weiner Index (H′), Simpson's diversity index (1-D), evenness Index (J) and Margalef richness index (Hoffman et al. 2008; Suryanarayanand and Kumaresan 2000; Kusari et al. 2012). All the diversity indexes were calculated both plant wise and also tissue wise.

Statistical analysis

Statistical analyses for biodiversity calculations were carried out by R 3.5.2 (Team 2019). One-way analysis of variance (ANOVA) was carried out to test the effect of tissue type (stem and leaf) on the colonization rate and species richness of endophytic fungi. Post hoc Tukey's Honest Significant Difference tests were performed to observe the significant differences among the tissue types at $P < 0.05$ level.

Results

Investigation of endophytic fungi isolated from A. asiatica

In our study, 82 fungal endophytes were isolated from the *A. asiatica* plants collected from the southern Hungarian areas and the strains were identified using molecular taxonomical tools (Table 1). The endophytic fungi distributed into 3 classes and 5 orders, where the members

Table 1. Endophytic fungi isolated in this study.

Plant part	Species	Collection code	Genbank ID
Leaf	*Alternaria* sp.	SZMC 27067	MT879608
Leaf	*Alternaria* sp.	SZMC 27068	MT879609
Leaf	*Alternaria* sp.	SZMC 27069	MT879610
Leaf	*Alternaria* sp.	SZMC 27070	MT879611
Leaf	*Alternaria* sp.	SZMC 27071	MT879612
Leaf	*Alternaria* sp.	SZMC 27072	MT879613
Leaf	*Alternaria* sp.	SZMC 27073	MT879614
Leaf	*Alternaria* sp.	SZMC 27074	MT879615
Leaf	*Alternaria* sp.	SZMC 27075	MT879616
Stem	*Aspergillus* sp.	SZMC 27076	MT994591
Stem	*Aspergillus* sp.	SZMC 27077	MT994592
Leaf	*Aspergillus* sp.	SZMC 27078	MT994593
Stem	*Aspergillus* sp.	SZMC 27079	MT994594
Stem	*Aspergillus* sp.	SZMC 27080	MT994595
Stem	*Aspergillus* sp.	SZMC 27081	MT994596
Stem	*Aspergillus* sp.	SZMC 27082	MT994597
Stem	*Aspergillus* sp.	SZMC 27083	MT994598
Stem	*Clonostachys* sp.	SZMC 27084	MT883288
Stem	*Cladosporium* sp.	SZMC 27085	MT883289
Stem	*Cladosporium* sp.	SZMC 27086	MT883290
Stem	*Cladosporium* sp.	SZMC 27087	MT883291
Stem	*Cladosporium* sp.	SZMC 27088	MT883292
Stem	*Cladosporium* sp.	SZMC 27089	MT883293
Leaf	*Penicillium* sp.	SZMC 27090	MT994617
Stem	*Clonostachys* sp.	SZMC 27091	MT940229
Leaf	*Clonostachys* sp.	SZMC 27092	MT940230
Leaf	*Curvularia* sp.	SZMC 27093	MT994617
Leaf	*Curvularia* sp.	SZMC 27094	MT994617
Leaf	*Diaporthe* sp.	SZMC 27095	MT940231
Leaf	*Diaporthe* sp.	SZMC 27096	MT940232
Leaf	*Diaporthe* sp.	SZMC 27097	MT940233
Leaf	*Didymella* sp.	SZMC 27098	MT940234
Leaf	*Didymella* sp.	SZMC 27099	MT940235
Leaf	*Didymella* sp.	SZMC 27100	MT940236
Leaf	*Didymella* sp.	SZMC 27101	MT940237
Leaf	*Didymella* sp.	SZMC 27102	MT940238
Leaf	*Didymella* sp.	SZMC 27103	MT994617
Stem	*Alternaria* sp.	SZMC 27104	MT997192
Stem	*Alternaria* sp.	SZMC 27105	MT997193
Stem	*Fusarium* sp.	SZMC 27106	MT997194
Leaf	*Fusarium* sp.	SZMC 27108	MT997196
Leaf	*Fusarium* sp.	SZMC 27109	MT997197
Leaf	*Fusarium* sp.	SZMC 27110	MT997198
Stem	*Fusarium* sp.	SZMC 27111	MT881636
Stem	*Fusarium* sp.	SZMC 27112	MT881637
Leaf	*Fusarium* sp.	SZMC 27113	MT881638
Stem	*Fusarium* sp.	SZMC 27114	MT881639
Leaf	*Fusarium* sp.	SZMC 27115	MT997199
Leaf	*Penicillium* sp.	SZMC 27116	MT997200
Leaf	*Penicillium* sp.	SZMC 27117	MT997201

Table 1. Continued.

Plant part	Species	Collection code	Genbank ID
Leaf	*Penicillum* sp.	SZMC 27118	MT997202
Leaf	*Penicillum* sp.	SZMC 27119	MT994761
Leaf	*Penicillum* sp.	SZMC 27120	MT994762
Stem	*Penicillum* sp.	SZMC 27121	MT994763
Leaf	*Penicillum* sp.	SZMC 27122	MT994764
Leaf	*Penicillum* sp.	SZMC 27123	MT994765
Leaf	*Phomopsis* sp.	SZMC 27124	MT994766
Leaf	*Phoma* sp.	SZMC 27125	MT994650
Leaf	*Phoma* sp.	SZMC 27126	MT994651
Leaf	*Phomopsis* sp.	SZMC 27127	MT994652
Stem	*Phomopsis* sp.	SZMC 27128	MT994653
Leaf	*Microsphaeropsis* sp.	SZMC 27129	MT994654
Leaf	*Simplicillium* sp.	SZMC 27130	MT994655
Stem	*Stemphylium* sp.	SZMC 27131	MT994656
Stem	*Trichoderma* sp.	SZMC 27132	MT881591
Stem	*Trichoderma* sp.	SZMC 27133	MT881592
Stem	*Trichoderma* sp.	SZMC 27134	MT994657
Stem	*Trichoderma* sp.	SZMC 27135	MT881593
Stem	*Trichoderma* sp.	SZMC 27136	MT881594
Stem	*Trichoderma* sp.	SZMC 27137	MT881595
Stem	*Trichoderma* sp.	SZMC 27138	MT881596
Leaf	*Trichoderma* sp.	SZMC 27139	MT881597
Stem	*Trichoderma* sp.	SZMC 27140	MT881598
Stem	*Trichoderma* sp.	SZMC 27141	MT881599
Stem	*Trichoderma* sp.	SZMC 27142	MT881600
Stem	*Phoma* sp.	SZMC 27143	MT994658
Stem	*Phoma* sp.	SZMC 27144	MT994659
Stem	*Phoma* sp.	SZMC 27145	MT994660
Stem	*Microsphaeropsis* sp.	SZMC 27146	MT994661
Stem	*Fusarium* sp.	SZMC 27147	MT994662
Stem	*Fusarium* sp.	SZMC 27148	MT994661

of Sordariomycetes were the most abundant (Fig. 1).

The isolation rate was recorded as 0.66 for leaf and 0.63 for stem and isolated fungi belong to 15 different genera. To characterize the biodiversity of endophytic fungi in the *A. asiatica*, the Shannon diversity index (*H'*) Simpson's diversity index (1-*D*), and Margalef's richness (*D mg*) have been calculated. The Shannon-index revealed higher certainty of endophytic fungal species consistency in the stem compared to the leaf. Moreover, the Simpson's-index clearly showed that the stem harbored slightly diverse fungal endophytes compared to the leaf. Finally, based on Margalef's-index the stems have higher taxonomic richness than the leaf in *A. asiatica* (Table 2). Although the number of fungi in the leaves was higher than those in the stems, the notable difference was comparatively low (Fig. 2).

Strains belonging to *Alternaria, Clonostachys, Didymella*, *Fusarium, Microsphaeropsis* and *Penicillium, Phoma* genera were isolated both from stem and leaves. However, the members of *Curvularia, Simplicillium* and *Phomopsis* genera were found only in leaves, while *Aspergillus*, *Stemphylium.* and *Trichoderma* were isolated only from the stem (Fig. 2, Table 1). These genera could be even tissue specific in *A. asiatica*, but to clarify this statement larger sample set would be favorable. It should also be considered that the host specificity of endophytic fungi can change the prevalence of their taxa in a particular plant and the divergence in the endophytic fungal community might be harbored in specific host tissues due to the histological difference and nutritional availability (Arnold et al. 2007).

Antimicrobial effects of fungal extracts of A. asiatica endophytes

Altogether, 328 extracts were tested against four bacte-

Table 2. Biodiversity parameters of endophytic fungi isolated from *A. asiatica*.

Diversity index	Stem	Leaves	Total
Simpson's (1-D)	0.1	0.13	0.07
Shannon (H')	2.62	2.36	2.96
Pielou's evenness (J)	0.89	0.87	0.9
Margeref richness	4.72	3.82	5.86

ria, two yeasts and two filamentous fungi (Fig. 3, Fig. 4, Table 3). Our results revealed that altogether, 54 hexane, 78 ethyl acetate, and 73 chloroform extracts of the ferment broth and 78 mycelial extracts were active against at least one test strain. Remarkably high number of extracts (53) were active against *B. subtilis*, and 50% of the extracts were active against *S. aureus* (Fig. 2). However, lower percentage of extracts were active against Gram-negative bacteria including *E. coli* (31%) and *P. aeruginosa* (28%). The extracts of *Didymella* sp. SZMC 27102 strain exhibited high activity against all of the tested bacteria and yeasts, while the extracts of *Phoma* sp. SZMC 27125 and SZMC 27126 showed a remarkable activity against Gram-positive bacteria and the mycelial extract of these endophytic fungi showed high activity against Gram-negative bacteria. However, their extracts did not show any activity against yeasts and filamentous fungi (Table 3). Most of the *Fusarium* extracts exhibited remarkable antimicrobial activities against yeasts, but none of them were active against the two tested filamentous fungal strains. The ethyl acetate extracts of two *Aspergillus* isolates (SZMC 27077, SZMC 27078) showed a significant inhibitory activity (>90%) against *B. subtilis, S. aureus, P. aeruginosa* and *C. albicans*.

During the yeast inhibition testing, *C. krusei* was found to be more resistant against the extracts than *C. albicans* (Fig. 3). In total, extracts of 46 strains were found to be possessing more than 90% inhibition against at least one test pathogen (Fig. 3). Taxa wise, *Aspergillus*, *Alternaria*, *Fusarium* and *Didymella* were found to have metabolites with effective yeast inhibition activity. Moreover, chloroform and mycelial extracts of *Trichoderma* isolates were mainly active against *R. solani* and *F. culmorum* (Table 3).

Discussion

Despite the biotechnological potential of endophytic fungi, the basic ecology about their relationship with the host plants is poorly understood. Furthermore, given the high biodiversity of plants in Hungary, examining their fungal endophytes could lead to the discovery of novel metabolites. Therefore, in our study the fungal endophytic community of *A. asiatica* was examined. The culturable endophytic fungi were identified using molecular techniques and their biodiversity, richness and tissue specificity were described. As these microorganisms have been generally identified as an abundant reservoir of novel antimicrobial compounds, the antimicrobial (i.e., antibacterial and antifungal) activities of the metabolites produced by the isolated fungi were also studied.

The fungi isolated from *A. asiatica* were characterized into 3 classes and 5 orders. All of the isolated fungi belonged to the phylum Ascomycota, which includes three classes, Dothideomycetes, Sordariomycetes and Eurotiomycetes. Our findings revealed that the leaves and stem parts of the *A. asiatica* are excellent reservoirs for endophytic fungi, where the most abundant genera were *Fusarium, Trichoderma, Penicillium* and *Alternaria*. Although *Alternaria* and *Fusarium* species are considered as plant pathogens, they might be latent when they are inside the living tissues until the environmental conditions are favourable and certain strains of them might have evolved to endophytic lifestyle due to loss of virulence (Freeman and Rodrigues 1993). These species are gaining a lot of attention recently for their bioactive

Table 3. Table 3. List of the endophytic fungi extracts showing inhibitory activities against plant pathogenic fungi.

Strain code	*F. culmorum*				*R. solani*			
	HEX	CLF	EtOAc	C:M	HEX	CLF	EtOAc	C:M
SZMC 27132	-	-	-	-	-	+	-	++
SZMC 27133	-	-	-	-	-	-	-	+
SZMC 27134	-	-	-	-	-	+	-	+
SZMC 27135	-	-	-	-	-	-	-	+
SZMC 27136	-	-	+	-	-	-	-	+
SZMC 27137	-	-	-	+	-	-	-	++
SZMC 27138	-	-	-	+	-	-	-	-
SZMC 27141	-	-	-	-	-	+	-	+++

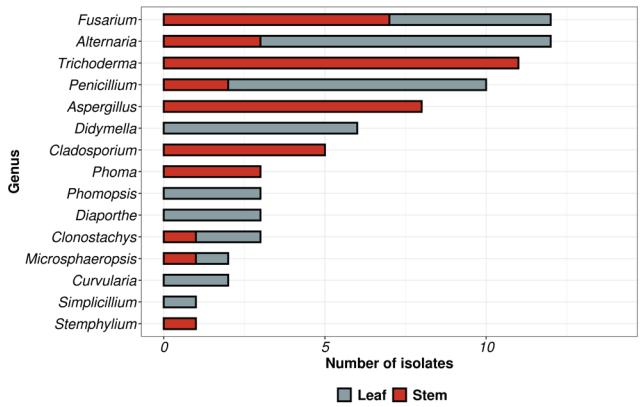

Figure 2. Distribution of endophytic fungi of *A. asiatica* at genus level.

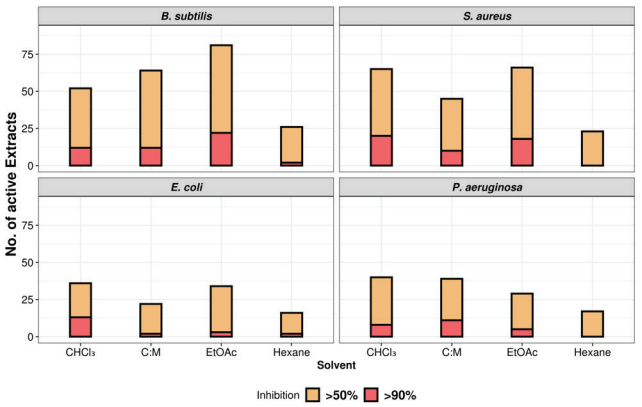

Figure 3. Summary of the antibacterial effects of endophytic extracts isolated from *A. asiatica*. C:M = chloroform:methanol (4:1 V/V) extract of mycelia.

compounds (Toghueo et al. 2019; Hellwig et al. 2002; Kaushik et al. 2020). Members of the *Trichoderma* genus were also found dominant in our study colonizing only the stems. In the literature, most of the studies reported the tissue specificity of *Trichoderma* species to roots and leaves (Rosemana et al. 2018). In addition, the colonization mechanism of *Trichoderma* sp. was also reported through systemic infection, which proved that the fungus could be re-isolated from stems rather than leaves and roots after the infection of roots (Rosemana et al. 2018).

In this work, five *Phoma* strains were isolated from stem and leaf. This genus is ubiquitous and inhabits a diverse range of hosts, from soil to air or from plants to animals (Aveskamp et al. 2010). Previously, extensive studies were carried out to clarify the significant generic boundaries in Didymellaceae, however, due to the lack of phylogenetic support of nearly 70 *Phoma* species belonging to Didymellaceae could not be assigned to definite genera (Aveskamp et al. 2010; Gruyter et al. 2013; Chen et al. 2017).

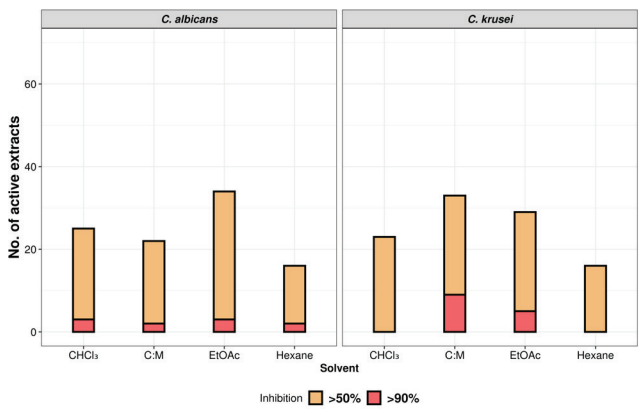

Fig. 4. Summary of the antifungal effects of endophytic extracts isolated from *A. asiatica*. C:M = chloroform:methanol (4:1 V/V) extract of mycelia.

In our cases, the isolation rate of the fungi were found to be the highest in stem, followed by leaf, whereas similar studies in other plants showed higher isolation rates in the leaf compared to stems (Alurappa and Chowdappa 2018). The tissue specificity are also affected by different environmental conditions. Previous studies showed that certain fungi, such as *Aspergillus* (El-Hawary et al. 2020) and *Penicillium* (Devi et al. 2012) species, did not exhibit tissue specificity. However, in our study, the *Aspergillus* strains were isolated only from stem.

Recently, an intensive research is required for effective antimicrobial drugs and the endophytic fungi are potential sources of these metabolites because they have been identified as an abundant reservoir of novel antimicrobial compounds (Strobel 2003). In the present work, 82 endophytic strains were isolated from the plant parts and the antimicrobial activity of their metabolites was evaluated. Altogether, 14.63% of the isolates had antibacterial effects with wide spectrum. Gram-positive bacteria were found to be more susceptible than Gram-negative bacteria and the observed antibacterial activity was higher than the antifungal activity. Altogether, 86.2% of the extracts were active against bacteria, whereas only 53% were active against yeasts and regarding Gram-positive bacteria, especially *B. subtilis* showed the highest sensitivity to the extracts. *Alternaria* and *Aspergillus* were the most predominant genera found to be exhibiting higher antibacterial activity than other fungi. Six out of 9 *Alternaria* strains had inhibitory activity against all the test organisms and at least one extract of all the *Aspergillus* isolates were active against all the test organisms. Furthermore, three and seven isolates showed inhibitory effects against the filamentous fungi *F. culmorum* and *R. solani*, respectively.

Acknowledgments

This work was supported by the Hungarian Government and the European Union within the frames of the Széchenyi 2020 Programme, through grant GINOP-2.3.2-15-2016-00012. The relating research group was also supported by the grant OTKA K-128659 from the Hungarian Scientific Research Fund providing infrastructure and research equipment.

References

Ahuja A, Yi Y-S, Kim M-Y, Cho JY (2018) Ethnopharmacological properties of *Artemisia asiatica*: A comprehensive review. J Ethnopharmacol 220:117-128.

Alurappa R, Chowdappa S (2018) Antimicrobial activity and phytochemical analysis of endophytic fungal extracts isolated from ethno-pharmaceutical plant *Rauwolfia tetraphylla* L. J Pure Appl Microbiol 12:317-332.

Aveskamp MM, de Gruyter J, Woudenberg JHC, Verkley GJM, Crous PW (2010) Highlights of the Didymellaceae: A polyphasic approach to characterise *Phoma* and related pleosporalean genera. Stud Mycol 65:1-60.

Chen Q, Hou LW, Duan WJ, Crous PW, Cai L (2017) Didymellaceae revisited. Stud Mycol 87:105-159.

Cragg GM, Newman DJ (2013) Natural products: a continuing source of novel drug leads. Biochim Biophys Acta 1830:3670-3695.

Demain AL, Sanchez S (2009) Microbial drug discovery: 80 years of progress. J Antibiot 62:5-16.

Devi NN, Prabakaran JJ, Wahab F (2012) Phytochemical analysis and enzyme analysis of endophytic fungi from *Centella asiatica*. Asian Pac J Trop Biomed 2:S1280-S1284.

El-Hawary SS, Moawad AS, Bahr HS, Abdelmohsen UR, Mohammed R (2020) Natural product diversity from the endophytic fungi of the genus *Aspergillus.* RSC Adv 10:22058-22079.

Freeman S, Rodriguez RJ (1993) Genetic conversion of a fungal plant pathogen to a nonpathogenic, endophytic mutualist. Science 260:75-78.

Garyali S, Kumar A, Reddy MS (2013) Taxol production by an endophytic fungus, *Fusarium redolens*, isolated from Himalayan yew. J Microbiol Biotechnol 23:1372-1380.

Gruyter J, Woudenberg JHC, Aveskamp MM, Verkley GJM, Groenewald JZ, Crous PW (2013) Redisposition of phoma-like anamorphs in Pleosporales. Stud Mycol 75:1-36.

Hajdú Z, Martins A, Orbán-Gyapai O, Forgo P, Jedlinszki N, Máthé I, Hohmann J (2014) Xanthine oxidase-inhibitory activity and antioxidant properties of the methanol extract and flavonoids of *Artemisia asiatica*. Rec Nat Prod 8:299-302.

Hellwig V, Grothe T, Mayer-Bartschmid A, Endermann R, Geschke F-U, Henkel T, Stadler M (2002) Altersetin, a new antibiotic from cultures of endophytic *Alternaria spp.* taxonomy, fermentation, isolation, structure elucidation and biological activities. J Antibiot 55:881-892.

Hoffman M, Gunatilaka M, Ong J, Shimabukuro M, Arnold AE (2008) Molecular analysis reveals a distinctive fungal endophyte community associated with foliage of montane oaks in Southeastern Arizona. J Arizona-Nevada Acad Sci 40:91-100.

Huang W-Y, Cai Y-Z, Xing J, Corke H, Sun M (2007) A potential antioxidant resource: Endophytic fungi from medicinal plants. Econ Bot 61:14.

Jalgaonwala RE, Mohite BV, Mahajan RT (2011) Natural products from plant associated endophytic fungi. J Microbiol Biotechnol Res 1:21-32.

Kaul S, Gupta S, Ahmed M, Dhar MK (2012) Endophytic fungi from medicinal plants: a treasure hunt for bioactive metabolites. Phytochem Rev 11:487-505.

Kaushik N, Díaz CE, Chhipa H, Julio LF, Andrés MF, González-Coloma A (2020) Chemical composition of an aphid antifeedant extract from an endophytic fungus, *Trichoderma sp*. EFI671. Microorganisms 8:420.

Khan AL, Gilani SA, Waqas M, Al-Hosni K, Al-Khiziri S, Kim YH, Ali L, Kang SM, Asaf S, Shahzad R, Hussain J, Lee IJ, Al-Harrasi A (2017) Endophytes from medicinal plants and their potential for producing indole acetic acid, improving seed germination and mitigating oxidative stress. J Zhejiang Univ Sci B 18:125-137.

Koul B, Taak P (2018) The *Artemisia* genus: A review on traditional uses, phytochemical constituents, pharmacological properties and germplasm conservation. J Glycomics Lipidomics 07:1-2.

Kumar S, Hyde K (2004) Biodiversity and tissue-recurrence of endophytic fungi in *Tripterygium wilfordii*. Fungal Divers 17:69-90.

Kusari S, Hertweck C, Spiteller M (2012) Chemical ecology of endophytic fungi: origins of secondary metabolites. Chem Biol 19:792-798.

Lam KS (2007) New aspects of natural products in drug discovery. Trends Microbiol 15:279-289.

Liu CH, Zou WX, Lu H, Tan RX (2001) Antifungal activity of *Artemisia annua* endophyte cultures against phytopathogenic fungi. J Biotechnol 88:277-282.

Newman DJ, Cragg GM (2016) Natural products as sources of new drugs from 1981 to 2014. J Nat Prod 79:629-661.

Oh TY (2005) Increased susceptibility of ethanol-treated gastric mucosa to naproxen and its inhibition by DA-9601, an *Artemisia asiatica* extract. World J Gastroenterol 11:7450-7456.

Rosmana A, Sjam S, Asman A, Jayanti NJ, Satriana S, Padang AT, Hakkar AA (2018) Systemic deployment of *Trichoderma asperellum* in theobroma cacao regulates co-occurring dominant fungal endophytes colonization. J Pure Appl

Microbiol 12:1071-1084.
Ryu BK, Ahn BO, Oh TY, Kim SH, Kim WB, Lee EB (1998) Studies on protective effect of DA-9601, *Artemisia asiatica* extract, on acetaminophen- and CCI4-induced liver damage in rats. Arch Pharm Res 21:508-513.
Sarker SD, Nahar L (2012) An introduction to natural products isolation. Methods Mol Biol 864:1-25.
Shukla S, Habbu P, Kulkarni VH, Jagadish K, Pandey A, Sutariya V (2014) Endophytic microbes: A novel source for biologically/pharmacologically active secondary metabolites. Asian J Pharmacol Toxicol 02:1-16.
Strobel G, Daisy B (2003) Bioprospecting for microbial endophytes and their natural products. Microbiol Mol Biol Rev 67:491-502.
Suryanarayanand TS, Kumaresan V (2000) Endophytic fungi of some halophytes from an estuarine mangrove forest. Mycol Res 104:1465-1467.
Talebi Bezmin Abadi A, Rizvanov AA, Haertlé T, Blatt NL (2019) World Health Organization report: Current crisis of antibiotic resistance. BioNanoSci 9:778-788.
Team RC (2019) R: A language and environment for statistical computing. R Foundation for Statistical Computing, Vienna, Austria. URL https://www.R-project.org/.
Toghueo RMK (2019) Bioprospecting endophytic fungi from *Fusarium* genus as sources of bioactive metabolites. Mycology 11:1-21.
Turbat A, Rakk D, Vigneshwari A, Kocsubé S, Thu H, Szepesi Á, Bakacsy L, D. Škrbić B, Jigjiddorj E-A, Vágvölgyi C, Szekeres A (2020) Characterization of the plant growth-promoting activities of endophytic fungi isolated from *Sophora flavescens*. Microorganisms 8:683.
Vigneshwari A, Rakk D, Németh A, Kocsubé S, Kiss N, Csupor D, Papp T, Škrbić B, Vágvölgyi C, Szekeres A (2019) Host metabolite producing endophytic fungi isolated from *Hypericum perforatum*. PLoS One 14:e0217060.
Wani K, Saboo S, Solanke P, Tidke P (2016) Production of novel secondary metabolites from endophytic fungi by using fermentation process. Indo Am J Pharm Res 6:4957-4961.
Weathers PJ, Arsenault PR, Covello PS, McMickle A, Teoh KH, Reed DW (2011) Artemisinin production in *Artemisia annua*: studies in planta and results of a novel delivery method for treating malaria and other neglected diseases. Phytochem Rev 10:173-183.
Weinstein MP (2018) Methods for dilution antimicrobial susceptibility tests for bacteria that grow aerobically, 11th ed. Clinical and Laboratory Standards Institute. Wayne, PA, USA.
White TJ, Bruns T, Lee S, Taylor J (1990) Amplification and direct sequencing of fungal ribosomal RNA genes for phylogenetics. In Innis MA, Gelfand DH, Shinsky JJ, White TJ, Eds., PCR Protocols: A Guide to Methods and Applications. Academic Press, San Diego, 315-322.
Yo HS, Ting ASY (2017) In vitro endophyte-host plant interaction study to hypothetically describe endophyte survival and antifungal activities in planta. Acta Biol Szeged 61(1):1-11.
Zhang H-W, Ying C, Tang Y-F (2014) Four ardeemin analogs from endophytic *Aspergillus fumigatus* SPS-02 and their reversal effects on multidrug-resistant tumor cells. Chem Biodivers 11:85-91.
Zhao J, Zhou L, Wang J, Shan T, Lingyun Z, Liu X, Gao L (2010) Endophytic fungi for producing bioactive compounds originally from their host plants. In Méndez-Vilas A, Ed., Current Research, Technology and Education Topics in Applied Microbiology and Microbial Biotechnology. Formatex Research Center, Spain, 567-576.

Acta Biologica Szegediensis

Volume 64(2):121-128, 2020
Acta Biologica Szegediensis
http://abs.bibl.u-szeged.hu/index.php/abs

DOI:10.14232/abs.2020.2.121-128

ARTICLE

Purification of surfactin compounds produced by a *Bacillus subtilis* strain

Attila Bartal, Henriett Hunkár, Gábor Endre, Mónika Vörös, Csaba Vágvölgyi, András Szekeres*

Department of Microbiology, Faculty of Science and Informatics, University of Szeged, Szeged, Hungary

ABSTRACT Surfactins are lipopeptide-type biosurfactants produced mainly by *Bacillus* species containing a peptide loop of seven amino acids and a hydrophobic fatty acid chain. These molecules exhibit various biological activities; therefore, their therapeutic and environmental applications are in the focus worldwide. In our work, a multi-step purification and separation process was developed to isolate surfactins from the ferment broth of *B. subtilis* SZMC 6179J strain. The process incorporates normal phase flash chromatography for pre-purifying the crude extract and two consecutive reverse phase HPLC separations for the isolation of the various surfactin molecules. The determination of the relative amounts of lipopeptides both in the crude extract and in each fraction of every separation step were carried out by HPLC-HESI-MS examinations. The ratio of surfactins in the crude extract was 21.35%, but after the preparative flash chromatographic separation the relative amount of surfactins was observed to be 30.44%. The preparative HPLC purification step resulted 85.39% purity of the surfactins. Nine different surfactin variants were isolated and identified from the fractions of this final semi-preparative HPLC purification, out of which three compounds were completely purified, and three others were detected in relative amounts of more than 95% in some fractions. **Acta Biol Szeged 64(2):121-128 (2020)**

KEY WORDS
Bacillus subtilis
HPLC
preparative purification
surfactin

ARTICLE INFORMATION
Submitted
20 October 2020.
Accepted
14 November 2020.
***Corresponding author**
E-mail: andras.j.szekeres@gmail.com

Introduction

Biosurfactants are natural products of various microorganisms such as bacteria, yeasts and fungi. They are constituted of peptides, saccharides or lipids or their combinations (Ward 2010). Biosurfactants have an amphiphilic nature due to possessing both hydrophilic and hydrophobic moieties, thus making these compounds able to lower the surface tensions of water/air, oil/air, or the oil/water interfaces (Santos et al. 2016). Most biosurfactants are either anionic or neutral, and few of them are cationic. The hydrophobic moieties of these molecules are made up of fatty acids, hydroxy fatty acids, or α-alkyl-β-hydroxy fatty acids possessing greater chain lengths. The hydrophilic parts can be carbohydrates, amino acids, cyclic peptides, phosphates, carboxylic acids, or different alcohols (Mulligan 2005). According to a recent study there are several causes for microorganisms to produce biosurfactants, mainly the necessity of changing the surface or interfacial properties of cells or the surrounding environment. These changes are mostly facilitating the formation and development of fruiting bodies and biofilms, the gliding movement or the swarming of cells. The amount of lipopeptides produced by the bacteria can be influenced by altering the culture conditions, for example with the application of different carbon sources and metal ions (Bartal et al. 2018) or the pH control of the ferment broth (Czinkóczky and Németh 2020). These compounds play an important role in controlling cell development, therefore they have various therapeutic activities including anti-microbial and anti-tumour effects (Mukherjee and Das 2010). Biosurfactants also possess important properties, such as low toxicity and specificity, moreover they are relatively easy to prepare. These bioactive compounds have attracted considerable interest during the past decade. Due to their characteristics, there were several attempts for their industrial applications, for example the bioremediation of organic chemicals, petroleum and petrochemicals, or their utilization as agrochemicals and fertilizers in agriculture. There are experiments for applications regarding food industry, cosmetics manufacturing, pharmaceuticals and detergents. Their attributes also propose the possibility for using biosurfactants as emulsifiers, demulsifiers, wetting agents, foaming agents and spreading agents (Volkering et al. 1997).

Lipopeptides are a wide group of microbial biosurfactants, consisting of a short linear or cyclic oligopeptide

linked to a fatty acid chain. They are produced by a high variety of microorganisms such as fungi, including *Aspergillus*, and several different bacteria, for example *Pseudomonas*, *Streptomyces*, and *Bacillus*. These compounds claimed the most attention due to the discovery of their antimicrobial, immunosuppressive, antitumor, and high surface activities (Cameotra and Makkar 2004; Gross and Loper 2009; Pirri et al. 2009; Raaijmakers et al. 2010). The proposed antimicrobial mechanism of lipopeptides is forming pores in the cellular membrane, resulting in an imbalance in ion flux leading to eventual cell death (Bender et al. 1999; Baltz 2009; Raaijmakers et al. 2010).

In 1968, Arima et al. isolated a substance in the form of needle-shaped white crystals from *Bacillus subtilis* and they named it "surfactin" due of its strong surface activity (Arima 1968). In addition to this property, surfactin was also proved to inhibit fibrin clot formation. Arima characterized surfactin as lipopeptide by its nature and its amino acids composition was also determined (Arima 1968). During 1969 several studies have been made to elucidate the full structure of surfactin (Kakinuma et al. 1969a, 1969b). The firstly described surfactin compound consists of a hydrophobic fatty acid "tail part" and a hydrophilic cyclic heptapeptide "head part" linked together by a lactone bridge (Bonmatin et al. 2003; Kakinuma et al. 1969b). Subsequent studies in the next decades revealed that surfactins have more variants having different fatty acid chain lengths and various changes in their amino acid sequences (Jenny et al. 1991; Lin et al. 1994; Yakimov et al. 1995; Kecskeméti et al. 2018). Surfactins have an acidic nature and can be dissolved in alkaline water and in polar organic solvents like methanol, ethanol, acetone, ethyl acetate, chloroform, methylene chloride and acetic acid, although it is insoluble in water, petroleum ester, hexane and other non-polar organic solvents. In its solid state, surfactin forms white, needle-shaped crystals, and it shows a powerful surface activity, exceeding that of sodium lauryl sulphate. Surfactin can lower the water's surface tension from 72 mN/m to 27 mN/m at very low concentrations (~0.005%). UV spectroscopic observations show that surfactin has no absorption in the range of 230 - 400 nm (Arima et al. 1968).

Recently there is a growing interest in studying surfactins, triggered by the increasing evidence for their potential as medical therapeutic agents, especially as antiviral, antimicrobial, anticancer, hemolytic, blood anticoagulant, and fibrinolytic agents (Al-Ajlani et al. 2007). Surfactin is produced mainly by the Gram-positive, endospore-forming bacteria *Bacillus subtilis* (Peypoux et al. 1999), as well as *B. pumilus*, *B. amyloliquefaciens*, *B. licheniformis*, and *B. mojavensis* (Alvarez et al. 2011; Chen et al. 2015).

In the past decades there has been a growing scientific and industrial attention towards using naturally produced biosurfactants instead of their chemically synthesized counterparts. The main reason behind this is the advantages of these natural compounds such as their low toxicity, easier biodegradability and possible specific activity amongst extreme conditions. While increasing number of the different surfactin variants reported, there is a lack of information regarding their exact structure and the possible differences in their biological activities. Therefore, the aim of our work was the purification of the different surfactin variants by various separation techniques for their further structural elucidation and to serve possibilities for the detailed examinations of their biological activities.

Materials and Methods

Culture conditions and sample preparation

The examined *Bacillus subtilis* strain SZMC 6179J was previously isolated from tomato rhizosphere and its antagonistic properties were characterized and reported by Vágvölgyi et al. (2013).

For the surfactin production, a liquid ferment broth was applied according to the method described by Besson et al. (1987). It contained 10 g/L glucose, 5 g/L glutamic acid, 1 g/L KH_2PO_4, 1 g/L K_2HPO_4, 1 g/L KCl, 500 mg/L $MgSO_4 \times 7\ H_2O$, 5 mg/L $FeSO_4 \times 7\ H_2O$, and 160 μg/L $CuSO_4 \times 5\ H_2O$. Bacteria were inoculated into 4 x 1 L medium in four 2-L Erlenmeyer flasks, then incubated on a rotary shaker at 120 rpm for 5 days at 25 °C. After this, the cells were removed from the ferment broth by centrifugation (4 °C, 8000 rpm, 15 min) using aliquots in 50 mL Falcon tubes. Peptides were precipitated from the supernatant acidified to pH 2 by the addition of hydrochloric acid (VWR Chemicals, Hungary). After an overnight incubation at 4 °C, the acidified ferment broth was centrifuged (4 °C, 8000 rpm, 15 min), the supernatant was discarded, and the collected pellet was resolved in 50 mL methanol. The remaining particulates were removed by centrifugation, and after the addition of 1 g silica gel the solvent methanol was evaporated by a rotational vacuum evaporator.

Separation methods

Flash chromatography

The crude extract from the *B. subtilis* strain SZMC 6179J containing the produced surfactin compounds was pre-purified for separation by a CombiFlash EZ Prep Streamline Flash and Preparative HPLC Chromatograph (Teledyne ISCO, USA). The sample evaporated on silica gel (Molar Chemicals, Hungary) was loaded into a RediSep 25 g cartridge (Teledyne ISCO, USA), while the silica gel used for

the purification was loaded into a Biotage 50g cartridge (Teledyne ISCO, USA). The applied elution program was isocratic using two solvents: 70% toluene (eluent A, Molar Chemicals, Hungary) and 30% methanol (eluent B, Molar Chemicals, Hungary) of five column volumes (500 mL). The flow rate was 40 mL/min and 20 mL fractions were collected into 30 mL test tubes leading to 25 fractions altogether and the length of the run was 12.5 min.

Preparative and semi-preparative HPLC methods

After the flash chromatographic run, a preparative HPLC purification was carried out to further cleanse the sample from contaminants for facilitating the actual isolation of the different surfactin variants by a semi-preparative HPLC separation. Both of them were performed by the aforementioned CombiFlash EZ Prep instrument (Teledyne ISCO, USA) in reverse phase and with the same solvents: eluent A was water and eluent B was a mixture of acetonitrile/methanol (1:1, V/V %, Molar Chemicals, Hungary), both solvents supplemented with 0.1% acetic acid (VWR International, Hungary).

The preparative step was achieved on a Phenomenex Gemini-NX (Phenomenex, USA) column (5μ, C18, 100 × 21.20 mm) using the following gradient elution time program: 30% of eluent B for 2 min followed by a sheer increase to 75% in 2 min. Then a slower, linear increase to 95% follows ending at 30 min, where this rate was held for 15 min, then decreased to the initial 30% in 2 min and remained constant until the pressure stabilized ending the run of 60 min in total. The flow rate was 10 mL/min, the injection volume was 5 mL and 20 mL fractions were collected into 30 mL test tubes, having 30 fractions in total.

The semi-preparative isolation was executed on a BioBasic-18 (Thermo Scientific, USA) column (5μ, C18, 250 × 10 mm) with an isocratic elution of 80% eluent B for 90 min. The flow rate was 5 mL/min, the injection volume was 1 mL and fractions collected every 5 mL into 13 mL test tubes, resulting in 90 fractions.

Analytical HPLC-MS methods

The purity of the crude extracts and the fractions of the flash chromatographic and preparative HPLC separations, as well as the identification and relative quantitative examination of the semi-preparative HPLC fractions were carried out by HPLC-HESI-MS measurements. The applied instrument was a Nexera XR HPLC (Shimadzu Corporation, Japan) coupled with a TSQ Quantum Access triple quadrupole mass spectrometer (Thermo Scientific, USA). Both the quantitative and qualitative acquisitions implemented the eluents of the preparative and semi-preparative HPLC isolations described above, and also the following reverse phase gradient elution time program was utilized in both cases: 5% eluent B for 2 min, increased to 80% in the following 2 min, then gradually raised to 95% at 24 min. This rate was held for 9 min, then dropped to 5% in 2 min, followed by a 5 min long equilibration stage, ending the run of 40 min in total. The flow rate was 0.2 mL/min and the column heater temperature was 30 °C. The applied column was a Gemini-NX (3μ, C18, 150 × 2 mm). The injection volume was 10 μL.

Both the purity checking, and the identifying measurements were carried out with heated electrospray ionization (HESI) ion source and in positive polarity. The spray voltage was +4000 V, the vaporizer temperature was 285 °C, the capillary temperature was 350 °C, the sheath gas pressure was 10 psi and the auxiliary gas pressure was 15 psi. The examinations of the purified fractions were achieved in full scan mode set between 900 – 1600 *m/z* values with the scan time of 1 sec/scan. The identification of the different surfactin variants were performed in single reaction monitoring (SRM) mode with a collision energy of 60 V. The *m/z* values of sodiated surfactin molecules were set as parent ion masses (*m/z* 1016.7, 1030.7, 1044.7, 1058.7, 1072.7, 1086.7, 1100.7, 1114.7) and for every parent ion, the first two internal fragment ions of every natural surfactin variant were set as a daughter ion (*m/z* 580.7, 594.7, 608.7, 622.7, 679.7, 693.7, 707.7, 721.7, 735.7) (Kecskeméti et al. 2018). Simultaneously with the SRM analyses, selected ion monitoring (SIM) mode was also used for the relative quantitative measurement of the detected isoforms and homologues, examining the parent ion *m/z* values listed above. With these two modes, 80 different scan events ran parallel, each for a scan time of 0.1 sec/scan.

Results

Analysis of crude surfactin extract

After the extraction of the lipopeptides from the ferment broth, the initial purity of the crude extract was measured by HPLC-HESI-MS examination in full MS mode (Fig. 1A). By calculating the integrated area of all peaks of the total ion chromatogram (TIC) of the sample and the extracted ion chromatogram (EIC) of all *m/z* values belonging to surfactins, which eluted from 20 min to 28 min, their ratio was observed in the crude extract to be 21.35%. As it can be seen, many contaminants appeared mostly at the lower retention time region, therefore the inclusion of a pre-purification step was recommended before loading our sample on a preparative HPLC column in large amounts. For that purpose, flash chromatographic separation was applied.

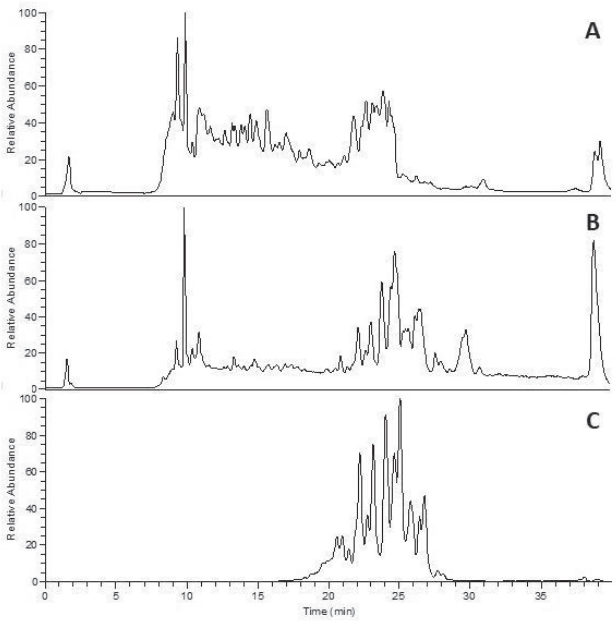

Figure 1. The total ion chromatogram of surfactins in the crude extract (A), in the 6th fraction of the flash chromatographic separation (B) and the 10th fraction of the preparative HPLC separation (C).

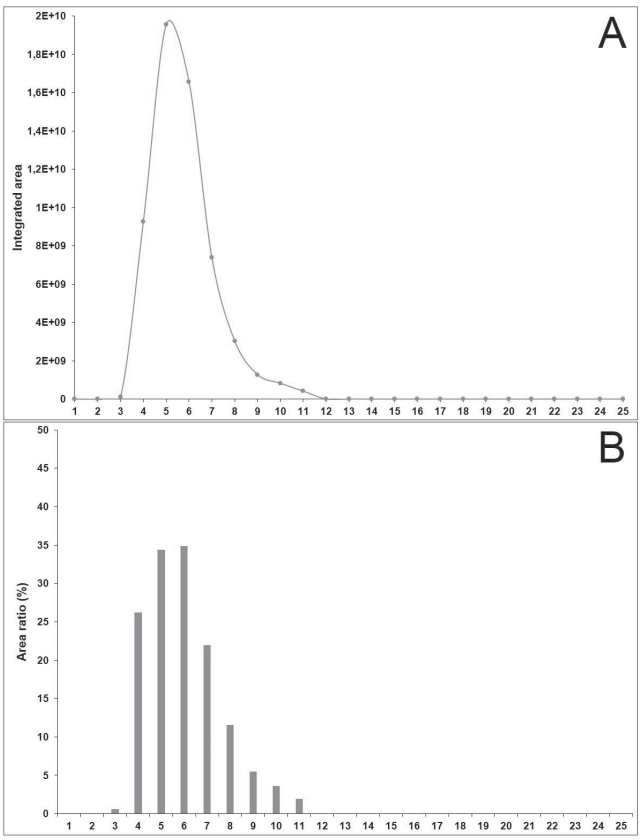

Figure 2. The intensities (A) and purities (B) of each fraction of the preparative flash chromatographic separation.

Flash chromatographic and preparative HPLC separation

Every fraction of the flash chromatographic separation was collected and their surfactin content and purity were measured by HPLC-HESI-MS technique in full MS mode. Although it could be observed that the relative amount of contaminants decreased considerably, the peak around the ten minute mark still exceeds the intensity of surfactins (Fig. 1B). Based on the calculation of the integrated peak areas of both the TICs and the EICs of all fractions the relative amount of surfactins and their purity were determined (Fig. 2). Based on these calculations, fractions 4 – 7 were pooled, while the rest were discarded. The ratio of surfactins in this pooled sample was 30.44%.

To further purify the sample from impurities, a preparative HPLC isolation was performed on the sample containing the combined fractions 4 - 7. Following the preparative HPLC separation, the resulting 30 fractions were collected and their relative surfactin content and its purity were measured also by HPLC-HESI-MS examinations. Comparing the chromatograms (Fig. 1), it can be outright seen that most of the contaminants were separated from surfactins, all the peaks possessing lower retention times disappeared, only some minor impurities can be observed among the peaks of surfactins, suggesting that these compounds bear similar affinity to the stationary phase, therefore eluted along with the lipopeptides to be isolated (Fig. 1C). After the evaluation of all fractions, the intensities and area ratios of surfactins were calculated (Fig. 3). For the most efficient isolation of the different surfactin variants, the combined fractions are recommended to be as pure as possible, while the sample should contain relatively high amount of surfactins. For these considerations, fractions 9 - 13 were merged and the rest of those that contain these lipopeptides were stored for subsequent purification. The final surfactin ratio of the pooled sample was 85.39%.

Semi-preparative HPLC separation

As a final step, a semi-preparative HPLC separation was carried out for the isolation of the different surfactin homologues and isoforms. The identification of the detected surfactin variants and their relative amounts were measured in all the fractions by HPLC-HESI-MS technique, in SRM and full MS modes, respectively (Fig. 4).

By the examination of the MS^2 spectra of all fractions of the semi-preparative HPLC separation, 9 molecules were identified altogether, with 4 different amino acid sequences ([Sur], [Val2], [Val7], [Val2,7]) and with 3 different fatty acid chain lengths (C13-C15). Out of the 9 variants, only C13-[Val2], C15-[Val7] and C15-[Sur] were

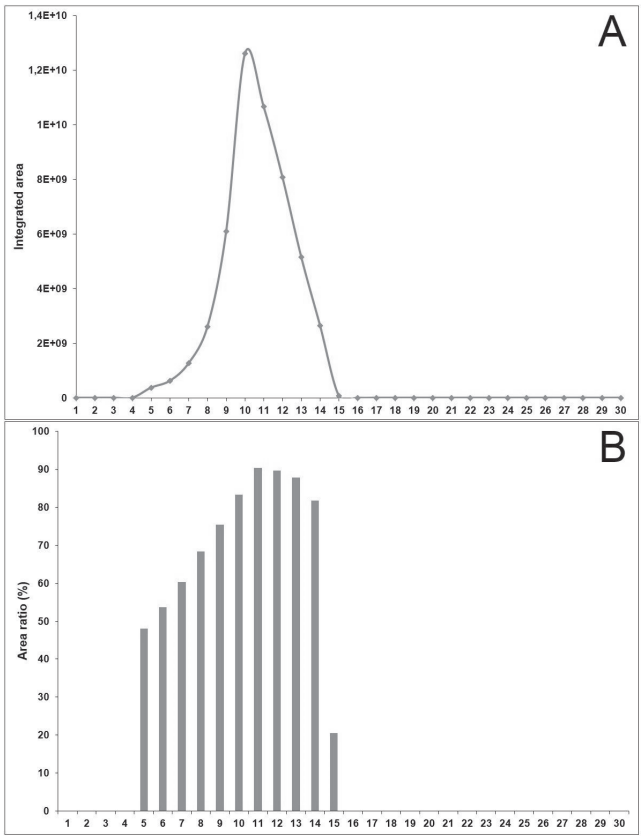

Figure 3. The intensities (A) and purities (B) of each fraction of the preparative HPLC separation.

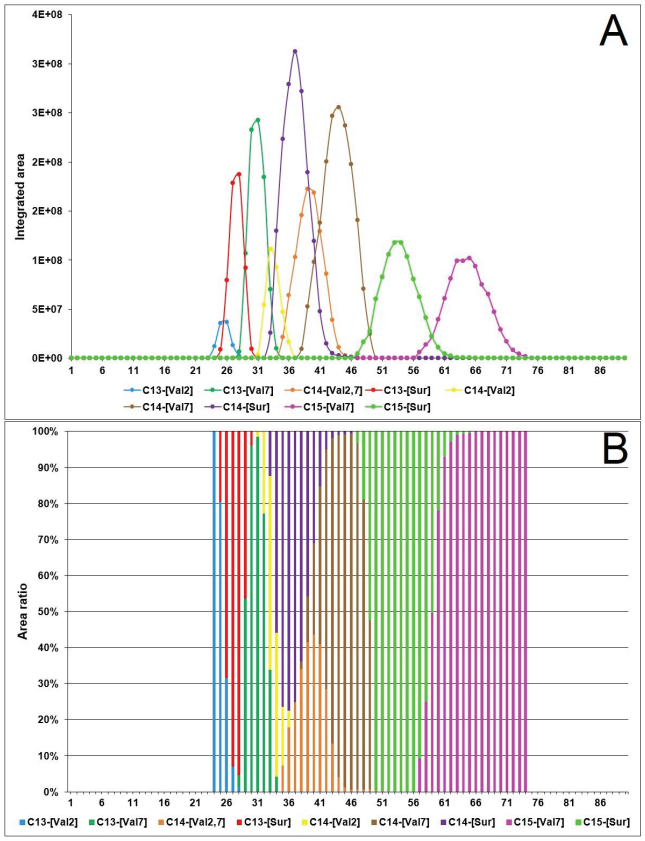

Figure 4. Fractogram of the identified surfactin variants (A) separated by semi-preparative HPLC technique and the ratios of surfactins in the fractions (B).

detected with more than 99% ratio in a fraction. In the cases of C15-[Val7], C14-[Val2,7], C13-[Sur], C14-[Val2], C14-[Val7] and [C14-Sur], their most pure fractions had ratios of 98.55%, 43.66%, 95.34%, 53.81%, 98.69% and 77.54%, respectively. The relative amounts of these molecules were also observed in comparison to the total integrated peak areas of every variant in every fraction (Fig. 5). Among the 9 molecules, C14-[Val7] and C14-[Sur] were found in the highest relative amounts, in 21.40% and 20.81%. They were followed by C14-[Val2,7], C15-[Val7], C15-[Sur] and C13-[Val7], with the area ratios of 12.13%, 11.10%, 11.05% and 10.93%, respectively. C13-[Sur] was observed in 7.12% of the total peak area, while C14-[Val2] had a ratio of 4.18% and C13-[Val2] had been found in the lowest relative amount, it only possesses 1,29% of the total surfactin amount detected in the fractions of the semi-preparative HPLC separation.

The efficiencies of the different separation steps

After each purification step the collected and merged fractions were evaporated and the weights of the dry matters were measured. The weights of surfactins and other impurities were calculated based on their respective peak area ratios of the HPLC-HESI-MS analyses, giving the efficiencies of the different separation techniques (Fig. 6).

In terms of peak area ratios, 21.35% of the total area belonged to surfactins in the crude extract. It was only

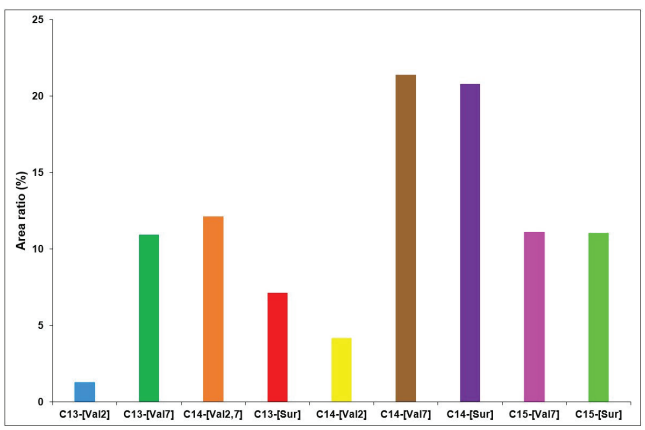

Figure 5. Ratios of the integrated peak areas of the different surfactin variants in fractions of the semi-preparative separation.

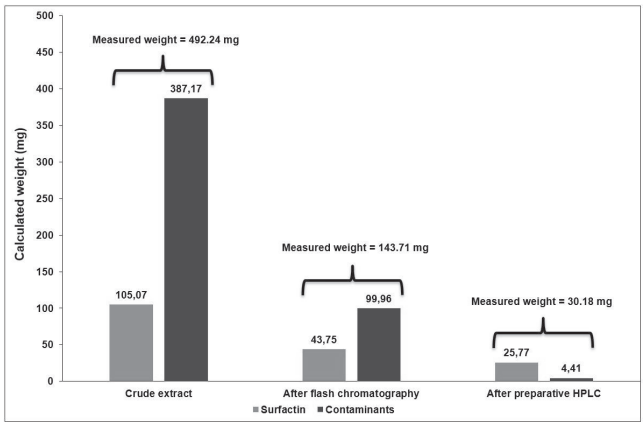

Figure 6. Measured weights of the dry matters after each separation step and the calculated weights of surfactins and the contaminants based on the peak area ratios of the HPLC-HESI-MS measurements.

increased to 30.44% after the flash chromatographic separation and the preparative HPLC purification technique raised the ratio of surfactins up to 85.39% altogether.

Based on these data and the measured weights of the dry matters, 74.18% of contaminants were removed by flash chromatography, and 95.59% of the remaining impurities were cleansed during preparative HPLC, leaving only 1.20% of the total amount of contaminants in the sample. On the other hand, the preparative flash chromatographic isolation removed 58.36% of surfactins as well, only to be further decreased by 41.10% by the preparative HPLC separation step. Thus, the calculated amount of surfactins remaining in the sample was only 24.53% that of the crude extract. This might be the explanation to the rather peculiar observation that only 9 different surfactin variants were detected in the fractions of the semi-preparative HPLC separation, although this strain is known to produce far more and in much higher variety of the different isoforms and homologues, which may have been lost during the purification process. Especially the loss of the molecules possessing longer fatty acid chains suggest that they were discarded among with the fractions collected later and having less area ratios than the ones being collected and merged.

In conclusion, the developed multi-step purification and separation of surfactins proved to be successful, more than 98% of the contaminants detected in the crude extract were removed and the C13-[Val2], C15-[Val7] and C15-[Sur] variants were completely isolated from the rest of the molecules, while three others were detected in more than 95% in some fractions. The efficiency of the separation however needs to be optimized, since around 75% of the calculated starting amount of surfactins were lost during the process, possibly including the homologues having more than 15 carbon atoms in their fatty acid chains. The flash chromatographic technique is especially in need of further development, subsequent repetitions of this step might be a suitable solution for decreasing the loss of surfactins and for increasing its purification potential.

Discussion

Surfactins have many potential applications, especially regarding therapeutic and environmental issues. The first example for the former was discovered by Arima et al. (1968); they observed that surfactin inhibits fibrin clot formation. Many other therapeutic activities were discovered later, e.g., antimycoplasmal, antibacterial and antiviral, anti-adhesive and anti-inflammatory effects (Vollenbroich et al. 1997; Kracht et al. 1999; Mulligan 2005; Heerklotz and Seelig 2006; Cho et al. 2006; Seydlová and Svobodová 2008). Furthermore, the use of surfactins as biosurfactans is an alternative to replace the chemically synthesized surfactant compounds. Biosurfactants are biodegradable and have lower toxicity (Kosaric 1992).

The length of the fatty acid chain and the amino acid sequence varies, resulting in numerous isoforms of the surfactins in previous works (Bonmatin et al. 2003). Although most of these variants were reported in the 1990s, our recent studies introduced novel surfactin molecules containing the following modifications: Val in the second amino acid position [Val2] (Bóka et al. 2016), aspartic acid 4-methyl ester at the fifth and Val in the seventh positions [AME5, Val7], leucine or isoleucine in the fourth and AME at the fifth positions [Lxx4, AME5] (Kecskeméti et al. 2018). Furthermore, it was also reported that the culture conditions of the producer strain could significantly influence the relative amounts of the individual members of surfactins produced allowing the selective production of certain groups of surfactins (Bartal et al. 2018).

However, the newly discovered surfactin variants were only characterized via spectrometric techniques and the confirmation of their exact structure will be important (for this the pure form of these compounds would be necessary in relatively large quantities). Furthermore, distinct surfactin variants could have different biological activities, as described by Aleti et al. (2016). They noted that two different surfactin variants with subtle structural differences had varying effects on bacterial biofilm formation on plant roots.

Therefore, in our work a multi-step purification and separation process was developed to isolate surfactins from the crude extract of the ferment broth of *B. subtilis* SZMC 6179J strain and to separate the different variants and homologues of this lipopeptide family. The method incorporates normal phase flash chromatography for

pre-purifying the crude extract and two consecutive reverse phase high performance liquid chromatographic techniques; one with a preparative column to further cleanse the sample from contaminants, which was followed by a semi-preparative RP-HPLC for the isolation of the various surfactin molecules. The measurement of the relative amounts of lipopeptides in the crude extract and in each fraction of every step was carried out by HPLC-HESI-MS examinations, as well as the identification of the different surfactin variants detected in the fractions of the semi-preparative HPLC separation.

The measured weight of the crude extract was 492.25 mg and the peak area ratio of surfactins in it was 21.35%. After the preparative flash chromatographic separation, fractions 4 - 7 were merged and kept for further purification. The weight of the dry matter found in these fractions was 143.71 mg and the relative amount of surfactins was observed to be 30.44%. Fractions 9 - 13 of the preparative HPLC purification step were collected together, their dry matter weighting 30.18 mg altogether, while the integrated peak area of surfactins were 85.39% that of the total area of peaks detected in this sample, meaning that more than 98% of impurities detected in the crude extract were removed by these separation steps, however, about 75% of surfactins were also lost during the process.

Examination of the fractions of the semi-preparative HPLC isolation technique showed that altogether 9 different surfactin variants were isolated and identified, out of which 3 compounds were completely purified, and other 3 were detected in relative amounts of more than 95% in some fractions.

These results suggest that the developed multi-step method is applicable for the purification of surfactin isoforms and homologues for subsequent structural characterization by spectroscopic techniques, however, further optimization is necessary to increase the efficiency of the whole process.

Acknowledgments

This work was supported by the grant OTKA K-128659 from the Hungarian Scientific Research Fund providing infrastructure and research equipment.

References

Aleti G, Lehner S, Bacher M, Compant S, Nikolic B, Plesko M, Schuhmacher R, Sessitsch A, Brader G (2016) Surfactin variants mediate species-specific biofilm formation and root colonization in *Bacillus*. Environ Microbiol 18:2634-2645.

Al-Ajlani MM, Sheikh MA, Ahmad Z, Hasnain S (2007) Production of surfactin from *Bacillus subtilis* MZ-7 grown on pharmamedia commercial medium. Microb Cell Fact 6:17.

Alvarez F, Castro M, Príncipe A, Borioli G, Fischer S, Mori G, Jofré E (2012) The plant-associated *Bacillus amyloliquefaciens* strains MEP2 18 and ARP2 3 capable of producing the cyclic lipopeptides iturin or surfactin and fengycin are effective in biocontrol of sclerotinia stem rot disease. J Appl Microbiol 112:159-174.

Arima K, Kakinuma A, Tamura G (1968) Surfactin, a crystalline peptidelipid surfactant produced by *Bacillus subtilis*: isolation, characterization and its inhibition of fibrin clot formation. Biochem Biophys Res Commun 31:488-494.

Bartal A, Vigneshwari A, Bóka B, Vörös M, Takács I, Kredics L, Manczinger L, Varga M, Vágvölgyi C, Szekeres A (2018) Effects of different cultivation parameters on the production of surfactin variants by a *Bacillus subtilis* strain. Molecules 23:2675.

Bender CL, Alarcón-Chaidez F, Gross DC (1999) *Pseudomonas syringae* phytotoxins: mode of action, regulation, and biosynthesis by peptide and polyketide synthetases. Microbiol Mol Biol Rev 63:266-292.

Besson F, Chevanet C, Michel G (1987) Influence of the culture medium on the production of iturin A by *Bacillus subtilis*. J Gen Microbiol 133:767-772.

Bóka B, Manczinger L, Kecskeméti A, Chandrasekaran M, Kadaikunnan S, Alharbi NS, Vágvölgyi C, Szekeres, A (2016) Ion trap mass spectrometry of surfactins produced by *Bacillus subtilis* SZMC 6179J reveals novel fragmentation features of cyclic lipopeptides. Rapid Commun Mass Spectrom 30:1581-1590.

Bonmatin JM, Laprévote O, Peypoux F (2003) Diversity among microbial cyclic lipopeptides: Iturins and surfactins. Activity-structure relationships to design new bioactive agents. Comb Chem High Throughput Screen 6:541-556.

Cameotra SS, Makkar RS (2004) Recent applications of biosurfactants as biological and immunological molecules. Curr Opin Microbiol 7:262-266.

Chen WC, Juang RS, Wei YH (2015) Applications of a lipopeptide biosurfactant, surfactin, produced by microorganisms. Biochem Eng J 103:158-169.

Cho JY, Kim, Dae S, Park HJ, Lim JH, Yun HI, Park SC, Kim SK, Rhee MH (2006) A comparison of the anti-inflammatory activity of surfactin A, B, C, and D from *Bacillus subtilis*. J Microbiol Biotechnol 16:1656-1659.

Czinkóczky R, Németh Á (2020) The effect of pH on biosurfactant production by *Bacillus subtilis* DSM10. Hung J Ind Chem 48:37-43.

Gross H, Loper JE (2009) Genomics of secondary metabolite production by *Pseudomonas* spp. Nat Prod Rep 26:1408-1446.

Heerklotz H, Seelig J (2007) Leakage and lysis of lipid membranes induced by the lipopeptide surfactin. Eur Biophys J 36:305-314.

Jenny K, Käppeli O, Fiechter A (1991) Biosurfactants from *Bacillus licheniformis*: structural analysis and characterization. Appl Microbiol Biotechnol 36:5-13.

Kakinuma A, Hori M, Isono M, Tamura G, Arima K (1969a) Determination of amino acid sequence in surfactin, a crystalline peptidelipid surfactant produced by *Bacillus subtilis*. Agric Biol Chem 33:971-972.

Kakinuma A, Sugino H, Isono M, Tamura G, Arima K (1969b) Determination of fatty acid in surfactin and elucidation of the total structure of surfactin. Agric Biol Chem 33:973-976.

Kecskeméti A, Bartal A, Bóka B, Kredics L, Manczinger L, Shine K, Alharby NS, Khaled JM, Varga M, Vágvölgyi C, Szekeres A (2018) High-frequency occurrence of surfactin monomethyl isoforms in the ferment broth of a *Bacillus subtilis* strain revealed by ion trap mass spectrometry. Molecules 23:2224.

Kosaric N (1992) Biosurfactants in industry. Pure Appl Chem 64:1731-1737.

Kracht M, Rokos H, Ozel M, Kowall M, Pauli G, Vater J (1999) Antiviral and hemolytic activities of surfactin isoforms and their methyl ester derivatives. J Antibiot (Tokyo) 52:613-619.

Lin SC, Carswell KS, Sharma MM, Georgiou G (1994) Continuous production of the lipopeptide biosurfactant of *Bacillus licheniformis* JF-2. Appl Microbiol Biotechnol 41:281-285.

Mukherjee AK, Das K (2010) Microbial surfactants and their potential applications: An overview. In Sen R, Ed., Biosurfactants. Advances in Experimental Medicine and Biology. Vol 672. Springer, New York, 54-64.

Mulligan CN (2005) Environmental applications for biosurfactants. Environ Poll 133:183-198.

Peypoux F, Bonmatin JM, Wallach J (1991) Recent trends in the biochemistry of surfactin. Appl Microbiol Biotechnol 51:553-563.

Pirri G, Giuliani A, Nicoletto SF, Pizzuto L, Rinaldi AC (2009) Lipopeptides as anti-infectives: a practical perspective. Cent Eur J Biol 4:258-273.

Raaijmakers JM, De Bruijn I, Nybroe O, Ongena M (2010) Natural functions of lipopeptides from *Bacillus* and *Pseudomonas*: more than surfactants and antibiotics. FEMS Microbiol Rev 34:1037-1062.

Santos DK, Rufino RD, Luna JM, Santos VA, Sarubbo LA (2016) Biosurfactants: Multifunctional biomolecules of the 21st century. Int J Mol Sci 17:401.

Seydlová G, Svobodová J (2008) Review of surfactin chemical properties and the potential biomedical applications. Cent Eur J Med 3:123-133.

Vágvölgyi C, Sajben-Nagy E, Bóka B, Vörös M, Berki A, Palágyi A, Krisch J, Skrbić B, Durišić-Mladenović N, Manczinger L (2012) Isolation and characterization of antagonistic *Bacillus* strains capable to degrade ethylenethiourea. Curr Microbiol 66:243-250.

Volkering F, Breure AM, Rulkens WH (1997) Microbiological aspects of surfactant use for biological soil remediation. Biodegradation 8:401-417.

Vollenbroich D, Pauli G, Ozel M, Vater J (1997) Antimycoplasma properties and application in cell culture of surfactin, a lipopeptide antibiotic from *Bacillus subtilis*. Appl Environ Microbiol 63:44-49.

Ward OP (2010) Microbial biosurfactants and biodegradation. Adv Exp Med Biol 672:65-74.

Yakimov MM, Timmis KN, Wray V, Fredrickson HL (1995) Characterization of a new lipopeptide surfactant produced by thermotolerant and halotolerant subsurface *Bacillus licheniformis* BAS50. Appl Environ Microbiol 61:1706-1713.

Acta Biologica Szegediensis

Volume 64(2):129-138, 2020
Acta Biologica Szegediensis
http://abs.bibl.u-szeged.hu/index.php/abs

DOI:10.14232/abs.2020.2.129-138

ARTICLE

Bioprospecting and biodiversity investigations of endophytic fungi isolated from *Juniperus communis*

Aruna Vigneshwari[1], Biljana D. Škrbić[2], László Kredics[1], Lubna Abbas[1], László Bakacsy[3], Csaba Vágvölgyi[1], András Szekeres[1]*

[1]Department of Microbiology, Faculty of Science and Informatics, University of Szeged, Szeged, Közép fasor 52., H-6726 Szeged, Hungary
[2]University of Novi Sad, Faculty of Technology Novi Sad, Bulevar cara Lazara 1, 21000 Novi Sad, Serbia
[3]Department of Plant Biology, Faculty of Science and Informatics, University of Szeged, Szeged, Közép fasor 52., H-6726 Szeged, Hungary

ABSTRACT Endophytes are a group of highly diverse microorganisms that reside within plant tissues without causing obvious symptoms on the host. In our study, *Juniperus communis* samples were collected from Hungary and used for the isolation of endophytic fungal strains. From 240 plant samples, 76 fungal isolates were recovered and subcultured for homogeneity. The isolates were identified using molecular taxonomical tools at the genus level and their biodiversity parameters were determined. The taxonomic diversity of the isolates was remarkably high, and the most abundant genera were *Fusarium*, *Alternaria* and *Trichoderma*. The secondary metabolites produced by the isolated endophytic fungi were extracted both from their mycelia and their ferment broth and their antimicrobial activities were tested against bacteria, yeasts, and filamentous fungi. In the antimicrobial tests, a total of 58 strains showed antimicrobial activity against at least one test organism. Altogether, 6.67% of the isolates have antibacterial effects with wide spectrum, and 10 strains showed remarkably high inhibitory percentage against yeast, while the extracts of 11 isolates proved to be active against filamentous fungi.
Acta Biol Szeged 64(2):129-138 (2020)

KEY WORDS
biodiversity
endophytic fungi
Juniperus communis
molecular identification

ARTICLE INFORMATION
Submitted
11 November 2020.
Accepted
16 December 2020.
***Corresponding author**
E-mail: andras.j.szekeres@gmail.com

Introduction

Throughout evolution, the dependence of human beings on nature has been everlasting. Natural products have among the important sources of medicine for millennia to alleviate and treat various diseases. However, despite the rise of combinatorial chemistry as an integral part of lead discovery process, natural products still play a major role in providing novel and interesting chemical scaffolds for drug discovery with an outstanding development in the areas of separation science (Liu et al. 2019). Although plants are considered as the biofactories of many valuable bioactive compounds, they possess the disadvantage of slow growth rate, while harvesting rare and endangered species also poses a risk (Jia et al. 2016). Therefore, it is necessary to find alternative approaches to produce medicinal plant-derived bioactive metabolites. In recent decades, endophytes have been recognized as sources of several bioactive compounds and are studied as potential sources of novel natural products for medical and commercial exploitation (Selvakumar and Panneerselvam 2018).

The term "endophyte" originally introduced by de Bary (1866) to distinguish fungi – living inside host tissues – from epiphytes, is derived from the Greek word "endon", meaning inside or within and "phyton", meaning plant. The meaning of the word has evolved to include any microorganism that inhabits plants during a period of its life cycle, especially within leaves, branches, and stems, without causing significant damage to its host (Wilson 1995). Endophytes possess a complex relationship with their hosts. They are symbiotic in nature, which may be mutualism, commensalism or saprophytism (Clay and Schardl 2002; Strobel and Daisy 2003). Endophytes can increase the competitive abilities and fitness of plants by increasing their nutrient uptake, resistance to drought and water stress, tolerance to heavy metal stress and high salinity, or their growth rate through biochemical pathways by producing plant growth hormones. For example, researchers proved that most of the endophytic fungi produce indole-3-acetic acid (Tan and Zou 2001; Turbat et al. 2020). It was also suggested that these endophytes initiate the biological degradation of the dead or dying host tissues (Tan and Zou 2001). Although almost all higher plants contain at least one endophytic micro-

organism, the relationship between microbes and their plant hosts remains one of the least studied biochemical systems, because it is difficult to find the exact physical relationship in the interaction. Given this fact, this long-held association might have created a specific genetic system in endophytes regarding their relationship with plants or vice versa (Strobel 2003).

Endophytic fungi are highly diverse, and more than 1 million species of this fungal group is estimated to be undiscovered (Sun and Guo 2012). They represent an important component of fungal biodiversity and it has also been observed that almost every plant examined to date harbors at least one species of endophytic fungi, while many plants, particularly woody plants, contain hundreds of endophytic species (Petrini 1986; Sahoo et al. 2017). However, various factors affect the distribution of the endophytic fungal community, such as environmental factors (temperature, humidity), and the type and age of the colonized host tissue (Sanchez-Azofeifa et al. 2012). Most of the studies reported that Dothideomycetes and Sordariomycetes are the dominant classes found in medicinal plants, but the diversity of the endophytic fungi also differs according to the geographical regions (Kharwar et al. 2008; Dhayanithy et al. 2019).

Endophytic fungi of medicinal plants are potential sources of novel bioactive compounds and some have also been proved to produce plant-associated therapeutic metabolites (Huang et al. 2007; Vigneshwari et al. 2019). The endophytic fungi such as *Acremonium*, *Alternaria, Aspergillus, Cephalosporium*, *Chaetomium, Chloridium, Choanephora, Colletotrichum, Fusarium, Gliocladium, Hypoxylon*, *Paecilomyces*, *Penicillium, Pestalotiopsis, Talaromyces*, and *Trichoderma* from different medicinal plants have been reported as sources of several bioactive compounds (Rana et al. 2019). A diverse array of endophytic metabolites exhibited antimicrobial activity against various pathogenic microbiota, and these can be used in pharmaceuticals, medicine, and agriculture (Gunatilaka et al. 2006; Yo et al. 2017; Sim et al. 2020).

The common juniper (*Juniperus communis L.*) is a bush or small evergreen tree which has been commonly referred to as herbal medicine in ancient times. It contains various chemical constituents including flavonoids, volatile oils, coumarins and therapeutically important anticancer lignans, podophyllotoxin and deoxypodophyllotoxin (Hartwell et al. 1953). Previous studies reported the isolation and characterization of endophytic fungi harboured in *Juniperus* plants sampled from the natural populations in Dortmund and Haltern (Germany), and Jammu and Kashmir (India). This resulted in the discovery of a deoxypodophyllotoxin-producing endophytic fungus harboured in *J. communis* (Kusari et al. 2009). The endophytic fungi isolated from *Juniperus* trees such as *Penicillium* and *Aspergillus* were also found to exhibit antimicrobial activities (Gherbawy and Elhariry 2016).

In our study, isolation and identification of endophytic fungi from *J. communis* were undertaken and their biodiversity parameters evaluated. Furthermore, the antimicrobial activities of metabolites extracted with different organic solvents from both the ferment broth and mycelia of isolated endophytic fungi were also determined.

Materials and Methods

Collection of J. communis samples

Fresh, healthy parts of the *J. communis* plants were collected during the late autumn of 2015, 2016 and 2017 (Table 1.). GPS coordinates of the sampling sites were recorded. All plant specimens have been identified and authenticated by experts. Collected specimens were placed into sealed plastic bags, labelled with the number and date of collection and stored at 4 °C until processing.

Isolation of endophytes

Isolation of endophytic fungi from plant parts was performed according to the method described by Garyali (2013) with minor modifications. The plant materials were rinsed in running tap water to remove dust and debris, and the specimens were cut into small segments of about 0.5 to 1 cm in length using a sterile blade. The leaf, twig, root, and cone parts were separated, and these parts were examined for their fungal endophyte content.

The plant segments were surface sterilized to kill the epiphytic microorganisms by sequentially immersing the plant material in 70% ethanol for 60 sec, washing with sterile distilled water and then steeping in 0.01% mercuric chloride (VWR International, Hungary) for 30 sec. Finally, the specimens were washed again with sterile distilled water 2-3 times and then allowed to dry on a sterile blotting paper. Each segment was placed onto the surface of PDA medium (VWR International, Hungary) supplemented with ampicillin (50 μg/mL, Merck, Hungary) in Petri dishes. They were incubated at 25 °C for 5-10 days and checked daily for the growth of fungal colonies. Pure isolates were obtained by picking individual colonies from the plates and transferring them onto fresh PDA medium where they were incubated at 25 °C for 10 days. Each fungal culture was checked again for purity, transferred separately to PDA slants, maintained at 4 °C and deposited in the Szeged Microbiological Collection (SZMC, Hungary; http://www.wfcc.info/ccinfo/collection/by_id/987).

Molecular identification of isolates

Genomic DNA was isolated from fungal mycelia grown in PDB medium (VWR International, Hungary) at 25 °C

for 7 days. Isolation and purification of genomic DNA was performed using the EZNA Fungal DNA Mini Kit (Omega Bio-tek, Norcross, USA) according to the manufacturer's instructions.

DNA fragments containing the ITS region of the ribosomal DNA gene cluster were amplified using the primers ITS1 and ITS4 (White et al. 1990). Polymerase chain reaction (PCR) was performed in a total volume of 25 μL consisting of 2.5 μL of PCR reaction buffer (10×Standard Reaction Buffer), 2 μL of 2mM dNTP, 0.5 μL of 10 μM ITS1 forward primer (5'-TCCGTAGGTGAACCTGCGG-3'), 0.5 μL of 10 μM ITS4 reverse primer (5'-TCCTCCGCTTATTGATATGC-3'), 2 μL of DNA template and 0.125 μL of *Pfu* DNA-polymerase (Fermentas). The PCR amplification profile consisted of an initial denaturation at 94 °C for 5 min, followed by 35 amplification cycles (30 sec at 94 °C, 40 sec at 48 °C, and 1 min 72 °C) and a final extension at 72 °C for 3 min. PCR products were separated using horizontal gel electrophoresis in 1% agarose gel supplemented with ethidium bromide at 0.1 μg/mL final concentration. Electrophoresis was performed for 30 min at 100 V. Separated DNA fragments were visualized using a UV transilluminator (UVP-BioDoc-It™ imaging Systems, Analytik Jena, Jena, Germany). 1000 bp marker (Fermentas) was used to determine the size of the products.

Amplified DNA fragments were sequenced (BaseClear, The Netherlands) and used for BLAST similarity search at the website of the National Center for Biotechnology Information (http://www.ncbi.nlm.nih.gov/BLAST). Genus level identification was carried out from the lowest expect value of the BLAST output.

Screening of bioactive metabolite-producing endophytic fungi

Secondary metabolite extraction

The isolated endophytic fungi were cultured for 7 days at 25 °C in 50 mL PDB medium. Then the mycelia were separated from the broth by filtration through a cheese cloth and dried overnight in an oven until constant weight. Then 25 mL distilled water was added to the dry material, which was then sonicated for 20 min after the addition of an aliquot of liquid nitrogen to maintain the chilled condition. After that the extraction of the aqueous samples was done with a 25 mL mixture of chloroform and methanol (4:1, V/V) and extraction was repeated 3 times. The ferment broths were extracted 3 times sequentially with 50-50 mL of hexane, ethyl acetate and chloroform, respectively, and both extract series were pooled. The organic solvents were removed by a rotary evaporator (IKA HB10 basic, VWR International, Hungary) in vacuum at 30 °C from each pooled extract including ethyl acetate, chloroform, as well as chloroform and methanol (4:1, V/V) fractions. The resulted 4 dry samples per each isolate were stored at -20 °C and resuspended in 1 mL of HPLC grade methanol (VWR International, Hungary) prior to use.

Activity assays against bacteria and yeast

For testing the antibacterial potential of the crude extracts, 400 μL of the methanolic extracts were transferred into new Eppendorf tubes and dissolved in 1 mL 10% methanol after evaporation. These extracts were tested against two Gram-negative (*Escherichia coli* SZMC 6271 and *Pseudomonas aeruoginosa* SZMC 23290), two Gram-positive bacteria (*Staphylococcus aureus* SZMC 14611 and *Bacillus subtilis* SZMC 0209) and two yeasts (*Candida albicans* SZMC 1533 and *C. krusei* SZMC 1352). For the assay, the suspensions of the microbes were prepared from overnight cultures, which were cultivated in Luria-Bertani broth (10 g tryptone, 5 g yeast extract and 5 g NaCl in 1 L distilled water) and yeast extract peptone dextrose broth (20 g peptone, 10 g yeast extract and 20 g glucose in 1 L distilled water) for the bacteria and yeasts, respectively, at 37 °C. Their concentrations were set to 4×10^5 cells/mL with sterile media. Then, 96-well plates were prepared by dispensing 100 μL suspension containing the bacterial or yeast cells, 100 μL of the extract dissolved in 10% of methanol was added into the wells, which were then incubated for 24 h at 37 °C. The mixture of 100 μL broth and 100 μL 10% methanol was used as the blank sample for background correction, while 100 μL of the microbial suspension supplemented with 100 μL 10% methanol was applied as the negative control. The positive control contained ampicillin (100 μg/mL, Merck, Hungary) for bacteria and nystatin (10 μg/mL, Merck, Hungary) for fungi. The inhibitory effects of each derivative were spectrophotometrically (SPECTROstar Nano, BMG Labtech, Ordenberg, Germany) determined at 620 nm after incubation, and the inhibition rate was calculated as the percentage of the positive control after blank correction.

Activity assay against filamentous fungi

To determine the potential antifungal activity of the fungal extracts against filamentous fungi, agar well diffusion assay was carried out. Evaporated samples of crude extracts (400 μL) were dissolved in 1 mL 10% methanol. Four holes with a diameter of 8 mm were bored into PDA plates, at the 2.5 cm distances around the centre of the plate. Then precultured (25 °C, 7 days) *Fusarium culmorum* SZMC 11039 and *Rhizoctonia solani* SZMC 21048 strains were placed in the centre of plates with agar plugs. After that, 100 μL of samples was applied into each hole. As solvent control, 10% methanol was used. Mycelial plug inoculated without any extracts was used as a control.

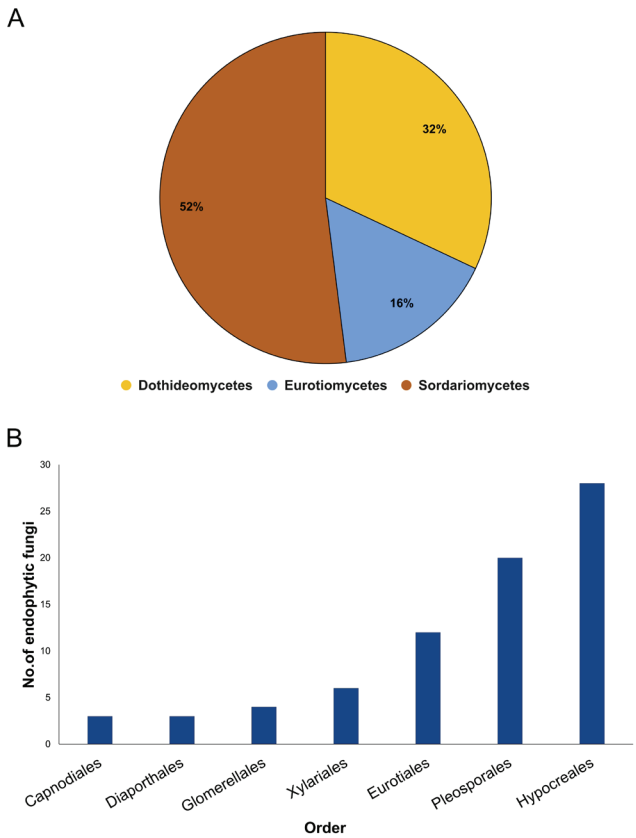

Figure 1. Distribution of endophytic fungi isolated from *J. communis* into classes (A) and orders (B).

Antifungal activity of the samples was determined by the size of the inhibition zone.

Biodiversity mapping of endophytic fungi of J. communis

Calculating isolation rate and diversity index

The isolation rate of endophytic fungi was calculated as the total number of tissue segments infected by fungi divided by the total number of tissue segments incubated (Kumar and Hyde, 2004).

The diversity of endophytic fungi isolated from 3 plants were evaluated using the, Shannon-Weiner Index (H′), Simpson's diversity index (1-D), evenness Index (J) and Margalef richness index (*D mg*) (Hoffman et al. 2008; Suryanarayanand and Kumaresan 2000; Kusari et al. 2012). All the diversity indices were calculated plantwise and also tissuewise to analyse the host and tissue specificity of endophytic fungi.

Statistical analysis

Statistical analyses for biodiversity calculations were carried out in R 3.5.2 (R core Team 2019). The diversity

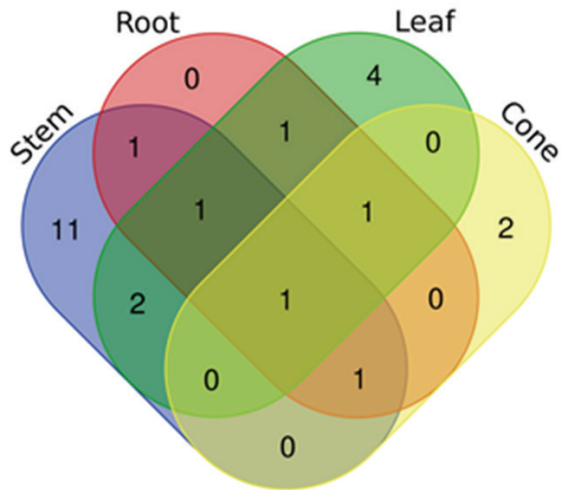

Figure 2. Venn diagram showing the common and unique fungi along the tissues of *J. communis*.

indices were calculated using the Vegan package from R 3.5.2 (Oksanen et al. 2018). One-way analysis of variance (ANOVA) was carried out to test the effect of plant species or tissue type (stem and root) on the isolation rate and genus richness of endophytic fungi. Post hoc Tukey's Honest Significant Difference tests were performed to observe the significant differences among the plant species or tissue types at $P < 0.05$ level.

Results

Investigation of endophytic fungi isolated from J. communis

The *J. communis* plant parts were collected from Southern Hungarian areas and their endophytes were isolated and purified, which was followed by sequence-based molecular identification (Table 1).

Altogether, 240 parts were tested involving 60 cuttings of leaf, stem, root and cone from 12 different plant samples of *J. communis*. A total of 75 endophytic fungi distributed into 3 main classes and 7 main orders were isolated from *J. communis* (Fig. 1). The isolation rates were 0.51, 0.3, 0.35 and 0.18 for stem, leaf, root and cone, respectively. The predominant class was found to be Sordariomycetes, similarly to previous studies on *Juniperus* endophytes (Kusari et al. 2009). Most of the isolates belonged to Hypocreales, while the rest of them were members of the taxa Pleosporales and Eurotiales (Table 1).

To characterize the biodiversity of *J. communis* EF, the Shannon diversity index (*H′*) Simpson's diversity index (1-*D*), and Margalef's richness (*D mg*) have been calculated. The Shannon-index revealed higher certainty of endo-

Table 1. Endophytic fungi isolated in this study.

Collection code	GPS coordinates	Plant part	Species	Genbank ID of ITS
SZMC 27149	N 46°53.338' / E 019°24.483'	Stem	*Alternaria* sp.	MT940776
SZMC 27150	N 46°53.340' / E 019°24.528'	Stem	*Alternaria* sp.	MT940777
SZMC 27151	N 46°53.340' / E 019°24.528'	Stem	*Alternaria* sp.	MT940778
SZMC 27152	N 46°53.338' E 019°24.483'	Stem	*Alternaria* sp.	MT940779
SZMC 27153	N 46°53.345' E 019°24.501'	Stem	*Alternaria* sp.	MT940780
SZMC 27154	N 46°53.345' E 019°24.501'	Stem	*Alternaria* sp.	MT940781
SZMC 27155	N 46°53.345' E 019°24.501'	Leaf	*Alternaria* sp.	MT940782
SZMC 27156	N 46°53.345' E 019°24.501'	Stem	*Alternaria* sp.	MT940783
SZMC 27157	N 46°53.345' E 019°24.501'	Stem	*Alternaria* sp.	MT940784
SZMC 27158	N 46°53.338' E 019°24.483'	Leaf	*Alternaria* sp.	MT940785
SZMC 27159	N 46°53.345' E 019°24.501'	Stem	*Alternaria* sp.	MT940786
SZMC 27160	N 46°53.345' E 019°24.501'	Stem	*Alternaria* sp.	MT940787
SZMC 27161	N 46°53.345' E 019°24.501'	Stem	*Alternaria* sp.	MT940788
SZMC 27162	N 46°53.345' E 019°24.501'	Stem	*Alternaria* sp.	MT940789
SZMC 27163	N 46°53.338' E 019°24.483'	Stem	*Alternaria* sp.	MT940790
SZMC 27164	N 46°53.345' E 019°24.501'	Stem	*Aspergillus* sp.	MT993364
SZMC 27165	N 46°53.345' E 019°24.501'	Stem	*Aspergillus* sp.	MT993365
SZMC 27166	N 46°53.338' E 019°24.483'	Stem	*Aspergillus* sp.	MT993366
SZMC 27167	N 46°53.345' E 019°24.501'	Stem	*Aspergillus* sp.	MT993367
SZMC 27168	N 46°53.345' E 019°24.501'	Stem	*Aspergillus* sp.	MT993368
SZMC 27169	N 46°53.330' E 019°24.478'	Stem	*Cladosporium* sp.	MT993369
SZMC 27170	N 46°53.330' E 019°24.478'	Stem	*Cladosporium* sp.	MT993370
SZMC 27171	N 46°53.330' E 019°24.478'	Stem	*Cladosporium* sp.	MT993371
SZMC 27172	N 46°53.338' E 019°24.483'	Stem	*Cladosporium* sp.	MT993372
SZMC 27173	N 46°53.330' E 019°24.478'	Root	*Cladosporium* sp.	MT994503
SZMC 27174	N 46°53.330' E 019°24.478'	Stem	*Colletotrichum* sp.	MT994504
SZMC 27175	N 46°53.330' E 019°24.478'	Leaf	*Colletotrichum* sp.	MT994505
SZMC 27176	N 46°53.330' E 019°24.478'	Stem	*Colletotrichum* sp.	MT994506
SZMC 27177	N 46°53.342' E 019°24.474'	Stem	*Curvularia* sp.	MT994507
SZMC 27178	N 46°53.330' E 019°24.478'	Stem	*Curvularia* sp.	MT994508
SZMC 27179	N 46°53.330' E 019°24.478'	Stem	*Didymella* sp.	MT994509
SZMC 27180	N 46°53.338' E 019°24.483'	Stem	*Fusarium* sp.	MT994510
SZMC 27181	N 46°53.342' E 019°24.474'	Stem	*Fusarium* sp.	MT994511
SZMC 27182	N 46°53.340' E 019°24.528'	Stem	*Fusarium* sp.	MT994512
SZMC 27183	N 46°53.338' E 019°24.483'	Leaf	*Fusarium* sp.	MT994513
SZMC 27184	N 46°53.342' E 019°24.474'	Root	*Fusarium* sp.	MT982177
SZMC 27185	N 46°53.340' E 019°24.528'	Root	*Fusarium* sp.	MT982178
SZMC 27186	N 46°53.338' E 019°24.483'	Root	*Fusarium* sp.	MT982179
SZMC 27187	N 46°53.340' E 019°24.528'	Root	*Fusarium* sp.	MT982180
SZMC 27188	N 46°53.340' E 019°24.528'	Root	*Fusarium* sp.	MT982181
SZMC 27189	N 46°53.340' E 019°24.528'	Root	*Fusarium* sp.	MT982182
SZMC 27190	N 46°53.338' E 019°24.483'	Root	*Fusarium* sp.	MT982183
SZMC 27191	N 46°53.340' E 019°24.528'	Root	*Fusarium* sp.	MT982184
SZMC 27192	N 46°53.340' E 019°24.528'	Root	*Fusarium* sp.	MT982185
SZMC 27193	N 46°53.340' E 019°24.528'	Root	*Fusarium* sp.	MT982186
SZMC 27194	N 46°53.342' E 019°24.474'	Root	*Fusarium* sp.	MT982187
SZMC 27195	N 46°53.340' E 019°24.528'	Root	*Fusarium* sp.	MT982188
SZMC 27196	N 46°53.340' E 019°24.528'	Root	*Fusarium* sp.	MT982189
SZMC 27197	N 46°53.338' E 019°24.483'	Root	*Penicillum* sp.	MT982190
SZMC 27198	N 46°53.340' E 019°24.528'	Leaf	*Penicillum* sp.	MT982191

Table 1. Continued.

Collection code	GPS coordinates	Plant part	Species	Genbank ID of ITS
SZMC 27199	N 46°53.342' E 019°24.474'	Leaf	*Penicillium* sp.	MT982192
SZMC 27200	N 46°53.340' E 019°24.528'	Leaf	*Penicillium* sp.	MT982193
SZMC 27201	N 46°53.338' E 019°24.483'	Leaf	*Penicillium* sp.	MT982194
SZMC 27202	N 46°53.342' E 019°24.474'	Leaf	*Penicillum* sp.	MT982195
SZMC 27203	N 46°53.340' E 019°24.528'	Leaf	*Penicillum* sp.	MT982196
SZMC 27204	N 46°53.340' E 019°24.528'	Leaf	*Pestalotiopsis* sp.	MT982197
SZMC 27205	N 46°53.340' E 019°24.528'	Leaf	*Pestalotiopsis* sp.	MT982198
SZMC 27206	N 46°53.338' E 019°24.483'	Leaf	*Pestalotiopsis* sp.	MT982199
SZMC 27207	N 46°53.340' E 019°24.528'	Leaf	*Bipolaris* sp.	MT982200
SZMC 27208	N 46°53.340' E 019°24.528'	Leaf	*Bipolaris* sp.	MT982201
SZMC 27209	N 46°53.338' E 019°24.483'	Leaf	*Phomopsis* sp.	MT982202
SZMC 27210	N 46°53.340' E 019°24.528'	Leaf	*Trichoderma* sp.	MT997192
SZMC 27211	N 46°53.342' E 019°24.474'	Leaf	*Trichoderma* sp.	MT997193
SZMC 27212	N 46°53.342' E 019°24.474'	Cone	*Trichoderma* sp.	MT997194
SZMC 27213	N 46°53.342' E 019°24.474'	Cone	*Trichoderma* sp.	MT997195
SZMC 27214	N 46°53.342' E 019°24.474'	Cone	*Trichoderma* sp.	MT997196
SZMC 27215	N 46°53.342' E 019°24.474'	Cone	*Trichoderma* sp.	MT997197
SZMC 27216	N 46°53.338' E 019°24.483'	Cone	*Trichoderma* sp.	MT997198
SZMC 27217	N 46°53.342' E 019°24.474'	Cone	*Trichoderma* sp.	MT997199
SZMC 27218	N 46°53.342' E 019°24.474'	Cone	*Trichoderma* sp.	MT997200
SZMC 27219	N 46°53.340' E 019°24.528'	Cone	*Trichoderma* sp.	MT997201
SZMC 27220	N 46°53.340' E 019°24.528'	Cone	*Xylaria* sp.	MT997202
SZMC 27221	N 46°53.338' E 019°24.483'	Cone	*Xylaria* sp.	MT997203
SZMC 27222	N 46°53.338' E 019°24.483'	Cone	*Xylaria* sp.	MT997204
SZMC 27031	N 46°53.338' E 019°24.483'	Stem	*Purpureocillium* sp.	MT997205

phytic fungal genus consistency in the stem compared to that of the other parts of *J. communis.* Moreover, the Simpson's-index clearly showed that the stem harboured highly diverse fungal endophytes compared to those harboured by other plant parts. Finally, based on Margalef's-index the stems had high taxonomic richness, while the cone had the lowest compared to the other tissues of *J. communis* (Table 2.).

The stems of *J. communis* harboured 11 unique fungi, whereas 4 and 2 were found in leaf and cone samples (Fig. 2). Interestingly, the roots of *J. communi*s did not harbour any unique fungi. This shows that some genus seems to be tissue specific. *Xylaria* sp. were found only in the cone, while *Pestalotiopsis* and *Bipolaris* were found only in the leaf and stem respectively, whereas *Curvularia*, *Aspergillus*, *Didymella* and *Purpureocillium* sp. were specifically found in stems (Fig. 3). *Fusarium* strains were more abundant in roots than in other tissues.

Antimicrobial effects of fungal extracts of J. communis endophytes

Gram-positive bacteria were found to be more susceptible to the extracted endophytic metabolites than Gram-negative ones due to the higher number of highly active (>90%) extracts (Fig. 4). For *B. subtilis*, the highest number of highly active extracts was recorded in the case of the

Table 2. Biodiversity parameters of endophytic fungi isolated from *J. communis*.

Diversity index	Stem	Root	Leaf	Cone	Total
Simpson's Dominance (D)	0.912	0.775	0.788	0.666	0.92
Shannon (H')	2.582	1.630	1.950	1.214	2.85
Pielou's evenness (J)	0.931	0.910	0.847	0.48	0.89
Margeref richness	4.218	1.894	3.176	1.365	5.32

Table 3. List of the endophytic fungi extracts showing inhibitory activities to plant pathogenic fungi (HEX – hexane; CLF – chloroform; C:M - chloroform: methanol (4:1) extract of mycelia; EtOAc – Ethyl acetate).

Collection code	*F. culmorum*				*R. solani*			
	HEX	CLF	EtOAc	C:M	HEX	CLF	EtOAc	C:M
SZMC 27198	-	-	-	-	-	-	-	+
SZMC 27206	-	-	-	+	-	-	++	-
SZMC 27209	-	-	-	+	-	-	-	-
SZMC 27210	-	-	-	-	-	-	-	+
SZMC 27211	-	-	-	-	-	-	-	+
SZMC 27212	-	-	-	+	-	-	-	+++
SZMC 27213	-	-	-	-	-	-	-	+
SZMC 27214	-	-	-	-	-	-	+	-
SZMC 27215	-	-	-	-	-	-	+	++
SZMC 27216	-	-	-	-	-	-	-	+
SZMC 27218	-	-	-	-	-	-	-	+++

ethyl acetate extracts of ferment broth (55), while the lowest amount of effective extracts (19) was obtained from the hexane-based solvent partitions. The mycelial extracts proved to be the most effective against *E. coli* and *P. aeruginosa*, as the numbers of the active extracts were 25 and 27, respectively. In the case of *S. aureus,* the highest number of effective extracts was obtained for the ethyl acetate extracts (43), followed by chloroform-partitioned ferment broth samples (37). It is important to highlight that strain SZMC 27155 was highly active against all bacteria, but it was not active against the tested yeasts and plant pathogenic fungi. The ethyl acetate and chloroform extracts of strains SZMC 27164 and SZMC 27031 showed remarkable inhibitory effects to all tested bacteria and the mycelial extracts of these isolates were also active against plant pathogenic fungi and yeasts. The *Trichoderma* isolates of this plant showed activity at least against one test microbe. The extracts of strain SZMC 27205 showed significant inhibitory activity to both Gram-positive and

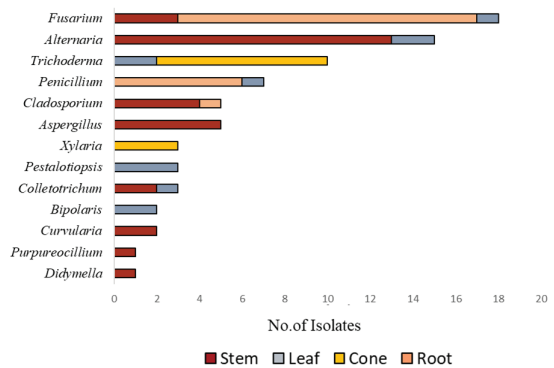

Figure 3. Distribution of endophytic fungi of *J. communis* at the genus level.

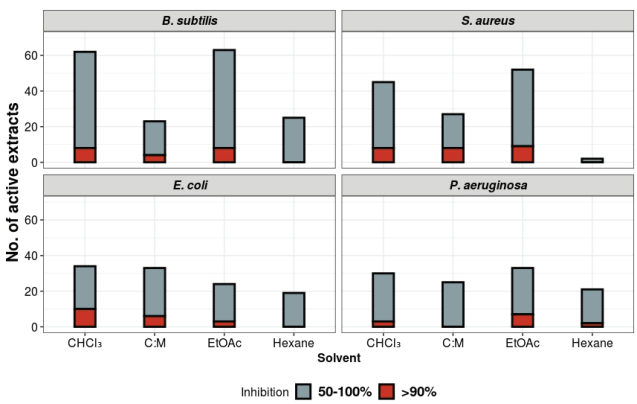

Figure 4. Summary of the antibacterial effects of endophytic extracts isolated from *J. communis* (C:M - chloroform:methanol (4:1, V/V) extract of mycelia).

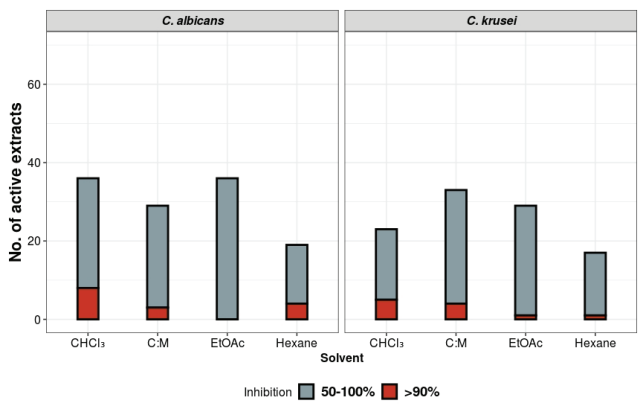

Fig. 5. Summary of the antifungal effects of endophytic extracts isolated from *J. communis* (C:M - chloroform:methanol (4:1, V/V) extract of mycelia).

Gram-negative bacteria. With respect to taxa, *Fusarium, Pestalotiopsis, Trichoderma, Aspergillus* and *Purpureocillium* strains showed high bioactivities and will be suitable for further investigations.

Altogether, 27 extracts showed inhibitory effects to yeasts, which is over 90% (Fig. 5). Interestingly, both the chloroform extract of the ferment broth and the mycelial extracts inhibited *C. albicans*, while *C. krusei* was mainly susceptible to the ethyl acetate extract of the ferment broth and to the mycelial extracts.

Previous works showed that the endophytic fungi of *J. communis* were excellent sources of antimicrobial compounds (Gherbawy and Elhariry 2016). In our study at least one solvent partition of 58 isolates was active against *B. subtilis, S. aureus* and *C. albicans*. However, only a few extracts, particularly the mycelial extracts were found to be active against the tested filamentous fungi (Table 3). Specifically, mycelial extracts of *Trichoderma* and *Purpureocillium* strains were active against both of the tested fungi. *F. culmorum* was found to be more resistant than *R. solani*.

Discussion

Endophytic fungi are highly diverse, and their investigation is very important from different plants to understand the biodiversity and structure of the endophytic fungal community, which mostly depends on the plant physiology, biogeographical factors and their interplay with other pathogenic microorganisms associated with their host plant (Arnold et al. 2007). Only a few studies have been carried out to study the endophytic fungal communities in Hungary (Knapp et al. 2012). Therefore, in the present work, 75 endophytic strains were isolated from *J. communis* from the Southern part of Hungary and the antimicrobial activities of their metabolites evaluated.

In our study, the culture-dependent method was followed for the molecular identification of fungal isolates. Based on ITS sequence analysis, the isolates were characterized into 7 orders of 3 classes. All the isolated fungi belonged to Ascomycota, which includes the classes Dothideomycetes, Sordariomycetes and Eurotiomycetes. Sordariomycetes was the dominant class (52%) followed by Dothideomycetes (32%) and Eurotiomycetes (16%). Such dominance of Sordariomycetes as endophytes has also been reported from several plants, e.g., *Phragmites* (Sim et al. 2018) and lichens (U'Ren et al. 2016) indicating that Sordariomycetes are ubiquitous among the plant kingdom. Totally, 14 genera (*Alternaria, Aspergillus, Bipolaris, Cladosporium, Colletotrichum, Curvularia, Didymella, Fusarium, Penicillium, Pestalotiopsis, Phomopsis, Purpureocillium, Trichoderma* and *Xylaria*) were identified (Table 1), where the relative abundances of *Fusarium, Alternaria* and *Trichoderma* were the highest (Fig. 3). The isolation rates of endophytic fungi were found to be the highest from stem followed by leaf, similarly to the results of previous studies on *J. communis* endophytes (Gherbawy and Elhariry 2016), whereas similar studies in other plants showed higher isolation rate values from the leaf compared to stems (Alurappa and Chowdappa 2018).

One of the most important properties of endophytic fungi is that they produce a wide variety of compounds that protect the plants from plant pathogens (Tan and Zou 2001; Strobel and Daisy 2003). In our cases, a total of 58 isolates (77%) showed antibacterial activity against at least one test microrganism. Altogether, 16% of the isolates had antibacterial effects with wide spectrum. Five strains showed remarkably high inhibitory values (>90%) to all the tested strains. Furthermore, regarding the antifungal activity, 43 and 31extracts were active against *C. albicans*, and *C. krusei*, respectively, while 3 and 11 showed inhibitory effects against *F. culmorum* and *R. solani*.

Future examinations could reveal the chemical nature of the active metabolites and their potential for practical (e.g., pharmaceutical, argricultural) applications.

Acknowledgments

This work was supported by the Hungarian Government and the European Union within the frames of the Széchenyi 2020 Programme (grant GINOP-2.3.2-15-2016-00012). The relating research group was also supported by the grant OTKA K-128659 from the National Research, Development and Innovation Office providing infrastructure and research equipment. B.D.S. and C.V. also acknowledge the contribution of the TÉT_16-1-2016-0148 (National Research, Development and Innovation Fund of Hungary) and HUSRB/1602/41/0031 (PLANTSVITA; Hungary-Serbia IPA CBC Programme) projects.

References

Alurappa R, Chowdappa S (2018) Antimicrobial activity and phytochemical analysis of endophytic fungal extracts isolated from ethno-pharmaceutical plant *Rauwolfia tetraphylla* L. J Pure Appl Microbiol 12:317-332.

Arnold AE, Engelbrecht MJB (2007) Fungal endophytes nearly double minimum leaf conductance in seedlings of a neotropical tree species. J Tropical Ecology 23(3):369-372._

Clay K, Schardl C (2002) Evolutionary origins and ecological consequences of endophyte symbiosis with grasses. Am Nat 160:S99-127.

de Bary, A (1866) Morphologie und Physiologie der Pilze, Flechten und Myxomyceten. W. Engelmann, Leipzig.

Dhayanithy G, Subban K, Chelliah J (2019) Diversity and biological activities of endophytic fungi associated with *Catharanthus roseus.* BMC Microbiol 19:22.

Garyali S, Kumar A, Reddy MS (2013) Taxol production by an endophytic fungus, *Fusarium redolens*, isolated from Himalayan yew. J Microbiol Biotechnol 23:1372-1380.

Gherbawy YA, Elhariry HM (2016) Endophytic fungi associated with high-altitude *Juniperus* trees and their antimicrobial activities. Plant Biosyst 150:131-140.

Gunatilaka AAL (2006) Natural products from plant-associated microorganisms: distribution, structural diversity, bioactivity, and implications of their occurrence. J Nat Prod 69:509-526.

Hartwell JL, Johnson JM, Fitzgerald DB, Belkin M (1953) Podophyllotoxin from *Juniperus* species; Savinin. J Am Chem Soc 75:235-236.

Hoffman M, Gunatilaka M, Ong J, Shimabukuro M, Arnold AE (2008). Molecular analysis reveals a distinctive fungal endophyte community associated with foliage of montane oaks in Southeastern Arizona. J Arizona-Nevada Acad Sci 40:91-100.

Huang W-Y, Cai Y-Z, Xing J, Corke H, Sun M (2007) A potential antioxidant resource: endophytic fungi from medicinal plants. Econ Bot 61:14.

Jia M, Chen L, Xin HL, Zheng CJ, Rahman K, Han T, Qin LP (2016) A friendly relationship between endophytic fungi and medicinal plants: A systematic review. Front Microbiol 7:906.

Kharwar RN, Verma VC, Strobel G, Ezra D (2008) The endophytic fungal complex of *Catharanthus roseus* (L.) G. Don. Curr Sci 95:228-233.

Knapp DG, Pintye A, Kovács GM (2012) The dark side is not fastidious – Dark septate endophytic fungi of native and invasive plants of semiarid sandy areas. PLoS One 7(2):e32570.

Kumar S, Hyde K (2004) Biodiversity and tissue-recurrence of endophytic fungi in *Tripterygium wilfordii.* Fungal Divers 17:69-90.

Kusari S, Hertweck C, Spiteller M (2012) Chemical ecology of endophytic fungi: origins of secondary metabolites. Chem Biol 19:792-798.

Kusari S, Lamshöft M, Spiteller M (2009) *Aspergillus fumigatus* Fresenius, an endophytic fungus from *Juniperus communis* L. Horstmann as a novel source of the anticancer pro-drug deoxypodophyllotoxin. J Appl Microbiol 107:1019-1030.

Liu M, Quinn RJ (2019) Fragment-based screening with natural products for novel anti-parasitic disease drug discovery. Expert Opin Drug Discov 14:1283-1295.

Oksanen J, Blanchet FG, Friendly M, Kindt R, Legendre P, Minchin P (2018) Vegan: Community Ecology Package. R Package Version. 2.4-6; 2018.

Petrini, O. (1986). Taxonomy of endophytic fungi of aerial plant tissues. In: Microbiology of the phyllosphere. In Fokkema NJ, van den Heuvel J, Eds., Cambridge University Press, Cambridge, UK, 175-187

Rana KL, Kour D, Kaur T, Devi R, Negi C, Yadav AN, Yadav N, Singh K, Saxena AN (2020) Endophytic fungi from medicinal plants: biodiversity and biotechnological applications. In Kumar A, Radhakrishnan EK, Eds., Microbial Endophytes, Woodhead Publishing, 273-305.

Sahoo S, Sarangi S, Kerry RG (2017) Bioprospecting of endophytes for agricultural and environmental sustainability. In Patra J, Vishnuprasad CN, Das G, Eds., Microbial Biotechnology, Singapore, Springer Singapore, 429-458.

Sanchez-Azofeifa A, Oki Y, Fernandes GW, Ball RA, Gamon J (2012) Relationships between endophyte diversity and leaf optical properties. Trees 26:291-299.

Selvakumar V, Panneerselvam A (2018) Bioactive compounds from endophytic fungi. In Gehlot P, Singh J. eds., Fungi and Their Role in Sustainable Development: Current Perspectives, Singapore, Springer Singapore, pp. 699–717.

Sim CSF, Cheow YL, Ng SL, Ting ASY (2018) Discovering metal-tolerant endophytic fungi from the phytoremediator plant *Phragmites*. Water Air Soil Pollut 229:68.

Sim CSF, Cheow YL, Ng SL, Ting ASY (2020) Can metal-tolerant endophytic biocontrol agents promote plant-growth under metal stress? Acta Biol Szeged 63(2):169-179.

Strobel G, Daisy B (2003) Bioprospecting for microbial endophytes and their natural products. Microbiol Mol Biol Rev 67:491-502.

Strobel GA (2003) Endophytes as sources of bioactive products. Microbes Infect 5:535–544.

Sun X, Guo LD (2012) Endophytic fungal diversity: Review of traditional and molecular techniques. Mycology 3:1-12.

Suryanarayanand TS, Kumaresan V (2000) Endophytic fungi of some halophytes from an estuarine mangrove forest. Mycol Res 104:1465-1467.

Tan RX, Zou WX (2001) Endophytes: A rich source of functional metabolites. Nat Prod Rep 18:448-459.

Team RC (2019) R: A language and environment for statistical computing. R Foundation for Statistical Computing, Vienna, Austria. https://www.R-project.org/.

Turbat A, Rakk D, Vigneshwari A, Kocsubé S, Thu H, Szepesi Á, Bakacsy L, Škrbić B, Jigjiddorj E-A, Vágvölgyi C, Szekeres A (2020) Characterization of the plant growth-promoting activities of endophytic fungi isolated from *Sophora flavescens*. Microorganisms 8:683.

U'Ren JM, Lutzoni F, Miadlikowska J, Arnold AE (2010) Community analysis reveals close affinities between endophytic and endolichenic fungi in mosses and lichens. Microb Ecol 60:340-353.

Vigneshwari A, Rakk D, Németh A, Kocsubé S, Kiss N, Csu-

por D, Papp T, Škrbić B, Vágvölgyi C, Szekeres A (2019) Host metabolite producing endophytic fungi isolated from *Hypericum perforatum*. PLoS One 14:e0217060.

White TJ, Bruns T, Lee S, Taylor J (1990) Amplification and direct sequencing of fungal ribosomal RNA genes for phylogenetics. In Innis MA, Gelfand DH, Shinsky JJ, White TJ, Eds., PCR protocols: A Guide to Methods and Applications. Academic Press, San Diego, 315-322.

Wilson D (1995) Endophyte - the evolution of a term, and clarification of its use and definition. Oikos 73:274-276.

Yo HS, Ting ASY (2017) In vitro endophyte-host plant interaction study to hypothetically describe endophyte survival and antifungal activities in planta. Acta Biol Szeged 61(1):1-11.

Acta Biologica Szegediensis

Volume 64(2):139-150, 2020
Acta Biologica Szegediensis
http://abs.bibl.u-szeged.hu/index.php/abs
DOI:10.14232/abs.2020.2.139-150

ARTICLE

Optimization of saccharification prospective from starch of sweet potato roots through acid-enzyme hydrolysis: structural, chemical and elemental profiling

Suman Jagatee[1], Sonali Priyadarshini[1], Chinmay Pradhan[1], Santi L. Sahoo[1], Rama C. Mohanty[1], Shidharth S. Ram[2,5], Mathummal Sudarshan[3], Tilahun A. Teka[4], Jyoti R. Rout[5]*

[1]Microbiology Laboratory, Post Graduate Department of Botany, Utkal University, Vani Vihar, Bhubaneswar-751004, Odisha, India.
[2]Institute of Physics, Bhubaneswar-751005, Odisha, India.
[3]UGC-DAE Consortium of Scientific Research, Kolkata Centre, Bidhan Nagar, Salt Lake, Kolkata-700098, India.
[4]Department of Postharvest Management, College of Agriculture and Veterinary Medicine, Jimma University, Jimma, Ethiopia.
[5]School of Biological Sciences, AIPH University, Bhubaneswar-752101, Odisha, India.

ABSTRACT The sweet potato root, a potent source of starch which is being considered as an efficient alternative for fuel ethanol production in recent times. The starchy substrate needs to be subsequently dextrinized and saccharified so as to enhance the utilization of its carbohydrates for ethanol production. In the present investigation, acid-enzyme process was conducted for the dextrinization and saccharification of sweet potato root flour (SPRF). The best optimized condition for dextrinization was achieved with an incubation period of 60 min, temperature 100 ºC and 1M HCl. However, for saccharification, the best result was obtained with an incubation of 18 h, pH 4, temperature 65 ºC and 1000 U concentration of Palkodex®. After the dextrinization process, maximum concentrations of total sugar and hydroxymethylfurfural (HMF) [380.44 ± 3.17 g/kg and 13.28 ± 0.25 mg/g, respectively] were released. Nevertheless, after saccharification, 658.80 ± 7.83 g/kg of total sugar was obtained which was about 73% more than that of dextrinization. After successful dextrinization and saccharification, the structural, chemical and elemental analysis were investigated using techniques such as scanning electron microscopy (SEM), Fourier-transforms infrared spectroscopy (FTIR) and energy-dispersive X-ray fluorescence spectrophotometer (EDXRF), respectively. Effective hydrolysis was demonstrated in thin layer chromatography (TLC) where the HCl was able to generate monomeric sugar such as glucose and maltose. On the other hand, only glucose is synthesized on the mutual effect of HCl and Palkodex®. The SEM findings indicate that the rough structure of both dextrinized and saccharified sample was gained due to the vigorous effect of both acid and enzyme subsequently. The saccharified SPRF when subjected to fermentation with *Saccharomyces cerevisiae* and *Zymomonas mobilis* separately, it was observed that *Z. mobilis* produced more stretching vibration of –OH than *S. cerevisiae*, which evidenced the better production of bioethanol. Additionally, evaluation of the influence of *S. cerevisiae* and *Z. mobilis* through elemental analysis revealed upsurge in the concentrations of S, Cl, Ca, Mn, Fe and Zn and decline in the concentrations of P, K and Cu in the fermented residue of *S. cerevisiae* and *Z. mobilis*, however, *Z. mobilis* showed little more variation than that of *S. cerevisiae.*

Acta Biol Szeged 64(2):139-150 (2020)

KEY WORDS
acid hydrolysis
dextrinization
EDXRF
FTIR
saccharification
SEM
sweet potato root flour (SPRF)

ARTICLE INFORMATION
Submitted
4 January 2021.
Accepted
27 January 2021.
***Corresponding author**
E-mail: E-mail: routjr@aiph.ac.in

Introduction

Petroleum is the key source of energy for the consumption of automobiles. Above and beyond the adverse global warming effect of fossil fuels, unpredictable oil price and political instability in the oil trading nations ensured a substantial rise in world-wide attention for alternate fuels. Both developed and industrialized countries consider biofuels such as ethanol and hydrogen as appropriate sources for the reason of energy security. Ethanol is one of the finest fluid alternatives of fossil fuel and has emerged as a promising energy substitute (Busic et al. 2018). Meanwhile, it is also reported that the plant biomass containing starch and sugar can be easily fermented to produce alcohol; however, the rate

of production depends upon feedstock availability (Limatainen et al. 2004; Abidin et al. 2014). Bioethanol is manufactured by fermenting sugar with microorganisms, in contrast to synthetically formed ethanol from petrochemical bases. It is produced by distilling the fermented sugars, which can be used as fuel in inner combustion engines, either neat or blended with petrol (Walker 2010). A study on bioethanol production in 2018 has revealed that the worldwide leaders in bioethanol production are USA with a production of about 16.06 billion gallons (primarily from maize and wheat) and Brazil, 7.92 billion gallons (from sugarcane), which accounts for approximately 84% of the total global ethanol (CSS 2019). Asia held the fourth position in the biosphere for ethanol production while China is the largest producer of ethanol in Asia, with an overall alcohol making of nearly 9.770 million liters in 2018 (Patni et al. 2011; USDA FAS 2018). Amongst all the Asian countries, India is having an optimistic viewpoint towards renewable energy technologies and is dedicated for the usage of renewable resources. In Asia, India is ranked as the second largest manufacturer of ethanol, with a yearly production of 2400 million liters in the year 2018 (USDA FAS 2019). In recent times, production of biofuel from tuber crops has been considered for experimental studies due to their high starch content. In India, as compared to yam and other tuber crops, cassava and sweet potato are being considered as the main tuber crops which are cultivated throughout all agro-climatic regions. However, no such exploitation is made for scale-up production of bioethanol by effective implication of sweet potatoes while they are rich in starch particles, the best source of carbohydrates for fermentable microorganisms (Lareo et al. 2013; Thatoi et al. 2014).

Currently, the degradation of carbohydrates from natural starch is a big challenge for the investigators as this process needs some tricky concepts for the development of simplified form of sugar that can be easily utilised by the microorganism. However, the high cost of the primary investment, involvement of enzymes, requirement of trained man-power and sophisticated laboratories are the limiting factors for the practice of process development (Surmely et al. 2004; Satapathy et al. 2020). The process of acid hydrolysis has several important advantages such as fast reaction rate, simple pre-treatment for starch feedstock, a cheap and easily available acid catalyst and a relatively low reaction temperature with high acid concentration. Inhibitor such as 5-HMF (5-hydroxymethylfurfural) is formed during the reaction of glucose dehydration but the optimization process in terms of temperature, concentration of acid, level of starch and duration of hydrolysis time may overcome this (Bharti and Chauhan 2016). The production of ethanol not only depends on the liquefaction process but also reliably manages as per the nature of the saccharified starch products. For this, a convenient way of enzyme implementation is to simplify the carbohydrates. However, the process of optimization of various starch molecules is a critical factor. The enzyme glucoamylase which is being used on industrial scale is very sensitive and effective for saccharification due to its efficiency of changing the functional properties, viscosity and gelatinization of starch (Cripwell et al. 2019; Strąk-Graczyk and Balcerek 2020). Afterward, ethanol is produced by fermentation of hydrolyzed sugar with the help of desired microorganisms like *Zymomonas mobilis, Saccharomyces cerevisiae, Saccharomyces uvarum, Candida tropicalis, Candida shehatae, Pichia stipites* and *Clostridium* species, etc. However, the yeast, *S. cerevisiae* as well as facultative bacterium, *Z. mobilis* are very promising contenders for the production of alcohol (Delgenes et al. 1996; Yang et al. 2016).

Sweet potato (*Ipomoea batatas* L.) which belongs to the family *Convolvulaceae* is ranked fifth as an essential food crop in developing countries on a fresh weight basis after wheat, rice, cassava and corn (Srinivas 2009). As a starch rich (18-30%) crop and due to its cheaper value and high biomass, it is widely accessed as a substitute of feedstock for grain and also acts as sugar substrate for fuel ethanol production (Qiu et al. 2010). The roots of this herbaceous perennial type of plant species are available throughout all the seasons and having some distinguished characteristics like high multiplication rate, low degeneration rate of the propagule, short life cycle, low illness and plague, and protect from erosive rains and drought stress (Lareo et al. 2013). Emphasizing on the food value of the sweet potato, the Center for Science in the Public Interest, USA ranked it as 'healthiest of all vegetables' due to presence of high value of dietary fiber, protein, vitamins A and C, complex carbohydrates, low levels of saturated fat, and essential elements like potassium, iron, calcium and sodium (Shao et al. 2017). Therefore, the present study is designed to investigate the impact of the hydrolysis process (at structural, chemical and elemental levels) through implementation of acid dextrinization and enzymatic saccharification on sweet potato root starch. This study may act as a baseline report for selecting and comparing the cost-effective strategy for the recovery of reducing and soluble sugar from starches.

Materials and Methods

Substrate and microorganisms

The sweet potato root flour (SPRF; used as substrate) and implemented microorganisms like *S. cerevisiae* MTCC 170 and *Z. mobilis* MTCC 92 used in the present study were obtained and processed as per our previously published paper (Jagatee et al. 2020).

Dextrinization and saccharification of sweet potato

SPRF diluted with distilled water (1:20) was separately treated with sulphuric acid, hydrochloric acid and perchloric acid and further screened for its dextrinization effects. For which, the freshly prepared slurry (5 g of SPRF in 100 ml of distilled water) was hydrolyzed with 1 ml of each acid having 1 M concentration at 100 °C for 60 min. The obtained hydrolysate was cooled and neutralized as per the methods of Koti et al. (2016). The total sugar content was measured using the anthrone reagent method (Hodge and Hofreiter 1962) and the reducing sugar was estimated by using alkaline copper and arsenomolybdate (Somogyi 1952). According to efficiency, further optimization of total sugar and HMF content (following the method of White 1979) was carried out by taking hydrochloric acid. To improve the dextrinization process, various parameters like temperature (80, 85, 90, 95, 100, 105, and 110 °C), incubation time (15, 30, 45, 60, 75, and 90 min), concentration (0.5, 1.0, 1.5, and 2.0 M of HCl) and volume (0.25, 0.5, 1.0, 1.5, and 2.0 ml of HCl) were tried and analyzed. After optimizing the dextrinization, saccharification process was carried out by taking Palkodex® (M/s Maps Enzymes, Ahmadabad, India) a glucoamylase enzyme that competently acts on starch and releases monomeric sugar compounds. To optimize the saccharification, a set of different temperatures (50, 55, 60, 65, and 70 °C), pH (3.5, 4.0, 4.5, 5.0, and 5.5), incubation time (1, 2, 4, 6, 8, 12, 18, and 24 h), enzyme volume (25, 50, 100, 150, 200, 250, and 300 µl) and enzyme concentration (125, 250, 500, 750, 1000, 1250, and 1500 U) respectively were tried with dextrinized SPRF. The dextrinized and saccharified samples were then collected and stored at -20 °C until further investigation.

Sugar analysis using TLC

To evaluate various fermentable sugar from dextrinized and saccharified sweet potato samples, TLC was performed by preparing 0.25 mm thick silica gel plates (20 × 20 cm in size). The dextrinized and saccharified sweet potato slurry was melded with water (1:5) in order to avoid the bulkiness of viscous mash. Separation of sugar was done with the help of butanol, ethanol and water with a ratio of 5:3:2 (v/v), respectively. The spots were developed by the application of 0.2% orcinol mixed with methanol: sulphuric acid (9:1; v/v) followed by incubation at 60 °C for about 2 h (Aquino et al. 2003). The glucose and maltose (1% each) were applied to develop the spot and were considered as standards.

Morphological analysis under SEM

The alteration in morphological appearance of SPRF (before and after dextrinization as well as saccharification) was observed under SEM (FEI Quanta 250, USA). The specimens were fixed on an aluminum stub with carbon tape on each side and the surface morphology was analyzed with a setup of accelerating voltage 10-15 kV (Jagatee et al. 2020).

Preparation of fermentation medium

For the preparation of 1 l of the medium, 50 g of saccharified SPRF was initially diluted with 500 ml of distilled water, supplemented with 2% $(NH_4)_2SO_4$ and 10% inoculums of *S. cerevisiae* was allowed to incubate for 48-120 h at 30 °C with pH 5.0. Similarly, for *Z. mobilis*, the fermentation was processed by taking the same 2% $(NH_4)_2 SO_4$ and 10% inoculum but incubated at 35 °C for 48-120 h at pH 5.5. To carry out the whole fermentation process, individual set up for *S. cerevisiae* and *Z. mobilis* were established under separate stationary conditions.

FTIR spectroscopy analysis

The fermented sample of saccharified SPRF was diluted with hexane and scanned in FTIR spectrophotometer (Nicolet iS5 spectrometer, Thermo-Fisher, Chicago, USA). With a resolution of 1.0 cm^{-1}, the spectra were processed through a scanning range of 1500-1800 cm^{-1} and 3000-3700 cm^{-1} and the compounds were quantified by using OMNIC software (Thermo Fisher, Chicago, USA). Hexane was used as a control for generating the data.

Elemental analysis using EDXRF spectrometer

Elemental profiling of both the saccharified and saccharified fermented SPRF was estimated using EDXRF spectrometer (Jordan Valley Ex-3600 EDXRF). The oven dried samples (150 mg/each pellet) were pressed to make the pellets with the help of table-top pelletizer (pressure: 100-110 kg/cm^2 for 5 min). The EDXRF instrument consisting of Rh anode X-ray tube (voltage 50 kV, current 1 mA) radiates signature X-rays for each element (Na-U) upon bombardment of X-rays on the samples. The elemental concentration is measured as the intensity of characteristic X-rays. The measurements were carried out in a vacuum condition and different filters were used (between the source and sample) for optimum identification of various elements. For detecting the P, S, Cl, K and Ca, no filter was used but a voltage of 6 kV and a current of 200 µA were applied, whereas for Mn, Fe, Cu and Zn, a 0.05 mm thick Ti filter was used with an applied voltage

Table 1. Screening of acids for dextrinization of sweet potato root flour (SPRF).

Acid	Total sugar (g/kg)	Reducing sugar (g/kg)
Control (as per normal procedure)	326.14 ± 3.87	190.91 ± 2.41
Sulphuric acid	298.42 ± 3.77	183.26 ± 1.78
Hydrochloric acid	340.63 ± 3.87	197.80 ± 3.22
Perchloric acid	201.28 ± 2.43	144.64 ± 2.04

of 14 kV and a current of 900 μA. The resulted X-ray fluorescence were detected by Si (Li) semiconductor detector (resolution 150 eV at 5.9 keV) and the quantification of the spectra was done by the in-built EX-WIN software (Rout et al. 2017).

Results

Screening of various acids for dextrinization of SPRF

The SPRF was initially treated with three significant acids such as sulphuric acid, hydrochloric acid and perchloric acid to release simple form of sugar, and the results are represented in Table 1. Among all treated acids, it was observed that the hydrochloric acid performed better dextrinization process as the concentration of total sugar (340.63 ± 3.87 g/kg) and reducing sugar (197.80 ± 3.22 g/kg) was yielded which is significantly improved than that of the control (326.14 ± 3.87 and 190.91 ± 2.41 g/kg of total and reducing sugar, respectively).

Standardization of the optimum conditions for acid dextrinization and enzyme saccharification

To obtain the non-reducing ends of starch molecule, hydrochloric acid and Palkodex® (glucoamylase) were used in the present experiment for evaluating the hydrolysing properties of SPRF. After initial screening, HCl was applied for better optimization of dextrinization process by interchanging different parameters like temperature, incubation time, concentration and volume of HCl. The results of HMF and total sugar content indicate the improved liquefying characteristic of SPRF, which facilitate the hydrolysis of complex carbohydrates. The environmental condition comprising of incubation time of 60 min, temperature of 100 °C, 1 M concentration of 1 ml HCl was found to be more suitable for better yielding of total sugar (380.44 ± 3.17 g/kg), which is comparatively better (16%) than that of the control one (326.14 ± 3.87 g/kg). Although, a significant variation in concentration of HMF (ranges from 2.74 ± 0.56 to 15.39 ± 0.23 mg/kg) was detected but in an optimum condition of dextrinization, 13.28 ± 0.25 mg/kg of HMF was achieved (Table 2). In case of saccharification, the efficiency of starch degrading glucoamylase enzyme (Palkodex®) was assessed by considering a different set of parameters like pH, temperature, incubation period, enzyme concentration and volume for releasing of monomeric sugar compounds. The best ideal condition for saccharification was noticed at pH 4.0, temperature 60 °C, incubation period of 18 h and 1000 U (200 μl) of enzyme. Under this condition more amount of total sugar (658.80 ± 7.83 g/kg) was released as compared to the optimized condition of dextrinized process (380.44

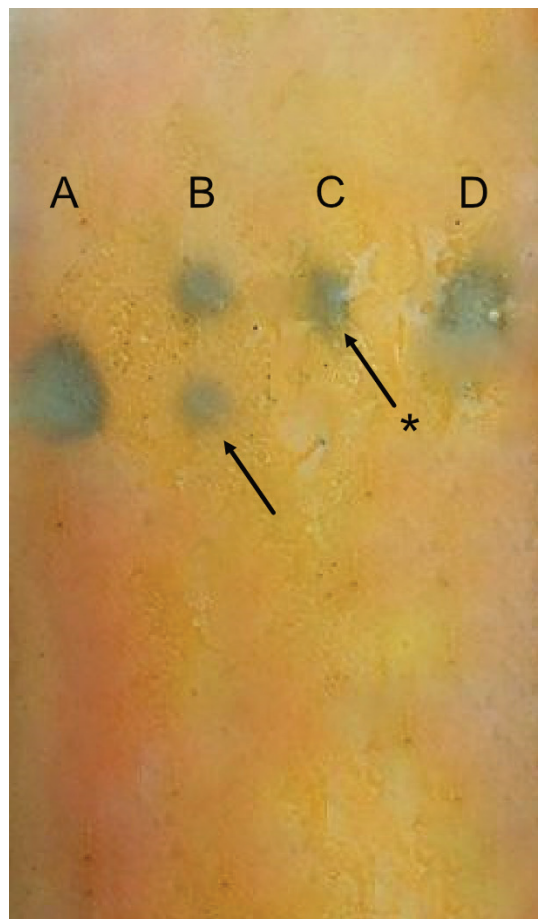

Figure 1. TLC chromatogram of untreated and treated SPRF. **A**: standard maltose; **B**: dextrinized SPRF; **C**: saccharified SPRF; **D**: standard glucose. The normal arrow and arrow with asterisk mark indicate maltose and glucose, respectively.

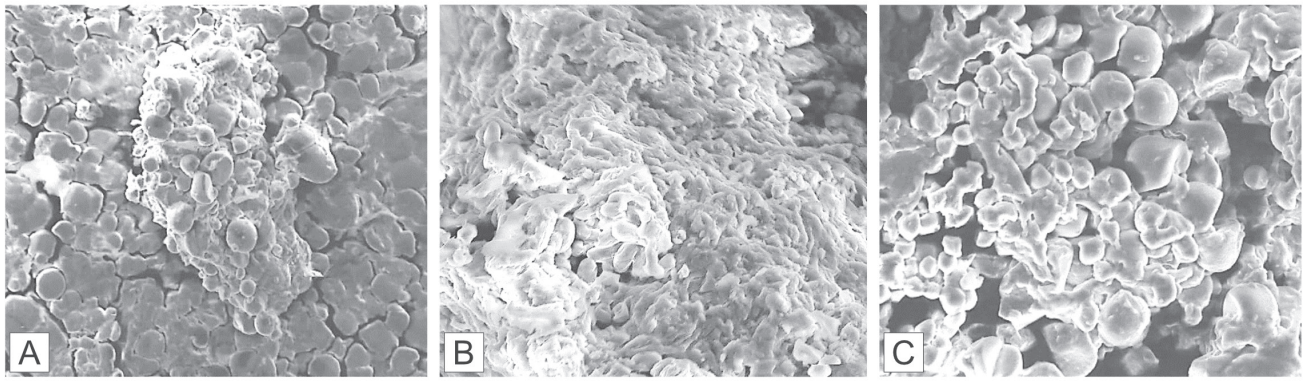

Figure 2. Scanning electron micrograph of untreated and treated SPRF. **A**: untreated SPRF; **B**: dextrinized SPRF; **C**: saccharified SPRF.

± 3.17 g/kg), and the increase is 73% (Tables 2,3).

TLC results of dextrinized and saccharified SPRF

For transformation of complex sugar into a simple form, HCl and glucoamylase were applied to carry out the dextrinization and saccharification process. TLC analysis revealed two fermentable sugars from dextrinized and saccharified sweet potato with maltose and glucose as standards (Fig. 1). The presence of both maltose (as compared with standard maltose) and glucose (as compared with standard glucose) was confirmed from the developed spot of acid hydrolyzed SPRF whereas, only glucose was detected from samples of saccharified SPRF. These results advocate that maltose and/or glucose are the main fermentable sugar components of sweet potato.

SEM analysis of dextrinized and saccharified SPRF

Certain acids and/or enzymes act upon the complex starch through which the complex structure breaks down into simple forms and can be noticeable under microscopic observation. A remarkable structural difference was witnessed among raw, dextrinized and saccharified SPRF samples when studied under SEM. An even granule surface of SPRF starch appeared in the untreated samples whereas both the dextrinized and saccharified SPRF samples exhibited an uneven surface of starch granules, indicating the breakdown of starch due to the vigorous action of HCl and glucoamylase. However, in comparison to the dextrinized sample, the saccharified sample has produced significant structural changes which indicate active involvement of both HCl and glucoamylase (Fig. 2).

FTIR spectra results of saccharified fermented SPRF

Two ethanologenic organisms, *S. cerevisiae* and *Z. mobilis* were subjected to ethanol production with the application of saccharified products. By maintaining the optimized fermentation condition i.e. incubation for 96 h at 30 °C and pH 5.0 (for *S. cerevisiae*) and incubation for 96 h at 35 °C and pH 5.5 (for *Z. mobilis*), the maximum production of ethanol [data not given] was separately standardised for both the microorganisms. To characterise the variation in functional group among the fermented samples, fermented SPRF samples were evaluated through FTIR spectroscopy. Significant variation of spectra was observed with respect to change of the functional components which also differed with the involvement of microorganisms tested (Fig. 3). The saccharified SPRF fermented with *S. cerevisiae* exhibited numerous significant peaks with respect to their specific functional groups such as 1512.26 cm^{-1} (N-O), 1676.12 cm^{-1} (C-N), 1716.11 cm^{-1} and 1772.28 cm^{-1} (C-O) due to variant compound development. Further, a varied range of band peaks between 3234.10 cm^{-1} to 3614.72 cm^{-1} were noticed due to bending of the O-H group (Fig. 3a,b). Similarly, due to N-O, C-C and C-O stretching, the saccharified SPRF fermented with *Z. mobilis* present a diverse range of peaks at 1530.17 cm^{-1}, 1641.78 cm^{-1}, 1646.69 cm^{-1} and 1783.57cm^{-1}. The absorption bands between 3263.37 cm^{-1} to 3608.95 cm^{-1} when taken into consideration for *Z. mobilis* fermented samples, contributed several peaks which is attributed to the stretching vibrations of -OH and water molecules (Fig. 3c,d). Such observations indicate the smooth conversion of ethanol by interchanging the functional complexity of starch of SPRF.

EDXRF results of saccharified fermented residues of SPRF

Elemental constituents of saccharified (control) and saccharified fermented SPRF residues were assessed to find out the differential impact of *S. cerevisiae* and *Z. mobilis* on substrate simplification during fermentation. Essential elements like potassium (K), sulphur (S), chlorine (Cl), calcium (Ca), manganese (Mn), iron (Fe), zinc (Zn), copper

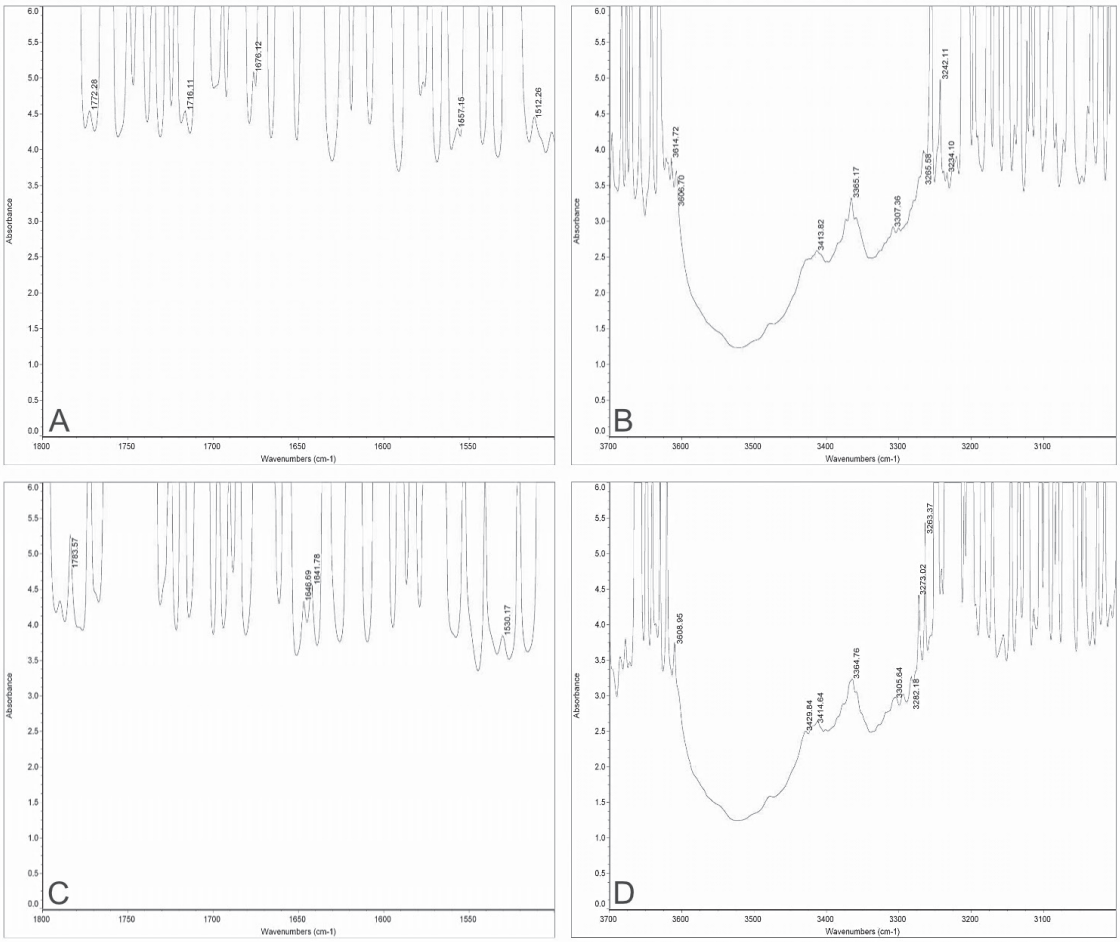

Figure 3. FTIR analysis of saccharified SPRF fermented with *S. cerevisiae* (A, B) and *Z. mobilis* (C, D). **A**: between 1500-1800 cm-1 spectral range of *S. cerevisiae*; **B**: between 3000-3700 cm-1 spectral range of *S. cerevisiae*. **C**: between 1500-1800 cm-1 spectral range of *Z. mobilis*; **D**: between 3000-3700 cm-1 spectral range of *Z. mobilis*.

(Cu) and phosphorus (P) were measured by using EDXRF spectrometer and the obtained results are presented in Table 4. It was observed that the acid-enzyme saccharified SPRF contains both macro and micronutrients such as P, S, Cl, K, Ca, Mn, Fe, Zn and Cu (2.12 ± 0.04, 0.75 ± 0.01, 3.37 ± 0.12,14.21 ± 0.36, 2.21 ± 0.04, 0.02 ± 0.003, 0.33 ± 0.001, 0.01 ± 0.002 and 0.03 ± 0.001 mg/g, respectively). However, a significant alteration of elemental constitution is noticed from both the fermented residues of *S. cerevisiae* and *Z. mobilis*. When the saccharified SPRF was utilized by *S. cerevisiae*, concentration of elements like P, K and Cu decreased to 1.80 ± 0.03, 13.14 ± 0.08 and 0.01 ± 0.003 mg/g whereas the concentration of S, Cl, Ca, Mn, Fe and Zn increased to 2.14 ± 0.28, 4.70 ± 0.07, 3.02 ± 0.02, 0.04 ± 0.005, 0.40 ± 0.01 and 0.16 ± 0.01 mg/g, respectively, after fermentation. Similar trends were also observed with respect to *Z. mobilis,* i.e. the concentration of P, K and Cu was slightly declined to 1.77 ± 0.02, 12.48 ± 0.10 and 0.01 ± 0.003 mg/g as compared to control. The increasing trend of S, Cl, Ca, Mn, Fe and Zn to 1.84 ± 0.03, 4.32 ± 0.10, 3.12 ± 0.03, 0.05 ± 0.001, 0.58 ± 0.004 and 0.17 ± 0.001 mg/g, respectively, as compared to control was also detected. However, the rate of decrease in concentration for all most all the elements was preferably higher in the fermented residues of *Z. mobilis* with respect to *S. cerevisiae* (Table 4).

Discussion

Acid-enzyme hydrolysis optimization

The SPRF slurry when exploited with acids for the liquefaction, yielded release of reducing sugar due to the cleavage of α and β glycosidic bonds. A comparative analysis of the liquefaction with different acids indicated greater release of reducing sugar with HCl than other acids (Putri and Rizaldi 2010). Similarly, Putri et al. (2012)

Table 2. Effect of temperature, incubation period, concentration and volume of HCl on acid hydrolysis (dextrinization) of sweet potato root flour (SPRF).

Concentration of HCl (M)	Volume (ml)	Temperature (°C)	Incubation period (min)	HMF (mg/kg)	Total sugar (g/kg)
Effect of temperature					
1.0	1.0	80	30	4.25 ± 0.17	295.21 ± 2.48
1.0	1.0	85	30	5.44 ± 0.19	310.34 ± 3.59
1.0	1.0	90	30	6.78 ± 0.20	328.45 ± 2.61
1.0	1.0	95	30	7.27 ± 0.26	340.26 ± 3.74
1.0	1.0	100	30	9.16 ± 0.29	354.15 ± 2.78
1.0	1.0	105	30	7.94 ± 0.28	348.73 ± 2.98
1.0	1.0	110	30	7.96 ± 0.28	347.64 ± 3.76
Effect of incubation time					
1.0	1.0	100	15	6.44 ± 0.12	334.23 ± 2.63
1.0	1.0	100	30	9.34 ± 0.14	354.14 ± 2.78
1.0	1.0	100	45	11.88 ± 0.17	371.42 ± 3.91
1.0	1.0	100	60	13.17 ± 0.27	380.14 ± 2.92
1.0	1.0	100	75	15.39 ± 0.23	380.31 ± 2.96
1.0	1.0	100	90	15.35 ± 0.29	380.40 ± 3.07
Effect of concentration					
0.5	1.0	100	60	7.92 ± 0.24	349.10 ± 3.18
1.0	1.0	100	60	13.28 ± 0.43	380.25 ± 2.94
1.5	1.0	100	60	13.28 ± 0.45	373.18 ± 2.91
2.0	1.0	100	60	13.28 ± 0.33	370.32 ± 3.09
Effect of volume					
1.0	0.25	100	60	2.74 ± 0.56	198.98 ± 2.19
1.0	0.5	100	60	3.53 ± 0.18	253.47 ± 2.34
1.0	1.0	100	60	13.28 ± 0.25	380.44 ± 3.17
1.0	1.5	100	60	13.29 ± 0.42	378.95 ± 2.97
1.0	2.0	100	60	13.39 ± 0.28	380.13 ± 3.10

also detected the reducing sugar from the sweet potato by implementing HCl, however a combination of HCl and *Aspergillus niger* has improved the properties of sugar synthesis. Additionally, Bharti and Chauhan (2016) and Azhar et al. (2017) stated that starch when hydrolyzed with a combination of acids resulted the release of compounds like HMF and 2-furaldehyde indicating a better dextrinization process. These furan derivatives pose a hindrance to ethanol production by inhibiting cell growth, so the production of HMF needs to be examined very carefully during the optimization process. In the present investigation, a significant upturn in the level of total soluble sugar along with HMF was obtained from the slurry of SPRF, through optimization of suitable environmental parameters involving temperature, incubation period and concentration of HCl. Temperature higher than 100 °C showed a momentous increase in HMF with minimum variation in the level of total sugar (Table 2). Kim and Hamdy (1985) have also observed increase in 5-HMF concentration at temperature above 100 °C, which on reaching the critical point inhibits the alcoholic fermentation. Increase in incubation period resulted an enhanced total sugar production till 60 minutes, after which the sugar level remained constant. This can be due to the polymerization of simple monosaccharides into polysaccharides. Whereas, optimizing the acid concentration, no such variation in total sugar and HMF was observed, and a higher level of sugar value at 1M concentration of HCl was detected in comparison to that of other strengths of HCl. Under acid hydrolysis, starch molecules randomly break down into simple sugar by dislocating the hydrogen bonds between starch chains, altering it to an entirely amorphous state, thereby developing a homogenous gelatinous substance (Judoamidjojo et al. 1992). However, during acid hydrolysis, starch usually breaks down into glucose and maltose and the ethanologenic organisms like *Z. mobilis* and *S. cerevisiae* cannot efficiently utilize the maltose as a substrate. Therefore, the acid hydrolyzed SPRF product needs to be carried out for the conversion of simple sugars with the application of moderately thermostable glucoamylase enzyme. Saccharification of starch with the help of glucoamylase enzyme is well

Table 3. Effect of pH, temperature, incubation period, enzyme concentration on saccharification of sweet potato root flour (SPRF).

Enzyme volume (µl)	Enzyme concentration (U)	pH	Temperature (°C)	Incubation period (h)	Total sugar (g/kg)
Effect of pH					
50	250	3.5	65	1	500.22 ± 6.31
50	250	4.0	65	1	515.14 ± 6.46
50	250	4.5	65	1	478.23 ± 7.35
50	250	5.0	65	1	451.54 ± 6.29
50	250	5.5	65	1	449.39 ± 5.92
Effect of temperature					
50	250	4.0	50	1	430.63 ± 5.28
50	250	4.0	55	1	478.58 ± 6.22
50	250	4.0	60	1	527.88 ± 4.33
50	250	4.0	65	1	515.12 ± 6.14
50	250	4.0	70	1	485.24 ± 6.08
Effect of incubation time					
50	250	4.0	60	1	527.90 ± 7.11
50	250	4.0	60	2	547.57 ± 6.19
50	250	4.0	60	4	557.26 ± 5.07
50	250	4.0	60	6	568.53 ± 6.13
50	250	4.0	60	8	580.91 ± 6.24
50	250	4.0	60	12	594.52 ± 7.10
50	250	4.0	60	18	611.46 ± 7.32
50	250	4.0	60	24	608.62 ± 6.26
Effect of enzyme concentration					
25	125	4.0	60	18	581.63 ± 6.34
50	250	4.0	60	18	611.42 ± 7.12
100	500	4.0	60	18	628.15 ± 7.34
150	750	4.0	60	18	642.36 ± 6.65
200	1000	4.0	60	18	658.80 ± 7.83
250	1250	4.0	60	18	648.49 ± 8.04
300	1500	4.0	60	18	647.94 ± 7.93

known for the development of glucose as its end product catalysing the α-(1-4) and α-(1-6) glycosidic linkages from the non-reducing terminus of starch molecule (Riaz et al. 2012). The potent application of glucoamylase from various sources have also been applied for the simplification of various carbohydrates where the rate of conversion is varied as per the nature of applied starches like raw starch (Cripwell et al. 2019), maize starch (Li et al. 2018), cassava starch (Pervez et al. 2014) rye starch (Strąk-Graczyk and Balcerek 2020) and raw flours starch (Xu et al. 2016).

Hydrolysis product analysis through TLC

Both the process of dextrinization and saccharification split into sugar consisting of reducing form the slurry form of SPRF starch. TLC analysis of the hydrolysis product confirmed the presence of maltose and glucose as the end products of the process. Particularly the treatment with acid is able to enhance the porosity of starch and then modify the granules, but this property may interact with the solubility and thermal properties of starch through which the starchy environment may generate some low weigh molecular product by rupturing some hydrogen bonds (Ulbrich et al. 2019; Vargas-León et al. 2019). Further, the combined treatment with enzymes like glucoamylase and HCl which is very common for the saccharification process was noted to simplify the sugar products. The release of glucose molecules from the slurry of acid treated SPRF typically depends on several factors like pH, temperature, incubation period, enzyme concentration and the maximum glucose is formed through break down of α-(1-4) and α-(1-6) chemical bonds (Riaz et al. 2012; Lincoln et al. 2019; Strąk-Graczyk and Balcerek 2020). Moreover, the glucoamylase-maltose complex (maltose first produced after acid hydrolysis) also insists on the rate of formation of glucose with interacting the non-reducing end side of the substrate (Chiba 1997; Salimi et al. 2019).

Table 4. Elemental analysis of saccharified and saccharified fermented residues of SPRF.

Elements tested	Control/saccharified sample (mg/g)	Saccharified fermented residue (mg/g)	
		S. cerevisiae fermented residue	*Z. mobilis* fermented residue
P	2.12 ± 0.04	1.80 ± 0.03	1.77 ± 0.02
S	0.75 ± 0.01	2.14 ± 0.28	1.84 ± 0.03
Cl	3.37 ± 0.12	4.70 ± 0.07	4.32 ± 0.10
K	14.21 ± 0.36	13.14 ± 0.08	12.48 ± 0.10
Ca	2.21 ± 0.04	3.02 ± 0.02	3.12 ± 0.03
Mn	0.02 ± 0.003	0.04 ± 0.005	0.05 ± 0.001
Fe	0.33 ± 0.001	0.40 ± 0.01	0.58 ± 0.004
Zn	0.01 ± 0.002	0.16± 0.01	0.17 ± 0.001
Cu	0.03 ± 0.001	0.01 ± 0.003	0.01 ± 0.003

Structural property of treated SPRF

The structural changes of SPRF starch obtained from the hydrolysis due to the combination of acid and enzyme are clearly viewed through scanning electron micrography. The structural appearance of starch granules with an irregular matrix as evidenced through SEM is a good indication of hydrolysis due to the simultaneous action of acid and enzyme. The action of hydrolysis by HCl alone (dextrinization) indicates starch degradation from roots of sweet potato due to its emulsification activity (Babu et al. 2015). The dextrinized sample then allowed for saccharification, in which glucoamylase is used for further hydrolysis to produce glucose. The glucoamylase consists of a catalytic domain associated with a starch-binding molecule linked with O-glycosylated linker region that vigorously acts upon the partly treated starch molecules to release monomeric form of sugar and resulted in the formation of rough surface of the substrate as compared to the dextrinized sample (Sauer et al. 2000; Betiku et al. 2013). A similar kind of experiment was also conducted to digest the complex starch molecules by the action of acids and some significant starch hydrolyzing enzymes (Zhang et al. 2010; de Souza et al. 2019; Strąk-Graczyk and Balcerek 2020).

Functional property of saccharified fermented SPRF

The efficacy of sweet potato as a substrate for the production of ethanol and the differences in the starch biodegradation involving both *S. cerevisiae* and *Z. mobilis* fermented SPRF were examined through FTIR analysis within the spectral range of 1500-1800 and 3000-3700 cm^1. Between the spectral range of 900-1200 cm^{-1}, no absorbance peak was detected from both the fermented microorganisms which indicated the utilization of resulted carbohydrates (Vodnar et al. 2010; Warren et al. 2016; Jagatee et al. 2020). However in the spectral range of 1500-1800 cm^{-1}, both *S. cerevisiae* and *Z. mobilis* fermented SPRF pronounced shifting of peak position corresponding the various functional groups which revealed the formation of aromatic C-C stretching, carbonyl C-O stretching, alkene C-C stretching, esters functional groups. Such stretching may be attributed to lipids and fatty acids with C-O stretching (Nandiyanto et al. 2019). Moreover, in the spectral range of 3000-3700 cm^{-1}, various absorbance shifting of peaks appeared which is a strong indication of polymeric, dimeric and internally bonded -OH stretch and such stretch in the acid-enzyme hydrolyzed slurry of SPRF corresponds to the better ethanol production potential (Nieuwoudt et al. 2006; Jivan et al. 2014; Nandiyano et al. 2019).

Elemental variation of fermented residue of SPRF

Sweet potato is being considered as an economically important food crop for its substantial level of starch as well as for the bioavailability of soluble sugars, vitamins, minerals and other nutrients. Additionally, the root parts of sweet potato have significant amount of essential elements like Ca and Fe (Senanayake et al. 2013). Hence, an effort was made to simplify and change the constituents of some valuable elements by implementing *S. cerevisiae* and *Z. mobilis* individually to the saccharified SPRF product and a considerable change of the constituents was achieved after the fermentation. The applied acid-enzyme hydrolysis method not only successfully synthesizes the simple form of sugar but also resulted in better bioavailability of some essential elements within the residue of fermented SPRF which is a good sign of further utilization of that type of waste biomaterials. As the fermented SPRF residues having various nutritional values along with good source of pectin and dietary fiber, the product can be used as the cattle and fish feed (Murugan et al. 2012; Jagatee et al. 2020). Moreover, the residual product may act as potential organic fertilizer for sustainable agriculture and improve the growth and metabolism of plants (Varzakas et al. 2016; Akoetey et al. 2017). The availability of specific carbohydrates is the key biomolecules for regulating the

fermentation process, however, the deployed microorganisms and producing certain enzymes play a central role by regulating the whole metabolic activity. The fluctuation of trace elements in the residue of fermented SPRF maybe an indication of their utilization by certain enzymes as a cofactor for better production of bioethanol (Choong et al. 2016; Nimbalkar et al. 2018).

Conclusion

The study concludes that the acid-enzyme hydrolysis can be an alternative and sustainable technology for the production of bioethanol. The experimental outcome obtained from the study validates the activation of hydrochloric acid and glucoamylase (Palkodex®) for the production of maltose and glucose from sweet potato starch. The saccharified substrate subjected to fermentation and the fermented residues of *Z. mobilis* and *S. cerevisiae* showed the presence of several absorbed peaks for ethanol functional group (-OH), indicating a more suitable substrate for the production of bioethanol. Moreover, the variation of elemental components of control as well as fermented sweet potato starch may act as a possible bioindicator for utilization of specific nutrients corresponding to the deployed microorganisms. These observations advocated further need of research on subcellular and molecular level to understand the role of individual element during each step of the fermentation process of bioethanol production.

Acknowledgments

The authors are grateful to Institute of Physics-Bhubaneswar, UGC DAE Consortium of Scientific Research–Kolkata and Kalyani Laboratories Pvt. Ltd.–Bhubaneswar for allowing to conduct the SEM, EDXRF and FTIR analysis, respectively. One of the authors (JRR) wish to thank the authorities of AIPH University for the support and encouragement to publish this work.

References

Abidin Z, Saraswati E, Naid T (2014) Bioethanol production from waste of the cassava peel (*Manihot esculenta*) by acid hydrolysis and fermentation process. Int J Pharm Tech Res 6(4):1209-1212.

Akoetey W, Britain MM, Morawicki RO (2017) Potential use of by products from cultivation and processing of sweet potatoes. Cienc Rural 47:1-8.

Aquino AC, Jorge AJ, Terenzi HF, Pohzeli ML (2003) Studies on thermostable alpha-amylase from thermophilic fungus *Scytalidium thermophilum*. Appl Microbiol Biotechnol 61:323-328.

Azhar SHM, Abdullaa R, Jambo SA, Marbawi H, Gansau JA, Faik AAM, Siti KFR (2017) Yeasts in sustainable bioethanol production: a review. Biochem Biophys 10:52-61.

Babu AS, Parimalavalli R, Jagannadham K, Rao JS (2015) Chemical and structural properties of sweet potato starch treated with organic and inorganic acid. J Food Sci Technol 52:5745-5753.

Betiku E, Akindolani OO, Ismaila AR (2013) Enzymatic hydrolysis optimization of sweet potato (*Ipomoea batatas*) peel using a statistical approach. Braz J Chem Eng 30:467-476.

Bharti B, Chauhan M (2016) Bioethanol production using *Saccharomyces cerevisiae* with different perspectives: substrates, growth variables, inhibitor reduction and immobilization. Ferment Technol 5(2):1-4.

Busic A, Marđetko N, Kundas S, Morzak G, Belskaya H, Santek MI, Komes D, Novak S, Santek B (2018) Bioethanol production from renewable raw materials and its separation and purification: a review. Food Technol Biotechnol 56(3):289–311.

Centre for Sustainable Systems (CSS) (2019) Biofuels factsheet. Centre for Sustainable Systems, University of Michigan. Pub. No. CSS08-09, 12 May 2020 (http://css.umich.edu/factsheets).

Chiba S (1997) Molecular mechanism in alpha-glucosidase and glucoamylase. Biosci Biotechnol Biochem 61(8):1233-1239.

Choong YY, Norli I, Abdullah AZ, Yhaya MF (2016) Impacts of trace element supplementation on the performance of anaerobic digestion process: a critical review. Bioresour Technol 209:369-379.

Cripwell RA, Rose SH, Favaro L, Van Zyl WH (2019) Construction of industrial *Saccharomyces cerevisiae* strains for the efficient consolidated bioprocessing of raw starch. Biotechnol Biofuels 12:201.

de Souza IA, Orsi DC, Gomes AJ, Lunardi CN (2019) Enzymatic hydrolysis of starch into sugars is influenced by microgel assembly. Biotechnol Rep 22:p.e00342.

Delgenes JP, Moletta R, Navarro JM (1996) Effects of lignocellulose degradation products on ethanol fermentations of glucose and xylose by *Saccharomyces cerevisiae, Zymomonas mobilis, Pichia stipitis* and *Candida shehatae.* Enzyme Microb Technol 19(3):220-225.

Hodge JE, Hofreiter BT (1962) Determination of reducing sugars and carbohydrates. In Whistler RL, Wolfrom ML, Eds., Methods in Carbohydrate Chemistry, Vol. 1, Academic Press, New York.

Jagatee S, Rout JR, Behera S, Ram SS, Sudarshan M, Pradhan C, Sahoo SL, Mohanty RC (2020) Effect of enzymatic hydrolysis on structural, chemical and elemental prop-

erties of sweet potato flour. Waste Biomass Valor. DOI: 10.1007/s12649-020-00984-9.

Jivan MJ, Yarmand M, Madadlou A (2014) Preparation of cold water-soluble potato starch and its characterization. J Food Sci Technol 51(3):601-605.

Judoamidjojo M, Said G, Hartoto L (1992) Fermentation technology, Bogor Agricultural Institute Press, Bogor.

Kim K, Hamdy M (1985) Acid hydrolysis of sweet potato for ethanol production. J Biotechnol Bioenergy 27:316-320.

Koti S, Govumoni SP, Gentela J, Rao LV (2016) Enhanced bioethanol production from wheat straw hemicellulose by mutant strains of pentose fermenting organisms *Pichia stipitis* and *Candida shehatae*. SpringerPlus 5:1545.

Lareo C, Ferrari MD, Guigou M, Fajardo L, Larnaudie V, Ramírez MB, Martínez-Garreiro J (2013) Evaluation of sweet potato for fuel bioethanol production: hydrolysis and fermentation. SpringerPlus 2:493.

Li Z, Wang D, Shi Y (2018) High-solids bio-conversion of maize starch to sugars and ethanol. Biosynth Nut Biomed 71(1-2):1800142.

Liimatainen H, Kuokkanen T, Kaariainen J (2004) Development of bio ethanol production from waste potatoes. In Pongrácz E, Ed., Proceedings of the Waste Minimization and Resources Use Optimization Conference, June 10, 2004. University of Oulu, Finland. 123-129.

Lincoln L, More VS, More SS (2019) Purification and biochemical characterization of extracellular glucoamylase from *Paenibacillus amylolyticus* strain. J Basic Microbiol 59(4):375-384.

Murugan S, Paramasivam SK, Nedunchezhiyan M (2012) Sweet potato as an animal feed and fodder. In Nedunchezhiyan M, Byju G, Eds., Sweet Potato. Fruit Vegetable and Cereal Science and Biotechnology 6(1). Global Science Books, Kagawa ken, Japan. 106-114.

Nandiyanto ABD, Oktiani R, Ragadhita R (2019) How to read and interpret FTIR spectroscope of organic material. Indones J Sci Technol 4(1):97-118.

Nieuwoudt HH, Pretorius IS, Bauer FF, Nel DG, Prior BA (2006) Rapid screening of the fermentation profiles of wine yeasts by Fourier transform infrared spectroscopy. J Microbiol Methods 67:248-256.

Nimbalkar PR, Khedkar MA, Parulekar RS, Chandgude VK, Sonawane KD, Chavan PV, Bankar SB (2018) Role of trace elements as cofactor: an efficient strategy toward enhanced biobutanol production. ACS Sustain Chem Eng 6:9304-9313.

Patni N, Pillai GS, Dwivedi AH (2011) Analysis of current scenario of biofuels in India specifically bio-diesel and bio-ethanol. Energy 4:8-10.

Pervez S, Aman A, Iqbal S, Siddiqui NN, Ul Qader SA (2014) Saccharification and liquefaction of cassava starch: an alternative source for the production of bioethanol using amylolytic enzymes by double fermentation process. BMC Biotechnol 14:49.

Putri LSE, Nasrulloh, Haris A (2012) Bioethanol production from sweet potato using combination of acid and enzymatic hydrolysis. Appl Mechanics Mater 110:1767-1772.

Putri LSE, Rizaldi F (2010) Taro as source of renewable energy. Proceedings of 2nd International Conference of the Institution of Engineering and Technology: Green Technology for Sustainable Global Development, Brunei Darussalam.

Qiu H, Huang J, Yang J, Rozelle S, Zhang Y, Zhang Y, Zhang Y (2010) Bioethanol development in China and the potential impacts on its agricultural economy. Appl Energy 87:76-83.

Riaz M, Rashid MH, Sawyer L, Akhtar S, Javed MR, Nadeem H, Wearc M (2012) Physiochemical properties and kinetics of glucoamylase produced from deoxy-d-glucose resistant mutant of *Aspergillus niger* for soluble starch hydrolysis. Food Chem 130:24-30.

Rout JR, Sahoo SL, Das R, Ram SS, Chakraborty A, Sudarshan M (2017) Changes in antioxidant enzyme activities and elemental profiling of *Abutilon indicum* L subjected to copper stress. Proc Natl Acad Sci, India, Sect. B, Biol Sci 87:1469-1478.

Salimi E, Saragas K, Taheri ME, Novakovic J, Barampouti EM, Mai S, Moustakas K, Malamis D, Loizidou M (2019) The role of enzyme loading on starch and cellulose hydrolysis of food waste. Waste Biomass Valor 10:3753-3762.

Satapathy S, Rout JR, Kerry RG, Thatoi H, Sahoo SL (2020) Biochemical prospects of various microbial pectinase and pectin: an approachable concept in pharmaceutical bioprocessing. Front Nutr 7:117.

Sauer J, Sigurskjold BW, Christensen U, Frandsen TP, Mirgorodskaya E, Harrison M, Roepstorff P, Svensson B (2000) Glucoamylase: structure/ function relationships, and protein engineering. Biochem Biophys Acta 1543:275-293.

Senanayake SA, Ranaweera KKDS, Gunaratne A, Bamunuarachchi A (2013) Comparative analysis of nutritional quality of five different cultivars of sweet potatoes (*Ipomea batatas* (L.) Lam) in Sri Lanka. Food Sci Nutr 1:284-291.

Shao A, Drewnowski A, Willcox DC, Kramer L, Lausted C, Eggersdorfer M, Mathers J, Bell JD, Randolph RK, Witkamp R, Griffiths JC (2017) Optimal nutrition and the ever-changing dietary landscape: a conference report. Eur J Nutr 56(1):1-21.

Somogyi M (1952) Note on sugar determination. J Biol Chem 200:245-247.

Srinivas T (2009) Economics of sweet potato production and marketing. In Loebenstein G, Thottappilly G, Eds., The Sweet Potato. Springer. 235-267.

Strąk-Graczyk E, Balcerek M (2020) Effect of pre-hydrolysis

on simultaneous saccharification and fermentation of native rye starch. Food Bioprocess Technol 13:923-936.
Surmely R, Alvarez H, Cereda MP, Vilpoux OF (2004) Hydrolysis of starch, in collections. In Cereda MP, Vilpoux OF, Eds., Latin American Starchy Tubers, Book 3: Technology, Use and Potentialities of Latin American Starchy Tubers. NGO Raizes and Cargill Foundation, Sao Paulo, Brazil. 389-469.
Thatoi H, Dash PK, Mohapatra S, Swain MR (2014) Bioethanol production from tuber crops using fermentation technology: a review. Int J Sustain Energy 35(5):443-468.
Ulbrich M, Daler JM, Flöter E (2019) Acid hydrolysis of corn starch genotypes. I. Impact on morphological and molecular properties. Carbohydr Polym 219:172-180.
United States Department of Agriculture. Foreign Agricultural Service (USDA FAS) (2018) China-Peoples Republic of Biofuels Annual. USDA Foreign Agricultural Services, USA. GAIN Report Number: CH19047, 12th May 2020 (https://apps.fas.usda.gov/newgainapi/api/report/downloadreportbyfilename?filename=Biofuels%20Annual_Beijing_China%20-%20Peoples%20Republic%20of_7-25-2018.pdf).
United States Department of Agriculture. Foreign Agricultural Service (USDA FAS) (2019) India Biofuels Annual. USDA Foreign Agricultural Services, USA. GAIN Report Number: CH19047, 13th May 2020 (https://apps.fas.usda.gov/newgainapi/api/report/downloadreportbyfilename?filename=Biofuels%20Annual_New%20Delhi_India_8-9-2019.pdf).
Vargas-Leóna EA, Falfan-Cortes RN, Navarro-Cortez RO, Hernández-Ávilad J, Castro-Rosasa J, Gómez-Aldapa CA (2019) Double chemical modification in rice starch: acid hydrolysis optimization process and phosphating. CyTA - J Food 17(1):632-639.
Varzakas T, Zakynthinos G, Verpoort F (2016) Plant food residues as a source of nutraceuticals and functional foods. Foods 5:88-100.
Vodnar DC, Paucean A, Dulf FV, Socaciu C (2010) HPLC characterization of lactic acid formation and FTIR fingerprint of pro- biotic bacteria during fermentation processes. Not Bot Hort Agrobot Cluj 38:109-113.
Walker GM (2010) Bioethanol: Science and Technology of Fuel Alcohol. Ventus Publishing ApS: Copenhagen. 1-114.
Warren FJ, Gidley MJ, Flanagan BM (2016) Infrared spectroscopy as a tool to characterise starch ordered structure--a joint FTIR-ATR, NMR, XRD and DSC study. Carbohydr Polym 139:35-42.
White JW (1979) Spectrophotometric method for hydroxymethylfurfural in honey. J Ass Off Anal Chem 62:509-514.
Xu Q, Yan Y, Feng J (2016) Efficient hydrolysis of raw starch and ethanol fermentation: a novel raw starch-digesting glucoamylase from *Penicillium oxalicum*. Biotechnol Biofuels 9:216.
Yang S, Fei Q, Zhang Y, Conteras LM, Utturkar SM, Brown SD, Himmel ME, Zhang M (2016) *Zymomonas mobilis* as a model system for production of biofuels and biochemicals. Microb Biotechnol 9(6):699-717.
Zhang L, Chen Q, Jin Y, Xue H, Guan J, Wang Z, Zhao H (2010) Energy-saving direct ethanol production from viscosity reduction mash of sweet potato at very high gravity (VHG). Fuel Proc Technol 91:1845-1850.

Acta Biologica Szegediensis

Volume 64(2):151-158, 2020
Acta Biologica Szegediensis
http://abs.bibl.u-szeged.hu/index.php/abs
DOI:10.14232/abs.2020.2.151-158

ARTICLE

Concomitant yield optimization of tannase and gallic acid by *Bacillus licheniformis* KBR6 through submerged fermentation: An industrial approach

Pradeep K. Das Mohapatra[1]*, Ishita Biswas[1], Keshab C. Mondal[2], Bikas R. Pati[2]

[1]Department of Microbiology, Raiganj University, Uttar Dinajpur-733 134, West Bengal, India
[2]Department of Microbiology, Vidyasagar University, Midnapore-721 102, West Bengal, India

ABSTRACT The present study is concerned with the evaluation of tannase and gallic acid production efficacy of *Bacillus licheniformis* KBR6 under different environmental conditions through submerged fermentation. Results have shown that different environmental conditions and mineral sources have differential influences on tannase and gallic acid production. Highest tannase and gallic acid yield was observed at incubation period of 18 h and 22 h, respectively. At tannic acid concentration of 15 g/l, maximum cell mass (0.75 g/l), cell yield coefficient (0.08 g/g), specific growth rate (37.5 mg/g/h), tannase yield (16.3 U/g) and specific tannase production rate (0.80 U/g/h) were observed, however, at higher tannic acid concentration a decrease in tannase yield and production rate were observed, but gallic acid production increased with increasing tannic acid concentration. Additional carbohydrate sources like glucose, fructose, and lactose showed positive influence on enzyme yield. Among the studied nitrogen sources urea and NH_4Cl, and of the phosphate sources KH_2PO_4 showed favourable effects on cell growth and simultaneous enzyme and gallic acid production. Temperature of 35 °C was found to be optimum for tannase and gallic acid production. Of all the studied metal ions Ca^{2+}, Mg^{2+} and Na^{+} showed positive effect whereas, Co^{2+}, Ag^{2+}, Pb^{2+}, Hg^{2+} showed inhibitory effects.
Acta Biol Szeged 64(2):151-158 (2020)

KEY WORDS
Bacillus licheniformis KBR6
gallic acid
submerged fermentation
tannase

ARTICLE INFORMATION
Submitted
4 December 2020.
Accepted
8 January 2021.
***Corresponding author**
E-mail: pkdmvu@gmail.com

Introduction

Tannin acyl hydrolase (E.C. 3.1.1.20), which is commonly called tannase, is an inducible enzyme especially in microbes, produced in the presence of hydrolysable tannins (Barthomeuf et al. 1994; Mondal et al. 2001a; Mukherjee and Banerjee 2006). Tannase hydrolyses the ester and depside linkages of hydrolysable tannins like tannic acid, gallotannins, epigallocatechin-3-gallate, esters of gallic acid into glucose and gallic acid (Iibuchi et al. 1968; Das Mohapatra et al. 2005; Jana et al. 2014).

Tannase has wide applications in food, beverage, brewing, cosmetic and chemical industries (Lekha and Lonsane 1997; Aissam et al. 2005). It is mainly used for the preparation of gallic acid, instant tea, acorn wine, coffee flavoured soft drinks, high-grade leather tannin, clarification of beer and fruit juice, detannification of food and production of wine (Coggon and Sanderson 1972; Lekha and Lonsane 1997; Mukherjee and Banerjee 2003; Aracri et al. 2019; Cavalcanti et al. 2020). It is also used to clean up highly polluting tannin from the effluent of the leather industry (Kim et al. 2020; Biswas et al. 2020).

Besides that, gallic acid (3,4,5, trihydroxy benzoic acid), a hydrolyzable product of tannic acid is an antioxidant and has several uses for the manufacture of propyl gallate, photosensitive resin, pyrogallol, ink and dye (Gaathon et al. 1989; Das Mohapatra et al. 2005; Patil et al. 2011). Conventionally it is produced from tannic acid by acid hydrolysis or by the action of enzyme tannase (Lekha and Lonsane 1997). Microbial process is the most specific, eco-friendly and cost-effective approach and at the same time pure gallic acid could be recovered from the process easily. The world-wide annual demand of gallic acid is about 8000 tones (Lokeswari 2010; Aguilar-Zarate et al. 2015). In India it is totally imported and mainly utilized as an intermediate in the production of trimethoxy benzaldehyde, which is used in the pharmaceutical industry to produce trimethoprim, a broad-spectrum antibiotic (Bajpai and Patil 1997; Aissam et al. 2005; Biswas et al. 2020). A combination of trimethoprim and sulphonamide is effective against many otherwise resistant species of bacteria.

Though tannic acid is generally considered as antinutrient and antimicrobial agent (Scalbert 1991), however, a large number of tannase-producing microorganisms

including bacteria, fungi and yeast can hydrolyse tannic acid into gallic acid and glucose (Mondal and Pati 2000; Banerjee et al. 2001; Sharma et al. 2007; Das Mohapatra et al. 2009). Production of tannase and gallic acid in tannin rich media through fungi has been reported earlier by many researchers (Rajakumar and Nandy 1983; Pourrat et al. 1987; Hadi et al.1994; Bajpai and Patil 1999; Banerjee et al. 2001; Mukherjee and Banerjee 2006). In this context there are comparatively few reports on simultaneous production of the two by bacteria. Using chestnut tannin as carbon source, Deschamps et al. (1983) first reported the production of extracellular tannase by *Bacillus pumilus*, *Bacillus polymixa*, *Corynebacterium* sp. and *Klebsiella pneumoniae*. Later, Deschamps and Lebeault (1984) reported the production of gallic acid from tara pod tannins by *K. pneumoniae* and *Corynebacterium* sp. Tannase-producing strains like *Streptococcus* sp. from faeces of koalas (Osawa and Mitsuoka 1990) and *Lactobacilli* from humans and fermented foods (Osawa et al. 2000) were also reported. Das Mohapatra et al. (2006) reported on tannase production by *Bacillus licheniformis* KBR6 by using eight different (*Acacia auriculiformis, Casuarina quisetifolia, Psidium guazava, Anacardium occidentale, Delonix regia, Eucalyptus tereticornis, Cassia fistula,* and *Ficus bengalensis*) plant extracts as tannin source. Aguilar-Zarate et al. (2015) reported on gallic acid production under anaerobic submerged fermentation by two bacilli strains identified as *Bacillus subtilis* AM1 and *Lactobacillus plantarum* CIR1. A preliminary study was done on isolation of tannase producer from soil, like *B. licheniformis* KBR6 and *Bacillus cereus* KBR9 (Mondal and Pati 2000; Mondal et al. 2001a).

Submerged fermentation involves the growth of the microorganism in a liquid medium in which various nutrients are either dissolved or suspended as particulate solids (Frost and Moss 1987). Submerged fermentation is mostly preferred, because sterilization and process control mechanisms are quite easier (Lekha and Lonsane 1997). In submerged fermentation, uniform growth of the microorganism occurred as a suspension owing to various gases and nutrients, which are either dissolved or suspended in a liquid medium (Frost and Moss 1987).

In this present work the tannase and gallic acid yield efficiency of *B. licheniformis* KBR6 through submerged fermentation has been studied.

Materials and Methods

Microorganism and mode of cultivation

A potent tannase-producing bacterium used in the present study was isolated from the lateritic sal forest soil of Midnapore district, West Bengal, India and was identified as *B. licheniformis* KBR6 (IMI. No.-379224) (Mondal and Pati 2000).

The selective medium used for growth of the organism was composed of (g/l): tannic acid, 10; K_2HPO_4, 0.5; KH_2PO_4, 0.5; $MgSO_4$, 0.5; $CaCl_2$, 1.0; NH_4Cl, 3.0. The pH of sterilized medium was adjusted to 5.0 using 0.5 M NaOH. Cultivation of *B. licheniformis* KBR6 was done in 250 ml Erlenmeyer flask containing 50 ml sterilized medium for 20 h on a rotary shaker (200 rpm) at 35 °C. The culture broth was centrifuged (5000 g for 15 min) and the supernatant was examined for production of tannase as well as gallic acid.

Determination of microbial growth

For measuring the growth, the cell concentration was determined by turbidimetry at 620 nm (SL 171 Mini Spec, Elico, India) and correlated to cell dry weight (mg/ml).

Measurement of tannin concentration

The remaining tannin content of the fermented broth was estimated by the modified method of Hagerman and Butler (1978). The tannin content of the fermented broth (0.5 ml) was precipitated by addition of 3 ml of BSA solution (1 mg/ml) and kept at room temperature for 15 min. After centrifugation (5000 g, 5 min), the precipitate was dissolved in 3 ml of SDS - triethanolamine solution (SDS 1%, w/v, and triethanolamine 5%, v/v, in distilled water). Then 1 ml of $FeCl_3$ reagent (0.01 M $FeCl_3$ in 0.01 N HCl) was added and incubated for 30 min for stabilization of colour. This coloured solution was diluted with distilled water and the absorbency was measured at 530 nm. The residual tannic acid in the fermented broth was determined from a standard curve and expressed as percentage of initial concentration.

Assay of tannase

The activity of extracellular tannase from *B. licheniformis* KBR6 was determined by the colorimetric method of Mondal et al. (2001b). For the assay, 0.1 ml of enzyme was mixed with 0.3 ml of tannic acid substrate solution (1.0% w/v tannic acid in 0.2 M citrate buffer, pH 5.0), and incubated at 50 °C for 30 min. The reaction was terminated by the addition of BSA solution (1 mg/ml), which also precipitated the residual tannic acid. A control reaction with heat-denatured enzyme was performed concomitantly. The tubes were then centrifuged (5000 g, 10 min) and the precipitates were dissolved in 2 ml of SDS-triethanolamine (1% w/v, SDS in 5% v/v, triethanolamine) solution. The absorbance was measured at 530 nm after addition of 1 ml of 0.13 M $FeCl_3$.

The specific extinction coefficient of tannic acid at 530 nm was 0.577 (Mondal et al. 2001b). Using this coefficient, one unit of tannase activity was defined as the amount of enzyme that can hydrolyse 1 μM of ester linkage of

tannic acid in 1 min at 50 ℃ and pH 5.0.

Estimation of gallic acid

The gallic acid in the culture medium was estimated following the method of Bajpai and Patil (1996). Culture supernatant was diluted 100-fold with 0.5 M acetate buffer (pH 6.0) and the absorbance was simultaneously measured at two specific wavelengths. Concentration of gallic acid was calculated by the following equation:

$$\text{Gallic acid } (\mu g/ml) = 21.77\ (A_{254.6}) - 17.17\ (A_{293.8})$$

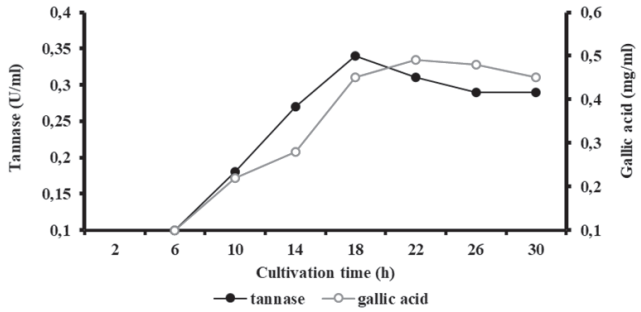

Figure 1. Effect of incubation period on tannase and gallic acid production.

Results

Effect of incubation period

Tannase and gallic acid production in relation to growth of *B. licheniformis* KBR6 were studied in submerged fermentation for 48 h. The formation of tannase was started from the early stages of growth of the bacterium and reached maximum at 18 h. The highest gallic acid production was found at 22 h (Fig. 1).

Effect of tannic acid concentration

The catalytic activity of *B. licheniformis* KBR6 was studied in a fermentation medium containing various tannic acid (sole substrate) concentrations (5 to 40 g/l) and represented in Table 1. Increasing the initial tannic acid concentration from 10 to 15 g/l favoured the growth of the organism. At 15 g/l tannic acid concentration maximum cell mass (0.75 g/l), cell yield co-efficient (0.08 g/g) and specific growth rate (37.5 mg/g/h) of the organism was observed. The highest tannase yield (16.3 U/g) and specific tannase production rate (0.80 U/g/h) were also obtained in this tannic acid concentration. It was also shown that somewhat higher concentration of tannic acid (20 g/l) decreased tannase yield (15.2 U/g) and specific tannase production rate (0.76 U/g/h). But the gallic acid yield coefficient and specific gallic acid production rate increased with increase in tannic acid concentration.

Effect of additional carbohydrate (extra carbon source) in tannic acid medium

Carbon source is known to influence the growth as well as constitutive element in the synthesis of any metabolite. In order to assess the effects of additional carbohydrates on the growth, extracellular tannase formation and gallic acid production by *B. licheniformis* KBR6, four different carbohydrates (2 g/l) viz, glucose, fructose, sucrose and lactose were added to the medium separately and then examined (Table 2). Maximum cell growth, gallic acid yield coefficient and specific growth rate of the organism were obtained in presence of glucose and fructose, whereas tannase yield coefficient and specific tannase production rate showed highest in presence of lactose. In absence of any additional carbon source, the catalytic activity of organism was significantly reduced.

Table 1. Effect of tannic acid concentration on gallic acid, tannase, and cell mass formation by *B. licheniformis* KBR6.

Parameters	Without tannic acid	Tannic acid (g/l)							
		5	10	15	20	25	30	35	40
C_{cm}	0.23	0.66	0.74	0.75	0.68	0.50	0.30	0.30	0.19
$Y_{c/s}$	0.23	0.07	0.07	0.08	0.07	0.05	0.03	0.03	0.02
$Y_{e/s}$	ND	8.1	14.1	16.3	15.2	12.4	11.3	10.9	7.8
$Y_{g/s}$	ND	61.4	75.8	77.5	80.0	80.0	82.0	84.0	83.0
q_e	ND	0.41	0.71	0.80	0.76	0.62	0.57	0.57	0.39
q_g	ND	3.0	3.1	3.8	4.1	4.06	4.1	4.2	4.3
q_c	11	33	37	37.5	34	25	15	15	9
S/s	ND	82.2	83.1	78.0	66.3	46.0	45.8	45.6	32.3

ND = Non detectable; C_{cm} = dry cell mass (g/l); $Y_{c/s}$ = cell yield coefficient (g dry cell mass per g tannic acid used); $Y_{e/s}$ = tannase yield coefficient (U of enzyme per g tannic acid used); $Y_{g/s}$ = gallic acid yield coefficient (g of gallic acid per g tannic acid used); q_e = tannase production rate (U/g/h); q_g = gallic acid production rate (mg/g/h); q_c = growth rate (mg/g/h); **S/s** = tannic acid consumed percentage

Table 2. Effect of carbon source (2 g/l) on tannase, gallic acid and cell mass formation by *B. licheniformis* KBR6.

Parameters	No carbohydrate	Glucose	Fructose	Sucrose	Lactose
C_{cm}	0.41	0.7	0.71	0.67	0.66
$Y_{c/s}$	0.04	0.07	0.07	0.07	0.07
$Y_{e/s}$	3.9	4.5	4.2	6.1	6.5
$Y_{g/s}$	0.125	0.269	0.252	0.216	0.185
q_e	0.195	0.225	0.21	0.305	0.325
q_g	4.1	4.3	4.4	4.4	4.0
q_c	20	35	35	33	33
S/s	66.2	32.2	35.0	40.8	44.2

C_{cm} = dry cell mass (g/l); **$Y_{c/s}$** = cell yield coefficient (g dry cell mass per g tannic acid used); **$Y_{e/s}$** = tannase yield coefficient (U of enzyme per g tannic acid used); **$Y_{g/s}$** = gallic acid yield coefficient (g of gallic acid per g tannic acid used); **q_e** = tannase production rate (U/g/h); **q_g** = gallic acid production rate (mg/g/h); **q_c** = growth rate (mg/g/h); **S/s** = tannic acid consumed percentage

Table 3 Effect of nitrogen source (3 g/l) on tannase, gallic acid and cell mass formation by *B. licheniformis* KBR6.

Parameter	No N_2 source	Urea	NH_4Cl	$(NH_4)_2SO4$	NH_4NO_3	$NaNO_3$	Creatinine	Ammonium oxalate
C_{cm}	0.34	0.78	0.74	0.71	0.73	0.07	0.08	0.07
$Y_{c/s}$	0.03	0.08	0.07	0.07	0.07	0.01	0.01	0.01
$Y_{e/s}$	2.1	9.4	14.8	7.1	11.7	2.8	2.8	5.5
$Y_{g/s}$	0.011	0.052	0.082	0.068	0.08	0.028	0.022	0.022
q_e	0.11	0.47	0.74	0.355	0.585	0.14	0.14	0.275
q_g	ND	2.6	4.1	3.4	4.0	1.4	1.1	1.1
q_c	10	39	37	35	36	3	4	3
S/s	12	63.2	54	43.4	50.1	11.4	12.9	10.9

ND = Non detectable; **C_{cm}** = dry cell mass (g/l); **$Y_{c/s}$** = cell yield coefficient (g dry cell mass per g tannic acid used); **$Y_{e/s}$** = tannase yield coefficient (U of enzyme per g tannic acid used); **$Y_{g/s}$** = gallic acid yield coefficient (g of gallic acid per g tannic acid used); **q_e** = tannase production rate (U/g/h); **q_g** = gallic acid production rate (mg/g/h); **q_c** = growth rate (mg/g/h); **S/s** = tannic acid consumed percentage

Effect of nitrogen source

The nitrogen source is an essential prerequisite for metabolic reaction of any living cell. In order to find out the suitable nitrogen source for tannase and gallic acid production, *B. licheniformis* KBR6 was grown in presence of various nitrogen sources (Table 3), and each nitrogen source was added to the basal medium at a concentration of 3 g/l Urea and NH_4Cl showed a favourable effect in respect to growth of the organism as well as gallic acid and enzyme production. Though the maximum growth of the bacterium occurred in the presence of urea, but the higher enzyme induction was observed in the presence of NH_4Cl. It is also observed that the gallic acid yield coefficient, the specific tannase and gallic acid production rates were also higher in presence of NH_4Cl. In relation to higher growth of bacteria, the tannic acid consumption percentage in presence of urea is much more (63.2%) as compared to other nitrogen sources. A negligible effect was observed in presence of the other nitrogen sources like $NaNO_3$, creatinine and ammonium oxalate.

Effect of phosphate source

The effect of different inorganic phosphates (KH_2PO_4,

Table 4 Effect of phosphate source (0.5 g/l) on tannase, gallic acid and cell mass formation by *B. licheniformis* KBR6.

Parameters	No phosphate source	KH_2PO_4	K_2HPO_4	$(NH_4)_2HPO_4$
C_{cm}	0.12	0.95	0.84	0.62
$Y_{c/s}$	0.01	0.10	0.08	0.06
$Y_{e/s}$	1.0	16.5	14.2	6
$Y_{g/s}$	0.11	0.071	0.069	0.058
q_e	0.015	0.825	0.71	0.3
q_g	1	3.5	3.4	2.9
q_c	6	47	42	31
S/s	1.73	82.2	75.8	45

ND = Non detectable; **C_{cm}** = dry cell mass (g/l); **$Y_{c/s}$** = cell yield coefficient (g dry cell mass per g tannic acid used); **$Y_{e/s}$** = tannase yield coefficient (U of enzyme per g tannic acid used); **$Y_{g/s}$** = gallic acid yield coefficient (g of gallic acid per g tannic acid used); **q_e** = tannase production rate (U/g/h); **q_g** = gallic acid production rate (mg/g/h); **q_c** = growth rate (mg/g/h); **S/s** = tannic acid consumed percentage

Table 5 Effect of temperature on tannase and gallic acid production by *B. licheniformis* KBR6.

Parameter	20 °C	25 °C	30 °C	35 °C	40 °C	45 °C
C_{cm}	0.15	0.25	0.32	0.52	0.27	0.25
$Y_{c/s}$	0.05	0.06	0.07	0.08	0.07	0.06
$Y_{e/s}$	2.9	6.5	11.3	14.4	10.2	5.3
$Y_{g/s}$	0.0	3.3	5.2	6.5	4.5	2.0

C_{cm} = dry cell mass (g/l); $Y_{c/s}$ = cell yield coefficient (g dry cell mass per g tannic acid used); $Y_{e/s}$ = tannase yield coefficient (U of enzyme per g tannic acid used); $Y_{g/s}$ = gallic acid yield coefficient (g of gallic acid per g tannic acid used)

K_2HPO_4 and $(NH_4)_2HPO_4$) was studied for tannase and gallic acid production by *B. licheniformis* KBR6. It has been observed that phosphate source in tannic acid medium is essential for bacterial growth and tannase production (Table 4). In this experiment 0.5 g/l of all the phosphate sources were used. The maximum gallic acid production, tannase yield co-efficient and specific rate of enzyme synthesis by the organism occurred in presence of KH_2PO_4 (Table 4). Whereas, the efficiency of the organism was similar for growth, tannase and gallic acid production in presence of both KH_2PO_4 and K_2HPO_4.

Effect of temperature

To find out optimum temperature for growth and tannase production the organism was grown at different temperature (20-50 °C). It was found that the organism could able to grow in between 20-45 °C. But maximum cell mass growth, tannase and gallic acid yield coefficient were observed at 35 °C (Table 5).

Effect of initial medium pH

Significant growth of organism and tannase and gallic acid production by the organism were observed in the wide range of pH (3.0 to 6.5), but maximum cell mass growth, tannase yield coefficient were found at pH 5.0, whereas highest gallic acid yield coefficient was observed at pH 5.5 (Table 6).

Effect of metal ions

Different cations (0.05%, w/v) were added in tannic acid medium to study their effects on growth, tannase and gallic acid production (Table 7). It has been observed that Ca^{2+}, Mg^{2+} and Na^{+} ions in tannic acid medium increased growth of microorganism, tannase and gallic acid production. Other metal ions like Mn^{2+}, Co^{2+}, Ag^{2+}, Pb^{2+}, Hg^{2+} were inhibitory to bacterial growth as well as tannase and gallic acid production.

Discussion

Simultaneous production of tannase and gallic acid by bacteria has comparatively little report. In comparison to fungal strains, bacteria are highly sensitive to tannic acid (Scalbert 1991). The organism *B. licheniformis* KBR6 produced maximum tannase and gallic acid at its active log phases (18 h and 22 h, respectively). It has also been observed that tannase production was directly proportional to the early (up to 20 h) growth of the organism. In this regard, Deschamp et al. (1983) reported that *Corynebacterium* sp. able to produce maximum tannase at early stages (6 h) of growth but the organism attained highest growth after 24 h. Similar findings were reported by Selwal et al. (2010) where enzyme production by *Pseudomonas aeruginosa* IIIB 8914 was started from its early growth but reached the highest level at 24 h, after which it get decreased.

Increasing the initial tannic acid concentration from 10 to 15 g/l favoured the growth of the organism. Furthermore, increasing substrate concentration (above 15

Table 6 Effect of pH on tannase and gallic acid production by *B. licheniformis* KBR6.

Parameter	3.0	4.0	4.5	5.0	5.5	6.0	6.5
C_{cm}	0.12	0.25	0.32	0.43	0.38	0.28	0.20
$Y_{c/s}$	0.04	0.05	0.06	0.08	0.07	0.05	0.05
$Y_{e/s}$	4.2	5.6	8.2	15.2	9.3	7.5	5.2
$Y_{g/s}$	2.0	3.3	4.2	5.5	6.5	4.2	2.2

C_{cm} = dry cell mass (g/l); $Y_{c/s}$ = cell yield coefficient (g dry cell mass per g tannic acid used); $Y_{e/s}$ = tannase yield coefficient (U of enzyme per g tannic acid used); $Y_{g/s}$ = gallic acid yield coefficient (g of gallic acid per g tannic acid used)

Table 7 Effect of metal ions on growth, tannase and gallic acid production.

Ions (0.05% w/v)	Dry biomass (mg/ml)	Tannase (U/ml)	Gallic acid (mg/ml)
Control	0.35 ± 0.03	0.30 ± 0.06	0.42 ± 0.08
$AgCl_2$	ND	ND	ND
$BaCl_2$	0.12 ± 0.03	0.08 ± 0.02	0.13 ± 0.01
$CaCl_2$	0.36 ± 0.08	0.33 ± 0.04	0.45 ± 0.01
$CoCl_2$	0.13 ± 0.02	0.08 ± 0.03	0.12 ± 0.03
$CuCl_2$	ND	ND	ND
$HgCl_2$	0.09 ± 0.04	0.06 ± 0.01	ND
$MgCl_2$	0.35 ± 0.05	0.37 ± 0.01	0.48 ± 0.05
$MnCl_2$	ND	ND	ND
NaCl	0.42 ± 0.06	0.33 ± 0.08	0.45 ± 0.14
$PbCl_2$	0.18 ± 0.03	0.14 ± 0.06	0.12 ± 0.01
$CaCl_2$+ $MgCl_2$	0.85 ± 0.10	0.35 ± 0.07	0.45 ± 0.03
$MgCl_2$ + NaCl	0.72 ± 0.09	0.36 ± 0.10	0.45 ± 0.04
$CaCl_2$ + NaCl	0.63 ± 0.07	0.31 ± 0.11	0.38 ± 0.02
$MgCl_2$+ NaCl + $CaCl_2$	0.92 ± 0.11	0.43 ± 0.05	0.55 ± 0.09

ND = Non detectable

g/l) resulted significant inhibition of bacterial growth as well as other growth-related parameters. This reveals that growth of *B. licheniformis* KBR6 is highly regulated by the tannic acid concentration in medium. The retardation of growth at higher tannic acid concentration was due to toxicity of substrate itself as it contained large quantity of phenolic groups, which causes precipitation of macromolecules including proteins and carbohydrates (Lewis and Starkey 1969; Scalbert 1991). In this experiment, an increment in the specific production rate and yield of gallic acid was observed with increasing the initial tannic acid concentration up to 20 g/l and after which there were no significant alteration observed with further enhancement of tannic acid. The initial rapid production of gallic acid was due to increase in growth as well as higher tannase in the medium. Above 20 g/l of tannic acid both growth and tannase synthesis inhibited but due to availability of substrate (tannic acid) to low concentration of enzyme, the gallic acid formation rate was not drastically altered. In the present study, an initial tannic acid concentration of 15 g/l was found to be a better tannase inducer than 10 or 20 g/l. Earlier most of the reports indicated that a specific tannic acid concentration is suitable for microbial tannase biosynthesis (Hadi et al. 1994; Bradoo et al. 1997). Raghuwanshi et al. (2011) reported maximum tannase production (11.2 IU/ml) in medium containing 2.0% tannic acid by *Bacillus sphaericus*.

The formation of extracellular enzyme is found to be strongly affected by the nature of additional carbon source used. The addition of lactose in tannic acid media enhanced tannase production about 1.7-fold. The requirement of additional carbon sources for tannase synthesis by fungal strains in tannic acid media have been reported by many workers (Hadi et al. 1994; Bradoo et al. 1997). Hadi et al. (1994) mentioned that carbohydrates act as a catabolic inducer for tannase biosynthesis in *Rhizopus oryzae*. Mondal et al. (2000) and Mondal and Pati (2000) observed that the addition of low concentrations of additional carbon sources like glucose, lactose and sucrose (0.1%) were supportive for enzyme production by *B. licheniformis* KBR6.

The nitrogen source in the culture medium is very essential for microbial growth. Organisms assimilate specific nitrogen source from their surrounding environment and mainly use it as a precursor of amino acid as well as cellular protein synthesis. In this experiment, the bacterium *B. licheniformis* KBR6 synthesized more tannase as well as gallic acids in presence of NH_4Cl. Lekha and Lonsane (1997) have also reported the nutritional requirement of specific nitrogen source in culture media for fungal tannase production. Sabu et al. (2006) reported an increase in the tannase production by *Lactobacillus* sp. ASR-S1 with NH_4NO_3 supplement in the medium containing tamarind seed powder (TSP). Belur et al. (2010a) observed enhanced tannase production by *Serratia ficaria* in presence of casein hydrolysate and yeast extract with NH_4NO_3 in fermentation medium. Raghuwanshi et al. (2011) observed maximum tannase production by *Bacillus sphaericus* with 0.25% ammonium chloride. Organic nitrogen sources (beef extract, peptone, etc.) were not used in the medium as these form insoluble complexes with tannic acid. Added advantages of inorganic nitrogen

sources are that, they are less expensive than organic one and at the same time they avoid the problems of complex formation during enzyme purification.

The inorganic phosphate sources are very much essential for tannase production from *B. licheniformis* KBR6. Different phosphate compounds in the basal medium for tannase production have been found in earlier reports (Hadi et al. 1994; Bradoo et al. 1997; Lekha and Lonsane 1997). This report is in accordance with the results reported by Das Mohapatra et al. (2009), where enzyme production by *B. licheniformis* KBR6 was optimised using KH_2PO_4.

It has been found that Ca^{2+}, Mg^{2+} and Na^{+} stimulated the tannase production by *B. licheniformis* KBR6. Micro- and macroelements act as an elementary composition of cell, but a particular ion has stimulatory effect to metabolic synthesis in specific group of microorganisms (Schlegel 1995). Beniwal et al. (2010) showed stimulatory effect of Ca^{2+} and Mg^{2+} ions for enzyme production by *Enterobacter cloacae* MTCC 9125.

Tannase is a most promising and applicable microbial enzyme in bioprocess industry. The enzymatic by product, gallic acid has also many uses in chemical industry. Both tannase and gallic acid can be produced by *B. licheniformis* KBR6 in tannic acid containing culture media. The optimal composition of this medium was tannic acid (15 g/l), glucose (2 g/l), NH_4Cl (3 g/l), KH_2PO_4 (0.5 g/l) and $MgCl_2$ (0.5 g/l). In this minimal medium bacterium can produce tannase in large amounts at short period of cultivation in comparison to other tannase producing fungi.

References

Aguilar-Zarate P, Cruz MA, Montañez J, Rodriguez-Herrera R, Wong-Paz JE, Belmares RE, Aguilar CN (2015) Gallic acid production under anaerobic submerged fermentation by two bacilli strain. Microb Cell Fact 14:209.

Aissam H, Errachidi F, Penninckx MJ, Merzouki M, Benlemlih M (2005) Production of tannase by *Aspergillus niger* HA37 growing on tannic acid and olive mill waste waters. World J Microbiol Biotechnol 21:609-614.

Aracri FM, Cavalcanti RMF, Guimaraes LHS (2019) Extracellular tannase from *Aspergillus ochraceus*: influence of the culture conditions on biofilm formation, enzyme production, and application. J Microbiol Biotechnol 29(11):1749-1759.

Bajpai B, Banerjee T, Patil S (1999) Gallotannin hydrolysis by immobilized fungal mycelia in a packed bed bioreactor. Indian J Exp Biol 37:94-97.

Bajpai B, Patil S (1996) Tannin acyl hydrolase (EC3.1.1.20) activity of *Aspergillus, Penicillium, Fusarium* and *Trichoderma.* World J Microbiol Biotechnol 12:217-220.

Bajpai B, Patil S (1997) Induction of tannin acyl hydrolase (EC 3.1.1.20) activity in some members of fungi imperfecti. Enzyme Microb Technol 20:612-614.

Banerjee D, Mondal KC, Pati BR (2001) Production and characterization of extracellular and intracellular tannase from newly isolated *Aspergillus aculeatus* DBF 9. J Basic Microbiol 41(6):313-318.

Barthomeuf C, Regerat F, Pourrat H (1994) Production, purification and characterization of a tannase from *Aspergillus niger* LCF 8. J Ferment Bioeng 77(3):320-323.

Belur PD, Mugeraya G, Kuppalu NR (2010a) Temperature and pH stability of a novel cell- associated tannase of *Serratia ficaria* DTC. Int J Biotechnol Biochem 6(5):667-674.

Beniwal V, Chhokar V, Singh N, Sharma J (2010) Optimization of process parameters for the production of tannase and gallic acid by *Enterobacter cloacae* MTCC 9125. J American Sci 6(8):389-397.

Biswas I, Mitra D, Bandyopadhyay AK, Das Mohapatra PK (2020) Contributions of protein microenvironment in tannase industrial applicability: An in-silico comparative study of pathogenic and non-pathogenic bacterial tannase. Heliyon 6:e05359.

Bradoo S, Gupta R, Saxena RK (1997) Parametric optimization and biochemical regulation of extracellular tannase from *Aspergillus japonicus*. Process Biochem 32(2):135-139.

Cavalcanti RMF, Martinez MLL, Oliveira WP, Guimaraes LHS (2020) Stabilization and application of spray-dried tannase from *Aspergillus fumigatus* CAS21 in the presence of different carriers. 3 Biotech 10:177.

Coggon P, Sanderson GW (1972) Manufacture of instant tea. Patent Ger. offen 2.304 073 (cl. A. 23f.) 16 August 1973.

Das Mohapatra PK, Mondal KC, Pati BR (2005) Effect of inorganic constituents on growth and tannase production by *Bacillus licheniformis* KBR6. Ind J Biol Sci 70:68-72.

Das Mohapatra PK, Mondal KC, Pati BR (2006). Production of tannase through submerged fermentation of tannin-containing plant extracts by *Bacillus licheniformis* KBR6. Pol J Microbiol 55(4):297-301.

Das Mohapatra PK, Pati BR, Mondal KC (2009) Effect of amino acids on tannase biosynthesis by *Bacillus licheniformis* KBR6. J Microbiol Immunol Infect 42(2):172-175.

Deschamps AM, Lebeault JM (1984) Production of gallic acid from tara tannins by bacterial strains. Biotechnol Lett 6(4):237-242.

Deschamps AM, Otuk G, Lebeault JM (1983) Production of tannase and degradation of chestnut tannin by bacteria. J Ferment Technol 61:55-59.

Frost GM, Moss DA (1987) Production of enzymes by fermentation. In Rehm HJ, Reed G, Eds., Biotechnology, Vol. 7a, VCH, Weinheim, 65-102.

Gaathon A, Gross Z, Rozhanski M (1989) Propyl gallate: enzymatic synthesis in a reverse micelle system. Enzyme Microb Technol 11:604-609.

Hadi TA, Banerjee R, Bhattacharyya BC (1994) Optimization of tannase biosynthesis by a newly isolated *Rhizopus oryzae*. Bioprocess Eng 11:239-243.

Hagerman AE, Butler LG (1978) Protein precipitation method for the quantitative determination of tannin. J Agric Food Chem 26(4):809-812.

Iibuchi S, Minoda Y, Yamada K (1968) Studies on tannin acyl hydrolase of microorganisms part III. Purification of enzyme and some properties of it. Agr Biol Chem 32(7):803-809.

Jana A, Halder SK, Banerjee A, Paul T, Pati BR, Mondal KC, Das Mohapatra PK (2014) Biosynthesis, structural architecture and biotechnological potential of bacterial tannase: A molecular advancement. Bioresour Technol 157:327-340.

Kim HS, Jeon DY, Javaid HMA, Sahar NE, Lee HN, Hong SJ, Kim YM (2020) Bio-transformation of green tea infusion with tannase and its improvement on adipocyte metabolism. Enzyme Microb Technol 135:109496.

Lekha PK, Lonsane BK (1997) Production and application of tannin acyl hydrolase: State of the art. Adv Appl Microbiol 44:215-260.

Lewis JA, Starkey RL (1969) Decomposition of plant tannins by some soil microorganisms. Soil Sci 107(4):235-241.

Lokeswari N, Sriramireddy D, Sudhakararao P, Varaprasad B (2010) Production of gallic acid using mutant strain of *Aspergillus oryzae*. J Pharm Res 3(6):1402-1406.

Mondal KC, Banerjee D, Banerjee R, Pati BR (2001a) Production and characterization of tannase from *Bacillus cereus* KBR9. J Gen Appl Microbiol 47:263-267.

Mondal KC, Banerjee D, Jana M, Pati BR (2001b) Colorimetric assay method for determination of the tannin acyl hydrolase (EC 3.1.1.20) activity. Anal Biochem 295:168-171.

Mondal KC, Banerjee R, Pati BR (2000) Tannase production by *Bacillus licheniformis*. Biotechnol Lett 22:767-769.

Mondal KC, Pati BR (2000) Studies on the extracellular tannase from newly isolated *Bacillus licheniformis* KBR6. J Basic Microbiol 40(4):223-232.

Mukherjee G, Banerjee R (2003) Production of gallic acid. Biotechnological routes (Part I). Chimica Oggi 21(1):59-62.

Mukherjee G, Banerjee R (2006) Effects of temperature, pH and additives on the activity of tannase produced by a co-culture of *Rhizopus oryzae* and *Aspergillus foetidus*. World J Mirobiol Biotechnol 22:207-212.

Osawa R, Kuroiso K, Goto S, Shimizu A (2000) Isolation of tannin degrading *Lactobacilli form* humans and fermented foods. Appl Env Microbiol 66(7):3093-3097.

Osawa R, Mitsuoka T (1990) Selective medium for enumeration of tannin-protein complex degrading *Streptococcus* spp. in faeces of koalas. Appl Env Microbiol 56(11):3609-3611.

Patil DB, Das SK, Das Mohapatra PK, Nag A (2011) Physicochemical studies and optimization of gallic acid production from the seed coat of *Terminalia belerica* Roxb. Ann Microbiol 61:649-654.

Pourrat H, Regerat F, Morvan P, Pourrat A (1987) Microbiological production of gallic acid from *Rhus coriaria*. L. Biotechnol Lett 9(10):731-734.

Raghuwanshi S, Dutt K, Gupta P, Misra S, Saxena RK (2011) *Bacillus sphaericus*: The highest bacterial tannase producer with potential for gallic acid synthesis. J Biosci Bioeng 111(6):635-640.

Rajakumar GS, Nandy SC (1983) Isolation, purification, and some properties *of Penicillium chrysogenum* tannase. Appl Environ Microbiol 46(2):525-527.

Sabu A, Augur C, Swati C, Pandey A (2006) Tannase production by *Lactobacillus* sp. ASR-S1 under solid-state fermentation. Proc Biochem 41:575-580.

Scalbert A (1991) Antimicrobial properties of tannins. Phytochem 30(12):3875-3883.

Schlegel HG (1995) Growth of microorganisms. In General Microbiology, Seventh ed., Cambridge University Press, 193-194.

Selwal MK, Yadav A, Selwal KK, Aggarwal NK, Gupta R, Gautam SK (2010) Optimization of cultural conditions for tannase production by *Pseudomonas aeruginosa* IIIB 8914 under submerged fermentation. World J Microbiol Biotechnol 26:599-605.

Sharma S, Agarwal L, Saxena RK (2007) Statistical optimization for tannase production from *Aspergillus niger* under submerged fermentation. Indian J Microbiol 47:132-138.

Acta Biologica Szegediensis

Volume 64(2):159-171, 2020
Acta Biologica Szegediensis
http://abs.bibl.u-szeged.hu/index.php/abs
DOI:10.14232/abs.2020.2.159-171

ARTICLE

Structure-based assortment of herbal analogues against spike protein to restrict COVID-19 entry through hACE2 receptor: An *in-silico* approach

Sourav Santra[1#], Sasti Gopal Das[1#], Suman Kumar Halder[2], Kuntal Ghosh[3], Amrita Banerjee[4], Amiya Kumar Panda[1,5] and Keshab Chandra Mondal[1,2*]

[1]BIF Center, Vidyasagar University, Midnapore-721102, West Bengal, India
[2]Department of Microbiology, Vidyasagar University, Midnapore-721102, West Bengal, India
[3]Department of Biological Sciences, Midnapore City College, Midnapore-721129, West Bengal, India
[4]Department of Biotechnology, Oriental Institute of Science & Technology, Midnapore-721102, West Bengal, India
[5]Department of Chemistry and Chemical Technology, Vidyasagar University, Midnapore-721102, West Bengal, India

ABSTRACT On-going global pandemic COVID-19 has spread all over the world and has led to more than 1.97 million deaths till date. Natural compounds may be useful to protecting health in this perilous condition. Mechanism of shuttle entry of SARS-COV-2 virus is by interaction with viral spike protein with human angiotensin-converting enzyme-2 (ACE-2) receptor. To explore potential natural therapeutics, 213 important phytochemicals of nine medicinal plants *Aconitum heterophyllum*, *Cassia angustifolia*, *Cymbopogon flexuosus*, *Cymbopogon martinii*, *Nux vomica*, *Phyllanthus urinaria*, *Swertia chirayita*, *Justicia adhatoda*, *Vetiveria zizanioides* were selected for in-silico molecular docking against the spike protein of SARS-COV-2 and compared with recently prescribed drug chloroquine, ramdesivir, lopinavir and hydroxychloroquine. Results revealed that rhamnocitrin of *P. urinaria*, 1,5-dihydroxy-3,8-dimethoxyxanthone of *S. chirayita* and laevojunenol of *V. zizanioides* potentially binds with the receptor binding site of SARS-COV-2 spike glycoprotein and more robustly destabilized the RBD-ACE-2 binding over chloroquine, ramdesivir, lopinavir and hydroxychloroquine. It was also found that laevojunenol, rhamnocitrin, and 1,5-dihydroxy-3,8-dimethoxyxanthone qualified the criteria for drug-likeness as per Lipinski rule. After attachment of the selected phytochemical with the spike protein the affinity of the later towards ACE-2 was minimized and the effect of 1,5-dihydroxy-3,8-dimethoxyxanthone and laevojunenol was superior. Hence, rhamnocitrin of *P. urinaria*, 1,5-dihydroxy-3,8-dimethoxyxanthone of *S. chirayita* and laevojunenol of *V. zizanioides*, are potential therapeutic molecules for SARS-COV-2, which upon binding with spike protein changes the affinity of the spike towards ACE-2 and therefore restrict the entry of the virus into a human cell. Subsequent clinical validation is needed to confirm these phytochemicals as drugs to combat COVID-19. **Acta Biol Szeged 64(2):159-171 (2020)**

KEY WORDS
angiotensin-converting-enzyme-2
COVID-19
medicinal plants
molecular docking
spike glycoprotein

ARTICLE INFORMATION
Submitted
12 December 2020.
Accepted
17 January 2021.
***Corresponding author**
E-mail: mondalkc@gmail.com

INTRODUCTION

Presently, the world's population is in under tremendous pressure, due to COVID-19 pandemic. Worldwide, more than 90 million people are infected and among them more than 1.97 million people died till date (as per WHO). Deaths are increasing by leaps and bounds due to community transmission and the scientists are deliberately trying to find drugs from natural and synthetic origin to use as a potential antiviral agent. The entry of the COVID-19 virus into human cells is mediated via transmembrane spike (S) glycoprotein that contributes to the cell receptor binding, tissue tropism, and pathogenesis. Spike protein has conserved motifs have three domains namely S1, S2 and N. The S1-domain has a conserved receptor-binding domain (RBD), which recognizes the angiotensin-converting enzyme-2 (ACE-2) receptor (Bourgonje et al. 2019; Yao et al. 2020) which is the initial step of entry mechanism into the host cells (Walls et al. 2020; Wang et al. 2020). The expression of ACE-2 is higher in the intestinal epithelium and pulmonary pneumocytes than other tissues. The interaction of S protein and ACE-2 results in imbalance of the renin-angiotensin system in the lungs as well as immunological intolerance, which leads to acute lung injury such as pulmonary oedema (Yao et al. 2020; Yang et al. 2007; Kuba et al. 2005). The entry of coronavirus into susceptible cells is a complex process that requires the concerted action of receptor binding and proteolytic processing of the S protein,

# Both the authors contributed equally.

which endorses virus-cell fusion (Walls et al. 2020). In recent time, chloroquine, hydroxychloroquine, remdesivir, lopinavir, arbidol are drugs of choice for COVID treatment but they have limitations and side effects (Wang et al. 2020; Cao et al. 2007; Rismanbaf et al. 2020; Yazdany et al. 2020). Under this emergency, several conventional and non-conventional medicines are being tested around the world to restrict viral transmission and to develop effective therapeutics. In this perspective, medicinal plants especially those employed in traditional medicine for the treatments of virus-allied symptoms have recently come under scientific surveillance as they contain bioactive compounds that could be useful for development of potential drugs against COVID like viral diseases.

Since ancient human civilization, many phytochemicals of diversified unique properties are being explored for customized treatments of variety of diseases owing to their analgesic, antipyretic, antioxidative, anticancer, immunomodulatory, anti-inflammatory, antimicrobial, anti-carcinogenic and many other notable properties (Jaiswal and Williams 2017; Suresh and Abraham 2020; Koparde et al. 2019). In global perspective, Lion's share of the world population still depends on plant derived products to formulate drugs to treat their health problems. Some selective herbal products have low cytotoxicity and high bioavailability and are effective for the treatment of different viral diseases (Divya et al. 2020). The potential biological roles of plant's secondary metabolites have now been explored in the blockage of virus particle's entry, their multiplication and pathogenesis (ul Qamar et al. 2020). Among the different plants, *P. urinaria* (commonly called gripe weed) have potential ethnomedicinal importance against asthma, bronchitis, cough, tuberculosis, fever, influenza, digestive pain, conjunctivitis and anaemia. Besides, this plant also effective against hepatitis A-C, herpes and HIV (Singh 2018). *S. chirayita* (also is known as *chirayta*) is useful for the cure of different diseases and containing anti-inflammatory, antioxidant and antiviral compounds. *S. chirayita* has also very good antiviral activity against herpes and papilloma virus (Singh 2018; Kumar and Van Staden 2016). Likewise, *V. zizanioides* (vetivergrass; Hindi: Khas-Khas) used to treat many skin and nervous disorders and claimed to inhibit the dengue NS2B–NS3 virus (Lavanya et al. 2016). *A. heterophyllum* also helps in the treatment of common cold, flu, and malaria bronchitis, persistent cough and upper respiratory tract infections (Paramanick et al. 2017). *C. flexuosus* commonly used against headaches, diabetes, rheumatism, hypertension, wounds, fever and bone fractures (Rajeswara Rao 2013). *Nux vomica* is used against colds and flu, particularly in the early stages of any virus infection (Singh 2018). These all plants are selected based on their ethno-botanical importance and the study of literature. The present study was aimed to explore the interaction of natural compounds of *A. heterophyllum, C. angustifolia, C. flexuosus, C. martinii, N. vomica, P. urinaria, S. chirayita, J. adhatoda, V. zizanioides* with the spike protein of the SARS-CoV-2 virus. The 3D structure of S protein was constructed and its binding ability against the 213 phytochemicals of the above-mentioned medicinal plants were evaluated. The post binding effect of the conjugated spike protein with ACE-2 was also addressed in order to explore the effectiveness of natural compounds as potential anti-COVID drug.

Table 1. Synthetic compounds and their binding energy with SARS-COV-2 spike glycoprotein.

SI No.	Compound names	Binding energy (kcal/mol)
1	Ramdesivir	-8.1
2	Lopinavir	-11.8
3	Chloroquine	-6.7
4	Hydroxychloroquine	-6.6

MATERIALS AND METHODS

Retrieval of protein sequence and prediction of homologous structure

The reference spike glycoprotein YP_009724390.1 sequence of human corona virus SARS-COV-2 collected from NCBI. Three-dimensional structure of corona viral spike glycoprotein (PDB ID: 6VSB) and human Angiotensin Converting Enzyme-2 (ACE-2) (PDB ID: 4APH) were retrieved from RCSB Protein Data Bank (https://www.rcsb.org/) in PDB format and modelling of the spike glycoprotein (YP_009724390.1) was carried out in SWISS-MODEL server (Waterhouse et al. 2018) and further analysed by using PyMol (DeLano 2002). Quality assessment of this spike glycoprotein model was validated by PROCHECK by analysing the Ramachandran plot (Laskowski et al. 1993).

Retrieval of ligands structure

Three-dimensional structure of 213 natural compounds of *A. heterophyllum, C. angustifolia, C.flexuosus, C. martinii, N. vomica, P. urinaria, S. chirayita, J. adhatoda, V. zizanioides* and drugs remdesivir, lopinavir, chloroquine and hydroxychloroquine was retrieved from Indian Medicinal Plants, Phytochemistry and Therapeutics (IMPPAT) database (Mohanraj et al. 2018), PubChem (Kim et al. 2016) on the basis of literature survey and listed in Table 1-3.

Protein-ligand docking

Prior docking, the water molecules were removed from the

Table 2. List of natural plant derived compounds whose binding energy is higher than -7 kcal/mol when binds with SARS-COV-2 spike glycoprotein.

No	Compound names	Plant species	Binding energy (kcal/mol)	H-bond interaction
1	Hetidine	*A. heterophyllum*	-9.7	371
2	Isoatisine	*A. heterophyllum*	-8.7	-
3	Hetisinone	*A. heterophyllum*	-8.6	370, 489
4	Veratridine	*A. heterophyllum*	-8.5	115, 167
5	6-benzoylheteratisine	*A. heterophyllum*	-8.4	377, 379
6	Hetisine	*A. heterophyllum*	-8.4	370
7	Atidine	*A. heterophyllum*	-8.3	377, 379, 457
8	Beta-carotene	*A. heterophyllum*	-8.3	-
9	Atisine	*A. heterophyllum*	-8.2	455
10	Dihydroatisine	*A. heterophyllum*	-8.1	338, 339
11	Aricine	*A. heterophyllum*	-8	370, 457
12	Benzoylmesaconine	*A. heterophyllum*	-8	488
13	Lactone atisenol	*A. heterophyllum*	-8	457
14	Lappaconitine	*A. heterophyllum*	-7.6	357, 473, 475
15	6-acetylheteratisine	*A. heterophyllum*	-7.4	379
16	Heterophyllisine	*A. heterophyllum*	-7.4	489
17	Aconitine	*A. heterophyllum*	-7.3	-
18	Anisoylaconine	*A. heterophyllum*	-7.3	377, 457, 473
19	Hypaconitine	*A. heterophyllum*	-7.3	371, 373
20	Mesaconitine	*A. heterophyllum*	-7.3	371, 373
21	Phytosterols	*A. heterophyllum*	-7.3	457
22	Jesaconitine	*A. heterophyllum*	-7.2	165, 355
23	Isorhamnetin 3-gentiobioside	*C. angustifolia*	-8.4	369, 417, 457, 487, 489, 493
24	Kaempferol	*C. angustifolia*	-8.1	457, 477
25	Aloe-emodin	*C. angustifolia*	-7.7	457, 477
26	Tinnevellinglucoside	*C. angustifolia*	-7.6	371, 403, 409, 505
27	Sennaglucosides	*C. angustifolia*	-9.8	343, 370, 371, 453, 476, 478, 493
28	Emodin-8-glucoside	*C. angustifolia*	-8.9	369, 371, 375, 376, 405, 406, 409
29	Rhein	*C. angustifolia*	-8.6	-
30	Isorhamnetin	*C. angustifolia*	-8.6	457, 477
31	Arundoin	*C. flexuosus*	-8.7	-
32	Phytosterols	*C. flexuosus*	-7.8	457
33	Humulene	*C. flexuosus*	-7.5	457
34	Caryophylene oxide	*C. martinii*	-7	478
35	Stryvomicine A	*N. vomica*	-9.2	-
36	Beta-colubrine chloromethochloride	*N. vomica*	-8.8	457, 477
37	Alpha-colubrine chloromethochloride	*N. vomica*	-8.5	
38	Oleanolic acid	*P. urinaria*	-8.7	370, 457
39	Trans-8,9-Dihydro-benz(a)anthracene-8,9-diol	*P. urinaria*	-8.7	-
40	Corilagin	*P. urinaria*	-8.7	379, 457, 487, 493
41	Naringin	*P. urinaria*	-8.7	343, 375, 403, 405, 437
42	Furosin	*P. urinaria*	-8.7	417, 456, 457, 493, 494
43	Kaempferol 7-methyl ether 4'-glucoside	*P. urinaria*	-8.7	417, 456, 457, 493, 494
44	Gallocatechingallate	*P. urinaria*	-8.6	457
45	Ellagic acid	*P. urinaria*	-8.5	371, 405, 408, 409
46	Cleistanthol	*P. urinaria*	-8.4	-
47	Quercetin	*P. urinaria*	-8.4	371, 455, 457, 477
48	Daucosterol	*P. urinaria*	-8.4	377, 488
49	Spruceanol	*P. urinaria*	-8.3	457, 490
50	Quercitrin	*P. urinaria*	-8.3	457, 488

Table 2. Continued.

No	Compound names	Plant species	Binding energy (kcal/mol)	H-bond interaction
51	13-Methyl-6,7,8,9,11,12,14,15,16,17-decahydrocyclopenta[a]phenanthrene-3,17-diol	*P. urinaria*	-8.2	-
52	Betulinic acid	*P. urinaria*	-8.2	408, 456, 457
53	Epigallocatechingallate	*P. urinaria*	-8.2	369, 379, 457, 487, 490
54	Rutin	*P. urinaria*	-8.2	372, 374, 375, 403, 405, 437, 439, 453, 505
55	Epicatechin-3-gallate	*P. urinaria*	-8.1	381, 417, 457, 487, 489
56	Beta-sitosterol	*P. urinaria*	-8.1	-
57	Glochidiol	*P. urinaria*	-8	408
58	Epicatechin	*P. urinaria*	-7.9	379, 381, 487, 489
59	Epigallocatechin	*P. urinaria*	-7.9	379, 381, 487, 489
60	Betulin	*P. urinaria*	-7.9	456, 457
61	Rhamnocitrin	*P. urinaria*	-7.9	379, 487, 489
62	Brevifolincarboxylic acid	*P. urinaria*	-7.8	375, 377, 415
63	Ethyl brevifolincarboxylate	*P. urinaria*	-7.5	371, 457, 477
64	Digallic acid	*P. urinaria*	-7.4	370, 457, 477, 478
65	Methyl brevifolincarboxylate	*P. urinaria*	-7.3	455, 457, 490
66	Urinatetralin	*P. urinaria*	-7.1	381
67	Episwertenol	*S. chirayita*	-9.7	-
68	Hopenol B	*S. chirayita*	-9.3	-
69	Erythrodiol	*S. chirayita*	-9.1	-
70	Friedlein	*S. chirayita*	-9.1	357
71	Chiratenol	*S. chirayita*	-8.9	-
72	Kairatenol	*S. chirayita*	-8.7	-
73	Swertanone	*S. chirayita*	-8.7	-
74	Oleanolic acid	*S. chirayita*	-8.6	-
75	Taraxasterol acetate	*S. chirayita*	-8.5	378, 408
76	Swertenol	*S. chirayita*	-8.3	466
77	Amarogentin	*S. chirayita*	-8.2	370, 371, 372, 457, 490
78	Swertiapuniside	*S. chirayita*	-8.1	372, 403, 439, 505, 506
79	Ursolic acid	*S. chirayita*	-8.1	457
80	1,8-Dihydroxy-2,6-dimethoxy-9H-xanthen-9-one	*S. chirayita*	-7.9	-
81	Mangiferin	*S. chirayita*	-7.9	379, 456, 457, 492
82	1,5-dihydroxy-3,8-dimethoxyxanthone	*S. chirayita*	-7.7	406, 409, 417
83	Swertianin	*S. chirayita*	-7.6	415, 377, 369
84	Decussatin	*S. chirayita*	-7.5	457, 477
85	Demethylbellidifolin	*S. chirayita*	-7.5	409
86	Isobellidifolin	*S. chirayita*	-7.5	371, 457
87	Swerchirin	*S. chirayita*	-7.5	371, 457
88	7,11-Epoxy-eremophila-1,9-dien-8-α-ol	*V. zizanioides*	-8.2	457
89	Eudesmane	*V. zizanioides*	-8	-
90	Cadalene	*V. zizanioides*	-7.9	-
91	Khusene	*V. zizanioides*	-7.9	-
92	10-epi-Acora-3,11-dien-15-al	*V. zizanioides*	-7.8	457, 478
93	Beta-vetivone	*V. zizanioides*	-7.8	457
94	15-nor-prezizaan-7-one	*V. zizanioides*	-7.7	457, 478
95	Isokhusimol	*V. zizanioides*	-7.7	457
96	Isovalencenol	*V. zizanioides*	-7.7	457, 477
97	Khusiol	*V. zizanioides*	-7.7	-
98	(1S,2S,8R)-2,6,7,7-tetramethyltricyclo[6.2.1.01,5] undecane	*V. zizanioides*	-7.7	-

Table 2. Continued.

No	Compound names	Plant species	Binding energy (kcal/mol)	H-bond interaction
99	Acora-2,4-diene	*V. zizanioides*	-7.6	-
100	Beta-cadinene	*V. zizanioides*	-7.6	-
101	Beta-vetivenene	*V. zizanioides*	-7.6	-
102	Khusimone	*V. zizanioides*	-7.6	-
103	Khusinol oxide	*V. zizanioides*	-7.6	478
104	7,15-epoxyprezizaane	*V. zizanioides*	-7.5	370
105	10-epi-Acor-3-en-5-one	*V. zizanioides*	-7.5	-
106	Allo-khusiol	*V. zizanioides*	-7.5	370
107	Alpha-vetispirene	*V. zizanioides*	-7.5	-
108	Eremophilane	*V. zizanioides*	-7.5	-
109	Khusilal	*V. zizanioides*	-7.5	457
110	Khusinodiol	*V. zizanioides*	-7.5	457
111	Khusitone	*V. zizanioides*	-7.5	-
112	13-nor-Eudesm-5-en-11-one	*V. zizanioides*	-7.4	457
113	Cedrane	*V. zizanioides*	-7.4	-
114	Epizizanal	*V. zizanioides*	-7.4	-
115	Isovetiselinenol	*V. zizanioides*	-7.4	-
116	Khusinol	*V. zizanioides*	-7.4	490
117	Laevojunenol	*V. zizanioides*	-7.4	489
118	11,12,13-tri-nor-cis-Eudesm-5-en-7-one	*V. zizanioides*	-7.3	-
119	Beta-Vetispirene	*V. zizanioides*	-7.3	-
120	Isokhusenic acid	*V. zizanioides*	-7.3	-
121	Isokhusinol oxide	*V. zizanioides*	-7.3	489
122	Nootkatone	*V. zizanioides*	-7.3	-
123	Cadin-4-en-10-ol	*V. zizanioides*	-7.2	-
124	Khusimol	*V. zizanioides*	-7.2	-
125	Ac1lb1ow	*V. zizanioides*	-7.1	-
126	Alpha-vetivone	*V. zizanioides*	-7.1	-
127	Cyclocopacamphenol	*V. zizanioides*	-7.1	457, 477
128	Epizizanone	*V. zizanioides*	-7.1	-
129	Khusol	*V. zizanioides*	-7.1	370

three-dimensional structure of the spike glycoprotein. The molecular docking study was performed for exploration of the binding affinity of the spike glycoprotein with the 213 selected natural phytochemicals in addition with remdesivir, lopinavir, chloroquine and hydroxychloroquine through AutoDock Vina [version 1.1.2] (Trott and Olson 2010). SARS-COV-2 spike protein S1 domain chains (A, B, C) have common reference active site of K417, G446, Y449, F486, N487, Y489, Q493, Q498, T500, N501, G502, Y505 (Walls et al. 2020; Wang et al. 2020; Yan et al. 2020; Lan et al. 2020). These sites were initially targeted for grid based molecular docking study with the selected natural phytochemicals. The grid box dimensions were 68 Å × 90 Å × 58 Å with a spacing of 1 Å and center set at coordinate 219.172, 224.276 and 287.134 in x, y, and z axis, respectively, centring around the ACE-2 binding domain. An array of ligands was screened based on binding energy at active site amino acid residues, and subsequently blindly docked with SARS-COV-2 spike protein using AutoDock with new grid dimension to cover the whole spike glycoprotein. The grid coordinate considered as 126 Å × 126 Å × 126 Å with a spacing of 1 Å and center set to coordinate 211.921, 226.209 and 247.631 in the x, y and z axis with 24 exhaustiveness, respectively. During blind docking, the size of grids was kept at maximum covering the whole surface of the protein to allow the ligand to bind in an unbiased binding pocket. Polar H charges of the Gasteiger-type were assigned to the receptor molecule and torsions were detected. Default settings of AutoDock Vina were used for docking studies.

Table 3. List of natural plant derived compounds whose binding energy is less than -7 kcal/mol when binds with SARS-COV-2 spike glycoprotein.

No	Compound names	Plant species	Binding energy (kcal/mol)
1	Phytosterols	*A. heterophyllum*	-6.9
2	Delphatines	*A. heterophyllum*	-6.7
3	Lycoctonine	*A. heterophyllum*	-6.6
4	Dl-borneol	*C. flexuosus*	-6
5	Citronellal	*C. flexuosus*	-5.7
6	Citral	*C. flexuosus*	-5.7
7	Methyleugenol	*C. flexuosus*	-5.6
8	Myrcene	*C. flexuosus*	-5.1
9	6-Methylhept-5-en-2-ol	*C. flexuosus*	-5
10	Triacontane	*C. flexuosus*	-4.9
11	Decanal	*C. flexuosus*	-4.8
12	Trans-2-Hepten-1-ol	*C. flexuosus*	-4.5
13	Beta-caryophyllene	*C. martinii*	-6.6
14	3-carene	*C. martinii*	-6.5
15	Carvylacetate	*C. martinii*	-6.4
16	P-cymene	*C. martinii*	-6.3
17	Alpha-terpineol	*C. martinii*	-6.3
18	Dihydrocarvone	*C. martinii*	-6.3
19	(-)-3-carene	*C. martinii*	-6.3
20	Beta-terpineol	*C. martinii*	-6.2
21	Perillyl alcohol	*C. martinii*	-6.2
22	D-carvone	*C. martinii*	-6.2
23	(-)-cis-carveol	*C. martinii*	-6.1
24	Cis,cis-farnesol	*C. martinii*	-6.1
25	Alpha-farnesene	*C. martinii*	-6.1
26	Limonene	*C. martinii*	-5.9
27	Eucalyptol	*C. martinii*	-5.8
28	Dihydrocarveol	*C. martinii*	-5.7
29	Geranyl acetate	*C. martinii*	-5.6
30	Geraniol	*C. martinii*	-5.3
31	6-Methyl-5-hepten-2-one	*C. martinii*	-5.2
32	6-Octen-1-ol, 3,7-dimethyl-, (R)-	*C. martinii*	-5.2
33	Geranyl butyrate	*C. martinii*	-5.1
34	(-)-Linalool	*C. martinii*	-4.9
35	2-Nonanol	*C. martinii*	-4.7
36	1,5-Hexadiyne	*J. adhatoda*	-5.4
37	2-(2,5-Hexadiynyloxy)tetrahydro-2H-pyran	*J. adhatoda*	-5.2
38	Heptasiloxane,1,1,3,3,5,5,7,7,9,9,11,11,13,13-tetradecamethyl-	*J. adhatoda*	-5.1
39	Hexasiloxane,1,1,3,3,5,5,7,7,9,9,11,11-dodecamethyl-	*J. adhatoda*	-4.7
40	Octasiloxane,1,1,3,3,5,5,7,7,9,9,11,11,13,13,15,15-hexadecamethyl-	*J. adhatoda*	-4.3
41	Pentasiloxane,1,1,3,3,5,5,7,7,9,9-decamethyl-	*J. adhatoda*	-4.3
42	Nirtetralin	*P. urinaria*	-6.9
43	Phyltetralin	*P. urinaria*	-6.9
44	Lintetralin	*P. urinaria*	-6.8
45	Hypophyllanthin	*P. urinaria*	-6.7
46	Syringin	*P. urinaria*	-6.7
47	Virgatusin	*P. urinaria*	-6.7
48	Dehydrochebulic acid trimethyl ester	*P. urinaria*	-6.6
49	Ferulic acid	*P. urinaria*	-6.5
50	5-demethoxyniranthin	*P. urinaria*	-6.5

Table 3. Continued.

No	Compound names	Plant species	Binding energy (kcal/mol)
51	Cucurbic acid	*P. urinaria*	-6.3
52	Methyl gallate	*P. urinaria*	-6.2
53	Niranthin	*P. urinaria*	-6.2
54	4-O-Methylgallic acid	*P. urinaria*	-6
55	Phyllanthin	*P. urinaria*	-5.9
56	(6r)-menthiafolic acid	*P. urinaria*	-5.9
57	4-hydroxybenzaldehyde	*P. urinaria*	-5.7
58	5-hydroxymethylfurfural	*P. urinaria*	-4.6
59	Dl-tryptophan	*S. chirayita*	-6.9
60	Gentianine	*S. chirayita*	-6.6
61	Enicoflavine	*S. chirayita*	-5.5
62	Dl-arginine	*S. chirayita*	-5.2
63	Nonacosyl_hentriacontanoate	*S. chirayita*	-5
64	Octadecanoate	*S. chirayita*	-4.8
65	Glutamate	*S. chirayita*	-4.2
66	Amorphane	*V. zizanioides*	-7
67	6,12-Epoxy-elema-1,3-diene	*V. zizanioides*	-6.9
68	13-nor-4,5-Epoxyeudesm-6-en-11-one	*V. zizanioides*	-6.9
69	Bisabolane	*V. zizanioides*	-6.7
70	3-carene	*V. zizanioides*	-6.5
71	15-nor-Funebran-3-one	*V. zizanioides*	-6.5
72	Beta-pinene	*V. zizanioides*	-6.5
73	Cis-Isoeugenol	*V. zizanioides*	-6.5
74	Cyclocopacamphan-12-al	*V. zizanioides*	-6.5
75	Isobisabolene	*V. zizanioides*	-6.5
76	Nootkatol	*V. zizanioides*	-6.4
77	Alpha-terpineol	*V. zizanioides*	-6.3
78	2-Methoxy-4-vinylphenol	*V. zizanioides*	-5.8
79	4-vinylphenol	*V. zizanioides*	-5.8
80	Eucalyptol	*V. zizanioides*	-5.8
81	Eugenol	*V. zizanioides*	-5.6
82	O-cresol	*V. zizanioides*	-5.5
83	M-cresol	*V. zizanioides*	-5.4
84	Oleamide	*V. zizanioides*	-5

Lipinski rule for validation of drug-likeness

Lipinski's rule of 5 helps to find out drug likeness of any experimental compound. Five rules are (i) molecular mass of the drug should be less than 500 Dalton, (ii) high lipophilicity (expressed as LogP less than 5), (iii) less than 5 hydrogen bond donors, (iv) less than 10 hydrogen bond acceptors, (v) molar refractivity should be between 40-130. The predictable drugs sites Lipinski Rule were checked by using SCFBio web-based database (Lipinski 2004).

Protein-protein docking

Spike glycoprotein (in free form and complex with selected phytochemicals) (Table 4) and ACE-2 were considered for protein-protein docking with receptor-binding domain (RBD) of the spike glycoprotein (S1 subunit) using HDOCK server (Yan et al. 2020). Precisely, the 19-41 amino acid resides of ACE-2 was employed for the docking with 417-505 amino acids of spike glycoprotein S1 subunit. In total, four ACE-2 docking experiments were performed with spike glycoprotein as per specification stated in Table 4.

RESULTS AND DISCUSSION

Homologous structure prediction of spike glycoprotein and its validation

The study of molecular docking and the ligand-based

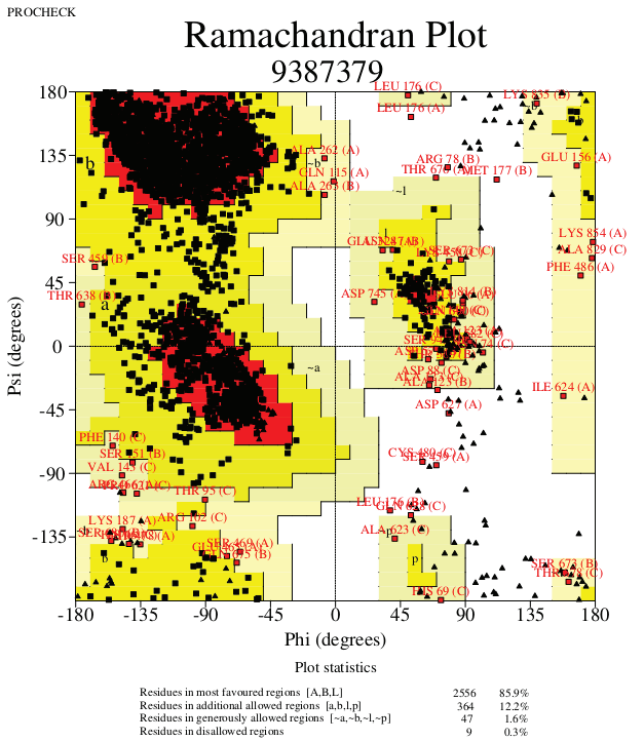

Figure 1. Ramachandran plot of COVID-19 SARS-CoV-2 spike glycoprotein.

computer-aided drug discovery approach involves energy, affinity and three-dimensional structural conformations-based analysis of ligands interaction with the target of interest. The binding ability of a ligand molecule to a specific target site depends on occurrence of proper cleft, proper hydrogen bonding and the nature of residues present at the target site and their interactive energy balance (Tripet et al. 2004). The binding affinity of a ligand for a targeted receptor is measured by binding energy. Lower binding energy implies that binding affinity is high whereas higher energy endorses the reverse (Zhou et al. 2020). In the present study, three-dimensional (3D) homologous structure of spike glycoprotein was generated from the reference protein sequence (YP_009724390.1) using the cryo-EM structure (6VSB) through SWISS-MODEL server and further analyzed through PyMol. PyMol is a molecular visualization tool; used here to align the predicted three-dimensional structure of the spike glycoprotein of SARS-CoV-2 into the cryo-EM structure of 6VSB. The Root-mean-square deviation (RMSD) of this model was computed as 0.278Å. Further, the predicted 3D structure was validated through RAMACHANDRAN plot using PROCHECK. The result revealed that 85.9% belongs to the most favourable region, 12.2% in allowed region, 1.6% in the generously allowed region, and only 0.3% in disallowed region (Fig. 1). Though cryo EM structure of SARS-COV-2 spike glycoprotein (6VSB) was available, some amino acids were not resolved properly at different locations due to its 3.46 Å resolution. To get the complete structure of spike, homology modelling was performed. Good quality structure with 98.1% residues at ordered form indicated the proper conformational packaging of protein.

Assessment of binding affinity of 213 ligands with spike protein and their subsequent screening

A spike glycoprotein of SARS-COV-2 has three domains namely S1, S2 and N. The S2 domain intercedes the membrane fusion process and the S1 domain utilizes human angiotensin-converting enzyme-2 (hACE-2) as the receptor to infect human cells (Pandey et al. 2020). The literature review revealed that the receptor-binding domain (RBD) of the S1 subunit of spike protein binds with the target cell ACE-2 receptor and forms the RBD-ACE-2 complex. According to recent report, ACE-2 could mediate SARS-CoV-2 binding by spike protein key residues of K417, G446, Y449, F486, N487, Y489, Q493, Q498, T500, N501, G502, Y505 (Walls et al. 2020; Wang et al. 2020; Yan et al. 2020; Lan et al. 2020). In this in-silico study, we attempted to explore the binding affinity of 213 phytochemicals in addition to remdesivir, lopinavir, chloroquine and hydroxychloroquine with the active site residues of the spike glycoprotein (Fig. 2A). The selection of the natural ligands of plant origin was primarily made on the basis of (i) minimal binding energy (<-7 kcal/mol) and (ii) formation of at least one H-bond with the active site residues (417-505) in the S1 subunit of the spike glycoprotein. These criteria were fulfilled by 23 compounds which were further blindly docked with whole spike glycoprotein

Table 4. Different complex of spike glycoprotein (free and ligand bound) and ACE2 docking in HDOCK and their binding score.

Molecular docking complex	HDOCK score	RMSD value
Spike glycoprotein dock with ACE2	-360.86	*0.51*
Spike glycoprotein and rhamnocitrin dock with ACE2	-360.86	*0.51*
Spike glycoprotein and 1,5-dihydroxy-3,8-dimethoxyxanthone dock with ACE2	-243.15	*481.28*
Spike glycoprotein and laevojunenol dock with ACE2	-238.13	*480.02*

Table 5. Physicochemical properties of natural plant derived compounds and their binding energy during molecular docking. Different capital alphabets before amino acids indicate different polypeptide chains.

Compound name	Amino acids at docked sites	Lipinski criteria for drug-likeness				
		MW (g/mol)	Hydrogen bond donor	Hydrogen bond acceptor	XLogP3-AA	Molar refractivity
Rhamnocitrin	B/PHE-490, B/SER-477, C/SER-371, B/ARG-457,	300.26	3	6	2.2	77.272881
1,5-dihydroxy-3,8-dimethoxyxanthone	B/GLU-406, B/GLN-409, B/LYS-417	288.26	2	6	2.37	77.145782
Laevojunenol	B/TYR-489	222.37	1	1	3.78	77.145782

(Table 1-2) to analyze the affinity of selected molecules at the active site of spike glycoprotein (417-505) instead of other cleft and pockets. It was evident that rhamnocitrin of *P. urinaria*, 1,5-dihydroxy-3,8-dimethoxyxanthone of *S. chirayita*, laevojunenol and khusinol of *V. zizanioides* are capable to bind with active site residues of the S1 subunit of spike glycoprotein (S) in 0 (zero) RMSD pose (Fig. 2). So, these three phytochemicals are the best ligand molecules for spike protein active site which restricts smooth interaction between spike and ACE-2.

The molecular docking study of spike protein with remdesivir revealed that this drug has the capability to bind with S1 domain through H-bond with the ARG403, ASP405 and ARG408 of B and PHE374, SER375 and TYR508 of C chain with binding energy of -8.1 kcal/mol. However, though remdesivir binds with the spike protein at S1 domain, but the site of attachment is not the active site of spike protein. Lopinavir interacts with the S2 subunit through amino acid residues GLN957, THR961 and associated with binding energy of -11.8 kcal/mol. Alongside, it was also revealed that chloroquine and hydroxychloroquine binds with LEU455, GLY485, PHE490,PRO491 and PRO559, PHE855, THR573, ILE587 residues of S2 domain having the binding energy of -6.7 and -6.3 kcal/mol, respectively (Table 3). It is evident that among the four drugs neither one is capable to bind at active site of spike glycoprotein.

The docking results were analysed based on a combination of binding energy, clustering score, shape complementarity, functional significance of the binding pocket and favourable interactions including H bonds.

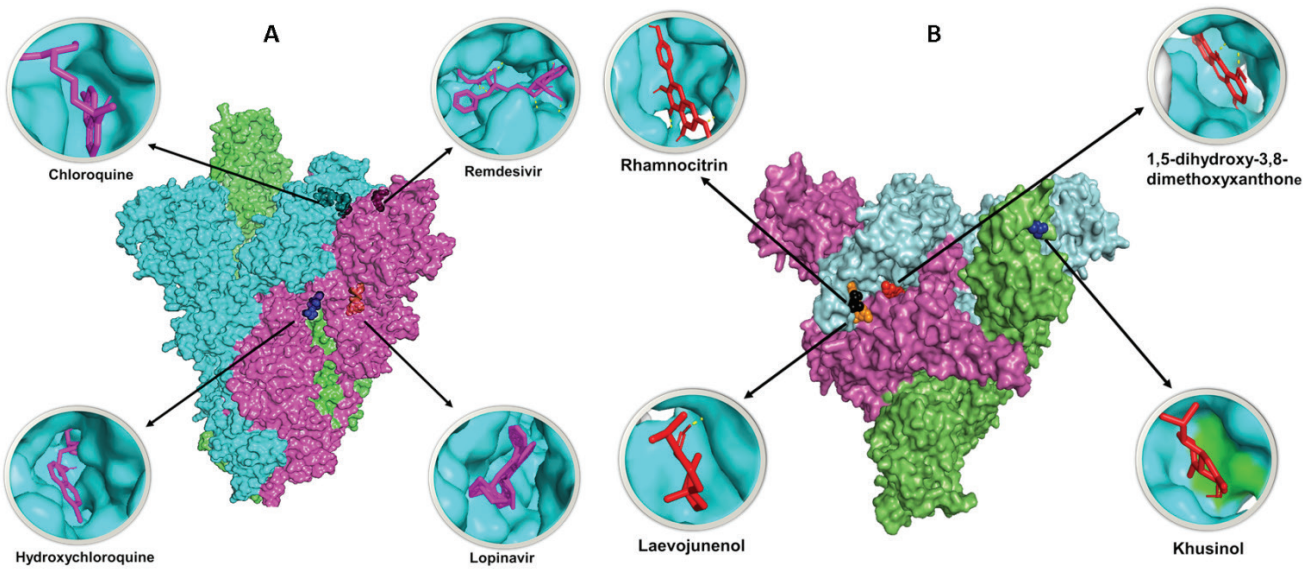

Figure 2. Binding of (A) remdesivir, lopinavir, chloroquine and hydroxychloroquine and (B) rhamnocitrin, 1,5-dihydroxy-3,8-dimethoxyxanthone, laevojunenol and khusinol with SARS-CoV-2 spike glycoprotein.

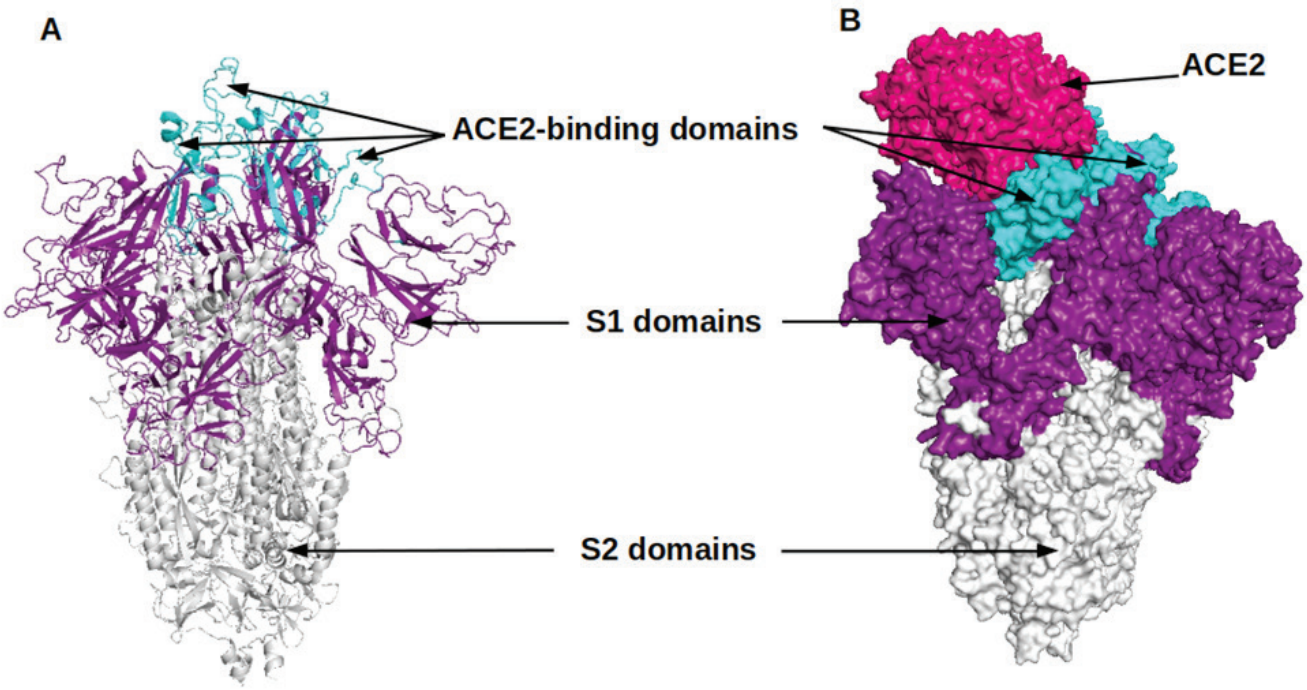

Figure 3. Binding of hACE2 with SARS-CoV-2 spike glycoprotein. (A) cartoon view and (B) surface view.

Validation of drug-likeness

Lipinski rule of five is a rule of thumb to check the drug's likeness of any chemical compound. It acts as a filter to screen potential therapeutic agents/drugs just at the initiation of the program, thereby minimizing the labour and costs of clinical drug development and to a large extent prevents late-stage clinical failures (Raj et al. 2019; Pandey et al. 2020). In this study, three selected phytochemicals were examined for their drug-likeness in the light of the rules (Table 5). The results clearly demonstrated that rhamnocitrin, 1,5-dihydroxy-3,8 dimethoxyxanthone and laevojunenol qualified the rule.

Ligand binding effect analysis on spike glycoprotein-ACE-2 interaction

Finally, the selected drugs were individually used to study effective inhibition of RBD-ACE2 complex formation. The interaction of spike glycoprotein with ACE-2 is depicted in Fig. 3. In order to verify the possible effect of the ligands in spike-ACE-2 interaction, the S glycoprotein-ligand docked complexes were further docked with ACE-2 protein in HDOCK web server. HDOCK is a web server-based protein-protein and protein-DNA/RNA docking tool. This web server based molecular docking revealed that the binding energy of spike protein-ACE-2 interaction was –360.86 and rmsd value 0.51 which decreased to -243.15 and 481.28 rmsd for 1,5-dihydroxy-3,8-dimethoxyxanthone, -238.13 and 480.02 for laevojunenol, -360.86 and 0.51 for rhamnocitrin separately pre-fixed with spike glycoprotein, respectively. Apart from the effect on binding energy, it was also evident that the binding of 1,5-dihydroxy-3,8-dimethoxyxanthone and laevojunenol triggers the shifting of interaction sites of both the partners from their active sites which may hamper the viral entry into human cell (Fig. 4). Also 1,5-dihydroxy-3,8-dimethoxyxanthone of *S. chirayita*, laevojunenol of *V. zizanioides* binding pose being poor, these compounds can be considered as potential inhibitor of S-glycoprotein and human ACE-2 interaction.

CONCLUSION

In conclusion, we can state that the present computer-aided *in-silico* study of exploration of preventive drugs against COVID-19 revealed that natural herbal phytochemicals like rhamnocitrin; 1,5-dihydroxy-3,8-dimethoxyxanthone and laevojunenol of *P. urinaria*, *S. chirayita*, and *V. zizanioides* have immense potential to restrict the onset of SARS-COV-2 disease due to their ability to interrupt the normal viral spike protein and ACE-2 interaction upon binding to the spike protein. The potential of 1,5-dihydroxy-3,8-dimethoxyxanthone and laevojunenol was proved to be superior. Maybe these compounds will be useful as potential preventive drugs, however, further experiments are necessary to validate their effects.

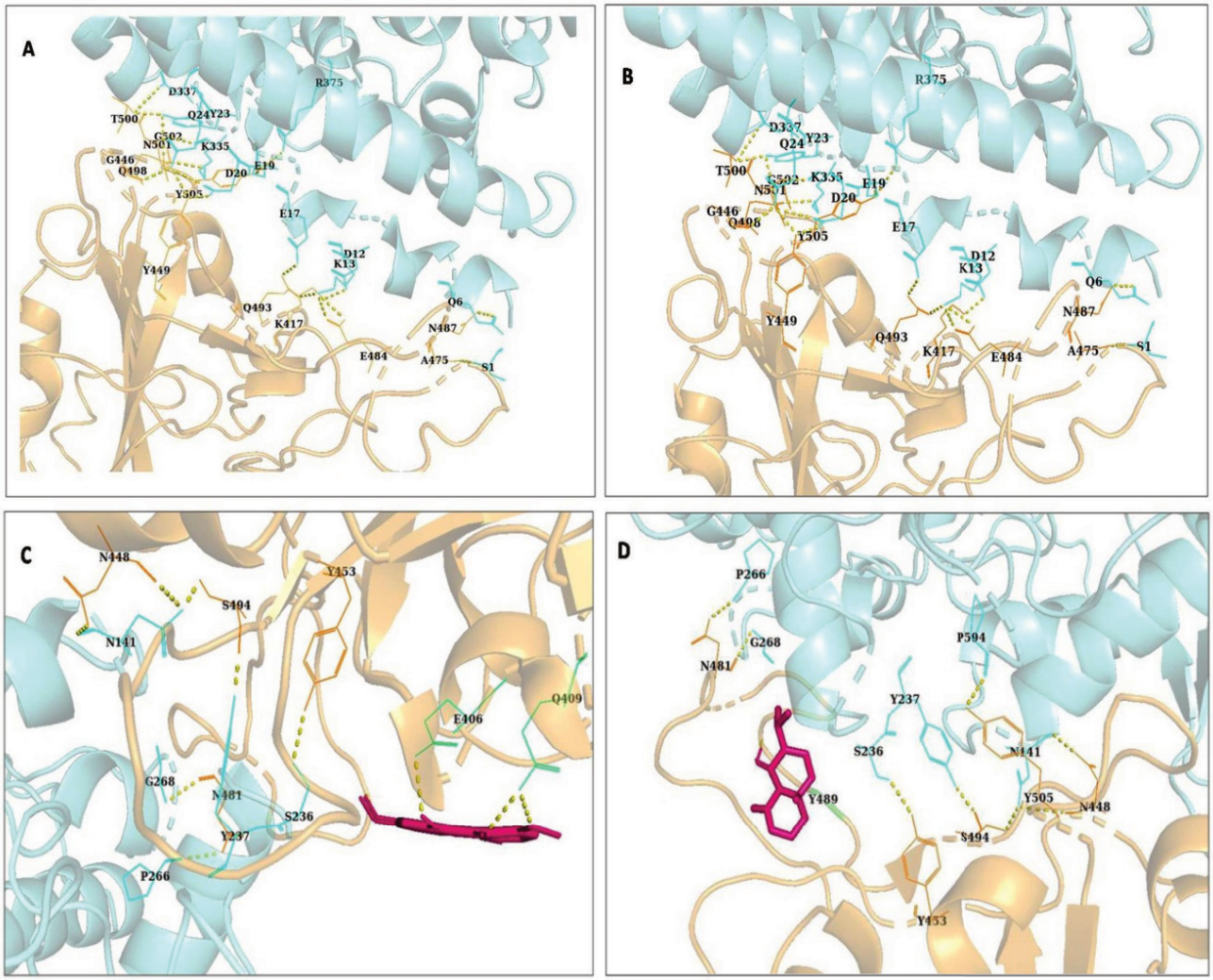

Figure 4. Spike protein bound with ACE2 in open condition (A). Binding of hACE2 with SARS-CoV-2 spike glycoprotein already bound 1,5-dihydroxy-3,8-dimethoxyxanthone (C) and laevojunenol (D). Change in binding position between hACE2 with SARS-CoV-2 spike glycoprotein was apparent in case of all except rhamnocitrin (B).

Acknowledgement

We would like to thank DBT, Government of India for financial assistant for BIF Center, Vidyasagar University, Midnapore-721102, West Bengal, India.

References

Bourgonje AR, Abdulle AE, Timens W, Hillebrands JL, Navis GJ, Gordijn SJ, Bolling MC, Dijkstra G, Voors AA, Osterhaus AD, van der Voort PH (2020) Angiotensin-converting enzyme-2 (ACE2), SARS-CoV-2 and pathophysiology of coronavirus disease 2019 (COVID-19). J Pathol 251(3):228-248.

Cao B, Wang Y, Wen D, Liu W, Wang J, Fan G, Ruan L, Song B, Cai Y, Wei M, Li X (2020) A trial of lopinavir–ritonavir in adults hospitalized with severe Covid-19. N Engl J Med 382:1787-1799.

DeLano WL (2002) Pymol: An open-source molecular graphics tool. CCP4 Newslett Prot Crystallogr 40(1):82-92.

Dev S (1999) Ancient-modern concordance in Ayurvedic plants: some examples. Environ Health Perspect 107(10):783-789.

Divya M, Vijayakumar S, Chen J, Vaseeharan B, Durán-Lara EF (2020) A review of South Indian medicinal plant has the ability to combat against deadly viruses along with COVID-19? Microb Pathog 104277.

Jaiswal YS, Williams LL (2017) A glimpse of Ayurveda–The forgotten history and principles of Indian traditional

medicine. J Tradit Compl Med 7(1):50-53.
Kim S, Thiessen PA, Bolton EE, Chen J, Fu G, Gindulyte A, Han L, He J, He S, Shoemaker BA, Wang J (2016) PubChem substance and compound databases. Nucleic Acids Res 44:D1202-D1213.
Koparde AA, Doijad RC, Magdum CS (2019) Natural products in drug discovery. In Pharmacognosy-Medicinal Plants. IntechOpen.
Kuba K, Imai Y, Rao S, Gao H, Guo F, Guan B, Huan Y, Yang P, Zhang Y, Deng W, Bao L (2005) A crucial role of angiotensin converting enzyme 2 (ACE2) in SARS coronavirus–induced lung injury. Nat Med 11(8):875-879.
Kumar V, Van Staden J. (2015) A review of *Swertia chirayita* (Gentianaceae) as a traditional medicinal plant. Front Pharmacol 6:308.
Lan J, Ge J, Yu J, Shan S, Zhou H, Fan S, Zhang Q, Shi X, Wang Q, Zhang L, Wang X. (2020) Structure of the SARS-CoV-2 spike receptor-binding domain bound to the ACE2 receptor. Nature 581(7807):215-220.
Laskowski RA, MacArthur MW, Moss DS, Thornton JM (1993) PROCHECK: a program to check the stereochemical quality of protein structures. J Appl Cryst 26(2):283-291.
Lipinski CA. (2004) Lead-and drug-like compounds: the rule-of-five revolution. Drug Discov Today Technol 1(4):337-341.
Lavanya P, Ramaiah S, Anbarasu A (2016) Ethyl 4-(4-methylphenyl)-4-pentenoate from Vetiveriazizanioides inhibits dengue NS2B–NS3 protease and prevents viral assembly: a computational molecular dynamics and docking study. Cell Biochem Biophys 74:337-351.
Mohanraj K, Karthikeyan BS, Vivek-Ananth RP, Chand RB, Aparna SR, Mangalapandi P, Samal A (2018) IMPPAT: A curated database of Indian Medicinal Plants, Phytochemistry and Therapeutics. Sci Rep 8(1):4329.
Pandey P, Rane JS, Chatterjee A, Kumar A, Khan R, Prakash A, Ray S (2020) Targeting SARS-CoV-2 spike protein of COVID-19 with naturally occurring phytochemicals: an in-silico study for drug development. J Biomol Struct Dyn 22:1-11.
Paramanick D, Panday R, Shukla SS, Sharma V (2017) Primary pharmacological and other important findings on the medicinal plant *"Aconitum heterophyllum"* (aruna). J Pharmacopunct 20(2):89-92.
Raj S, Sasidharan S, Dubey VK, Saudagar P (2019) Identification of lead molecules against potential drug target protein MAPK4 from *L. donovani*: An *in-silico* approach using docking, molecular dynamics and binding free energy calculation. PloS One 14(8):e0221331.
Rajeswara Rao BR (2013) Biological activities and medicinal uses of the essential oil and extracts of lemongrass (*Cymbopogon flexuosus, C. citratus, C. pendulus* and *C. species*). In Govil JN, Bhattacharya S, Eds., Recent Progress in Medicinal Plants: Essential Oils I. Vol. 36. Studium Press LLC, Houston, USA. pp. 213-257.
Rismanbaf A, Zarei S (2020) Liver and kidney injuries in COVID-19 and their effects on drug therapy; a letter to editor. Arch Acad Emerg Med 8(1):e17.
Singh DD (2018) Assessment of antimicrobial activity of hundreds extract of twenty Indian medicinal plants. Biomed Res 29(9):1797-1814.
Suresh A, Abraham J (2020) Phytochemicals and their role in pharmaceuticals. In Patra J, Shukla A, Das G, Eds., Advances in Pharmaceutical Biotechnology. Springer, Singapore. pp. 193-218.
Tripet B, Howard MW, Jobling M, Holmes RK, Holmes KV, Hodges RS (2004) Structural characterization of the SARS-coronavirus spike S fusion protein core. J Biol Chem 279(20):20836-20849.
Trott O, Olson AJ (2010) AutoDock Vina: improving the speed and accuracy of docking with a new scoring function, efficient optimization, and multithreading. J Comput Chem 31(2):455-461.
ul Qamar MT, Alqahtani SM, Alamri MA, Chen LL (2020) Structural basis of SARS-CoV-2 3CLpro and anti-COVID-19 drug discovery from medicinal plants. J Pharm Anal 10(4):313-319.
WHO Coronavirus Disease (COVID-19) Dashboard (https://covid19.who.int/) [accessed 13 January 2021].
Walls AC, Park YJ, Tortorici MA, Wall A, McGuire AT, Veesler D (2020) Structure, function, and antigenicity of the SARS-CoV-2 spike glycoprotein. Cell 181(2):281-292.
Wang Q, Zhang Y, Wu L, Niu S, Song C, Zhang Z, Lu G, Qiao C, Hu Y, Yuen KY, Wang Q (2020) Structural and functional basis of SARS-CoV-2 entry by using human ACE2. Cell 81(4):894-904.
Waterhouse A, Bertoni M, Bienert S, Studer G, Tauriello G, Gumienny R, Heer FT, de Beer TA, Rempfer C, Bordoli L, Lepore R (2018) SWISS-MODEL: homology modelling of protein structures and complexes. Nucleic Acids Res 46(W1):W296-303.
Yan R, Zhang Y, Li Y, Xia L, Guo Y, Zhou Q (2020) Structural basis for the recognition of SARS-CoV-2 by full-length human ACE2. Science 367(6485):1444-1448.
Yan Y, Tao H, He J, Huang SY (2020) The HDOCK server for integrated protein–protein docking. Nat Protoc 15(5):1829-1852.
Yang XH, Deng W, Tong Z, Liu YX, Zhang LF, Zhu H, Gao H, Huang L, Liu YL, Ma CM, Xu YF (2007) Mice transgenic for human angiotensin-converting enzyme 2 provide a model for SARS coronavirus infection. Comp Med 57(5):450-459.
Yao X, Ye F, Zhang M, Cui C, Huang B, Niu P, Liu D (2020) In vitro antiviral activity and projection of optimized dosing design of hydroxychloroquine for the treatment of severe acute respiratory syndrome coronavirus 2

(SARS-CoV-2). Clin Infect Dis 71(15):732-739.
Yazdany J, Kim AH (2020) Use of hydroxychloroquine and chloroquine during the COVID-19 pandemic: what every clinician should know. Ann Int Med 172(11):754-755.
Zhou P, Yang XL, Wang XG, Hu B, Zhang L, Zhang W, Si HR, Zhu Y, Li B, Huang CL, Chen HD (2020) A pneumonia outbreak associated with a new coronavirus of probable bat origin. Nature 579(7798):270-273.

Acta Biologica Szegediensis

Volume 64(2):173-179, 2020
Acta Biologica Szegediensis
http://abs.bibl.u-szeged.hu/index.php/abs
DOI:10.14232/abs.2020.2.173-179

ARTICLE

Characterization of amylase and protease activity in the digestive tract of two teleosts (*Labeo rohita* and *Anabas testudineus*) with different feeding habits

Sanjeet Debnath, Surjya Kumar Saikia*

Aquatic Ecology and Fish Biology Laboratory, Department of Zoology, Visva-Bharati, Santiniketan, West Bengal, India

ABSTRACT Two teleosts (Rohu, *Labeo rohita* and Koi, *Anabas testudineus*), both with contrasting feeding habits (herbivorous versus carnivorous) were studied for amylase and protease activity concerning different regions of their digestive tracts. Significant differences in enzymatic activity across different regions of the digestive tracts were observed. Rohu, with three equal regions of the stomachless gut, showed the highest amylolytic activity at the posterior digestive tract but the highest proteolytic activity is limited to mid region. Contrary to such observation, Koi with three distinct regions of the digestive tract (stomach, pyloric caeca and intestine), the pyloric caeca exhibited the highest specific activity for both amylase and total protease. The optimum pH and temperature conditions were determined concerning the activity for both amylase and protease.
Acta Biol Szeged 64(2):173-179 (2020)

KEY WORDS
α-amylase
digestive enzyme
digestive tract
Rohu
Koi
protease

ARTICLE INFORMATION
Submitted
11 June 2020.
Accepted
04 October 2020.
***Corresponding author**
E-mail: surjyasurjya@gmail.com

Introduction

Like other vertebrates, the activity of digestive enzymes in fish is influenced by the abiotic factors, such as temperature (Kuz'mina 1996), particular timing of day (Kuz'mina and Strelnikova 2008) and different seasons (Kofuji et al. 2005), and biotic factors, including the preference of food (Ugolev and Kuz'mina 1993), the age of the organism (Kuz'mina 1996), state of infestation with parasites (Izvekova and Solovyev 2012), etc. Hence, careful investigation of the pattern of the digestive activity of different enzyme would provide not only the complete information of the digestive physiology of fish, but also the age, health and feeding ecology of the organism. The α-amylase and protease were one of the major digestive enzymes found in digestive tract (DT) of fish, which are widely studied for the above purpose.

In India and rest of South-East Asia, Rohu (*Labeo rohita*) has been the most preferred cultivable fish over many other freshwater species and extensively cultivated in India, Nepal, Bangladesh, Myanmar, Sri Lanka and Pakistan (Talwar and Jhingran 1991). This Indian Major Carp (Rohu), has always been receiving special attention as a potential animal crop over centuries for alleviating malnutrition in human populations because of its capability to retain high amounts of vitamins and other micronutrients at a reasonable cost (Mohanty et al. 2016). On the other hand, the cultivation of climbing perch (*Anabas testudineus*), locally known as Koi, is gaining importance as one of the most potential candidates for aquaculture because of its high market demand and greater consumer preference throughout all the seasons (Uddin et al. 2016). It is a good source of protein, fat, vitamins, amino acids and fatty acids (Bogard et al. 2015; Paul et al. 2017). Being an air-breathing fish, Koi is also a model of interest for several scientific studies for its low maintenance effort, as well as easy availability and hardy nature (e.g., Munshi et al. 2018). Wide spreading aquaculture of Koi has been a great demand among the entire Indian sub-continent including Bangladesh, Myanmar, and Indonesia.

Voluminous research works have been carried out on the growth and feeding biology of Indian Major Carps (see review Majumder and Saikia 2020). But, except few (e.g., Mandal and Ghosh 2010; Singh et al. 2018), these studies have not addressed the details of the digestive physiology, particularly the activity of the crucial digestive enzymes along the digestive tract. These studies considered the whole intestine as an overall source of activity of a particular enzyme. As a result the specific region wise performance of an enzyme remains shadowed. Similarly, studies on Koi with regard to the effects

of toxicants on the digestive system were performed (Samanta et al. 2014; Kole et al. 2017). Banerjee and Ray (2018) reported the seasonal variation in the activity of digestive enzymes of Koi. However, these studies are not elaborate since these studies treated whole gut as site of activity of a particular enzyme. Of late, more precise explanation of digestive enzyme activity across the gut length of fish has been started (e.g., Weinrauch et al. 2019). More precise observation of the process of the activity of digestive enzymes will provide supportive information to improvise diet formulations for optimum supplementary feeding. In the present study, an attempt has been made to characterize region wise enzyme activities keeping in mind the optimum pH and temperature. This study establishes the optimum pH and temperature for amylase and protease activity in the tissue extracts of digestive tract from Rohu and Koi. The feeding habits of both the fishes were compared keeping in view of the activity of enzymes across different regions of digestive tract.

Material and methods

Experimental animals

A total of 20 fish were collected from local fish pond (23°37'N, 87°49'E) during February, 2020 using gill net (08:00-09:00) and brought alive to the laboratory. In laboratory fishes were kept unfed in glass aquaria (45 x 30 x 30 cm, 30 L) for 24 hours before analysis. Throughout the experiment, the water temperature was 28.67 ± 1.87 °C; dissolved oxygen 7.61 ± 0.26 mg/L; pH 7.48 ± 0.21; conductivity 623 ± 15.2 μS; photoperiod 12 :12 (light hour : dark hour).

Preparation of extracts

On the second day of collection, a small amount of food was introduced to stimulate the digestive function in the two fish species. After one hour, fish were euthanized with the help of ice-cold water and dissected on ice board. The DT was dissected out from esophagus to anus, washed in chilled distilled water and blotted with paper towel. For Rohu, the DT was divided lengthwise into three equal segments viz. anterior, middle and posterior starting from the esophagus to anus. Like Rohu, the short DT of Koi was also divided into three parts based on the morphological difference and identified as the stomach, pyloric caeca and intestine. Tissues were initially stored in -40 °C until use. Later, 10% tissue homogenate were prepared at 4 °C in a buffer containing 100 mM Tris-HCl, pH 7.4, centrifuged at 10 000 g at 4 °C for 10 min, and the supernatants (or the DT extracts) were collected carefully.

Table 1. Activity of amylase and protease in different sections of the digestive tract of *L. rohita* (n = 10). Values are expressed as mean ± SE. Means with different alphabets within a group show statistically significant difference at $p < 0.05$.

Digestive tract (DT)	Specific activity (U/mg protein)	
	Amylase	Total protease
Anterior DT	0.400 ± 0.005^{a}	0.316 ± 0.005^{c}
Mid DT	0.246 ± 0.004^{b}	0.523 ± 0.016^{a}
Posterior DT	0.182 ± 0.022^{c}	0.483 ± 0.012^{b}

Estimation of digestive enzymes

Amylase

The activity of amylase was measured following the method of Bernfeld (1955) using potato-starch as the substrate. The specific activity was expressed as the measure of unit activity per μg protein, where one-unit activity was the amount of enzyme required to liberate 1 μg of maltose per hour form the assay mixture.

Protease

Casein was used as substrate to measure the activity of protease according to Walter (1984). One unit of enzyme activity in each sample was expressed as the amount of enzyme required to liberate 1 μg of tyrosine in one hour per μg protein. Method suggested by Lowry et al. (1951) was followed to estimate the amount of total protein in the DT extracts.

Optimal range of pH and temperature

Firstly, the individual optimum pH for each type of enzyme from different region of DT was determined spectrophotometrically using a range of buffer solutions (pH 1.0 to 10.0) as the assay medium. The buffers used were as follows: 0.2 M KCl-HCl buffer (pH 1.0 and 2.0), 0.2 M glycine-HCl buffer (pH 3.0), 0.1 M citrate buffer (pH 4.0, 5.0, 6.0), 0.2 M Tris-HCl buffer (pH 7.0, 8.0, 9.0), 0.2 M glycine-NaOH (pH 10.0), respectively. Finally, the optimal temperatures for the same digestive enzymes were determined by measuring their activity at several temperatures starting from 20 °C to 45 °C with 5 °C interval where, the pH condition was kept constant to the previously determined optimum level. The spectrophotometric enzyme activity assays were performed in triplicate.

Data analysis

Data from the replicates for digestive enzymes were combined for statistical analysis. One-way ANOVA was performed and multiple comparisons between mean values were made using Tukey's post hoc test. The alpha level

was maintained less than 0.05 for all statistical analysis. Results are reported as mean values with SD. Minitab 18 was used for all statistical analysis.

Results

Measurement and distribution of digestive enzymes

The activity of amylase and protease from different parts of DT in Rohu is summarized in Table 1. Amylase activity in the anterior DT was much higher than the rest. The mid DT showed significantly less amylolytic activity than the anterior part ($p < 0.05$) but, had higher activity when compared to the posterior region. On the other hand, in the mid DT, the protease activity was much higher than that in other parts. Levels of protease activity were in descending order in the DT were as follows: mid DT, posterior DT, and anterior DT. The distribution of the activity of amylase and protease in different digestive locations throughout the DT in Koi are summarized in Table 2. The pyloric caeca showed the maximum amylase activity followed by the intestine and stomach. Also, for proteolytic activity, pyloric caeca showed the dominant portion of the DT. There are no significant ($p < 0.05$) difference between the total digestive protease activity in stomach and intestine.

Characteristics of amylase and protease

The results showed that the optimum pH value for amylase activity was 8.0 in both the anterior and mid DT in Rohu (Fig. 1a). On the other hand, the last segment of the DT showed an optimum pH of 7.0 for the amylolytic activity. The optimal temperature for amylase activity was 35 °C throughout the DT (Fig. 1b).

Proteolytic enzyme showed optimum activity at pH 8.0 in both anterior and middle region of the DT in Rohu (Fig. 1c). However, the posterior region of the DT showed the highest proteolytic activity at pH 7. The optimum temperature for proteases, found in the DT of Rohu, to achieve the maximum activity was 35 °C (Fig. 1d)

In Koi, the optimum pH value, at which the amylase activity peaked the highest value was 3 in both stomach and pyloric caeca (Fig. 2a). In intestine, the highest activity of amylase was found at pH 8.0. Protease activity was at its peak in stomach at pH 2.0. In both pyloric caeca and intestine, pH 7.0 was recorded as optimum value for highest activity (Fig. 2c). The optimum temperature for both amylase and protease activity were 35 °C (Fig. 1b, 1d) throughout all regions of DT.

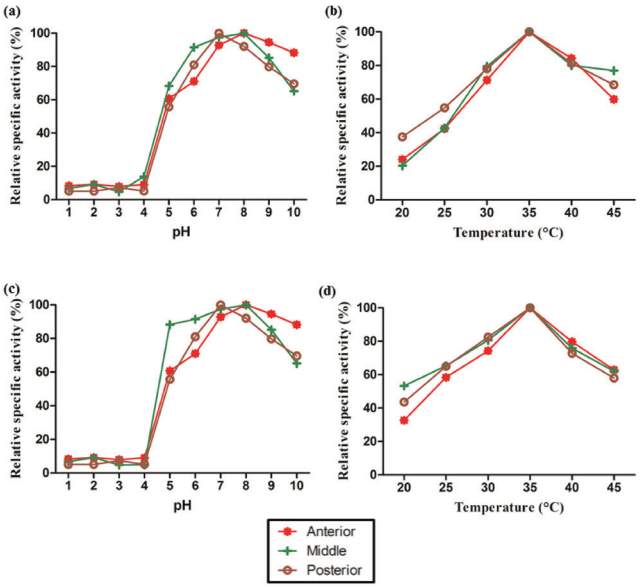

Figure 1. Effect of pH and temperature on the activity of amylase and protease of *L. rohita*. Fig. 1a and 1b represent effect of pH and temperature on relative specific activity of digestive amylase respectively. Fig. 1c and 1d represent effect of pH and temperature on relative activity of total protease, respectively. Enzyme activity was expressed as relative specific activity (RSA). RSA% = $(Z_i/Z_{max}) \times 100$ [Z_i = enzyme activity at specific pH or temperature value; Z_{max} = maximum enzyme activity]. In all cases, n = 10.

Table 2. Activity of amylase and protease in different sections of the digestive tract of *A. testudineus* (n = 10). Values are expressed as mean ± SD. Means with different alphabets within a group show statistically significant difference at $p < 0.05$.

Digestive tract (DT)	Specific activity (U/mg protein)	
	Amylase	Total protease
Stomach	0.099 ± 0.014[b]	0.285 ± 0.004[b]
Pyloric caeca	0.175 ± 0.004[a]	0.308 ± 0.001[a]
Intestine	0.113 ± 0.002[c]	0.281 ± 0.001[b]

Discussion and conclusions

Biochemical studies of the digestive enzymes reflect the dietary specializations of the respective organism (Day et al. 2011). The present study aimed to study the ability to digest dietary carbohydrate and protein by two freshwater teleosts with different feeding habits and topologically dissimilar DTs. It also aimed to establish the optimum pH and temperature for the studied digestive enzymes along different parts of their DT. In the current study, the highest amylase activity was reported in the anterior DT for Rohu, and the activity was apparently twice than the mid and posterior DT. Here pancreatic amylase, which is found in association to hepatopancreas act as source of higher activity of amylase. It is known as the primary glucosidase available in fish (Candiotto et al. 2018). Fishes generally lack the salivary amylase prevalent

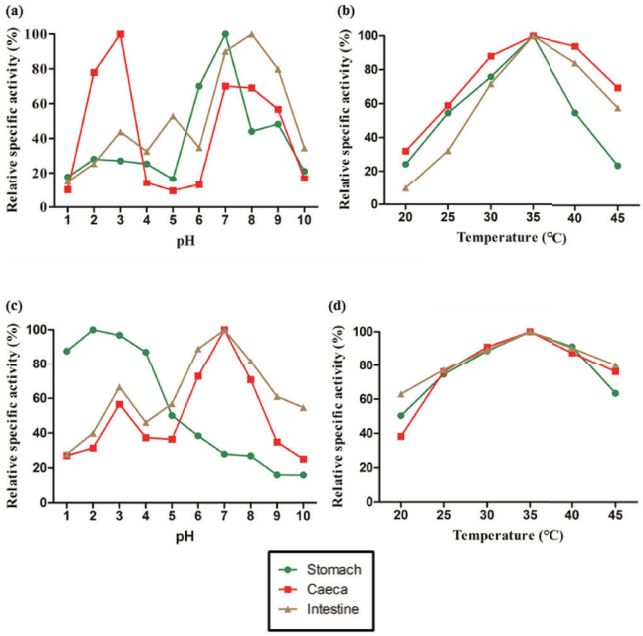

Figure 2. Effect of pH and temperature on the activity of amylase and protease of *A. testudineus*. Fig. 2a and 2b represent effect of pH and temperature on relative specific activity of digestive amylase, respectively. Fig. 2c and 2d represent effect of pH and temperature on relative activity of total protease, respectively. Enzyme activity was expressed as relative specific activity (RSA). RSA% = $(Z_i/Z_{max}) \times 100$ [Z_i = enzyme activity at specific pH value; Z_{max} = maximum enzyme activity]. In all cases, n = 10.

in mammals, but intestinal α-amylase is produced in the exocrine pancreas (Krogdahl et al. 2005). Day et al. (2011) found a similar pattern of amylase activity in *Arrhamphus sclerolepi krefftii*, which was again a stomachless herbivore fish. Similar result was observed by Parra et al. (2007) for α-amylase in Pacific bluefin tuna *Thunnus orientalis* under culture conditions. Hidalgo et al. (1999) observed higher activity of amylase in omnivorous species *Cyprinus carpio* and found that amylase activity determined in the hepatopancreas of carp was high compared to digestive tract. It is known that amylase activity depends on the natural diet of fish species, and herbivorous and omnivorous fish have more amylase activity than carnivorous fish (Liu et al. 2016). Being an herbivore, Rohu has to consume a lot of plant materials rich in starch. Moreover, Ray et al. (2010) reported that Rohu has a sac like region (intestinal bulb) in the anterior portion of the DT, which is responsible for the temporary storage of the ingested food material. The requirement of high amylolytic activity in the anterior DT can be linked with the storage of plant based food at this region. Moderate amylolytic activity was enough for the breakdown of starch in the mid and anterior portion because the fish has a long DT. The longer the length of the DT the greater the chance of the action of digestive enzymes in herbivore fish and it may compensate the low specific activity of digestive enzyme. On the other hand, the results revealed that the pyloric caeca of Koi is the most active site for both α-amylase and proteases. Similar result was reported in the study of Caruso et al. (2009), where the amylase and total protease activity in pyloric caeca of starved blackspot seabream (*Pagellus bogaraveo*) were potentially higher than the rest parts of the DT. The overall activity of amylase was higher in Rohu than Koi. This fact is in agreement with the popular principal that the amylase activity is always higher in the herbivorous fish species when compared to the carnivorous ones (Krogdahl et al. 2005).

The optimum pH for amylase activity in the Rohu was 8.0 for both the anterior and mid DT but at the posterior region of the DT, it was 7.0. However, in Koi the maximum activity of digestive amylase was obtained at pH 3.0 in stomach in addition with some significant activity of digestive amylase was also found at the range of pH 7.0 to pH 9.0. Subsequently the pyloric caeca and the intestine of Koi showed the optimum amylolytic activity at pH 8.0, having a relatively weak tendency towards acidic amylase activity. Study of several authors (Parra et al. 2007; Xiong et al. 2011; Champasri and Champasri 2017) in different fish reveals that the general trend of digestive amylase activity picks at natural or alkaline pH in the intestine, and in stomach the amylase activity was slightly acidic (Munilla-Moran and Saborido-Rey 1996; Fernández et al. 2001; Xiong et al. 2011). Besides, diverse feeding habits of Koi may be one of the reasons of the activity observed within a wider range of pH. The amylase activity has been reported within a wide range shows quite different feeding habits (Kawai and Ikeda 1971; Kuz'mina et al. 1996). Highest activity of amylase recorded at 35 °C in all parts of the DT in both fish species. It is known that temperature ranging from 30 °C to around 55 °C was responsible for amylase activity in wild fish (Ugolev and Kuz'mina 1993; Parra et al. 2007; Xiong et al. 2011; Champasri and Champasri 2017; Candiotto 2018). But, in most cases, temperature of gut lumen in fish is closely linked to that of the environment as well as the water temperature and may have manifold effects on fish digestion (Munilla-Moran and Saborido-Rey 1996).

In the present study total proteolytic activity of both Rohu and Koi were measured. Study on proteolytic activity means the study of pepsin, trypsin, chymotrypsin, aminopeptidase, carboxypeptidase that, which act as a battery of enzymes (Torrissen 1987; Unajak et al. 2012). In Rohu, highest activity of protease was found in mid region of the DT followed by the posterior region. The lowest activity was found in the anterior DT. Day et al. (2011) made a similar observation in another stomachless fish *Strongylura krefftii*, where proteases were more

active at mid and distal intestine than the proximal parts. However, in Koi the proteolytic activity of the stomach and the intestine showed no significant difference but for the stomach the optimum activity achieved at acidic pH, whereas in the intestine the highest activity was taken place at the neutral pH. Similar result was obtained in case of *Glyptosternum maculatum*, where protease activity was highest in stomach followed by anterior intestine (Xiong et al. 2011). In contrast to stomachless fish, proteolytic activity is highest in low pH condition when a stomach is present in fish (Kuz'mina 1990; Hidalgo et al. 1999**).**

On the other hand, the pyloric caeca in Koi exhibited maximum proteolytic activity at neutral pH (pH 7.0) and in compared to stomach (highest activity at pH < 2.0), the proteolytic activity in intestine and pyloric ceaca were far higher at neutral pH. Thus the proteolytic digestion in Koi takes place near neutral environment outside the stomach. In general, the maximum activity of protease at highly acidic pH in the stomach may be due to the stomach was bearing the gastric cells. Earlier, Lobel (1981) noted that the fish with a thin-walled stomach, with ability to considerably widen in the presence of large food items, the gastric pH was lower than in fish with a thick-walled stomach. Apparently, Koi maintains an ability to digest protein food in all the components across the gut with variable pH. Such adjustment is often noticed in fishes with diversified food habits (Moyano et al. 2001). The optimum pH for total protease activity was 8.0 in both the anterior and mid region of the DT of Rohu, but the posterior portion showed optimum proteolytic activity at pH 7.0. It gives clear indication that neutral to alkaline range of pH has been the environment of gut in Rohu for protease digestion. The absence of stomach may be the probable reason why Rohu lacks acidic protease activity. These findings were similar with other findings where the optimum activity was close to pH 8.0 (Hidalgo 1999; Pena et al. 2015; Aissaoui et al. 2017). All three regions showed some degree of acid protease activity at pH 5.0 to pH 6.0. In the case of the current study, the maximum activity of protease was found to be at 35 °C and it was somewhat in agreement with the study of Ugolev and Kuz'mina (1993), Munilla-Moran and Saborido-Rey (1996) and Aissaoui et al. (2017), where they showed the activity of proteases falls within a range of 35 °C to 40 °C in various other fishes.

Although the observations here are compared for herbivorous versus omnivorous fish species and variable ranges of optimal activity of enzymes are presented under different pH as well as temperatures levels, it is to be kept in mind that there are different other factors, like time of ingestion of food, environmental temperature, emptiness of the stomach, food types available in the stomach for omnivorous, age of fish etc to effect the release of digestive enzymes at different frequencies throughout the gut (Solovyev et al. 2017). Nevertheless, it is also possible that the existence of more than one peak of optimal pH found in the above cases of Rohu and Koi indicates the possible existence of isoenzymes. Optimum pH and temperature for the enzyme activity varies along different regions of the DT (Fernández et al. 2001; Xiong et al. 2011; Solovyev et al. 2015) and within different fish (Fernández et al. 2001; Alarcón et al. 2001) as several isoforms may possibly present for a particular enzyme.

There is a strong relationship between the environment and the internal physiological state of fish, as it is an ectothermic aquatic organism. Concerning this relation, the internal physiological environment of the fish also modulated or affected by the environmental conditions. Various seasons are with various temperatures and as a rule of thumb, pH decreases with an increase in temperature. So, the self-adjustment of the ectothermic aquatic animal obviously affects its gastrointestinal digestive purpose accordingly (Solovyev and Izvekova 2016). Our study mainly conveyed the unique pattern of the complete activity of amylase and protease from different positions along with the DT of *L. rohita* and *A. testudineus* across a series of pH and temperature values. We established the specific distribution of major digestive enzymes working in various digestive sections in the studied fish species. The study also demonstrated typical patterns of varying activity depending on location in the digestive tract, pH and temperature. It is the primary study of the digestive physiology of *L. rohita* and *A. testudineus*, and further research should be carried out to learn greater details regarding its digestion and nutrition. In this context, this study surely going to guide the researchers who are working with the diet preparation or feed formulation of the studied fish species.

Acknowledgments

This work was supported by the Council of Science & Industrial Research (CSIR), India. Authors also acknowledge the facility supported under the programmes DST-FIST and CAS (UGC) in the Department of Zoology, and DST-PURSE in Siksha Bhavana, Visva-Bharati, West Bengal, India.

References

Aissaoui N, Marzouki MN, Abidi F (2017) Purification and biochemical characterization of a novel intestinal protease from *Scorpaena notata*. Int J Food Prop 20:2151-2165.

Banerjee G, Ray AK (2018) The effect of seasonal temperature on endogenous gut enzyme activity in four air-breathing fish species. Croat J Fish 76:60-65.

Bernfeld P (1955) Amylases alpha and beta. In Colowick S, Kaplan N, Eds., Methods in Enzymology I. Academic Press, New York. 149-158.

Bogard JR, Thilsted SH, Marks GC, Wahab MA, Hossain MA, Jakobsen J, Stangoulis J (2015) Nutrient composition of important fish species in Bangladesh and potential contribution to recommended nutrient intakes. J Food Compost Anal 42:120-133.

Candiotto FB, Freitas-Júnior AC, Neri RC, Bezerra RS, Rodrigues RV, Sampaio LA, Tesser MB (2018) Characterization of digestive enzymes from captive Brazilian flounder *Paralichthys orbignyanus*. Braz J Biol 78:281-288.

Caruso G, G Denaro M, Genovese L (2009) Digestive enzymes in some teleost species of interest for Mediterranean aquaculture. Open Fish Sci J 2:74-86.

Champasri C, Champasri T (2017) Biochemical characterization, activity comparison and isoenzyme analysis of amylase and alkaline proteases in seven cyprinid fishes. J Fish Aquat Sci 12:264-272.

Day RD, German DP, Tibbetts IR (2011) Why can't young fish eat plants? Neither digestive enzymes nor gut development preclude herbivory in the young of a stomachless marine herbivorous fish. Comp Biochem Physiol B 158:23-29.

de la Parra AM, Rosas A, Lazo JP, Viana MT (2007) Partial characterization of the digestive enzymes of Pacific bluefin tuna *Thunnus orientalis* under culture conditions. Fish Physiol Biochem 33:223-231.

Fernández I, Moyano FJ, Díaz M, Martínez T (2001) Characterization of α-amylase activity in five species of Mediterranean sparid fishes (Sparidae, Teleostei). J Exp Mar Biol Ecol 262:1-12.

Hidalgo MC, Urea E, Sanz A (1999) Comparative study of digestive enzymes in fish with different nutritional habits. Proteolytic and amylase activities. Aquaculture 170:267-283.

Hsu YL, Wu JL (1979) Relationship between feeding-habits and digestive proteases of some freshwater-fishes. Bull Inst Zool Acad Sin 18:45-53.

Izvekova GI, Solovyev MM (2012) Activity of digestive hydrolases in fishes infected with cestodes. Usp Sovrem Biol 132:601-610.

Kawai SI, Ikeda S (1971) Studies on digestive enzymes of fishes. I. Carbohydrases in digestive organs of several fishes. Bull Japan Soc Sci Fish 37:333-337.

Kofuji PY, Akimoto A, Hosokawa H, Masumoto T (2005) Seasonal changes in proteolytic enzymes of yellowtail *Seriola quinqueradiata* (Temminck & Schlegel; Carangidae) fed extruded diets containing different protein and energy levels. Aquac Res 36:696-703.

Kole D, Mondal S, Ghosh AR (2018) Effects of arsenic (III) and chromium (VI) toxicity on digestive enzymes' activities of *Anabas testudineus* (Bloch)Proc Zool Soc 71:178-185

Krogdahl Å, Hemre GI, Mommsen TP (2005) Carbohydrates in fish nutrition: digestion and absorption in postlarval stages. Aquac Nutr 11:103-122.

Krogdahl Å, Hemre GI, Mommsen TP (2005) Carbohydrates in fish nutrition: digestion and absorption in postlarval stages. Aquac Nutr 11:103-122.

Kuz'mina VV (1990) Temperature influence on the total level of proteolytic activity in the digestive tract of some species of freshwater fishes. J Ichthyol 30:97-100.

Kuz'mina VV (1996) Influence of age on digestive enzyme activity in some freshwater teleosts. Aquaculture 148:25-37.

Kuz'mina VV, Strel'nikova AP (2008) Influence of diurnal rhythms of feeding during intestine total amylolytic activity and activity of alkaline phosphatase in juvenile fish. Inland Water Biol 1:182-191.

Liu H, Guo X, Gooneratne R, Lai R, Zeng C, Zhan F, Wang W (2016) The gut microbiome and degradation enzyme activity of wild freshwater fishes influenced by their trophic levels. Sci Rep 13:24340.

Lobel PS (1981) Trophic biology of herbivorous reef fishes: alimentary pH and digestive capabilities. J Fish Biol 19:365-397.

Lowry OH, Rosebrough NJ. Farr AL, Randall RJ (1951) Protein measurement with the Folin phenol reagent. J Biol Chem 193:265-275.

Majumder S, Saikia SK (2020) Ecological intensification for feeding rohu *Labeo rohita* (Hamilton, 1822): A review and proposed steps towards an efficient resource fishery. Aquac Res 51(1):3072-3078.

Mandal S, Ghosh K (2010) Inhibitory effect of *Pistia* tannin on digestive enzymes of Indian major carps: an in vitro study. Fish Physiol Biochem 36:1171-1180.

Mohanty BP, Sankar TV, Ganguly S, Mahanty A, Anandan R, Chakraborty K, Paul BN, Sarma D, Dayal JS, Mathew S, Asha KK (2016) Micronutrient composition of 35 food fishes from India and their significance in human nutrition. Biol Trace Elem Res 174:448-458.

Moyano FJ, Savoie L (2001) Comparison of in vitro systems of protein digestion using either mammal or fish proteolytic enzymes. Comp Biochem Physiol A 128:359-368.

Munilla-Morán R, Saborido-Rey F (1996) Digestive enzymes in marine species. II. Amylase activities in gut from seabream (*Sparus aurata*), turbot (*Scophthalmus maximus*) and redfish (*Sebastes mentella*). Comp Biochem Physiol B 113:827-834.

Munshi M, Tumu KN, Hasan MN, Amin MZ (2018) Biochemical effects of commercial feedstuffs on the fry of climbing perch (*Anabas testudineus*) and its impact on Swiss albino mice as an animal model. Toxicol Rep 5:521-530.

Paul BN, Chanda S, Bhowmick S, Sridhar N, Saha GS, Giri SS (2017) Nutrient profile of Indian climbing perch, *Anabas testudineus*. SAARC J Agric 15:99-109.

Peña E, Hernández C, Álvarez-González CA, Ibarra-Castro L, Puello-Cruz A, Hardy RW (2015) Comparative characterization of protease activity in cultured spotted rose snapper juveniles (*Lutjanus guttatus*). Lat Am J Aquat Res 43:641-650.

Ray AK, Roy T, Mondal S, Ringø E (2010) Identification of gut-associated amylase, cellulase and protease-producing bacteria in three species of Indian major carps. Aquac Res 41:1462-1469.

Samanta P, Pal S, Mukherjee AK, Senapati T, Ghosh AR (2014) Effects of almix herbicide on metabolic enzymes in different tissues of three teleostean fishes *Anabas testudineus*, *Heteropneustes fossilis* and *Oreochromis niloticus*. Int J Sci Res Env Sci 2:156-163.

Singh G, Bhatnagar A, Alok K, Ajay SA (2018) Enzymatic profiling and feeding preferences of Catla: *Catla catla*, Rohu: *Labeo rohita* and Mrigala: *Cirrhinus mrigala* in rural polyculture ponds. J Aquac Res Dev 9:1-8.

Solovyev MM, Izvekova GI (2016) Seasonal changes in pH values in the intestine of fish from Lake Chany (West Siberia). Inland Water Biol 9:400-404.

Solovyev MM, Kashinskaya EN, Izvekova GI, Glupov VV (2015) pH values and activity of digestive enzymes in the gastrointestinal tract of fish in Lake Chany (West Siberia). J Ichthyol 55:251-258.

Talwar PK, Jhingran AG (1991) Inland Fisheries of India and Adjacent Countries. Vol. I. Oxford and IBH Publishing, New Delhi, India.

Torrissen KR (1987) Genetic variation of trypsin-like isozymes correlated to fish size of Atlantic salmon (*Salmo salar*). Aquaculture 62:1-10.

Uddin KB, Moniruzzaman M, Bashar MA, Basak S, Islam AS, Mahmud Y, Lee S, Bai SC (2016) Culture potential of Thai climbing perch (*Anabas testudineus*) in experimental cages at different stocking densities in Kaptai Lake, Bangladesh. Aquac Aquar Conserv Legis 9:564-573.

Ugolev AM, Kuz'mina VV (1993) Digestive Processes and Adaptations in Fish. St. Petersburg: Gidrometeoizdat.

Unajak S, Meesawat P, Paemanee A, Areechon N, Engkagul A, Kovitvadhi U, Kovitvadhi S, Rungruangsak-Torrissen K, Choowongkomon K (2012) Characterisation of thermostable trypsin and determination of trypsin isozymes from intestine of Nile tilapia (*Oreochromis niloticus L.*). Food Chem 134:1533-1541.

Walter HE (1984) Proteinases: methods with haemoglobin, casein and azocoll as substrates. In Bergmeyer HU, Bergmeyer J, GraBl M. Methods of Enzymatic Analysis, Vol 5, 3rd Ed., Verlag Chemie, Weinheim, Germany, 270-277.

Weinrauch AM, Schaefer CM, Goss GG (2019) Activity and post-prandial regulation of digestive enzyme activity along the Pacific hagfish (*Eptatretus stoutii*) alimentary canal. PLOS ONE 14:e0215027.

Xiong DM, Xie CX, Zhang HJ, Liu HP (2011) Digestive enzymes along digestive tract of a carnivorous fish *Glyptosternum maculatum* (Sisoridae, Siluriformes). J Anim Physiol An Nutr 95:56-64.

Acta Biologica Szegediensis

Volume 64(2):181-189, 2020
Acta Biologica Szegediensis
http://abs.bibl.u-szeged.hu/index.php/abs
DOI:10.14232/abs.2020.2.181-189

ARTICLE

Histomorphological perspectives of preputial and clitoral glands of soft-furred field rat *Millardia meltada*

Thangavel Rajagopal[1,2]*, Ganesan Ramya Vaideki[1], Ganesan Saibaba[2], Ponnirul Ponmanickam[2,3], Shanmugam Achiraman[2,4], Swaminathan Rajanarayanan[2,5] Mohammad Abdulkader Akbarsha[6], Govindaraju Archunan[2]*

[1]Department of Zoology, Thiagarajar College (Autonomous), Madurai-625 009, Tamil Nadu, India.
[2]Pheromone Technology Lab, Department of Animal Science, School of Life Sciences, Bharathidasan University, Tiruchirappalli - 620 024, Tamil Nadu, India.
[3]Department of Zoology, Ayya Nadar Janaki Ammal College (Autonomous), Sivakasi-626 124, Tamil Nadu, India.
[4]Department of Environmental Biotechnology, School of Environmental Science, Bharathidasan University, Tiruchirappalli - 620 024, Tamil Nadu, India.
[5]Department of Biotechnology, St. Michael College of Engineering and Technology, Kalayarkoil-630 551, Tamil Nadu, India.
[6]Research Co-ordinator, National College (Autonomous), Tiruchirappalli, 620001, Tamil Nadu, India.

ABSTRACT The present study was an attempt to understand the sexual dimorphism of the integumentary scent glands of soft-furred field rat *Millardia meltada* from the perspectives of anatomy, morphology and histology with view to correlate with the sex-specific pheromones they produce. The scent gland of male is known as preputial gland, and female, the clitoral gland. The rats, that are agricultural pests were field caught, the glands of males and females of almost identical size were dissected out, and subjected to gravimetric, morphometric and histological analyses. Both glands are yellowish-brown, pear-shaped, and dorsoventrally compressed. The mean weight, length and width of preputial glands are significantly ($p < 0.05$) larger than that of the clitoral glands. The preputial gland is composed of sebaceous glandular lobules and apocrine glandular lobules whereas the clitoral gland is formed only of sebaceous glandular lobules. The sebaceous glandular lobules of both preputial and clitoral glands are filled with a wax-like material. Thus, the scent glands of the soft-furred male field rats exhibit sexual dimorphism in respect histoarchitecture of the glands and the nature of the secretory material. This sexual dimorphism of the scent glands may reflect control by male and female sex hormones impinging on specific roles as sex attractant pheromones.
Acta Biol Szeged 64(2):181-189 (2020)

KEY WORDS
apocrine glandular lobes
clitoral gland
myoepithelial cells
preputial gland
sebaceous glandular lobes
soft-furred field rat

ARTICLE INFORMATION
Submitted
11 January 2021.
Accepted
14 January 2021.
***Corresponding author**
E-mail: deer_raj@yahoo.co.in (T. Rajagopal);
garchu56@yahoo.co.in (G. Archunan)

Introduction

Rodent pests, distributed worldwide, are a huge menace in that they affect human health by spreading diseases and human welfare by damaging food crops and stored food grains. Soft-furred field rat, *Millardia meltada*, is one such rodent pest widely distributed in India, Pakistan, Nepal, Bangladesh and Sri Lanka, mostly found in gravelly areas, bunds of fields, largely cultivated areas of tropical and sub-tropical dry deciduous forests, tropical grasslands, irrigated croplands and grasslands with gravel, wherein the preferred habitats are agriculture lands, water courses, embankments, and dry rocky hills. This rat's infestation causes pre-harvest losses of up to 1-10% in rice and wheat crops (Greaves 1989). The very high reproductive fitness of rats in general and field rat in particular overrides the conventional pest control strategies whereupon control of this pest has been gruesome. Effective olfactory (chemical) communication between male and female rats plays a vital role in this high reproductive fitness (Archunan 2009). In most mammals, the olfactory communication is mediated by pheromones which are emitted into the environment via urine, feces, saliva, and the secreted fluids of diverse integumentary scent glands. Laterocaudal, supraorbital, orbital, circumcaudal, infracaudal, preputial, clitoral, armpit, metatarsal, tarsal, preorbital, interdigital, flank, cheek, chin, anal, perineal, ventral, midventral, supracaudal, etc. are some such integumentary scent glands. They are located under the dermal layer of the skin (Balakrishnan and Alexander 1985; Archunan and Ponmanickam 2010; Rajagopal and Archunan 2011; Alexandre-Pires et al. 2014; Yilmaz et al. 2017).

Among the integumentary scent glands of rats prepu-

tial glands in the male and clitoral glands in the female are very prominent (Kannan et al. 1998; Kannan and Archunan 2001; Archunan and Ponmanickam 2010). These two glands are the prime sources of pheromones in rats and have several critical functions including conspecific attraction through releasing specific volatiles as well as non-volatile substances, mother-young bondage, etc. (Archunan 2009; Archunan and Ponmanickam 2010). According to Zhang et al. (2008) the male rats are attracted towards the females by odors emanating from the clitoral gland and this attraction is more at the time of estrus than the other phases of the reproductive cycle. Achiraman et al. (2011) found the concentration of squalene to be significantly higher in clitoral gland secretion at the time of estrus which, therefore, could be an ovulation-indicating chemosignal in female rat. Zhang et al. (2008) identified farnesol in female rats and squalene in male rats as the major chemosignals. The predominant pheromone compound farnesol and its carrier protein α_{2u}-globulin have been reported in preputial gland secretion of the laboratory rat (Ponmanickam and Archunan 2006; Ponmanickam et al. 2009; Ponmanickam et al. 2010) and house rat (Kamalakkannan et al. 2006; Rajkumar et al. 2010). The preputial gland becomes atrophied after castration, and testosterone replacement restores it to its the original size, which suggest that the preputial gland and the glandular proteins, *visa vi* pheromone carrier protein, are testosterone dependent (Kamalakkannan et al. 2006; Ponmanickam et al. 2010). It is interesting to note that rat pub preputial gland releases a pheromone, dodecyl propionate, which regulates the maternal anogenital licking behavior that forms an aspect of the mother-young bond (Brouette-Lahlou et al. 1999; Ponmanickam et al. 2009). The preputial gland also enhances the poison bait efficiency by inhibiting the bait shyness when tested in house rat (Selvaraj and Archunan 2006).

The histomorphology of male preputial and female clitoral glands has been studied in a very few rat and mouse species. For instance, Knoblaugh et al. (2018) found that the preputial glands of rats and mice are lobulated and consist of a connective tissue capsule that surrounds large, cavernous ducts lined by stratified squamous epithelium and acini. The acini are composed of eosinophilic, pale, foamy, secretory sebaceous cells with dark nuclei and peripheral, flat, elongated basal cells (Ponmanickam et al. 2016). Gourbal and Gabrion (2006) investigated the histomorphological alterations induced by the parasite (*Taenia crassiceps*) in male preputial and female clitoral glands of mice, and found disorganization of the acinar cells of male preputial gland, but no impact was reflected in the histomorphology of the female clitoral glands. It was suggested that this difference between infected male and female mice might be related to the different sex hormones (Gourbal and Gabrion 2006). According to Ramachandran et al (2018) the histological preparations of the preputial gland of *M. meltada* show acinar cells with sebum. Immunohistochemical analysis revealed the presence of α_{2u}-globulin, the carrier protein, in the sebum. The sebum is secreted into the central duct of the preputial gland and excreted through the urethra when it contains volatile compounds (e.g., farnesol and 6-methyl-1-heptanol) for chemical communication. Barring this, there has been no focused study of comparative histomorphology of male preputial glands and female clitoral glands. Hence, the present investigation was taken up to explore the sex-specific differences in the histomorphology of preputial and clitoral glands of soft-furred field rat, *M. meltada*.

Materials and Methods

Animal

Adult male and female rats *Millardia meltada* were collected from paddy fields in and around Madurai and Tiruchirappalli districts and housed separately in polypropylene cages (40 x 25 x 15 cm) with rice husk to 2 cm height as bedding material, at 12 h light: 12 h dark cycle, and temperature 24 ± 1 °C, when they were fed with formulated rat pellet food (Sai Durga Feeds and Foods, Bangalore) and water *ad libitum*. The bedding material was changed twice a week. The study was conducted under approval from the Institutional Animal Ethics Committee (IAEC) of Bharathidasan University, Tiruchirappalli, India (Approval No. BDU/IAEC/2012/71).

Dissection of preputial and clitoral glands

Six adult intact male and female rats were dissected under sodium pentabarbital anesthesia (Fig. 1). The preputial and clitoral glands were removed carefully, and the rats were sacrificed under excess ketamine (2 mg/kg, iv). The length and width of the glands were measured using a graph sheet, and then weighed in a monopan balance (Rajagopal and Archunan 2011).

Histological study

Immediately thereafter the glands were fixed separately in Bouin's fluid and subjected to routine histological analysis (Humason 1979). After several changes of 70% alcohol, until the yellow color of Bouin's fluid disappeared, the tissues were dehydrated by passing through ascending grades of alcohol, cleared in xylene, infiltrated with molten paraffin, and finally embedded in paraffin wax. Transverse and longitudinal sections at 3-5 μm

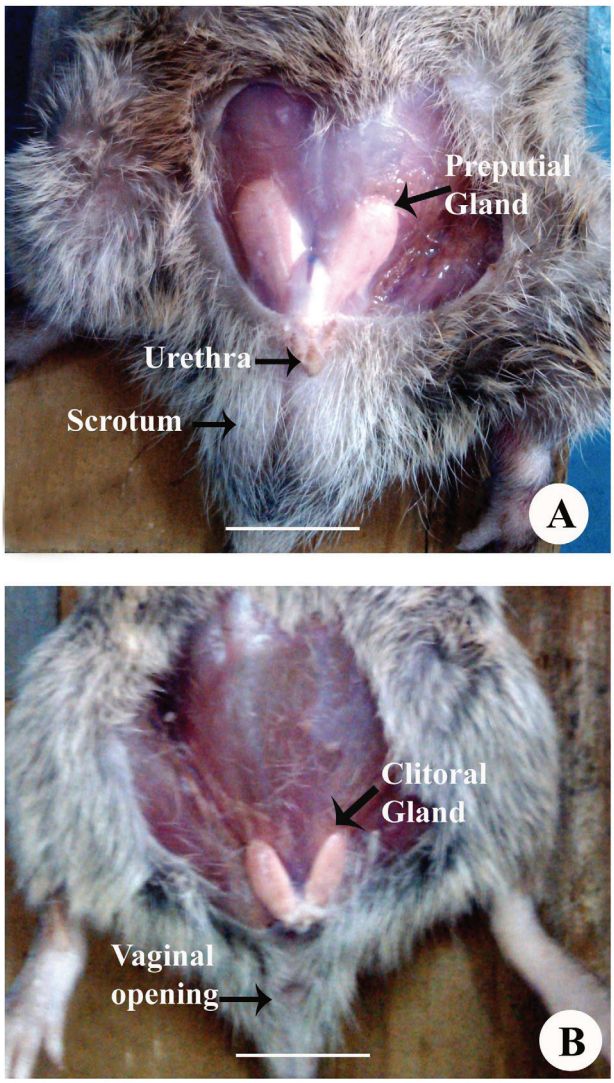

Figure 1. Ventral dissection of male (A) and female (B) soft-furred field rat, *Millardia meltada*, showing preputial and clitoral glands, respectively. Bar = 1 cm

thickness were obtained using a rotary microtome (Leica, Germany). The sections, thus obtained, were stained in Harris hematoxylin and eosin, dehydrated using alcohol, cleared in xylene and mounted in DPX adhesive resin.

Data processing

The data with respect to length, width and weight were used to calculate the respective means and standard deviations. Paired sample *t*-test was conducted and *p* value less than 0.05 was taken to indicate significant difference.

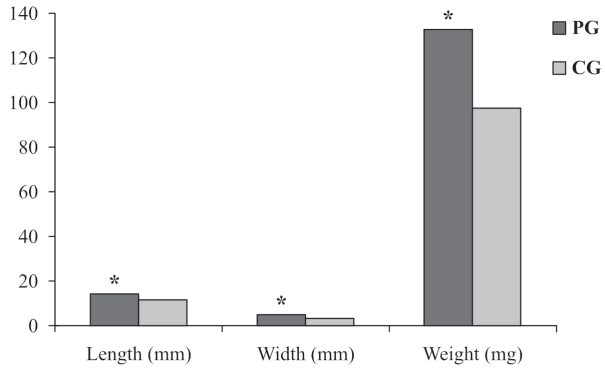

Figure 2. Mean values of the morphometric parameters (length, width, and weight) of male preputial (PG) and female clitoral glands (CG). *$p < 0.05$, preputial gland (PG) compared to clitoral gland (CG).

Results

Morphological observation

The scent glands are located underneath the dermis and embedded in the subcutaneous fat. The preputial glands are bilateral and located in the subcutaneous adipose tissue, laterocranial to the penis (Fig. 1A), while the clitoral glands are situated on either side of the clitoris and immediately adjacent to the inguinal portion of the mammary gland (Fig. 1B). The paired glands (both preputial and clitoral) are yellowish-brown, pear-shaped, and dorsoventrally compressed. The preputial gland of adult male rat measured 14.16±3.81 mm long, and 4.41 ± 1.05 mm wide and weighed 132.6 ± 12.10 mg. The clitoral gland of adult female rat measured 11.25 ± 2.13 mm long, and 2.95 ± 0.75 mm wide and weighed 97.5 ± 10.85 mg. Thus, the morphometric parameters [length: t = 10.03, df = 11; width: t = 5.99, df = 11 and weight: t = 13.47, df = 11] of preputial and clitoral glands differ significantly ($p < 0.05$) (Fig. 2).

The density and diameter of sebaceous glands were found to vary between preputial gland of male and clitoral gland female rats under microscopic investigation. The paired t-test clearly showed that the density of sebaceous gland is significantly (t = 7.97, df = 11, $p < 0.05$) higher in male preputial gland (14.65 ± 1.14 units/mm^2) than the female clitoral gland (8.35 ± 0.52 units/mm^2). Further, the diameter of sebaceous gland varied significantly (t = 13.58, df = 11, $p < 0.05$) in the male preputial gland (29.90 ± 1.56 μm) compared to female clitoral gland (18.71 ± μm). The density (6.44 ± 0.48 units/mm^2) and diameter (24.69 ± 0.88 μm) of apocrine gland was also noted in the preputial glands of male rat.

Histological observation

The secretory units of preputial gland are formed of se-

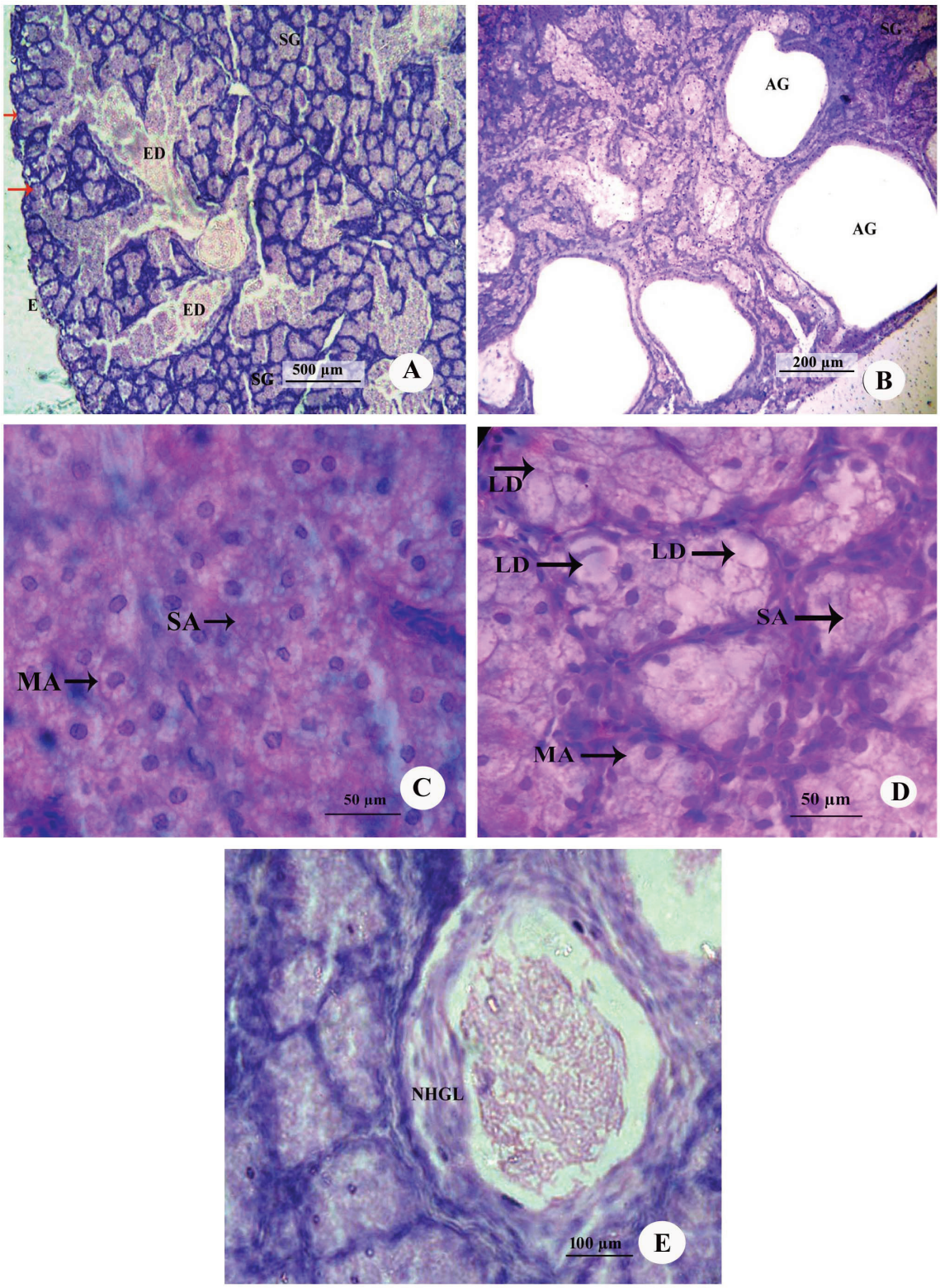

Figure 3. Hematoxylin-eosin-stained sections of preputial gland of male rat. A, Sebaceous glandular lobular portion; B, Apocrine glandular lobular portion; C, Ordinary sebaceous glandular lobules; D, Modified sebaceous glandular lobules; E, Sebaceous glandular portion with a secretory acinus with the lumen distended with secretory material released from the cells by necrosis. Abbreviations: **ED**: Excretory duct; **E**: Epidermis; **SG**: Sebaceous gland; **AG**: Apocrine gland; **NHGL**: Normal alveolar holocrine glandular lobules; **SA**: Serous acini; **MA**: Mucus acini; **LD**: Lipid droplets.

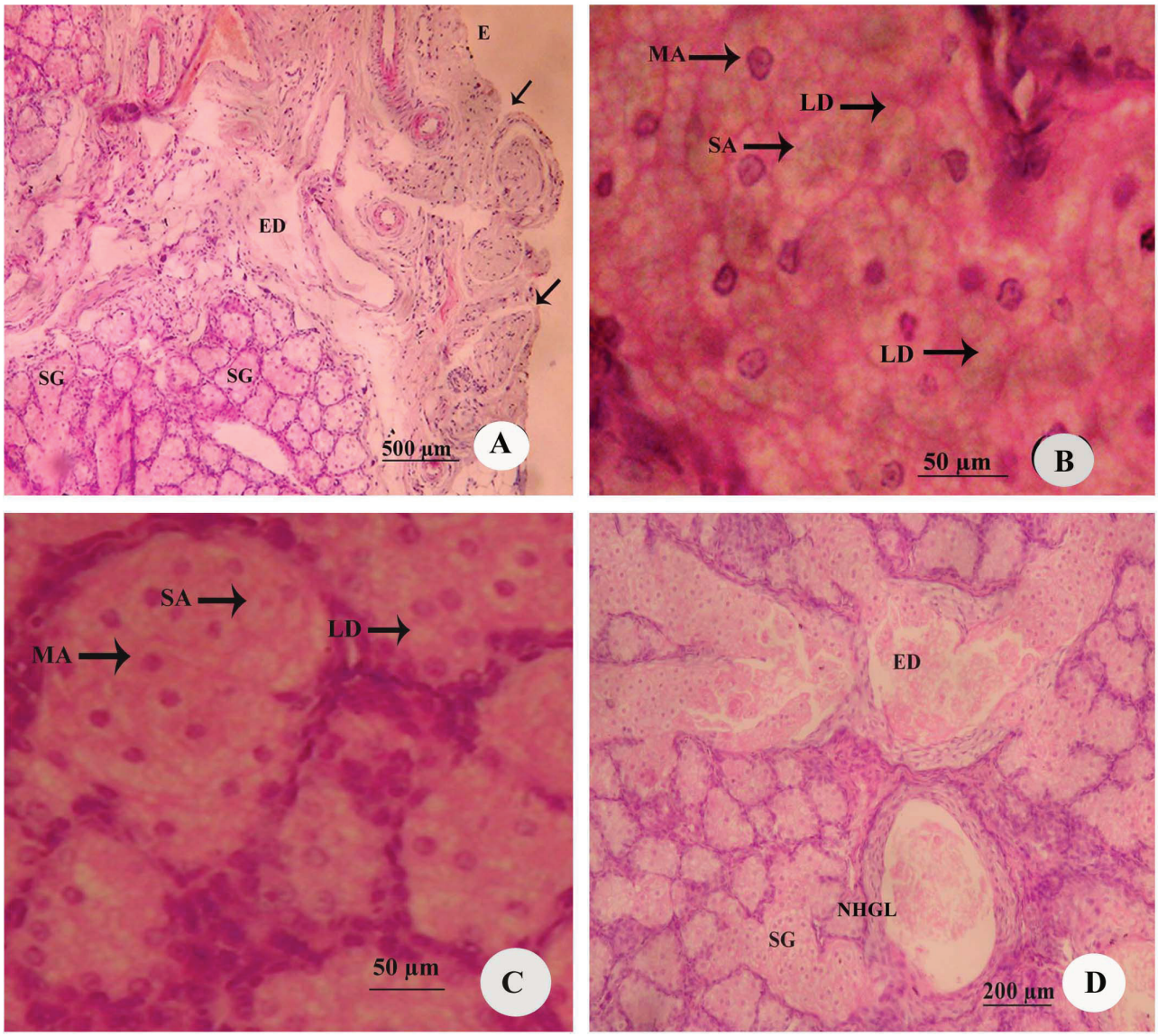

Figure 4. Hematoxylin-eosin stained sections of clitoral gland of female rat. A, Sebaceous glandular lobules; B, Ordinary sebaceous glandular lobules; C, Modified sebaceous glandular lobules; D, Sebaceous glandular portion with a secretory acinus distended with secretory material released from cells by necrosis. Abbreviations: **ED**: Excretory duct; **E**: Epidermis; **SG**: Sebaceous gland; **NHGL**: Normal alveolar holocrine glandular lobules; **SA**: Serous acini; **MA**: Mucus acini; **LD**: Lipid droplets.

baceous secretory lobules and apocrine secretory lobules (Fig. 3A, B). On the other hand, the secretory units of clitoral glands are only sebaceous glandular lobules (Fig. 4A). The sebaceous secretory gland lobules of preputial as well as clitoral glands are formed of both ordinary and modified sebaceous glandular lobules (Fig. 3C, D; Fig. 4B, C). The ordinary sebaceous glandular lobules are small and superficially located. The secretory acini formed of the modified sebaceous glandular lobules are teardrop-shaped and very large as compared to acini formed of the ordinary type of glandular lobules. The modified sebaceous glandular lobules consist of four types of cells: peripheral cells, differentiating cells, mature cells and necrotic cells. Peripheral cells are flat with oval nucleus and form a thin layer. Differentiating cells are large, polyhedral in shape, and contain centrally located nucleus in the eosinophilic cytoplasm. The differentiating cells progressively transform into mature cells which have a foamy cytoplasm. Necrotic cells possess pyknotic nuclei and on lysis release the content into the lumina.

In both preputial and clitoral glands the secretory material of sebaceous cells is released by holocrine mechanism into the branched tubuloalveolar system wherein the secretory acini open into numerous lateral ducts that fuse to form a wide central duct through which the secretion is conveyed to the lumen of the pouch (Fig. 3E; Fig. 4D). At the distal end of the gland the central duct, containing membrane-bound secretory granules, opens onto the skin at the transition of the parietal layer of the prepuce and the end of the urethra in the tip of the penis in the case of preputial gland and vagina in the case of clitoral gland. The sebaceous type acinar cells look foamy, with small granules in the cytoplasm. The glandular epithelioid acini are composed of flat basal cells adjacent to the basement membrane and lateral to the secretory cells in the central parts of the acini. The cells are closer to the center of the alveoli and become progressively large, and the cytoplasm is distended with fat droplets due to which the cytoplasm takes honeycomb-like appearance (Fig. 3C, D; Fig. 4B, C). The apocrine secretory units of preputial glands consist of an inner layer of cuboidal cells that rest directly on the basement membrane and an outer layer of myoepithelial cells. The cuboidal cells that line the secretory acini possess acidophilic vacuolated cytoplasm and spherical, centrally located nucleus. The cells often exhibit apical protrusions. The secretory material is released in the form of droplets by apocrine mechanism and get stored in the lumina (Fig. 3B).

Discussion

The significant difference of the morphometric parameters (i.e., length, width, and weight) between preputial and clitoral glands is to be perceived as manifestation of the sexual difference of the pheromone secreting glands between male and female soft-furred field rat which is in agreement with the condition in Iranian sheep (Abbasi et al. 2009), Egyptian sheep (Awaad et al. 2015), Awassi sheep (Yilmaz et al. 2017), and Bandicoot rat (Ponmanickam et al. 2016). In another context, the preorbital gland length, width and weight were higher in dominant male (i.e., adult) than subordinate male (i.e., sub-adult and adolescent) blackbucks (Rajagopal and Archunan 2011). According to Zhang et al. (2008) the scent glands of rats do not exhibit sexual differences, but gonadectomy resulted in significant decrease of size of the scent glands of both sexes. The dominant male mice are characterized by higher testosterone levels and heavier preputial glands than subordinate male mice (Mckinney and Desjardins 1973). Further, the diameter of sebaceous gland has a higher in size in male preputial gland compared to female clitoral gland. It is reported that the higher development of the sebaceous gland in the male fallow deer could depend on the higher social responsibility (dominance hierarchy) / production of testosterone (Schaal 1982; Moawad 2016). Therefore, the larger size and higher weight of male scent gland are to be taken to reflect manifestation of the androgen-support. These findings indicate that the size of scent glands is influenced by sex hormones and function to express their respective reproductive statuses to the opposite sex.

Microscopic examination of preputial and clitoral glands revealed a clear fibrous capsule around each. The histological structure of preputial gland is heterogeneous in that it has holocrine sebaceous and apocrine secretory cells, whereas sebaceous secretory cells alone are present in the entire clitoral gland. This is a clear histomorphological manifestation of sexual dimorphism. Similar findings have been made on intermandibular glands of lesser mouse deer (Agungpriyono et al. 2006), infraorbital gland of the barking deer (Adnyane et al. 2011) and preorbital gland of the blackbuck (Rajagopal and Archunan 2011), but the finding contradicts the observation made on infraorbital glands of the Japanese serow (Atoji et al. 1987), and Formosan serow (Atoji et al. 1996) and interdigital glands of sheep (Misk and Misk 2013). According to Zhang et al. (2008) rat male scent gland secretion is rich in squalene compared to female gland, whereas farnesol content was lower in male scent gland than female gland. Squalene is a female-attractant and farnesol a male-attractant. Thus, these compounds are sex-specific (Zhang et al. 2008). One of our studies showed that the amount of protein was higher in preputial glandular secretion than clitoral gland (Archunan et al. 2004). In addition, though the 20 kDa protein was found in both male and female scent glands of rat, the intensity was higher in male than female and it was suggested that this protein is indeed a sex-associated protein (Archunan et al. 2004). Thus, this study substantiates histological difference between the preputial and clitoral glands of soft-furred field rat indicating sexual dimorphism. We suggest that the sex-specific nature of pheromone and protein may be due to the variations in the histoarchitectutre of the glands and sex hormone-dependence of their morphology and secretion.

As far as sebaceous secretory portion of both preputial and clitoral glands are concerned, we found ordinary as well as modified glandular lobules. The modified sebaceous glandular lobules have been found in the scent glands of several mammalian species such as antelope *Madoqua* sp. (Richter 1971), antelope/red duiker *Cephalophus natalensis* (Mainoya 1978), royal antelope *Neotragus pygmaeus* (Kuhn 1976), steenbok *Raphicerus campestris* (Cohen and Gerneke 1976), and oribi *Ourebia ourebi* (Sokolov et al. 1994). Nevertheless, both modified and ordinary sebaceous glandular lobules produce sebum which is an oily/waxy

substance documented to be concerned with olfactory communication in several mammals (Rajagopal and Archunan 2011; Yilmaz et al. 2017; Ramachandran et al. 2018; SankarGanesh et al. 2018). The modified sebaceous glandular lobules of the preputial glands of male mouse are larger than in the female clitoral glands, and this feature is greatly influenced by a variety of hormones (Bronson and Caroom 1971). An immunohistochemical study revealed the presence of α_{2u}-globulin in the sebum produced in modified sebaceous glandular lobules of preputial gland. The sebum is discharged by holocrine mechanism into the central duct of the preputial gland and excreted through the urethra. The putative pheromones (e.g., farnesol) are bound to the α_{2u}-globulin (Ramachandran et al. 2018). Ilayaraja et al. (2014) conducted research to confirm that farnesol binds with the α_{2u}-globulin efficiently. The present study suggests that sebaceous secretory cells of scent glands of male and female rats secrete different odoriferous volatile substances. These substances provide for olfactory communication between conspecifics (Kannan et al. 1998; Zhang et al. 2008; Achiraman et al. 2011; Ramachandran et al. 2018).

In the present study, the apocrine glandular lobules were found only in the preputial gland, i.e., male. The myoepithelial cells observed in the apocrine glandular lobules revealed evidence of apocrine secretion of the secretory cells. The myoepithelial cells surround the secretory acini and facilitate discharge of the secretory material by way of their contraction (Abbasi et al. 2009; Awaad et al. 2015). Apocrine glands have been reported in sheep, horse, antelope, cow and a few marsupials, and these glands function as scent glands to produce pheromones (Robertshaw 1987; Rajagopal and Archunan 2011). According to Satoh et al. (1994) the myoepithelial cells of apocrine glands are endowed with capability to provide compression pressure for glandular expulsion of the secretory material. It is remarkable that the pheromonal compounds derived mainly from the sebaceous gland on discharge to the outside can adhere to objects in view of the carrier proteins (Atoji et al. 1987; Agungpriyono et al. 2006; Rajagopal and Archunan 2011). Previous studies have shown that the lumen of the apocrine gland is filled with dense secretory materials which are discharged directly onto the excretory duct through prepuce (Karahan et al. 2007; Abbasi et al. 2009; Rajagopal and Archunan 2011; Awaad et al. 2015). The present study suggests that the apocrine secretory gland in the male rats would produce sex-specific volatile substances as an aspect of the preputial glands that might facilitate better adhesion capacity and high persistence in the scented site during the expression of territorial/scent marking in male rats.

To the best of our knowledge this is the first comprehensive comparative histomorphological analysis of preputial and clitoral glands, the male and female scent glands respectively, of soft-furred field rat. Preputial glands of male rat are relatively larger in size than the clitoral glands of female rat. Preputial gland is composed of sebaceous and apocrine secretory glandular lobules whereas clitoral gland is made up only of sebaceous glandular lobules. These findings indicate that the scent glands of the soft-furred male and female field rats show sexual dimorphism. Based on the morphometric and histomorphological observation, we conclude that the soft-furred field rat scent glands (preputial and clitoral) would play role in the production of sex-specific volatile substances through sebaceous and apocrine secretory glands for olfactory communication. Further ultrastructural and immunohistochemical studies of different rodent species and correlation between pheromone production and behaviors would throw light on importance of these glands in pheromonal communication which can be made use of in the rodent pest management programs.

Acknowledgements

The authors thank the Principal and the Management of Thiagarajar College (Autonomous), Madurai, for providing facilities and the constant encouragement. GA thanks the University Grants Commission (UGC), New Delhi, for the award of UGC-BSR Faculty Fellowship. The authors declare that there is no conflict of interest.

References

Abbasi M, Gharzi A, Mohammadzadeh S, Karimi H (2009) Morphology and histology of the interdigital gland in an Iranian native breed of sheep. J Anim Vet Adv 8:1157-1161.

Achiraman S, Archunan G, Abirami B, Kokilavani P, Suriyakala U, SankarGanesh D, Kamalakkannan S, Kannan S, Habara Y, Sankar R (2011) Increased squalene concentrations in the clitoral gland during the estrous cycle in rats: an estrus-indicating scent mark? Theriogenology 76:1676-1683.

Adnyane IKM, Ziki ABZ, Noordin MM, Wahyuni S, Agungpriyono S (2011) Morphological study of the infraorbital gland of the male barking deer, *Muntiacus muntjak*. Afr J Biotechnol 10:17891-1797.

Agungpriyono S, Atoji Y, Yamamoto Y, Zuki AB, Novelino S (2006) Morphology of the intermandibular gland of the lesser mouse deer, *Tragulus javanicus*. Anat Histol Embryol 35:325-333.

Alxandre-Pires G, Martins C, Galvao AM, Correia M, Ramilo D, Quaresma M, Ligeiro D, Nunes T, Calderia RM, Ferreira Dias G (2014) Morphological aspects and

expression of estrogen and progesterone receptors in the interdigital sinus in cyclic ewes. Microsc Res Tech 77:313-325.

Archunan G (2009) Vertebrate pheromones and their biological importance. J Exp Zool India 12:227-239.

Archunan G, Kamalakkannan S, Achiraman S, Rajkumar R (2004) Identification of glandular (preputial and clitoral) proteins in house rat (*Rattus rattus*) involved in pheromonal communication. Indian J Exp Biol 42:1032-1035

Archunan G, Ponmanickam P (2010) Preputial gland: A potent pheromone source in rodents. In Logan EW, Jason MA, Eds., The Biology of Odors: Sources, Olfaction and Response. Nova Science Publishers, Hauppauge, New York, 321-340.

Atoji Y, Sugimura M, Suzuki Y (1987) Lectin histochemical study on the infraorbital gland of the Japanese serow (*Capricornis crispus*). Acta Morphol Neerl Scand 25:201-213.

Atoji Y, Yamamoto Y, Suzuki Y (1996) Infraorbital glands of a male Formason serow (*Capricornis crispus swinhoei*). Eur J Morphol 34:87-94.

Awaad AS, Tawfiek MG, Moawad UK, Abdel Razek AH, Abedellaah BA (2015) Morphohistological and surgical anatomy of the sinus interdigitalis in Egyptian native breeds of sheep. Beni-Suef Univ J Basic Appl Sci 4:157-166.

Balakrishnan M, Alexander KM (1985) Sources of body odour and olfactory communication in some Indian mammals. Indian Rev Life Sci 5:277-313.

Bronson FH, Caroom D (1971) Preputial gland of the male mouse: attractant function. J Reprod Fertil 25:379-382.

Brouette-Lahlou I, Godinot F, Vernet-Maury E (1999) The mother rat's vomeronasal organ is involved in detection of dodecyl propionate, the pup's preputial gland pheromone. Physiol Behav 66:427-436

Cohen M, Gerneke DH (1976) Preliminary report on the intermandibular cutaneous glandular area and the infraorbital gland of the steenbok. J S Afr Vet Assoc 47:35-37.

Gourbal BEF, Gabrion C (2006) Histomorphological study of the preputial and clitoral glands in BALB/c mice with experimental *Taenia crassiceps* infections. J Parasitol 92:189-192.

Greaves JH (1989) Rodent pest and their control in the near East. FAO of the UN plant production and protection, Issue No. 95. Food and Agricultural Organization, Rome, Italy.

Humason GL (1979) Animal Tissue Techniques, 4th Ed. W. H. Freeman, San Francisco.

Ilayaraja R, Rajkumar R, Rajesh D, Muralidharan AR, Padmanabhan P, Archunan G (2014) Evaluating the binding efficiency of pheromone binding protein with its natural ligand using molecular docking and fluorescence analysis. Sci Rep 4:1-7.

Kamalakkannan S, Achiraman S, Rajkumar R, Rameshkumar K, Archunan G (2006) Identification of sex-associated protein in the preputial gland of house rat: a new insight in RPM. Acta Physiol Hung 93:145-152.

Kannan S, Rameshkumar K, Archunan G (1998) Sex attractants in male preputial gland: Chemical identification and their role in reproductive behaviour of rats. Curr Sci 74:689-691.

Kannan S, Archunan G (2001) Chemistry of clitoral gland secretions of the laboratory rat: Assessment of behavioural response to identified compounds. J Biosci 26:247-252.

Karahan S, Yildiz D, Bolat D (2007) Scanning electron microscopic features of the ovine interdigital sinus. Acta Vet Hung 55:417e24.

Knoblaugh SE, True L, Tretiakova M, Hukkanen RR (2018) Comparative anatomy and histology. In Treuting PM, Dintzis SM, Montine KS, Eds., A Mouse, Rat, and Human Atlas. Academic Press, London, UK, 335-365.

Kuhn HJ (1976) Antorbitaldruse und tranennasengang von *Neotragus pygmaeus*. Z Säugetierkde 41:369-380.

Mainoya JR (1978) Histological aspect of preorbital and interdigital glands of red duiker (*Cephalopus natalensis*). East Afr Wildl J 16:256-272.

McKinney TD, Desjardins C (1973) Postnatal development of the testis, fighting behavior and fertility in house mice. Biol Reprod 9:279-294.

Misk TN, Misk NA (2013) Surgical excision of interdigital pouch and cyst in sheep. *Int J Vet Med* Res Rep 1:1-8.

Moawad UK (2016) Morphological, histochemical and morphometric studies of the preorbital gland of adult male and female Egyptian native breeds of sheep (*Ovis aries*). Asian J Anim Vet Adv 11:771-782.

Ponmanickam P, Archunan G (2006) Identification of α_{2u}-globulin in the rat preputial gland by MALDI-TOF analysis. Indian J Biochem Biophys 34:319-322.

Ponmanickam P, Jebamercy G, Archunan G, Kannan S (2009) Detection of α_{2u}-globulin in rat pup preputial gland by MALDI-TOF mass spectrometry. Curr Zool 55:296-300.

Ponmanickam P, Palanivelu K, Govindaraj S, Baburajendran R, Habara Y, Archunan G (2010) Identification of testosterone-dependent volatile compounds and proteins in the preputial gland of rat *Rattus norvegicus*. Gen Comp Endocrinol 167:35-43.

Ponmanickam P, Muniasamy S, Rajagopal T, Rengarajan RL, Archunan G (2016) Identification of $GABA_{\beta}$ receptor protein and farnesol in the preputial gland of bandicoot rat (*Bandicota indica*). Adv Zool Bot 4:37-45.

Rajagopal T, Archunan G (2011) Histomorphology of preorbital gland in territorial and non-territorial male blackbuck, *Antelope cervicapra* L., a critically endangered species. Biologia 66:370-378.

Rajkumar R, Ilayaraj R, Liao CC, Archunan G, Achiraman S, Prakash S, Ng WV, Tsay YG (2010) Detection of alpha(2u)-globulin and its bound putative pheromones in

the preputial gland of the Indian commensal rat (*Rattus rattus*) using mass spectrometry. Rapid Commun Mass Spectrum 24:721-728.

Ramachandran R, Achiraman S, Rajagopal T, SankarGanesh D, Kamalakkannan S, Ponmanickam P, Rajkumar R, Ramya Vaideki G, Padmanabhan P, Archunan G (2018) Localization of α_{2u}-globulin in the acinar cells of preputial gland, and confirmation of its binding with farnesol, a putative pheromone, in field rat (*Millardia meltada*). PLoS One 13:1-15.

Robertshaw D (1983) Apocrine sweat glands. In Goldsmith LA, Ed., Biochemistry and Physiology of the Skin. Oxford University Press, New York, 642-653.

Richter J (1971) Unterschungen an antorbitaldrusen von Madaqua (Bovidae; Mammalia). Z Säugetierkd 36:334-342.

SankarGanesh D, Ramachandran R, Ashok R, Saravanakumar VR, Sukirtha R, Archunan G, Achiraman S (2018) Buck odor production in the cornual gland of male goat, *Capra hircus*- Validation with histoarchitecture, volatile and proteomic analysis. Indian J Biochem Biophys 55:183-190.

Satoh Y, Oomori Y, Ishikawa K, Ono K (1994) Configuration of myoepithelial cells in various exocrine glands of guinea pigs. Anat Embryol 189:227-236.

Selvaraj R, Archunan G (2006) Efficacy of male scent glands and urine in masking poison bait odour in female house rats, *Rattus rattus*. J Pest Sci 79:255-258.

Sokolov VE, Chernova OF, Fekadu K (1994) The skin of some Ethiopian ungulates. Russian Academy of Science, Moscow, 147

Yilmaz B, Yilmaz R, Demircioglu I, Arican I (2017) Morphological and histological structure of the interdigital gland in Awassi sheep (*Ovis aries*). Turk J Vet Anim Sci 41:380-386.

Zhang JX, Sun L, Zhang JH, Feng ZY (2008) Sex- and gonad-affecting scent compounds and 3 male pheromones in the rat. Chem Senses 33:611-621.

Acta Biologica Szegediensis

Volume 64(2):191-198, 2020
Acta Biologica Szegediensis
http://abs.bibl.u-szeged.hu/index.php/abs

DOI:10.14232/abs.2020.2.191-198

ARTICLE

Acidic ambiance induced post-oxidative stress affects AMPK-PGC1α-SIRT1 axis in the skeletal muscles of zebrafish *Danio rerio* Hamilton, 1822

Sabarna Chowdhury[1], Subhendu K Chatterjee[1], Samir Bhattacharya[2], Sudipta Maitra[3] and Surjya K Saikia[1]*

[1]Aquatic Ecology and Fish Biology Laboratory, Department of Zoology, Centre for Advanced Studies, Visva-Bharati (A Central University), Santiniketan, West Bengal, India
[2]Molecular Endocrinology Laboratory, Department of Zoology, Centre for Advanced Studies, Visva-Bharati (A Central University), Santiniketan, West Bengal, India / Currently at The University of Burdwan, Golapbag, Barddhaman, West Bengal, India
[3]Molecular and Cellular Endocrinology Laboratory, Department of Zoology, Centre for Advanced Studies, Visva-Bharati (A Central University), Santiniketan, West Bengal, India

ABSTRACT The present study was aimed to understand whether acidic pH induces oxidative stress in zebrafish affecting metabolic sensor protein and thereby, the mitochondrial functions in the skeletal muscle of zebrafish. The experiments performed in aquaria involved the study of the changes of HIF1α, AMPK, PGC1α and SIRT1 levels together with the levels of mitochondrial Tfam and Nrf1. The results obtained from investigation of superoxide dismutase (SOD), catalase and glutathione revealed that the fish undergoes oxidative stress within a short duration of exposure to acidic ambiance. Further analysis with MDA and HIF1α helped to understand the effects of post oxidative stress on skeletal muscle of the fish at pH 5.0 (± 0.5). Of the three tissues studied (gill, brain and skeletal muscle) the effect was maximum in skeletal muscle as depicted by MDA level at 2 hours beyond which it declines augmenting death or mortality (15%) to the fish. Consequently, HIF1α was increased as an adaptive strategy against metabolic disruption during the first 2 hours period. However, on exposure to pH 5.0 (± 0.5) for 2 hours, there were decrease of the metabolic sensors viz. AMPK and SIRT1 followed by mitochondrial gene transcriptional co-activator PGC1α. The expression of mitochondrial transcription factors Tfam and Nrf1 were also reduced confirming perturbation in mitochondrial function affecting low ATP production compared to control. This was also supported by the decrease of COXII as well as mitochondrial complex I activity. All these results confirm that the metabolic machinery of zebrafish is affected when pH was lowered to 5.0 (± 0.5).

KEY WORDS
AMPK
malondialdehyde
mitochondrial bioenergetics
mitochondrial biogenesis
PGC1α
SIRT1

ARTICLE INFORMATION
Submitted
12 November 2020.
Accepted
28 December 2020.
***Corresponding author**
E-mail: surjyasurjya@gmail.com

INTRODUCTION

For last forty years, acidification in water bodies, largely in lakes throughout the world has invited extensive and vigorous research approach regarding aquatic resource management (Mcdonald 1983). Acidification of freshwater bodies became a global problem involving Europe, USA and Asia (Schindler 1988; Psenner 1994). Aquatic animals including fish live in a narrow range of pH, which is near neutral, therefore, any change in pH range adversely affects their normal biological functioning (Mcdonald 1983; Wood 1989). Of these, the metabolic mechanisms are found to be the most susceptible biological functions (Bhaskar and Govindappa 1985). A high alkaline or acidic stress may affect the physiological system, especially ion transporting cells in fish (Kwong et al. 2014). Thus, a sudden change in pH may lead to acute stress and a chronic pH state may cause death. Besides, acidic environment induced physiological impairments may disturb the overall homeostatic condition during growth in fish.

The zebrafish (*Danio rerio*), a small teleost has become the most widely used animal model for the study of various biological phenomena of vertebrates. Recently, this fish was subjected to study under different stress conditions for stress related diseases (Steenberger et al. 2011). However, very limited studies on the stress tolerance, especially with pH are performed on zebrafish. Reported studies address toxicological effect on embryos of zebrafish (Dave 1984, 1985; Andrade et al. 2017). Zahangir et al.

(2015) reported secondary stress responses of 'pH stress' on zebrafish where the haematological parameters were primarily assessed. However, metabolic regulator proteins related to mitochondrial functions due to pH stress have not been studied, yet.

In the present study, responses during oxidative stress and its post traumatic consequences caused by acidic pH were analysed through oxidative stress indicators and specified biochemical parameters, especially malondialdehyde (MDA) level in fish body. Being a by-product of lipid peroxidation, MDA has been widely used as a biochemical index of oxidative stress in mammals (Eze et al. 2008). The results of MDA, therefore, supported the changes of oxidative stress indicators like superoxide dismutase (SOD) and catalase enzyme activity and glutathione. The hypoxia inducible factor-1α (HIF1α) from skeletal muscle tissue was also studied to affirm the oxidative stress. At first instance, analysis of metabolic regulator proteins like AMP-activated protein kinase (AMPK), peroxisome proliferator-activated receptor gamma coactivator-1α (PGC1α) and sirtuin 1 (SIRT1 or NAD-dependent deacetylase sirtuin-1) were performed, which was followed by the analysis of transcription factor A of mitochondria (Tfam) and nuclear respiratory factor 1 (Nrf1). These were followed by the analysis of mitochondrial complex I activity, expression of cytochrome oxidase II (COX II) and synthesis of ATP to elucidate a better understanding on the metabolic impairments.

MATERIALS AND METHODS

Stress exposure to zebrafish

Zebrafish stock was kept in aquarium under laboratory environment (pH 6.5-7.5, temperature 25-28 °C, dissolved oxygen (DO) 7-10 mg/l). After one week of acclimatization, zebrafish (weight: 0.7 g, total length: 3.8 cm, n = 10) were collected in separate aquarium for further study. The experiments were set with three different levels of pH to measure the responses of tissues against acidic stress. These three pH levels were acidic (AC, 5.0 ± 0.5), near neutral (NN, 6.0 ± 0.45) and neutral (N, 7.0 ± 0.3). The pH levels were maintained by application of weak organic acid following a regression equation as $Y = 7.675 – 0.008X$ (Y = pH and X = Volume acetic acid, µl, $R^2 = 0.997$). A portable digital pocket-sized pH meter (HI98107P) was used to record the pH of the aquaria. The responses in fish tissues were measured in terms of MDA level from the respective tissues. For each analysis, ten fishes were sampled for collection of tissues.

Three tissues (skeletal muscle, brain and gills) were evaluated for maximum stress response against the three pH levels, *viz*. AC, NN and N. The values were recorded till the first mortality occurred in the treated fish population. Two norms were standardized after these three experiments. These were, (i) the highly responsive tissue and (ii) the effective pH level to assess the biochemical parameters of the highly responsive tissue. Once the above norms were set, a new set of fish were treated with the effective pH level and only the highly responsive tissue was subjected to all specified biochemical analysis. In this case, the effective duration of treatment period (mortality ≈ 15%) was determined beforehand.

To understand the progression and resulting effect of acidic stress, the specified biochemical parameters like SOD, catalase, and glutathione levels were measured for a period of two hours (the effective duration at 15% mortality) with 30 min intervals. The tissue samples thus collected were also used for assessing levels of metabolic sensors related to mitochondria after 2 h of acidic stress exposure.

Although not mandatory for the purpose, attempts were made to maintain all ethical norms for the fish in the subject during the experiment. Before tissue collection, fishes were narcotized using MS222.

Tissue collection and processing

Tissues (skeletal muscle, gill and brain) were collected (n = 10) from zebrafish and processed for further analysis. Before every analysis, the pooled tissues kept in lysis buffer (phosphate buffer) were homogenized using micro tissue homogenizer. The tissues homogenized were then centrifuged in 10000 g for 15 min. The supernatant was collected and used for all biochemical assessment. For western blot analysis, tissue proteins of 100 µg from the lysate were used.

Biochemical assays

The biochemical assessment was performed for MDA, other antioxidant enzymes and antioxidant (SOD, catalase, glutathione), mitochondrial complex I and ATP. MDA assay was performed according to the method of Aust (1985). MDA is a product of lipid peroxidation and reacts with TBA (thiobarbituric acid) to give a red species named TBARS (thiobarbituric acid reactive substance). The antioxidant enzyme SOD assay was performed following the method of Ewing and Janero (1995), while catalase assay together with reduced glutathione quantification were performed using microplate assay kits (G-Biosciences, ITAK1061 and ITAK1006). The ATP produced and the mitochondrial complex I activity were quantified using microplate assay kits (ATP assay kit, Sigma MAK190 and Cayman Chemical Mitocheck, Mitochondrial Complex I activity assay kit 700930).

Electrophoresis and immunoblotting

The desired quantity of tissue protein was resolved on 10% SDS-PAGE and were transferred to PVDF membranes through transfer buffer (25 mM Tris, 193 mM glycine, 20% methanol, pH 8.5) for 1.5 hours. Western blot analysis was performed for HIF1α, PGC1α, AMPK, SIRT1, Tfam, Nrf1 and COXII using specific antibodies (Table 1) against the protein/factor of interest. Membrane bound primary antibodies were visualized using corresponding secondary antibodies at 1:1000 dilutions, which was tagged with alkaline phosphatase and developed with corresponding substrates, 5-bromo-3-chloro-3-indolyl phosphate/nitrobluetetrazolium (BCIP/NBT). Band intensities were quantified by utilizing Image J software (NIH, Bethesda, MD).

Statistical analysis

Homogeneity of variances of data sets were tested using Levene's statistics. The Kruskal-Wallis H test was computed where Levene's statistics did not comply to $p > 0.05$. In case of all analyses, α level was fixed at 0.05. SPSS 16.0 was used for all statistical analyses.

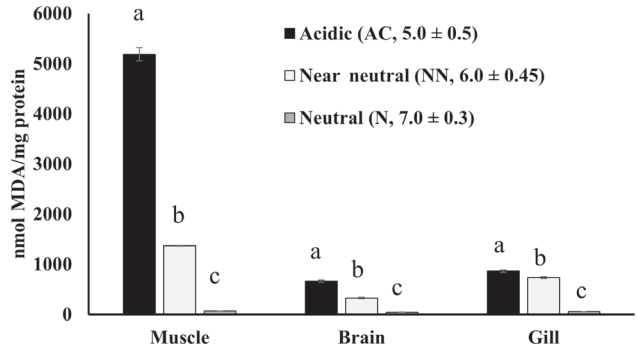

Figure 1. Determination of MDA levels in three different tissues (skeletal muscle, brain and gills) of zebrafish under three different pH conditions: acidic (AC, 5.0 ± 0.5), near neutral (NN, 6.0 ± 0.45) and neutral (N, 7.0 ± 0.3). Data are shown as Mean ± SE. Bars with different lower-case letters show statistically significant difference at $p < 0.05$.

RESULTS

The present study examined three different tissues from adult zebrafish, which were subjected to three pH levels, *viz.*, AC, NN and N (control). The formation of MDA in skeletal muscle tissue was significantly higher than the control (Kruskal-Wallis H Test, $\chi 2 = 25.806$, $p = 0.00$; Fig. 1). Out of all the three pH levels, mean rank of pH 5.0 ± 0.5 showed maximum effect on skeletal muscle as reflected from MDA levels (Fig. 1). It was also observed that increased formation of MDA in skeletal muscle tissue was comparatively higher than brain and gill tissues (Fig. 1). We have, therefore, considered skeletal muscle of zebrafish as primary tissue affected by acidic ambiance. The difference in the formation of MDA in skeletal muscle among three pH levels (namely AC, NN and N), were found statistically significant (Kruskal-Wallis H Test, $\chi 2 = 25.806$, $p=0.00$; Fig. 1). Here, the AC showed highest rank in terms of MDA formation in skeletal muscle compared to other pH levels. The maximum level

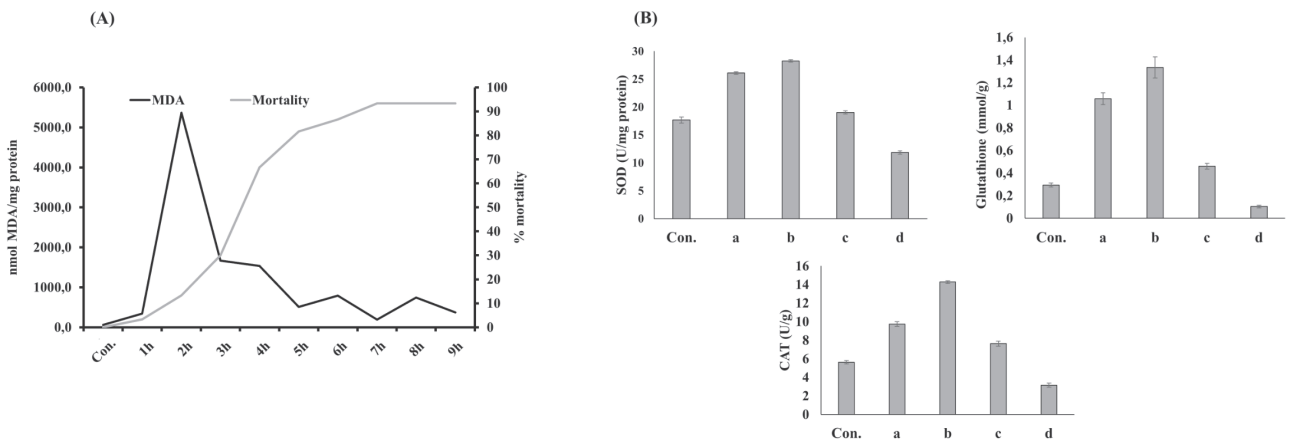

Figure 2. Formation of MDA in skeletal muscle tissue of zebrafish. (A) Formation of MDA in skeletal muscle tissue and percent mortality estimated over 9-h gradient with 1 h interval. The MDA formation was highest on exposure for 2 h to pH 5 (± 0.5). (B) catalase, glutathione and SOD produced under pH 5.0 ± 0.5 in the zebrafish skeletal muscle when treated for 30 min, 1 h, 1.5 h and 2 h. Bars with different lower-case letters show statistically significant difference at $p < 0.05$.

On figure B: **a**, pH 5 ± 0.5 for 30 min; **b**, pH 5 ± 0.5 for 1 h; **c**, pH 5 ± 0.5 for 1.5 h; **d**, pH 5 ± 0.5 for 2 h

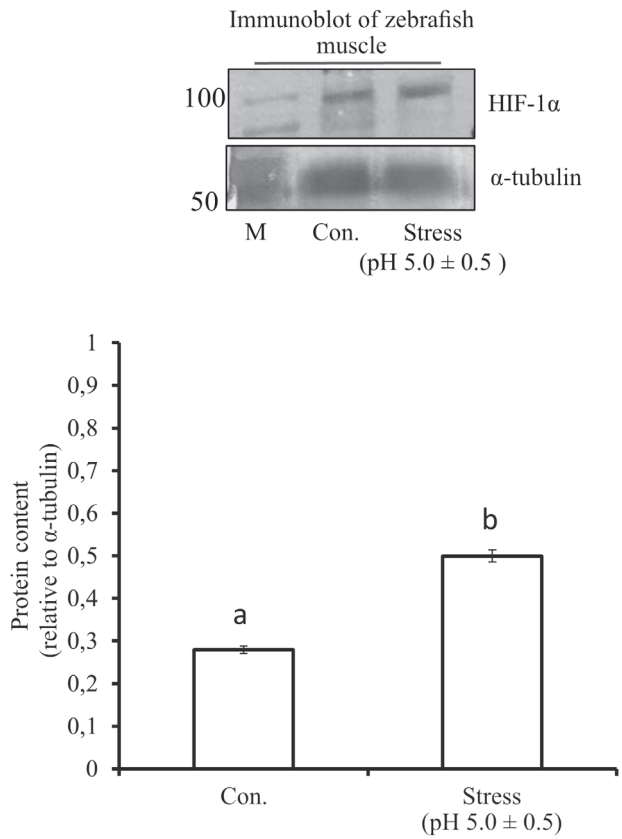

Figure 3. Immunoblot of a stress marker protein, HIF1α and its densitometry analysis after 2 h of stress exposure of zebrafish to pH 5.0 ± 0.5. Data are shown as Mean ± SE. Bars with different lower-case letters show statistically significant difference at $p < 0.05$.

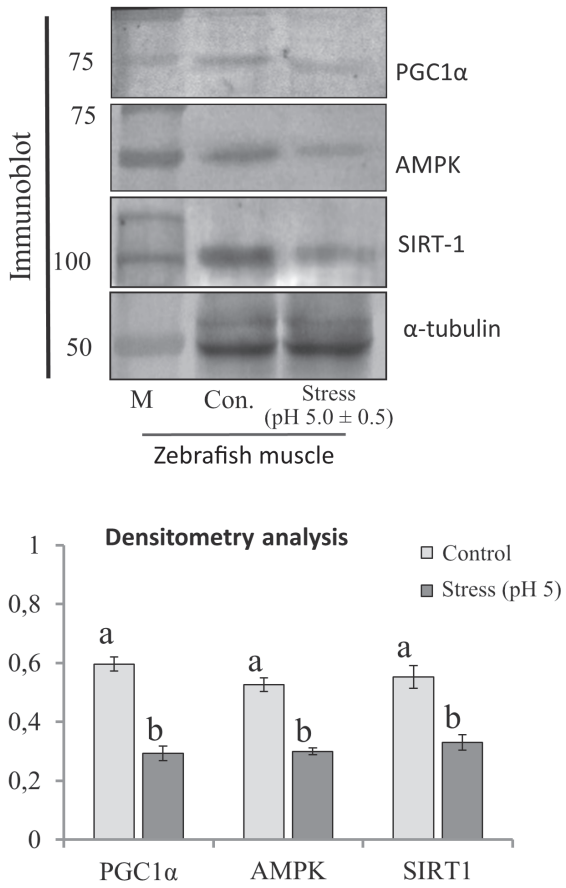

Figure 4. Immunoblots of AMPK, SIRT1 and PGC1α and, their densitometry analysis compared to control after 2 h of stress exposure of zebrafish to pH 5.0 ± 0.5. Data are shown as Mean ± SE. Bars with different lower-case letters show statistically significant difference at $p < 0.05$.

of MDA in skeletal muscle tissue (5000 nmol MDA/mg protein) was recorded at the second hour of treatment. Beyond this period, fish mortality starts (Fig. 2A). Thus, it was standardized that the skeletal muscle is the highly responsive tissue for oxidative stress induced by acidic ambiance, and it experiences elevated oxidative stress during 2-hours-exposure to acidic ambiance. All these outcomes were supported by the results of SOD, catalase and glutathione assays of the skeletal muscle of fish at 30 min, 1 h, 1.5 h and 2 h intervals under pH 5.0 ± 0.5. The results showed that, compared to control, the acidic ambiance markedly induced the elevation of catalase and SOD antioxidant enzymes activities along with the oxidative stress protective glutathione compound between 30 min to 1 h of exposure to acidic stress. Beyond this period, at 2 h, the activities of antioxidant enzymes (catalase and SOD) and glutathione were declined steeply and reached below the normal level (control) (Fig. 2B). The Kruskal-Wallis H Test showed statistically significant difference of activities of SOD ($\chi2 = 45.155$, $p = 0.000$), glutathione ($\chi2 = 45.161$, $p = 0.00$) and catalase ($\chi2 = 46.874$, $p = 0.00$) from the control. HIF-1α, an oxidative stress marker protein was also significantly increased at pH 5.0 ± 0.5. There is a significant increase in the expression of the protein ($\chi2 = 8.308$, $p = 0.004$) than the control, which is quite prominent from the densitometric analysis, when exposed under acidic ambiance for 2 h (Fig. 3).

Immunoblots of AMPK, PGC1α and SIRT1 from skeletal muscle tissue showed that the amount of AMPK, PGC1α and SIRT1 were decreased under acidic pH (Fig. 4). Both the metabolic sensors (AMPK and SIRT1) were significantly decreased ($\chi2 = 8.366$, $p = 0.004$ and $\chi2 = 7.908$, $p = 0.005$, respectively), which in turn resulted in the significant decreased amount of the master regulator PGC1α ($\chi2 = 8.396$, $p = 0.004$), which is the transcriptional coactivator of the energy homeostatic pathway in mitochondria. It is reasonable to think that reduced level of PGC1α results in the decrease in expressions of the PGC1α –regulated Tfam, Nrf1 (transcription factors in-

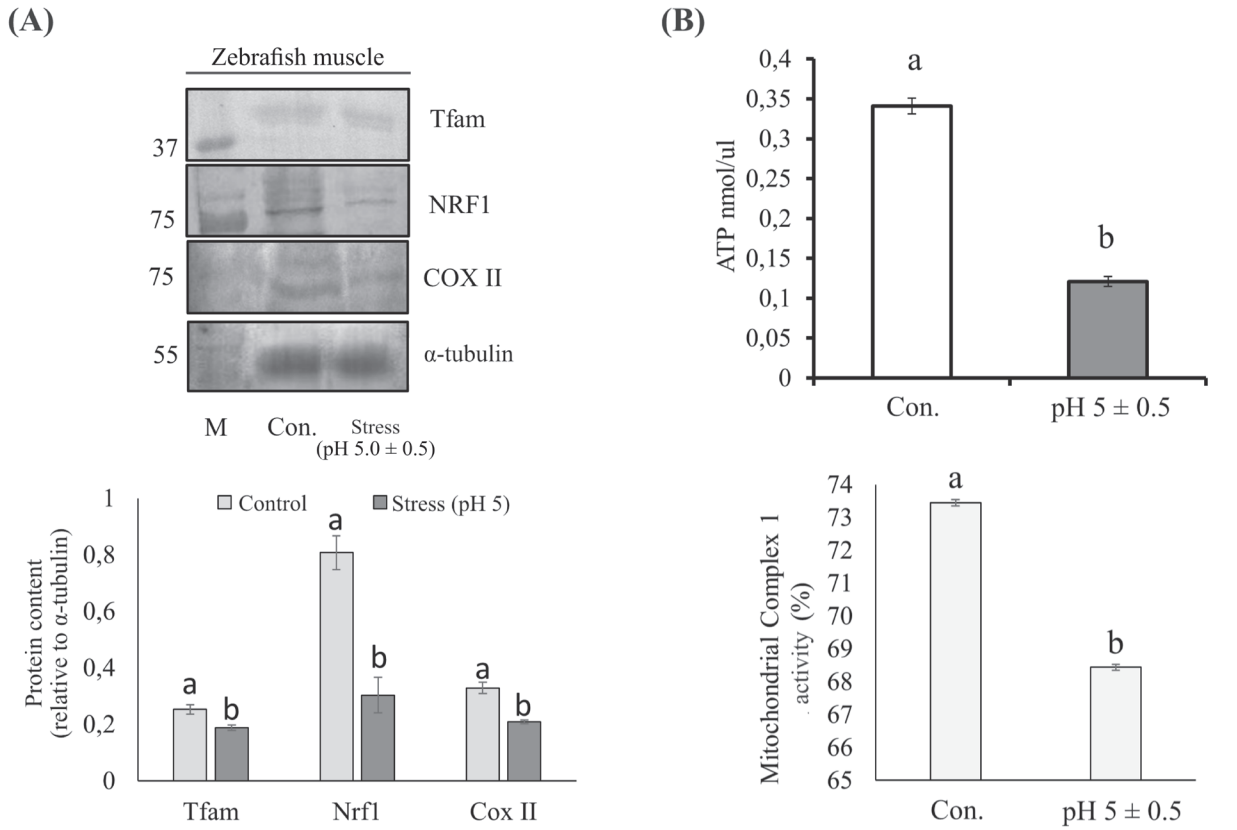

Figure 5. Immunoblots of Tfam, COXII and Nrf1 along with ATP synthesis and mitochondrial complex I activity. (A) Immunoblots of Tfam, COXII and Nrf1 and, their densitometry analysis after 2 h of stress exposure of zebrafish to pH 5.0 ± 0.5. (B) ATP production and mitochondrial complex I activity in skeletal muscle tissue on exposure of zebrafish to pH 5.0 ± 0.5 stress exposure of 2 h showing significant decrease in ATP production and mitochondrial complex I activity after 2 h. Data are shown as Mean ± SE. Bars with different lower-case letters show statistically significant difference at $p < 0.05$.

volved in mitochondrial biogenesis) and COXII (one of the essential subunits of the complex IV of electron transport chain). Indeed, significant decrease of Tfam ($\chi 2 = 5.026$, $p = 0.025$), Nrf1 ($\chi 2 = 8.308$, $p = 0.004$) and COXII ($\chi 2 = 8.308$, $p = 0.004$) protein levels were observed at pH 5 ± 0.5 (Fig. 5A). Under stress condition at pH 5.0±0.5, the production of ATP and mitochondrial complex I activity of electron transport chain also showed a significant reduction ($\chi 2 = 5.333$, $p=0.021$ and $\chi 2 = 14.329$, $p=0.00$, respectively) that may correlate with the damage to the mitochondrial bioenergetics (Fig. 5B).

DISCUSSION

It is evident from the result that the zebrafish skeletal muscle experienced highest oxidative stress on exposure for 30 min to 1 h to acidic ambience. However, the oxidative stress indicators steeply declined from 1-2 h. It is not confirmed whether the physiological health of the fish came under threat for such short exposure or not. The assessment of the formation of MDA is also significantly higher in its skeletal muscle tissue compared to brain and gill under low pH condition, indicating the resultant post traumatic physiological challenge. Such outcome was also confirmed by the changes in HIF-1α levels and other stress indicators like SOD and catalase activity and glutathione level at pH 5.0 ± 0.5 at 2 h. The 15% mortality at 2 h further supported the possible failure of the fish to withstand the oxidative stress induced damage. As outlined earlier, the present study aims to understand the metabolic impairment at this point faced by zebrafish through AMPK-SIRT1-PGC1α axis under acidic ambiance.

Earlier, few studies reported that zebrafish can tolerate pH from 4.0-10.7 (Kwong et al. 2014; Zahangir et al. 2015). However, in the present study, results of oxidative stress indicators confirmed that the skeletal muscle of the fish experienced high oxidative stress within 1 hour to the exposure of pH 5.0 ± 0.5. The use of MDA and HIF-1α

as biomarker of stress further established that the after-effects of oxidative stress exists even though the oxidative stress indicators were declined in the skeletal muscle at 2 h. Thus, a cellular hypoxic condition might persist even after the exhibition of surge evident from oxidative stress indicators. Such possibility cannot be ignored since the fish displayed unrest behaviour after exposure of 2 h in acidic ambiance with more frequent gulping at the water surface. Although, this level of pH is not lethal in general, it led the fish to suffer from high oxidative stress, which is reflected from the observation discussed above. Probably, such observation was overlooked by previous researchers, since their studies were not based on formation of MDA in skeletal muscle tissue. In general, MDA is suggested as the efficient stress-marker for animals, especially mammals (Nielsen et al. 1997). Being one of the final products of polyunsaturated fatty acids peroxidation in the cells, its formation indicates the generation of free radicals in tissues (Gawel et al. 2004; Dahake et al. 2016). As mentioned earlier, the results shown by MDA were correlated to the results of stress indicators (SOD, catalase and glutathione). These stress indicators are the part of antioxidant defence system which are either enzymatic (SOD and catalase) or non-enzymatic (glutathione) and are frequently used to evaluate oxidative stress level in animals (Huang et al. 2020). The enhanced level of HIF-1α protein indicates insufficient O_2 in cell that creates hypoxia and mediates the re-establishment of homeostasis in oxidatively stressed cell (Samenza 2005). The cellular hypoxic condition probably persists, even at 2 h, when antioxidant surge exhausted. Under such condition, amount of HIF-1α increases, as seen in the present study, and helps to generate adaptive response in cell through metabolic and bioenergetic pathways arresting ATP production through decrease in expression of metabolic sensors like AMPK, PGC1α and SIRT1 (Muoio and Kove 2007; Majumdar et al. 2010). In this study, the increase of HIF-1α protein level was indeed accompanied by decrease of AMPK, PGC1α and SIRT1.

Out of all metabolic sensors, the AMPK and SIRT1 act as sensors of cellular energy status for restoration of cellular damage (Han et al. 2013). This homeostatic defence mechanism is a natural biological phenomenon and takes place in all eukaryotes (Hardie et al. 2012a, 2012b; Hardie 2013; Han et al. 2016). The activation of AMPK is found to be linked with increase in AMP:ATP ratio and increased ADP concentrations, both of which are linked to an energetic drop (Canto and Auwerx 2009; Hardie 2011; Mihaylova and Shaw 2011). In case of oxidative stress, the AMPK works as a cellular sensor for degraded AMP:ATP and ADP:ATP ratios and gets activated to recover the energy balance (Auciello et al. 2014). Under the acidic ambiance, in the skeletal muscle of zebrafish, the levels of AMPK and SIRT1 proteins significantly decreased within 2 h compared to the stress-free condition, indicating a direct effect of pH 5.0 ± 0.5 on skeletal muscle tissue.

It is well known that the master metabolic regulator PGC1α that promotes the expression of mitochondrial genes, functions synergistically with AMPK and SIRT1 for ATP production under oxidative stress conditions (Canto and Auwerx 2009; Jeninga et al. 2010). In compliance to the above role, the level of PGC1α protein was found to be significantly decreased in the present study. This directly indicates that the energy synthesis processes are intervened at acidic pH level of 5.0 ± 0.5. The present study also showed significant decrease of mitochondrial complex I activity and COXII protein level that directly indicates a decreased performance of mitochondrial functions. Indeed, reduction in activities of both mitochondrial complex I and COXII, which are parts of the electron transport chain, is indicative of impaired mitochondrial bioenergetics (Rato et al. 2014). Similarly, decrease of AMPK levels results in reduced activation of PGC1α, which in turn results in the perturbation of normal mitochondrial biogenesis processes. The decrease of mitochondrial functions is further reflected by the significantly decreased levels of Tfam and Nrf1 proteins under acidic ambiance compared to control conditions. In mammals, these two transcription factors are directly involved in mitochondrial biogenesis under stress condition (Sharma et al. 2013). There is decrease in mitochondrial derived ATP production in mammals under oxidative stress (Zhang et al. 2006). Congruently, in the present study, the mitochondrial bioenergetics seems to be disrupted resulting in low ATP production under acidic ambiance.

CONCLUSION

This study explains that zebrafish experiences oxidative stress in skeletal muscle when ambiance turned to acidic, to a level at pH 5.0 ± 0.5 within 30 min to 1 h, which was evident from the response of oxidative stress indicators (SOD and catalase activities and glutathione level). Beyond this point, even though the oxidative stress indicators (SOD and catalase activities and glutathione level) declined, the oxidative stress induced traumatic condition persists. This is evident from the analysis of MDA or HIF1α levels or other regulators related to energy homeostasis associated directly or indirectly with mitochondria (such as PGC1α). The fish, although strived to resume adaptive homeostatic strategy at pH 5.0 ± 0.5, the increase in the rate of mortality explains state of metabolic dysfunction. Surprisingly, when the fish was kept under acidic ambiance for a period up to 9 h, the rate of mortality reached up to

90% and MDA level was reduced to 1000 nmol MDA/mg protein. Whether these adaptations at miniscule scale of 10% is due to naturally inherent counter mechanism or it is just a failure of progressive rate of adaptive response in 90% of population, is not clear. As of now, this study hints that, acidic ambiance induced post oxidative stress affects the mitochondrial biogenesis and bioenergetics in zebrafish greatly impairing its metabolic adaptability.

ACKNOWLEDGEMENT

Authors acknowledge National Agriculture Science Fund (NASF) [Project Ref. NASF/ABA/6018/2016-17], The Indian Council of Agricultural Research (ICAR) for financial assistance and DIST FIST- II and CAS-II of Department of Zoology, Visva-Bharati for instrumental assistance. Authors are also thankful to DST-PURSE of Siksha Bhavana, Visva-Bharati for technical assistance.

REFERENCES

Andrade TS, Henriques JF, Almeida AR, Soares AMVM, Scholz S, Domingues I (2017) Zebrafish embryo tolerance to environmental stress factors-Concentration-dose response analysis of oxygen limitation, pH, and UV-light irradiation. Environ Toxicol Chem 36:682-690.

Auciello FR, Ross FA, Ikematsu N, Hardie DG (2014) Oxidative stress activates AMPK in cultured cells primarily by increasing cellular AMP and/or ADP. FEBS Lett 588:3361-3366.

Aust SD (1985) Lipid peroxidation. In Greenwald RA, ed., Handbook Methods for Oxygen Radical Research. CRC Press Revivals, Florida, 203-210.

Bhaskar M, Govindappa S (1985) Physiological and metabolic patterns in muscle of fish, *Tilapia mossambica* on acclimation to altered pH. Ambio 14:349-351.

Canto C, Auwerx J (2009) PGC-1α, SIRT1 and AMPK, an energy sensing network that controls energy expenditure. Curr Opin Lipidol 20:98-105.

Dahake HS, Warade J, Kansara GS, Pawade Y, Gangle S (2016) Study of malondialdehyde as an oxidative stress marker in schizophrenia. IJRMS 4:4730-4734.

Dave G (1984) Effect of pH on pentachlorophenol toxicity to embryos and larvae of zebrafish (*Brachydanio rerio*). Bull Environ Contam Toxicol 33:621-630.

Dave G (1985) The influence of pH on the toxicity of aluminium, cadmium and iron to eggs and larvae of the zebrafish, *Brachydanio rerio.* Ecotoxicol Environ Saf 10:253-267.

Ewing JF, Janero DR (1995) Microplate superoxide dismutase assay employing a nonenzymatic superoxide generator. Anal Biochem 232:243-248.

Eze JI, Anene BM, Chukwu CC (2008) Determination of serum and organ malondialdehyde (MDA) concentration, a lipid peroxidation index, in *Trypanosoma brucei* infected rat. Comp Clin Pathol 17:67-72

Gawel S, Wardas M, Niedworok E, Wardas P (2004) Malondialdehyde (MDA) as a lipid peroxidation marker. WIAD 57:453-455.

Han G, Zhang S, Marshall DJ, Ke C, Dong Y (2013) Metabolic energy sensors (AMPK and SIRT1), protein carbonylation and cardiac failure as biomarkers of thermal stress in an intertidal limpet: linking energetic allocation with environmental temperature during aerial emersion. J Exp Biol 216:3273-3282.

Han X, Tai H, Wang X, Wang Z, Zhou J, Wei X, Ding Y, Gong H, Mo C, Zhang J, Qin J, Ma Y, Huang N, Xiang R, Xiao H (2016) AMPK activation protects cells from oxidative stress-induced senescence via autophagic flux restoration and intracellular NAD(+) elevation. Aging cell 15:416-427.

Hardie DG, Ross FA, Hawley SA (2012a) AMP-activated protein kinase: A target for drugs both ancient and modern. Chem and Biol 19:1222-1236.

Hardie DG, Ross FA, Hawley SA (2012b) AMPK: A nutrient and energy sensor that maintains energy homeostasis. Nat Rev Mol Cell Biol 13:251-262.

Hardie DG (2013) AMPK: A target for drugs and natural products with effects on both diabetes and cancer. Diabetes 62:2164-2172.

Hardie DG (2011) Signal transduction: How cells sense energy. Nature 472:176-177.

Huang X, Li Y, Wang T, Liu H, Shi J, Zhang X (2020) Evaluation of the oxidative stress status in zebrafish (*Danio rerio*) liver induced by three typical organic UV filters (BP-4, PABA, PBSA). Int J Environ Res Public Health 17:1-13.

Jeninga EH, Schoonjans K, Auwerx J (2010) Reversible acetylation of PGC-1: connecting energy sensors and effectors to guarantee metabolic flexibility. Oncogene 29:4617-4624.

Kwong RWM, Kumai Y, Perry SF (2014) The physiology of fish at low pH: the zebrafish as a model system. J Exp Biol 217:651-662.

Majumdar AJ, Wong WJ, Simon MC (2010) Hypoxia inducible factors and the response to hypoxic stress. Mol Cell 40:294-309.

Mcdonald DG (1983) The effects of H+ upon the gills of freshwater fish. Can J Zool 61:691-703.

Mihaylova MM, Shaw RJ (2011) The AMPK signalling pathway coordinates cell growth, autophagy and metabolism. Nat Cell Biol 13:1016-1023.

Miranda S, Foncea R, Guerrero J, Leighton F (1999) Oxidative stress and upregulation of mitochondrial biogenesis genes in mitochondrial DNA-depleted HeLa cells. Bio-

chem Biophys Res Com 258:44-49.
Muoio DM, Koves TR (2007) Skeletal muscle adaptation to fatty acid depends on coordinated actions of the PPARs and PGC1α: implications for metabolic disease. Appl Physiol Nutr Metab 32:874-883.
Nielsen F, Mikkelsen BB, Nielsen JB, Andersen HR, Grandjean P (1997) Plasma malondialdehyde as biomarker for oxidative stress: reference interval and effects of life-style factors. Clin Chem 43:1209-1214.
Psenner R (1994) Environmental impacts on freshwaters: acidification as a global problem. Sci Total Environ 143:53-61.
Rato L, Duarte AI, Tomas GD, Santos MS, Moreira PI, Socorro S, Cavaco JE, Alves MG, Oliveira PF (2014) Pre-diabetes alter testicular PGC1α/SIRT3 axis modulating mitochondrial bioenergetics and oxidative stress. Biochim Biophys Acta 1837:335-344.
Samenza GL (2004) Hydroxylation of HIF1: Oxygen sensing at the molecular level. Physiology 19:176-182.
Schindler DW (1988) Effects of acid rain on freshwater ecosystems. Science 239:149-157.
Sharma DR, Sunkaria A, Wani WY, Sharma RK, Kandimalla RJL, Bal A, Gill KD (2013) Aluminium induced oxidative stress results in decreased mitochondrial biogenesis via modulation of PGC-1α expression. Toxicol Appl Pharm 273:365-380.
Steenberger PJ, Richardson MK, Champagne DL (2011) The use of the zebrafish model in stress research. Prog Neuropsychopharmacol Biol Psychiatry 35:1432-1451.
Wood CM (1989) The physiological problems of fish in acid waters. In Morris R, Brown DJA, Taylor EW, Brown JA, ed., Acid Toxicity and Aquatic Animals. Cambridge University Press, England, 125-152.
Zahangir MM, Haque F, Islam MS (2015) Effects of acute water pH stress on the stress indicators in zebrafish (*Danio rerio*). Proceedings of 5th International Conference on Environmental Aspects of Bangladesh (ICEAB 2014). Paper ID E76.
Zhang X, Wu XQ, Lu S, Guo YL, Ma X (2006) Deficit of mitochondria-derived ATP during oxidative stress impairs mouse MII oocyte spindles. Cell Res 16:841-850.

Acta Biologica Szegediensis

Volume 64(2):199-206, 2020
Acta Biologica Szegediensis
http://abs.bibl.u-szeged.hu/index.php/abs

DOI:10.14232/abs.2020.2.199-206

ARTICLE

Antioxidant and hepatoprotective property of squalene for counteracting the oxidative damage induced by methotrexate in experimental rats

Edakkukaran Sudhakaran Sumi, Pavan Kumar Dara, Rosemol Jacob Mannuthy, Balaraman Ganesan, Rangasamy Anandan, Suseela Mathew*

Biochemistry and Nutrition Division, ICAR-Central Institute of Fisheries Technology, Cochin 682 029, Kerala, India

ABSTRACT Methotrexate (MTX), an antifolate drug, is extensively prescribed for patients suffering from diseases like cancer, psoriasis, neoplasms, and rheumatoid arthritis. Despite its effectiveness, MTX sometimes finds limited application because its undesirable side effects, including hepatic or renal impairment, bone marrow toxicity and gastrointestinal mucosal injury. Squalene, a highly unsaturated isoprenoid compound, isolated from shark liver oil has great potential in neutralizing the damaging effects triggered by free radicals. Therefore, in this study, the protective role of dietary squalene supplementation on oxidative stress induced by methotrexate in experimental rats was evaluated. A significant reduction was displayed in the activities of catalase (CAT) and superoxide dismutase (SOD) in MTX-intoxicated groups compared to other groups. Similarly, the activities of glutathione dependant enzymes (GPx and GST) and reduced glutathione (GSH) in MTX-induced groups were shown to be lower compared to the untreated control. Increased LPO (lipid peroxide) level was found in MTX-intoxicated groups compared to other groups. In addition, alterations in the levels of liver marker enzymes like AST, ALP, ALT, and LDH were noticed in MTX intoxicated groups compared to other groups. Biochemical results were confirmed by the histopathological examination of liver sections. In conclusion, the result obtained in the present study proposes that squalene exerts antioxidant activity and is capable of ameliorating oxidative stress and liver injury induced by MTX. **Acta Biol Szeged 64(2):199-206 (2020)**

KEY WORDS
hepatotoxicity
histopathology
methotrexate
squalene

ARTICLE INFORMATION
Submitted
01 July 2020.
Accepted
22 December 2020.
***Corresponding author**
E-mail: suseela1962@gmail.com

Introduction

Methotrexate (MTX) is a widely used anti-neoplastic drug which is considered as first line treatment option to patients suffering with cancer (Uzar et al. 2006a). Additionally, MTX is a prescribed medicine for other diseases like psoriasis, Crohn's disease, autoimmune diseases (e.g., rheumatoid arthritis), immunological abnormalities, and systemic inflammation (Cetinkaya et al. 2006). It causes acute life-threatening side effects in overdose situations (Funk et al. 2013; Schwartzberg et al. 2014). However, the most severe and widespread problems of toxicity associated MTX treatment are fever, non-productive cough and dyspnoea, pneumonitis and pulmonary fibrosis (Imokawa et al. 2000; Jakubovic et al. 2013; Hsu et al. 2003). MTX-induced toxic effect is dependent on the applied dose and found to be occurring up to 60% of disease cases (Neuman et al. 1999). MTX in higher doses has restricted applications in disease management because of its serious life-threatening effects on liver (Liang et al. 2004). Methotrexate prevents the formation of tetrahydrofolate (THF) by dihydrofolate reductase (DHFR) and thus decreases reduced folate species and hence, the synthesis of purine and pyrimidine precursors, which are necessary for the synthesis of nucleic acids (Channa Keshava et al. 1998; Goodsell et al. 1999). Johovic et al. (2003) reported that methotrexate inhibits cytosolic enzymatic activities of NADP-dependent dehydrogenases and NADP malic enzyme to reduce the availability of NADPH in cells *via* pentose phosphate inhibition pathway. However, the exact mechanism underlying the MTX-toxicity remains unclear. Previous studies have hypothesized that MTX application induces oxidative damage in tissues (Miketova et al. 2005; Armagan et al. 2008). Like other anticancer synthetic drugs, oxidative stress is reported to have a significant role in the pathophysiology of tissue toxicity induced by MTX (Atessahin et al. 2005; Fadillioglu et al. 2003; Uz et al. 2005; Quiles et al. 2002). Earlier studies also reported that MTX toxicity results in significant reduction in efficacy of the antioxidant enzymes defence system and increased sensitivity of cells to ROS (Kolli

et al. 2014; Abd et al. 2016). Antioxidants perform an essential role in living organisms, and they are capable to stop free radical generation. To conquer the adverse effect of MTX toxicity, it has been recommended to use antioxidants (Block et al. 2008; Miyazono et al. 2004).

Squalene is a marine biomolecule having six isoprene units. It is abundantly available in shark liver oil and other sources including olive oil, rice bran oil etc. Squalene is an integral part of Mediterranean diet and is incorporated in traditional medicine as it plays an essential role in the treatment of several diseases. Squalene is a highly effective natural antioxidant, reported to have ability to protect cells from oxidative stress and lipid peroxidation (Kabuto et al. 2013). It is key intermediate in cholesterol metabolism and exerts lipid lowering and membrane stabilizing property (Farvin et al. 2004; Farvin et al. 2005). Detoxifying activities of squalene were studied and was suggested to be having a potential to ameliorate the harmful effects of different compounds namely hexachlorobiphenyl, perchlorobenzene, arsenic, theophylline, phenobarbital and cyclophosphamide (Richter et al. 1982; Kamimura et al. 1992; Fan et al. 1996; Senthilkumar et al. 2006a). Relevant studies reported that squalene exhibits anti-neoplastic effect (Smith 2000; Sotiroudis and Kyrtopoulos 2008). Though squalene has been identified as a natural antioxidant capable of reducing the side effect of anti-cancer agents, the ameliorating effects of squalene against hepatotoxicity associated with MTX administration have not been explored yet. With this rationale, this study was designed to demonstrate the protective role of squalene to counteract the oxidative stress mediated by MTX administration and to serve as a free radical inhibitor.

Materials and methods

Drug and chemicals

Methotrexate was procured from Sisco Research Laboratory (Mumbai, India). Squalene was obtained as a kind gift from Aasha Biochem (Kerala, India). Remaining reagents/chemicals used in this study were of standard analytical chemicals and were obtained either from Sigma Chemical (USA) or Sisco Research Laboratory (Mumbai, India).

Animals

Ten-week-old male Wistar strain albino rats, weighing 100-120 g were selected for the study. All animals were housed individually in hygienic and standard environmental conditions of temperature 28 ± 2 ˚C, humidity 60-70%, 12 h light and 12 h dark cycle in polypropylene cages. During the experimental period, the animals were fed with a standard diet (M/s Sai Foods, Bangalore, India; the diet contained carbohydrate 56.2%, crude protein 22%, ash 7.5%, total fat 4.2%, crude fibre 3%, glucose 2.5%, vitamin 1.8%, sand silica 1.4%, calcium 0.8%, phosphorus 0.8 %, and provide metabolizable energy of 3600 kcal.) and water ad libitum. The experiment was carried out according to the guidelines of the Committee for the Purpose of Control and Supervision of Experiments on Animals (CPCSEA), New Delhi, India and approved by the Institutional Animal Ethics Committee of the Central Institute of Fisheries Technology, Cochin.

Experimental design

The experimental animals were separated into four groups, each group having six animals. Group I (CO-SAL) and Group II (CO-MTX) animals were fed on commercial feed with added coconut oil at 1.5% level and Group III (SQ-SAL) and Group IV (SQ-MTX) animals were fed on commercial feed with added squalene at 1.5% level for a period of 30 days. Group I and III were intraperitoneally (i.p.) injected with 0.5 ml normal saline (0.9%) and Group II and IV with 0.5 ml methotrexate (20 mg/kg body weight) on 30th day (Saeed et al. 2018). During the experimental period body weight of all the animals was properly documented. At the end of the experiment, i.e. 48 h after the MTX/normal saline administration, the experimental rats were sacrificed. The sera obtained from the collected blood samples were stored properly and used for performing various assays including total protein (Lowry et al. 1951), total bilirubin (Frederick and Robert Lee 1974), AST (Mohur and Cook 1957), ALT (Mohur and Cook 1957), LDH (King 1965a) and ALP (King 1965b). The results obtained for AST, ALT, LDH were expressed in μmol of pyruvate liberated/h/mg protein and ALP in μmol of phenol liberated h/mg protein.

Liver samples were weighed, and a small portion of liver tissue was fixed in 10% buffered formalin for histopathological observations. Accurately weighed liver tissue samples were homogenized in phosphate buffer at 4 ˚C with a tissue homogenizer. The homogenate obtained was further centrifuged and the supernatant collected were used for conducting different assays like SOD (Misra and Fridovich 1972), catalase (Takahara et al. 1960), GST (Habig et al. 1974), GSH (Ellman 1959), GPx (Paglia and Valentine 1967) and LPO (Ohkawa et al. 1979). The obtained results were expressed as SOD: one unit of the SOD activity is the amount of protein required to give 50% inhibition of epinephrine autoxidation. Catalase: μmol H_2O_2 decomposed/min/mg protein; GST: μmol 1-chloro-2,4-dinitrobenzene conjugate formed/min/mg protein; GSH: μmol/mg wet tissue; GPx: μmol GSH oxidized/min/mg protein; LPO: μmol malonaldehyde liberated/mg protein.

Table 1. Effect of dietary squalene supplementation on body weight and relative liver weight of experiments rats receiving different treatments.

Groups	Group I (CO-SAL)	Group II (CO-MTX)	Group III (SQ-SAL)	Group IV (SQ-MTX)
Body weight (g)	202.66 ± 2.51^{c}	181.33 ± 1.52^{a}	203.05 ± 0.50^{c}	196.66 ± 2.08^{b}
Relative liver weight (%)	2.15 ± 0.06^{a}	2.94 ± 0.05^{c}	2.12 ± 0.03^{a}	2.32 ± 0.01^{b}

Values that have a different superscript letter (a, b, c, d) differ significantly ($p < 0.05$) among each other.

Histopathological examination

Liver tissues were processed by the standard histopathological procedure to observe microscopic changes. Briefly, liver tissue section was embedded in paraffin and 5 μm sections were cut separately. The sections were deparaffinized using xylene and ethanol and then washed with PBS and permeabilization solution (0.1 M citrate, 0.1% Triton X-100). The deparaffinised sections were stained with haematoxylin and eosin. The histopathological examination of tissues of animals was carried out under fluorescence microscope (Olympus BX 60, PA, USA).

Statistical analysis

The results were stated as mean ± SD for 6 animals. The statistical comparisons among studied groups were performed with SPSS software program (SPSS.16.0 for Windows, SPSS, Chicago, IL) using one-way analysis of variance (ANOVA). Duncan's multiple range comparison tests were performed among groups.

Results and Discussion

Influence of MTX treatment on body weight and relative liver weight

In the present study, it was observed that MTX injection at single dose results in the decline of the body weight of both group II and group IV animals. A signifcant reduction in the body weight was found in Group II animals in comparison with other group animals (Table 1). These variations in body weight might possibly be due to oxidative tissue damage in response to MTX induced toxic effect, which was reversed by dietary squalene supplementation. Oxidative stress is one of the key mechanisms involved in drugs induced liver toxicity. A reduced body weight in experimental rats after single dose methotrexate injection (i.p.) was reported in previous studies (Moghadam et al. 2015). In addition, it was also reported that the MTX administration (20 mg/kg, single i.p. injection) in experimental rats initiates tissue damage and subsequent weight loss in comparison with normal control rats (Khafaga and El-Sayed 2018). Squalene pretreatment might have inhibited the cell damage due to MTX toxicity and maintained the body weight to near normalcy by its tissue protecting activity against oxidative stress. The results were in line with the previous reports which described that squalene exhibited antioxidant defense mechanism in tissue and protected the cell membrane from oxidative stress (Farvin et al. 2005)

Significant changes observed in the relative liver weight of Group II MTX intoxicated rats (Table 1) possibly due to the oxidative tissue damage induced by methotrexate. Prior treatment with squalene reversed these changes in relative liver weight. In consistence with current study, it has been reported that acute tissue damage and alterations in relative liver weights of experimental rats receiving a single dose methotrexate (20 mg/kg body weight) indicated its toxic effect on tissue (Moghadam et al. 2015). Furthermore, other investigators also reported that a single intra-peritoneal injection of MTX initiates oxidative stress which is evidenced by an elevated level of relative liver weight in MTX intoxicated groups compared to control (Asmaa and Yasser 2018; Mukherjee et al. 2013). Prior supplementation of squalene in Group IV animals perhaps protected the liver cell against oxidative damage induced by methotrexate. Squalene is effective

Table 2. Effect of dietary squalene supplementation on total protein and total bilirubin content of experimental rats receiving different treatments.

Parameters	Group I (CO-SAL)	Group II (CO-MTX)	Group III (SQ-SAL)	Group IV (SQ-MTX)
Total protein (mg/100 ml)	7.57 ± 0.07^{c}	5.25 ± 0.05^{a}	7.54 ± 0.10c	6.49 ± 0.06^{b}
Total bilirubin (mg/100 ml)	0.200 ± 0.00^{a}	1.30 ± 0.00^{c}	0.204 ± 0.00^{a}	0.291 ± 0.00^{b}

Values that have a different superscript letter (a, b, c, d) differ significantly ($p < 0.05$) among each other.

Table 3. Effects of dietary squalene supplementation on enzymatic antioxidant levels and lipid peroxide content of experimental rats receiving different treatments.

Parameters	Group I (CO-SAL)	Group II (CO-MTX)	Group III (SQ-SAL)	Group IV (SQ-MTX)
SOD	3.82 ± 0.01^{d}	1.04 ± 0.00^{a}	3.41 ± 0.02^{c}	2.71 ± 0.02^{b}
CAT	10.23 ± 0.31^{c}	2.11 ± 0.02^{a}	11.19 ± 0.26^{d}	9.48 ± 0.41^{b}
GST	7.19 ± 0.02^{c}	3.88 ± 0.02^{a}	7.61 ± 0.06^{d}	6.40 ± 0.04^{b}
GSH	21.48 ± 0.51^{d}	7.99 ± 0.42^{a}	17.13 ± 0.20^{c}	13.96 ± 0.18^{b}
GPx	2.13 ± 0.07^{c}	1.21 ± 0.10^{a}	1.91 ± 0.05^{b}	1.8 ± 0.03^{b}
LPO	1.18 ± 0.03^{a}	2.99 ± 0.01^{d}	1.58 ± 0.01^{b}	1.71 ± 0.02^{c}

Values that have a different superscript letter (a, b, c, d) differ significantly ($p < 0.05$) among each other.

in counteracting oxidative stress and cellular damage occurred in tissue by its antioxidant and membrane stabilizing activity. Earlier it was reported that squalene pretreatment in experimental animals effectively restored the impaired tissue that was exposed to drug treatment (Farvin et al. 2004).

Influence of MTX treatment on total protein and total bilirubin level

Total serum protein levels of MTX administrated groups (Group II and IV) were lower in comparison with other groups (Table 2). Significant decline was noticed in Group II animals when compared with other groups. Observed changes in total protein level depict impaired liver function probably due to methotrexate administration. These observations were in accordance with the previous reports which displayed significant depletion of serum protein level in MTX intoxicated groups than untreated groups (Moghadam et al. 2015). Dietary squalene supplementation helps to maintain the serum total protein levels to near normal in experimental animals. Normalized protein levels in squalene treated group marks its protection of liver functions against methotrexate toxicity. The resultant observation is in accordance with the earlier report which stated that squalene treatment aids to restore serum protein levels to near normal in cyclophosphamide intoxicated groups vs untreated group (Senthilkumar et al. 2006a). The total bilirubin level was found to be increased in Group II animals compared to other groups (Table 2). Squalene supplementation prevented the increase of total bilirubin levels and maintained to normal in group IV animals. Abdulzahra and Mohammed (2014) indicated that total serum bilirubin level was found to be higher in rats treated with MTX group compared with untreated groups. Increased total bilirubin level indicates the hepatotoxicity and these results concur with the previous studies (Moghadam et al. 2015). Squalene provides protection to liver cells and effectively prevents the elevation of serum biochemical parameters by its membrane stabilizing activity. In the present study, prior supplementation of squalene decreased total serum bilirubin levels thereby reduced the biochemical alteration induced by methotrexate. The present results were in accordance with the previous studies (Senthilkumar et al. 2006a).

Effect of dietary squalene on antioxidant enzyme levels of MTX administrated rats

Table 3 shows the protective action of dietary squalene supplementations on enzymatic and non-enzymatic antioxidant levels as well as lipid peroxide content in experimental groups. SOD and CAT levels in liver tissue were decreased significantly in MTX-administered Group II animals as compared to other animals. This may possibly be due to the formation of superoxide anions and these ions inactivate or reduce the activity of SOD. In fact, SOD and CAT levels of liver induced by MTX treatment causes marked alteration in the antioxidant status, signifying that the cells may possibly be more susceptible to reactive oxygen species (Uzar et al. 2006b), leading to failure in the efficacy of defence mechanism of antioxidant enzymes at cellular level (Miyazono et al. 2004). Squalene is an efficient singlet oxygen scavenging molecule like that of vitamin E. In the present study, squalene in Group IV inhibited MTX induced inactivation of SOD and CAT enzyme activity and retained the cellular antioxidant status to near normal. Antioxidant activity of squalene is assumed to protect the liver cells from cellular damage induced by MTX and these observations were in line with the previous reports (Senthilkumar et al. 2006b).

Methotrexate administration resulted in substantial depletion in GST, GSH, GPx levels in group II compared with others (group I, III and IV). MTX intoxication might have reduced the cellular defence against toxic metabolites in liver of experimental animals. MTX causes significant decrease in antioxidant enzymatic level in experimental animals and supplementation of certain antioxidants like melatonin, taurine is effective in preventing this mechanism. (Jahovic et al. 2003; Cetiner et al. 2005). However,

Table 4. Effects of dietary squalene supplementation on serum biochemical parameters of experimental rats receiving different treatments.

Parameters	Group I (CO-SAL)	Group II (CO-MTX)	Group III (SQ-SAL)	Group IV (SQ-MTX)
AST	129.28 ± 0.44[a]	274.81 ± 0.23[c]	130.28 ± 0.28[a]	179.81 ± 0.33[b]
ALT	136.48 ± 0.52[a]	255.38 ± 0.54[d]	147.47 ± 0.71[b]	164.95 ± 0.16[c]
LDH	199.38 ± 0.58[a]	377.67 ± 0.66[c]	195.77 ± 0.40[a]	231.10 ± 0.20[b]
ALP	126.39 ± 0.60[b]	197.19 ± 0.66[d]	123.36 ± 0.25[a]	157.26 ± 0.53[c]

Values that have a different superscript letter (a, b, c, d) differ significantly ($p < 0.05$) among each other.

the observed reduction of antioxidant enzymatic level was restored in Group IV animals by squalene supplementation. Squalene possibly acts as a potent antioxidant as well as oxygen scavenging molecule and improves antioxidant defence status in liver tissue, which prevents MTX induced toxicity. It has been previously reported that squalene enhances antioxidant defence mechanism in hepatocytes of experimentally induced rats during drug toxicity by its antioxidant activity (Rajesh and Lakshmanan 2008).

Lipid peroxidation is an oxidative degradation process and is also responsible for nucleotide degradation. In the present study, the LPO level of MTX administrated group (Group II) was significantly higher than other groups. The LPO levels of squalene treated groups (Group I and IV) and Group I were in same range. Oxidative stress along with free radical generation and intense lipid peroxidation are major problems associated with MTX toxicity (Sener et al. 2006). MTX administration in experimental animals might initiate peroxidation of membrane lipids and production of free radicals which was reversed by dietary squalene supplementation. Squalene significantly counteracts the MTX induced lipid peroxidation and oxidative stress which is probably related to its free radical scavenging property. Senthilkumar et al. (2006b) stated that squalene is effective in attenuating lipid peroxidation reactions in the liver of experimental rats induced by anticancer drug and this observation is in line with the present study. Previously, it was reported that dietary squalene supplementation enhanced the antioxidant defense mechanism in experimental animals by reducing the elevated LPO level in cardiac tissue (Farvin et al. 2007). In addition, the protective effect of squalene against arsenic toxicity is mainly through the eradication of free radicals by means of its antioxidant and membrane stabilizing properties (Rajesh and Lakshmanan 2008).

Effect of dietary squalene on AST, ALP, ALT and LDH levels of MTX administrated rats

The levels of AST, ALP and ALT of MTX treated groups (Group II and IV) were increased in comparison with other groups, indicating impaired liver functions (Table 4). The lactate dehydrogenase (LDH) activity was also increased in MTX administrated groups (Group II and IV), whereas the prior squalene supplementation in Group IV animals showed significantly lower values than Group II animals (Table 4). Elevated levels of these marker enzymes in the liver tissue of experimental animals could be the indication of MTX related hepatotoxicity. MTX administration and its effect on liver marker enzymes were also reported by other investigators (Karthikeyan 2004; Ramadan et al. 2008). Moghadam et al. (2015) reported an increased serum ALT, AST and LDH activities in liver tissue homogenate due to hepatotoxicity induced by MTX. Methotrexate is metabolised in liver and such toxic metabolites produce oxidative stress subsequently initiating acute liver injury in experimental animals. In the present study, the treatment with squalene prior to the MTX injection resulted in the reduction of these parameters to control levels. Squalene by its free radical scavenging property possibly trapped the toxic metabolites produced in liver during the activation of this anticancer drug. Similarly, dietary squalene supplementation could be effective in preventing experimentally induced oxidative damage in hepatocytes and subsequent liver toxicity by its potential antioxidant and membrane stabilising activity. Earlier it was reported that dietary squalene supplementation effectively prevented the elevation of serum AST, ALT, ALP and LDH levels in kidney and liver tissue of experimental animals induced by cyclophosphamide (anticancer drug) by means of its antioxidant and free radical scavenging activity (Senthilkumar et al. 2006a). In addition, squalene supplementation decreased serum diagnostic marker enzymes' level and exerts protection on cardiac tissue of experimental animals by its membrane stabilising property (Farvin et al. 2004).

Histopathological examination

The examination of liver sections showed normal architecture of central vein, blood sinusoidal, portal triad and nucleus of hepatocytes in group I and III (Fig. 1 and

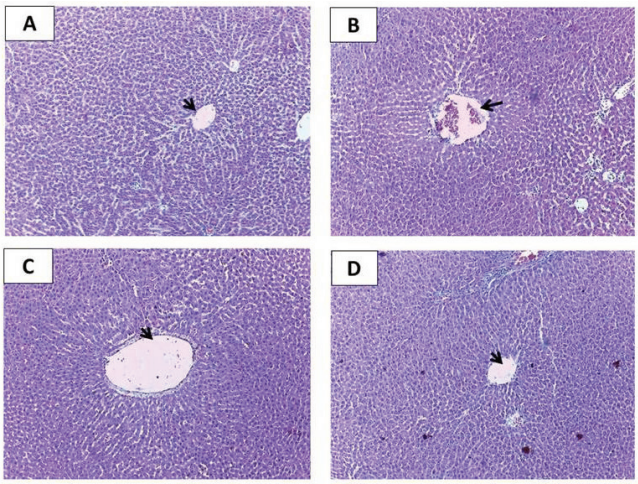

Figure 1. Histopathological analysis of liver sections of experimental animals. A; Microscopic view from the liver tissue of Group I. B; Microscopic view from the liver tissue of Group II. C; Microscopic view from the liver tissue of Group III. D; Microscopic view from the liver tissue Group IV. Arrow mark showing the central vein.

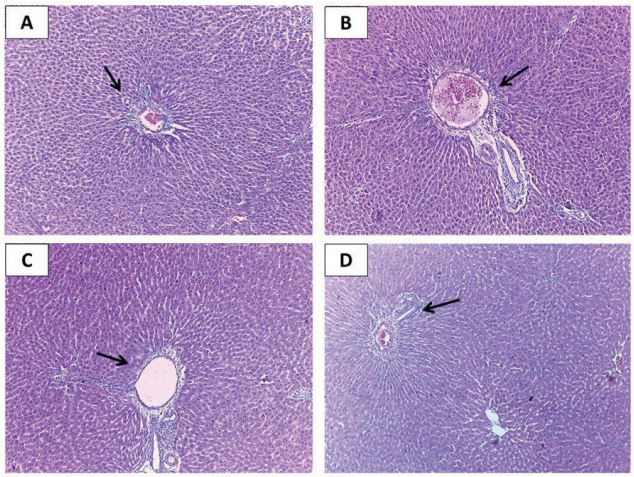

Figure 2. Histopathological analysis of liver sections of experimental animals. A; Microscopic view from the liver tissue Group I. B; Microscopic view from the liver tissue Group II. C; Microscopic view from the liver tissue Group III. D; Microscopic view from the liver tissue Group IV. Arrow mark showing portal triad structures (portal vein, hepatic artery, and bile duct).

2). But MTX administrated groups (Group II and IV) displayed irregular central vein with massive inflammatory reactions, degenerative changes in portal triad, swelling of nucleus in hepatocytes and blood sinusoids were compressed. Dietary squalene supplementation to experimental animals considerably improved cell structure with regenerative changes in portal triad and cell sinusoidal with separated blood sinusoids. Histological studies also confirmed the hepatoprotective effect of squalene on MTX induced toxicity.

The histopathological observations in this study, confirmed that squalene inverted the increase of free radical generation. Thus, it is likely that the hepatoprotective mechanism of squalene could be due to its antioxidant activity and its ability to scavenge a wide range of free radicals. Earlier it was reported that squalene inhibit generation of free radicals and lipid hydroperoxides (Kabuto et al. 2013).

Conclusion

In conclusion, dietary supplementation of squalene can attenuate methotrexate-induced liver dysfunctions. Squalene could reduce the free radical formation during MTX induced toxicity. Therefore, squalene might serve as a potential as well as effective dietary supplement in reducing the complications of MTX induced liver injury and related hepatotoxicity during cancer treatment. Hence, the results of present study suggest that the oral in-take of squalene has prominent attenuating effect against oxidative stress and subsequent liver injury induced by MTX and can serve as therapeutic alternative.

Acknowledgements

The authors would like to express their sincere gratitude to ICAR for providing funds to carry out the research work under ICAR-National Fellow Scheme. The authors acknowledge the Director, ICAR-Central Institute of Fisheries Technology (ICAR-CIFT), Cochin, Kerala, India for providing the facilities to carry out this work and also for granting permission to publish the data acquired from the study. The authors are grateful to the Mrs. PA Jaya (Senior Technical Assistant) ICAR-Central Institute of Fisheries Technology (CIFT), Cochin, Kerala for providing technical support to carry out the analyses. Squalene used in the experiments was obtained as a gift from Mr. Sreedharan (Aasha Biochem, Kerala, India).

References

Abd El-Twab SM, Hoyden WG, Hussein OE, Mahmoud AM (2016) 18β-Glycyrrhetinic acid protects against methotrexate-induced kidney injury by up-regulating the Nrf2/ARE/HO-1 pathway and endogenous antioxidants. Ren Fail 38(9):1516-1527.

Abdulzahra MD, Mohammed HF (2014) The possible protective effect of green tea extract against methotrexate-induced liver injury in male rats. Pharmanest 5(3):2034-

2038.
Armagan A, Uzar E, Uz E, Yilmaz HR, Kutluhan S, Koyuncuoglu HR, Soyupek S, Cam H, Serel TA (2008) Caffeic acid phenethyl ester modulates methotrexate-induced oxidative stress in testes of rat. Hum Exp Toxicol 27:547-552.
Atessahin A, Yilmaz S, Karahan I, Ceribasi AO, Karaoglu A (2005) Effects of lycopene against cisplatin-induced nephrotoxicity and oxidative stress in rats. Toxicology 212:116-123.
Block KI, Koch AC, Mead MN, Tothy PK, Newman RA, Gyllenhaal C (2008) Impact of antioxidant supplementation on chemotherapeutic toxicity: A systematic review of the evidence from randomized controlled trials. Int J Cancer 123:1227-1239.
Cetiner M, Sener G, Sehirli AO, Eksioglu-Demiralp E, Ercan F, Sirvanci S, Gedik N, Akpulat S, Tecimer T, Yegen BC (2005) Taurine protects against methotrexate-induced toxicity and inhibits leukocyte death. Toxicol Appl Pharmacol 209(1):39-50.
Cetinkaya A, Bulbuloglu E, Kurutas E and Kantarceken B (2006) N-acetylcysteine ameliorates methotrexate–induced oxidative liver damage in rats. Med Sci Monit 12(8):274-278.
Keshava C, Keshava N, Whong W-Z, Nath J, Ong T-m (1998) Inhibition of methotrexate-induced chromosomal damage by folinic acid in V79 cells. Mutat Res 397:221-228.
Ellman GL (1959) Tissue sulfhydryl groups. Arch Biochem Biophys 82:70-77.
Fadillioglu E, Yilmaz HR, Erdogan H, Sogut S (2003) The activities of tissue xanthine oxidase and adenosine deaminase and the levels of hydroxyproline and nitric oxide in rat hearts subjected to doxorubicin: protective effect of erdosteine. Toxicology 191:153-158.
Fan S, Ho I, Yeoh FL, Lin C, Lee T (1996) Squalene inhibits sodium arsenite-induced sister chromatid exchanges and micronuclei in Chinese hamster ovary-K cells. Mutat Res 368:165-169.
Farvin KHS, Anandan R, Kumar SHS, Shiny KS, Sankar TV, Thankappan TK (2004) Effect of squalene on tissue defence system in isoproterenol-induced myocardial infarction in rats. Pharmacol Res 50:231-236.
Farvin KHS, Anandan R, Sankar TV, Nair PGV, Thankappan TK (2005) Protective effect of squalene against isoproterenol induced myocardial infarction in rats. J Clin Biochem Nutr 37:55-60.
Farvin KHS, Kumar SHS, Anandan R, Mathew S, Sankar TV, Nair PGV (2007) Supplementation of squalene attenuates experimentally induced myocardial infarction in rats. Food Chem 105:1390-1395.
Frederick C Pearlman, Robert TY Lee (1974) Detection and measurement of total bilirubin in serum, with use of surfactants as solubilizing agents. Clin Chem 20(4):447-453.
Funk RS, Van HL, Becker ML, Leeder JS (2013) Low-dose methotrexate results in the selective accumulation of aminoimidazole carboxamide ribotide in an erythroblastoid cell line. J Pharmacol Exp Ther 347(1):154-63.
Goodsell DS (1999) The molecular perspective: methotrexate. Stem Cells 17:314-315.
Habig WH, Pabst MJ, Jakoby WB (1974) Glutathione-S-transferases: the first enzymatic step in mercapturic acid formation. J Biol Chem 249:7130-7139.
Hsu PC, Lan JL, Hsieh TY, Jan YJ, Huang WN (2003) Methotrexate pneumonitis in a patient with rheumatoid arthritis. J Microbiol Immunol Infect 36:137-140.
Imokawa S, Colby TV, Leslie KO, Helmers RA (2000) Methotrexate pneumonitis: review of the literature and histopathological findings in nine patients. Eur Respir J 15:373-81.
Jahovic N, Cevik H, Sehirli AO, Yegen BC, Sener G (2003) Melatonin prevents methotrexate-induced hepatorenal oxidative injury in rats. J Pineal Res 34:282-287.
Kabuto H, Yamanushi TT, Janjua N, Takayama F, Mankura M (2013) Effects of squalene/squalane on dopamine levels, antioxidant enzyme activity, and fatty acid composition in the striatum of Parkinson's disease mouse model. J Oleo Sci 62(1):21-28.
Kamimura H, Koga N, Ogari K, Yoshimura H (1992) Enhanced elimination of theophylline phenobarbital and strychnine from the bodies of rats and mice by squalene treatment. J Pharmacobiodyn 15:215-221.
Karthikeyan S (2004) Hepatotoxicity of isoniazid: A study on the activity of marker enzymes of liver toxicity in serum and liver tissue of rabbits. Indian J Pharmacol 36:247-249.
Khafaga AF, El-Sayed YS (2018) Spirulina ameliorates methotrexate hepatotoxicity via antioxidant, immune stimulation, and proinflammatory cytokines and apoptotic proteins modulation. Life Sci 196:9-17.
King J (1965a) The dehydrogenases or oxidoreductases - lactate dehydrogenase. In Van D, Ed., Practical Clinical Enzymology. Van Nostrand, London. 83-93.
King J (1965b) The hydrolases- acid and alkaline phosphatases. In Van D, Ed., Practical Clinical Enzymology. Van Nostrand, London. 191-208
Kolli VK, Natarajan K, Isaac B, Selvakumar D, Abraham P (2014) Mitochondrial dysfunction and respiratory chain defects in a rodent model of methotrexate-induced enteritis. Hum Exp Toxicol 33(10):1051-1065.
Liang LS, Jackson J, Min W, Risovic V, Wasan KM, Burt HM (2004) Methotrexate loaded poly(L-lactic acid) microspheres for intra-articular delivery of methotrexate to the joint. J Pharm Sci 93:943-956.
Lowry OH, Rosebrough NJ, Farr AL, Randall RJ (1951) Protein measurement with Folin-phenol reagent. J Biol Chem 193:265-275.

Miketova P, Kaemingk K, Hockenberry M, Pasvogel A, Hutter J, Krull K, Moore IM (2005) Oxidative changes in cerebral spinal fluid phosphatidylcholine during treatment for acute lymphoblastic leukemia. Biol Res Nurs 6:187-195.

Misra HP, Fridovich I (1972) The role of superoxide ion in the auto-oxidation of epinephrine and a simple assay for superoxide dismutase. J Biol Chem 247:3170-3175.

Miyazono Y, Gao F, Horie T (2004) Oxidative stress contributes to methotrexate induced small intestinal toxicity in rats. Scand J Gastroenterol 39:1119-1127.

Moghadam AR, Tutunchi S, Namvaran-Abbas-Abad A, Yazdi M, Bonyadi F, Mohajeri D, Mazani M, Marzban H, Łos MJ, Ghavami S (2015) Pre-administration of turmeric prevents methotrexate-induced liver toxicity and oxidative stress. BMC Complement Altern Med 15:246.

Mohur A, Cook IJY (1957) Simple methods for measuring serum levels of glutamic-oxalo acetic and glutamic-pyruvic transaminase in routine laboratories. J Clin Pathol 10:394-399.

Mukherjee S, Ghosh S, Choudhury S, Adhikary A, Manna K, Dey S, Sa G, Das T, Chattopadhyay S (2013) Pomegranate reverses methotrexate-induced oxidative stress and apoptosis in hepatocytes by modulating Nrf2-NF-κB pathways. J Nutr Biochem 24(12):2040-2050.

Neuman MG, Cameron RG, Haber JA, Katz GG, Malkiewicz IM, Shear NH (1999) Inducers of cytochrome P450 2E1 enhance methotrexate-induced hepatotoxicity. Clin Biochem 32:519-536.

Ohkawa H, Onishi N, Yagi K (1979) Assay for lipid peroxides in animal tissue by thiobarbituric acid reaction. Anal Biochem 95:351-358.

Paglia DE, Valentine WN (1967) Studies on the quantitative and qualitative characterization of erythrocyte glutathione peroxidise. J Lab Clin Med 70:158-169.

Quiles JL, Huertas JR, Battino M, Mataix J, Ramirez-Tortosa MC (2002) Antioxidant nutrients and adriamycin toxicity. Toxicology 180:79-95.

Ramadan AM. Hemeida, Omar M. Mohafez (2008) Curcumin attenuates methotraxate-induced hepatic oxidative damage in rats. J Egypt Nat Cancer Inst 20(2):141-148.

Rangasamy Rajesh, Pindath Thandayan Lakshmanan (2008) Antioxidant defense of dietary squalene supplementation on sodium arsenite-induced oxidative stress in rat myocardium. Int J Biomed Pharm Sci 2(2):98-102.

Richter E, Schafer SG (1982) Effect of squalene on hexachlorobenzene (HCB) concentrations in tissue of mice. J Environ Sci Health 17:195-203.

Mehrzadi S, Fatemi I, Esmaeilizadeh M, Ghaznavi H, Kalantar H, Goudarzi M (2018) Hepatoprotective effect of berberine against methotrexate induced liver toxicity in rats. Biomed Pharmacother 97(2):233-239.

Schwartzberg LS, Vogel WH, Campen CJ (2014) Methotrexate and fluorouracil toxicities: A collaborative practice approach to prevention and treatment. ASCO Post 5(7):234- 236.

Sener G, Eksioglu-Demiralp E, Cetiner M, Ercan F, Sirvanci S, Gedik N, Yegen BC (2006) L-Carnitine ameliorates methotrexateinduced oxidative organ injury and inhibits leukocyte death. Cell Biol Toxicol 22:47-60.

Senthilkumar S, Devaki T, Manohar BM, Babu MS (2006a) Effect of squalene on cyclophosphamide-induced toxicity. Clin Chim Acta 364(1-2):335-342.

Senthilkumar S, Yogeeta SK, Subashini R, Devaki T (2006b) Attenuation of cyclophosphamide induced toxicity by squalene in experimental rats. Chem Biol Interact 160(3):252-260.

Smith TJ (2000) Squalene: potential chemopreventive agent. Expert Opin Investig Drugs 9:1841-1848.

Sotiroudis SA, Kyrtopoulos (2008) Anticarcinogenic compounds of olive oil and related biomarkers. Eur J Nutr 47:69-72.

Takahara S, Hamilton BH, Nell JV, Kobra TY, Ogawa Y, Nishimura ET (1960) Hypocatalasemia: A new genetic carrier state. J Clin Invest 29:610-619.

Uz E, Oktem F, Yilmaz HR, Uzar E, Ozguner F (2005) The activities of purine-catabolizing enzymes and the level of nitric oxide in rat kidneys subjected to methotrexate: protective effect of caffeic acid phenethyl ester. Mol Cell Biochem 277:165-170.

Uzar E, Koyuncuoglu HR, Uz E, Yilmaz HR, Kutluhan S, Kilbas S, Gultekin F (2006a) The activities of antioxidant enzymes and the level malondialdehyde in cerebellum of rats subjected to methotrexate: protective effect of caffeic acid phenethyl ester. Mol Cell Biochem 291:63-68.

Uzar E, Sahin O, Koyuncuoglu HR, Uz E, Bas O, Kilbas S, Yilmaz HR, Yurekli VA, Kucuker H, Songur A (2006b) The activity of adenosine deaminase and the level of nitric oxide in spinal cord of methotrexate administered rats. Toxicol 218:125-133.

Acta Biologica Szegediensis

Volume 64(2):207-219, 2020
Acta Biologica Szegediensis
http://abs.bibl.u-szeged.hu/index.php/abs
DOI:10.14232/abs.2020.2.207-219

ARTICLE

Pollen morphology of the genus *Impatiens* L. (Balsaminaceae) and its systematic implications

Muthulakshmipechiammal Pechimuthu, Rajendran Arumugam*, Samydurai Ponnusamy

Phytodiversity Research Laboratory, Department of Botany, Bharathiar University, Coimbatore- 641 046, Tamil Nadu, India.

ABSTRACT Pollen morphology of 18 species from the genus *Impatiens* collected from different localities in Nilgiris, Tamil Nadu was evaluated using scanning electron microscopy (SEM) during the period of February 2017 to November 2019. From the observation of pollen it was found to be structurally monad; prolate, sub-prolate and prolate-spheroidal in equatorial view; and circular, rectangular, triangular, quinquangular, elliptic and quadrangular in polar view. The apertures varied from dicolpate, tricolpate to tetracolpate. The main ornamentation type was reticulate in most of the species except *Impatiens fruticosa* which showed echinate ornamentation. The variations in pollen structure within the species were useful for the identification and classification of the genus *Impatiens*. The high structural diversity renders important taxonomic value for species differentiation. **Acta Biol Szeged 64(2):207-219 (2020)**

KEY WORDS

Impatiens
micromorphology
palynology
scanning electron microscopy (SEM)
taxonomy

ARTICLE INFORMATION

Submitted
08 September 2020.
Accepted
16 November 2020.
***Corresponding author**
E-mail: arajendran222@yahoo.com

Introduction

The genus *Impatiens* L. is a highly diverse genus of the family Balsaminaceae representing with over 1000 species distributed in tropical and subtropical regions (Janssens et al. 2018). In India, there are more than 210 species within Himalaya and the Western Ghats as the two major diversity centres (Shajitha et al. 2016). The Western Ghats is one of the richest areas in the world considering the distribution of species of *Impatiens* where about 103 species of *Impatiens* are endemic (Bhaskar 2012). They usually occur in wet and moisture conditions from sea level to 4000 m altitude, valleys, along streams, while some species tolerate drier habitats (Yu et al. 2015).

The vegetative morphology of *Impatiens* is conserved, always having a glandular-toothed leaf, fleshy semi-succulent stem and reflected in the hypervariable floral morphology in which the spurred sepal and the lateral petals show extreme variability (Fig. 1-2). High levels of convergent evolution on flower morphology are probably the main reason why it has been so difficult in the past to divide the genus into natural groups based on macromorphological data only (Janssens et al. 2012).

Representatives of the genus are known for their convergent phenotypic adaptation often making it extremely difficult to divide the genus into natural groupings using morphological data (Janssens et al. 2018). Grey-Wilson (1980b) suggested that due to their hypervariable flower morphology, enormous species diversity within the genus was the result of repeated hybridization events. Though macromorphological characters are very useful for taxonomic identification of many plant species, yet these cannot be used to distinguish between kinds of closely related species that are morphologically indistinguishable but belong to different species. Therefore, to bring out morphological differences that may exist between closely related species, SEM analysis of micromorphological investigations of pollen grains are used.

A reticulate rectangular pollen grains in genus *Impatiens* with four apertures was first reported by Huynh in 1968. Janssens et al. (2012) investigated pollen morphology in 115 species and described as four-aperturate to tri-aperturate, and the polar view ranged from circular, quadrangular, elliptic, and sub-elliptic to rectangular. Yu et al. (2015) provided a new classification for the genus *Impatiens* based on morphological and molecular evidence.

Janssens et al. (2005) carried out a palynological study and variation was noticed from the results of pollen morphology. In their study, representative of samples of 11 African and 8 Asian taxa were used for observation using SEM, but the palynological evolution of Asian *Impatiens* species was unable to conclude. Janssens et al. (2018) characterized pollen morphology as circular, rectangular or elliptic and reticulate sexine ornamentation for most of the African *Impatiens* species. Lens et al. (2005)

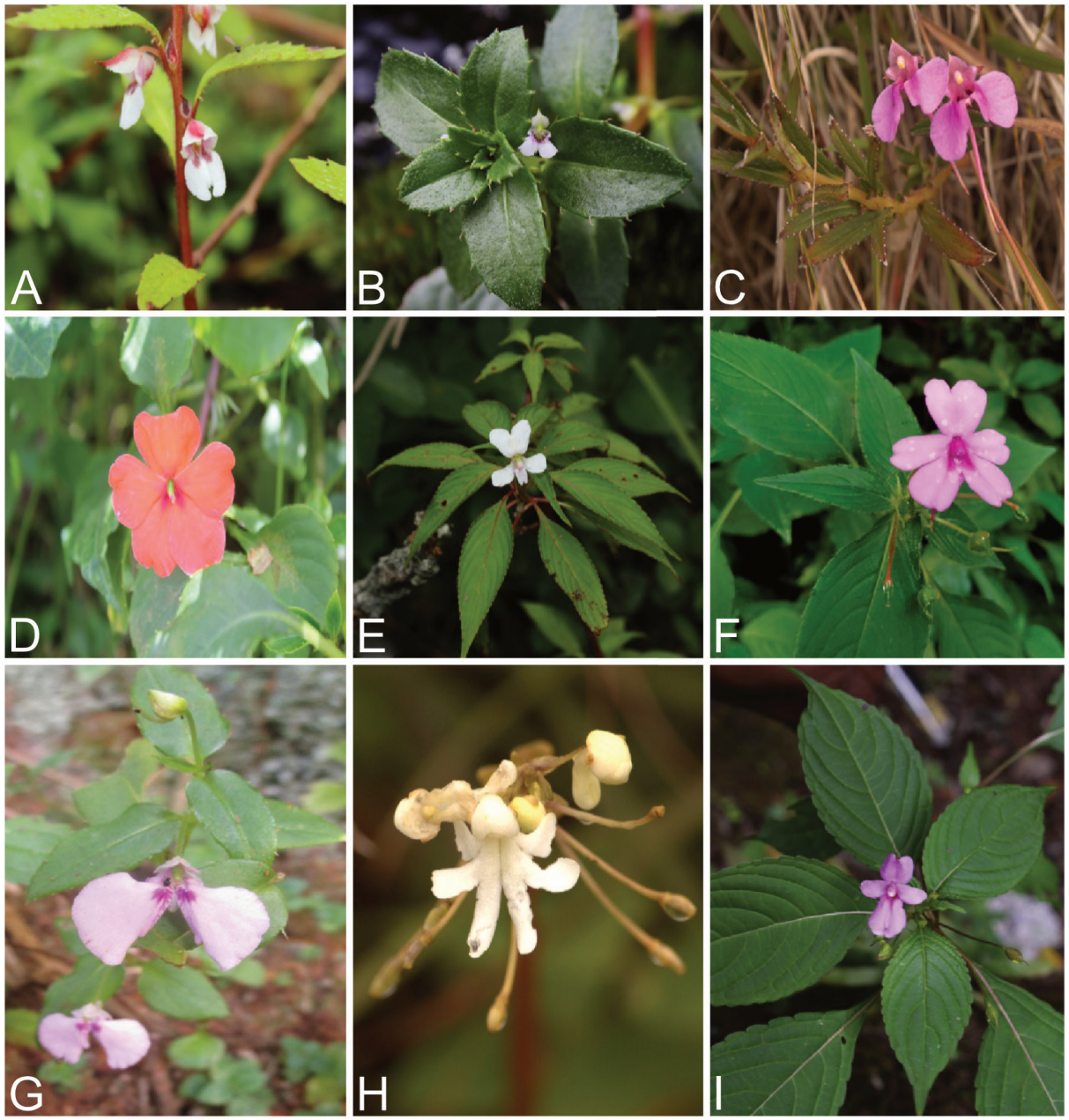

Figure 1. **A**: *Impatiens scabriuscula* Heyne; **B**: *Impatiens pendula* Heyne *ex* Wight & Arn.; **C**: *Impatiens fasciculata* Lam.; **D**: *Impatiens walleriana* Hook. f. **E**: *Impatiens cuspidata* Wight & Arn.; **F**: *Impatiens gardneriana* Wight; **G**: *Impatiens tenella* B. Heyne *ex* Wight & Arn.; **H**: *Impatiens clavicornu* Turcz.; **I**: *Impatiens latifolia* Wight.

carried out a detailed pollen morphological description of Balsaminaceae, Tetrameristaceae and Pellicieraceae by means of light microscopy, SEM and transmission electron microscopy revealed main aperture type in four-aperturate, colpate rectangular pollen grain with reticulate sexine ornamentation.

Bigazzi and Selvi (1998) suggested that palynological features are not changeable with environmental changes and have strong selection forces at work in dispersal, water-stress, pollination, germination, stigmatic interactions and possess strong taxonomic characteristics for species-genera identifications.

Taxonomically, *Impatiens* is notoriously difficult to classify due to the semi-succulent stems and fleshy leaves, flowers are extremely fragile, providing well-dried herbarium specimens is challenging and in dried specimens

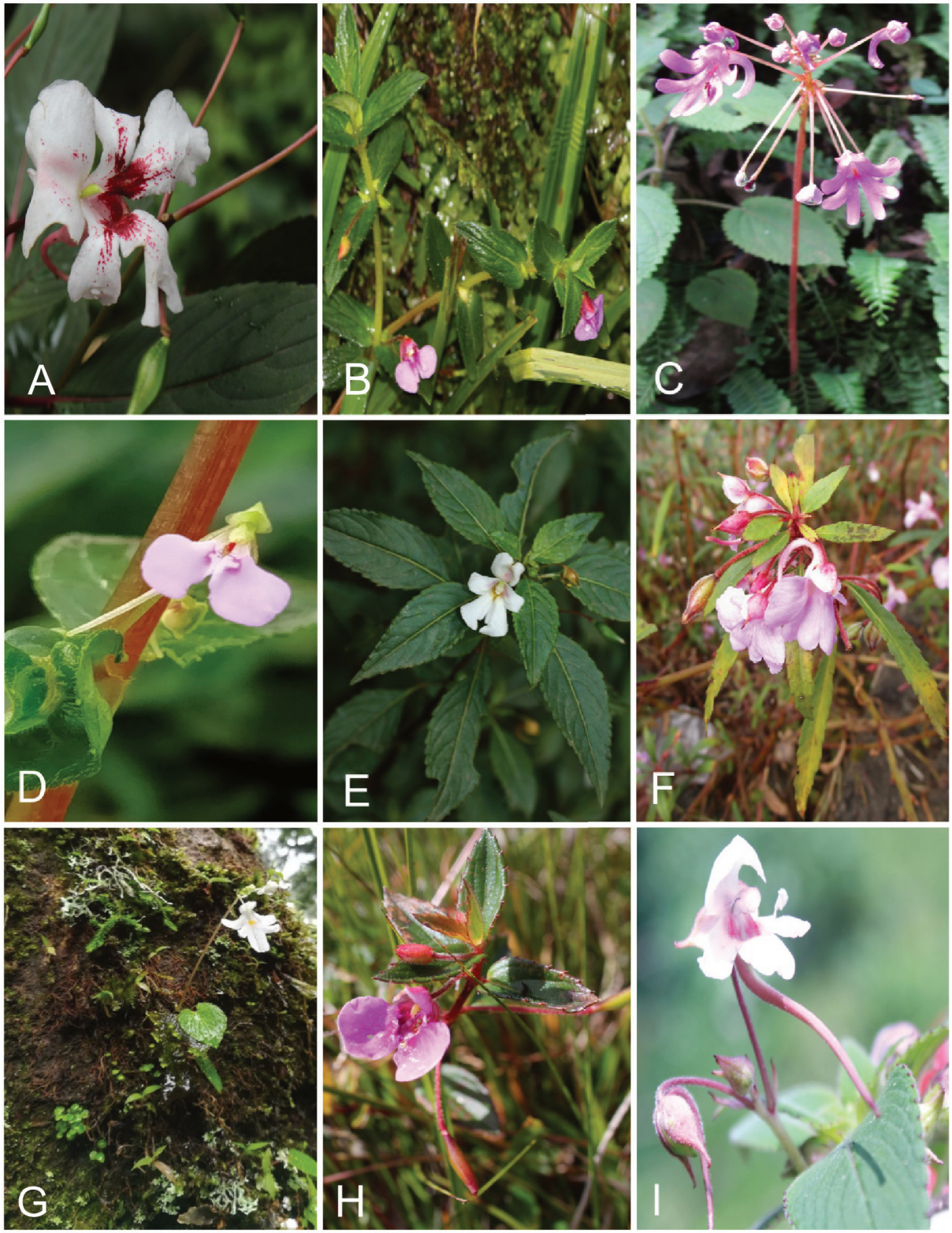

Figure 2. **A**: *Impatiens grandis* Heyne; **B**: *Impatiens oppositifolia* L.; **C**: *Impatiens levingei* Gamble *ex* Hook. f.; **D**: *Impatiens minor* (DC.) Bennet; **E**: *Impatiens leschenaultii* (DC.) Wall. *ex* Wight & Arn.; **F**: *Impatiens balsamina* L.; **G**: *Impatiens modesta* Wight; **H**: *Impatiens rufescens* Benth. *ex* Wight & Arn.; **I**: *Impatiens fruticosa* Lesch. *ex* DC.

most are folded and coalesced (Yu et al. 2015). Accordingly, Grey-Wilson (1980a, 1980b) suitable micromorphological characters to tackle the taxonomic complexity within the genus, as macromorphological characters have often proven unsuitable. Pollen grains can be retained in soil for a long period of time and its morphology is considered as conservative characters for plant classification because the shape of pollen grains specific to the taxonomic rank such as family, genus and species. Improved determination keys have been derived from extensive pollen analysis which could serve as a base for pollen studies by archaeologists, botanists, geologists, and immunologists (Erdtman 1986).

SEM offers distinct advantages for examination of unstained preparations of pollen and was used for the purpose of observing variations in the morphology of pollen of many plant taxa. Several studies (Lens et al. 2005; Janssens 2005, 2008, 2012) on the pollen morphology of *Impatiens* described their importance to understand the taxonomy of particular species. Even though several studies have been carried out, still the pollen morphology of this genus *Impatiens* require deeper understanding.

Material and methods

For palynological study, the specimens were collected along with its flower. Fresh pollen samples were collected from various localities of Nilgiris during the period of 2017-2019. The collected plant specimens were identified with the help of local floras (Gamble and Fischer 1915; Gamble 1921; Gamble 1934; Nair et al. 1983; Mattew 1991) and regional floras, revisions, monographs, and pertinent literature. The voucher specimens were deposited in the Herbarium of Department of Botany, Bharathiar University (BUH), Coimbatore. Further, the pollens were examined using scanning SEM.

The selected pollens were mounted directly on aluminum stubs using double sided adhesive tape and were sputter coated with in a thin layer of gold. Each taxon was studied for qualitative and quantitative character. SEM imaging was carried out with FEI Quanta 200 SEM (FELMI-ZFE, Graz, Austria) at the pollen laboratory. SEM micrographs were used mainly for studying the general shape, size, type of ornamentation, aperture characters and get more detailed information on the sculpturing.

Fifty pollen grains of each species were examined and an average measurement for the polar axis and equatorial axis, and lumen diameter were observed by ImageJ software. The P/E ratios were calculated. Pollen terminology follows the Punt et al. (2007). The terminology of pollen shape in polar view by the following Reitsma (1970). Terms for shape classes in equatorial view are adopted from Erdtman (1971). The ratio of polar length to equatorial length was calculated using the following formula.

The ratio of polar length to equatorial length = P/E

Where P denotes the diameter of the Polar axis and E denotes the diameter of the Equatorial axis.

Based on the palynological characters dichotomous taxonomic key for *Impatiens* was prepared. To evaluate the significant variations in quantitative character among the *Impatiens* taxa were determined by subjecting the data to one-way analysis of variance (ANOVA) using SPSS (version 16.0).

Results

The pollen morphology of 18 taxa of the genus *Impatiens* L. (Balsamiaceae) was investigated. A comprehensive description of the SEM data according to the pollen features in terms of the size, shape, shape in polar view, exine ornamentation, symmetry, polarity, polar length (P), equatorial length (E), the ratio of polar length to equatorial length (P/E) and the diameter of lumen measured for fifty pollen grains of each specimen are provided (Table 1 and 2).

All the collected species of *Impatiens* are monad. Most of the pollen grains were isopolar but certain species showed heteropolar grains, such as in *Impatiens fruticosa, Impatiens clavicornu, Impatiens levingei*, *Impatiens latifolia* and *Impatiens rufescens.* The pollen grain was radially symmetrical in *I. clavicornu*, *I. cuspidata*, *I. pendula, I. levingei*, *I. gardneriana, I. grandis*, *I. rufescens* and bilateral symmetrical in the remaining species. Selected SEM micrographs of examined pollen grains are presented in Fig. 3-6.

Size

According to size of the pollen grains it can be categorized into small size, large size and very large size (Kermp 1965). The pollen of the Nilgiris *Impatiens* species is generally small and medium sized. The small pollen grains were observed in *I. modesta, I. balsamina, I. pendula and I. rufescens* whereas the rest of the species are medium sized. The mean of the polar axis varies from 22.90 μm in *I. balsamina* to 36.19 μm in *I. walleriana*. The minimum equatorial axis (14.66 μm) is reported in *I. balsamina* and the maximum equatorial axis (28.52 μm) is reported in *I. gardneriana* (Table 1).

Shape in equatorial view

According to Erdtman (1952) the shapes of the pollen grains determine the ratio of polar axis and equatorial diameter. The highest P/E ratio was recorded in *I. walleriana* (1.78 μm) and the lowest was observed in *I. modesta*

Table 1. Dimensions and size variation in pollen grains of the *Impatiens* taxa.

Number	Taxon	Polar axis (P) µm		Equatorial axis (E) µm		P/E	Lumen diameter	Size
		Mean	Range	Mean	Range			
1	*I. balsamina L.*	22.90 ± 2.691^{i}	16.18 - 26.47	14.66 ± 1.913^{f}	10.12 - 18.59	1.56	1.20 ± 0.44^{g}	Small
2	*I. clavicornu* Turcz.	27.94 ± 2.810^{f}	21.61 - 33.34	24.29 ± 31.10^{bcd}	18 - 31.10	1.15	2.86 ± 1.00^{a}	Medium
3.	*I. cuspidata* Wight & Arn.	29.68 ± 2.608^{de}	24.50 - 34.21	22.34 ± 2.157^{cde}	16.08 - 27.75	1.32	1.80 ± 0.53^{def}	Medium
4.	*I. latifolia* Wight	31.07 ± 3.375^{c}	25.05 - 38.65	19.56 ± 2.174^{def}	16.36 - 23.23	1.58	2.11 ± 0.65^{bc}	Medium
5.	*I. fasciculata* Lam.	33.01 ± 2.273^{b}	27.61 - 38.09	22.19 ± 2.234^{cde}	16.45 - 26.87	1.48	1.68 ± 0.53^{ef}	Medium
6.	*I. fruticosa* Lesch. *ex* DC.	30.28 ± 2.491^{cd}	25.60 - 35.73	27.28 ± 2.287^{bc}	21.56 - 32.17	1.10	-	Medium
7.	*I. grandis* Heyne	27.73 ± 1.966^{c}	24.24 - 32.74	23.04 ± 2.235^{bc}	17.25 - 26.08	1.20	1.80 ± 0.52^{def}	Medium
8.	*I. gardneriana* Wight	31.46 ± 4.840^{c}	24.29 - 48.54	28.52 ± 3.729^{b}	22.38 - 35.25	1.10	2.20 ± 0.87^{b}	Medium
9.	*I. levingei* Gamble *ex* Hook. f.	25.94 ± 3.184^{g}	18.89 - 31.62	17.56 ± 2.265^{ef}	14.67 - 22.82	1.46	1.58 ± 0.44^{f}	Medium
10.	*I. leschenaultii* (DC.) Wall. *ex* Wight & Arn.	28.64 ± 3.860^{ef}	21.81 - 36.87	19.96 ± 2.911^{def}	16.39 - 28.31	1.43	1.91 ± 0.33^{cde}	Medium
11.	*I. modesta* Wight	23.10 ± 2.824^{i}	16.2 - 29.64	20.45 ± 3.053^{def}	15.18 - 28.19	1.09	1.96 ± 0.63^{bcd}	Small
12.	*I. minor* (DC.) Bennet	25.19 ± 2.586^{gh}	17.94 - 29.39	16.80 ± 2.455^{ef}	11.57 - 20.84	1.49	1.71 ± 0.56^{def}	Medium
13.	*I. oppositifolia* L.	28.67 ± 2.163^{ef}	24.26 - 33.45	19.68 ± 1.544^{def}	16.78 - 22.77	1.45	1.84 ± 0.53^{de}	Medium
14.	*I. pendula* Heyne *ex* Wight & Arn.	24.16 ± 2.400^{hi}	18.65 - 29.26	20.62 ± 2.689^{def}	14.16 - 24.57	1.17	1.19 ± 0.33^{g}	Small
15.	*I. rufescens* Benth. *ex* Wight & Arn.	23.83 ± 2.476^{i}	18.75 - 26.31	18.84 ± 2.260^{def}	14.73 - 20.92	1.26	1.28 ± 0.30^{g}	Small
16.	*I. scabriuscula* Heyne	28.36 ± 2.558^{f}	21.38 - 34.11	17.50 ± 2.637^{ef}	13.15 - 22.67	1.62	1.12 ± 0.34^{g}	Medium
17.	*I. tenella B.* Heyne *ex* Wight & Arn.	28.38 ± 2.862^{f}	20.76 - 33.42	17.38 ± 2.693^{ef}	12.69 - 23.56	1.63	1.58 ± 0.44^{f}	Medium
18.	*I. walleriana* Hook. f.	36.19 ± 4.634^{a}	28.06 - 44.18	20.24 ± 2.723^{def}	14.66 - 26.44	1.78	1.94 ± 0.63^{cde}	Medium
		F= 71.953* **		**F= 16. 522*** **			**F=52.023*** **	**Df-17,908**

Means ± Standard Error in a row followed by a same letter(s) are not significantly (P > 0.05) different according to Duncan's Multiple Range Test.
Df- Degree of freedom
***= Significant at 0.001% level

Table 2. Details of pollen morphological characteristics in selected species of *Impatiens*.

Number	Taxon	Shape	Polar view	Sexine ornamentation	Symmetry	Polarity	Number of aperature
1	*I. balsamina L.*	Prolate	Rectangular	Reticulate	Bilateral	Isopolar	Dicolpate
2	*I. clavicornu* Turcz.	Subprolate	Circular	Reticulate	Radial	Heteropolar	Tricolpate
3.	*I. cuspidata* Wight & Arn.	Subprolate	Elliptic - circular	Reticulate	Radial	Isopolar	Monocolpate
4.	*I. latifolia* Wight	Prolate	Elliptic	Reticulate	Bilateral	Heteropolar	Monocalpate
5.	*I. fasciculata* Lam.	Prolate	Elliptic	Reticulate	Bilateral	Isopolar	-
6.	*I. fruticosa* Lesch. *ex* DC.	Prolate - spheroidal	Quadrangular	Echinate	Bilateral	Heteropolar	-
7.	*I. grandis* Heyne	Subprolate	Elliptic	Reticulate	Radial	Isopolar	-
8.	*I. gardneriana* Wight	Prolate - spheroidal	Elliptic - circular	Reticulate	Radial	Isopolar	-
9.	*I. levingei* Gamble *ex* Hook. f.	Prolate	Triangular	Reticulate	Radial	Heteropolar	Tricolpate
10.	*I. leschenaultii* (DC.) Wall. *ex* Wight & Arn.	Prolate	Rectangular	Reticulate	Bilateral	Isopolar	-
11.	*I. modesta* Wight	Prolate - spheroidal	Circular	Reticulate	Bilateral	Isopolar	-
12.	*I. minor* (DC.) Bennet	Prolate	Rectangular	Reticulate	Bilateral	Isopolar	-
13.	*I. oppositifolia* L.	Prolate	Elliptic	Reticulate	Bilateral	Isopolar	-
14.	*I. pendula* Heyne *ex* Wight & Arn.	Subprolate	Circular	Reticulate	Radial	Isopolar	-
15.	*I. rufescens* Benth. *ex* Wight & Arn.	Subprolate	Quinquangular	Reticulate	Radial	Heteropolar	Monocolpate
16.	*I. scabriuscula* Heyne	Prolate	Rectangular	Reticulate	Bilateral	Isopolar	Bicolpate
17.	*I. tenella B.* Heyne *ex* Wight & Arn.	Prolate	Rectangular	Reticulate	Bilateral	Isopolar	-
18.	*I. walleriana* Hook. f.	Prolate	Rectangular	Reticulate	Bilateral	Isopolar	Tetracolpate

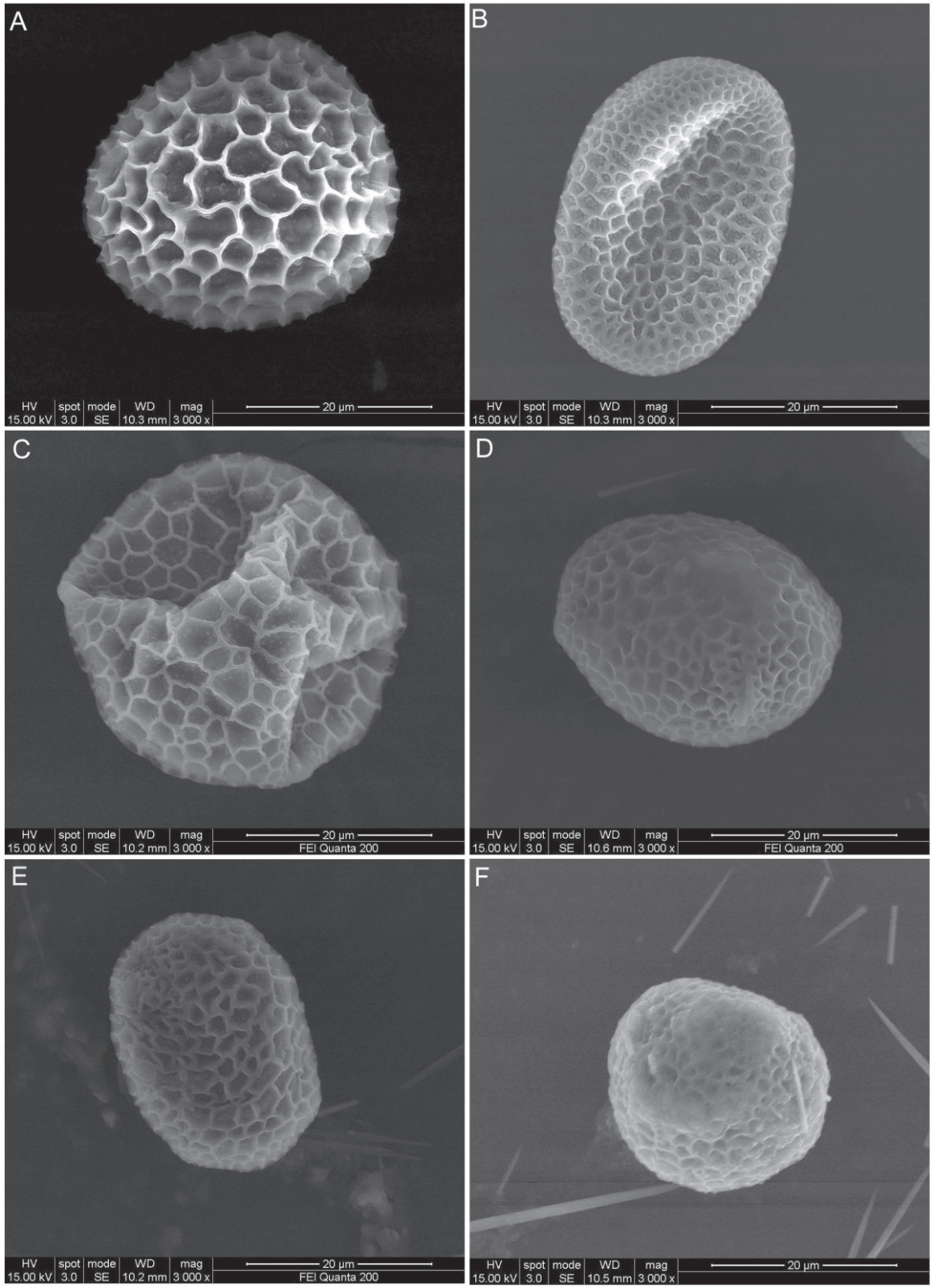

Figure 3. **A**: *Impatiens clavicornu* Turcz.; **B**: *Impatiens fasciculata* Lam.; **C**: *Impatiens gardneriana* Wight; **D**: *Impatiens grandis* Heyne; **E**: *Impatiens leschenaultii* (DC.) Wall. *ex* Wight & Arn.; **F**: *Impatiens pendula* Heyne *ex* Wight & Arn.

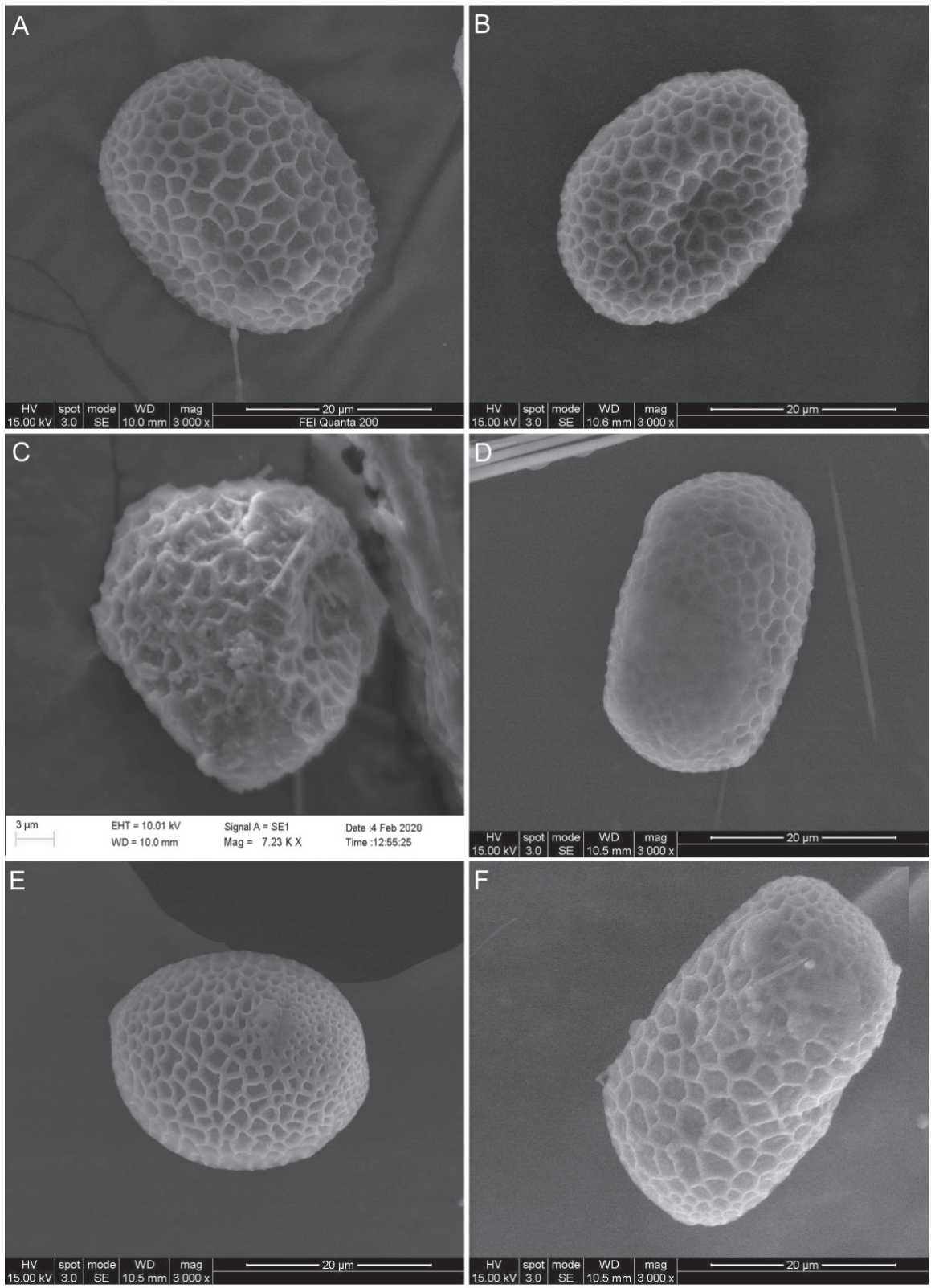

Figure 4. **A**: *Impatiens minor* (DC.) Bennet; **B**: *Impatiens oppositifolia* L.; **C**: *Impatiens rufescens* Benth. *ex* Wight & Arn.; **D**: *Impatiens tenella* B. Heyne *ex* Wight & Arn; **E**: *Impatiens cuspidata* Wight & Arn; **F**: *Impatiens walleriana* Hook. f.

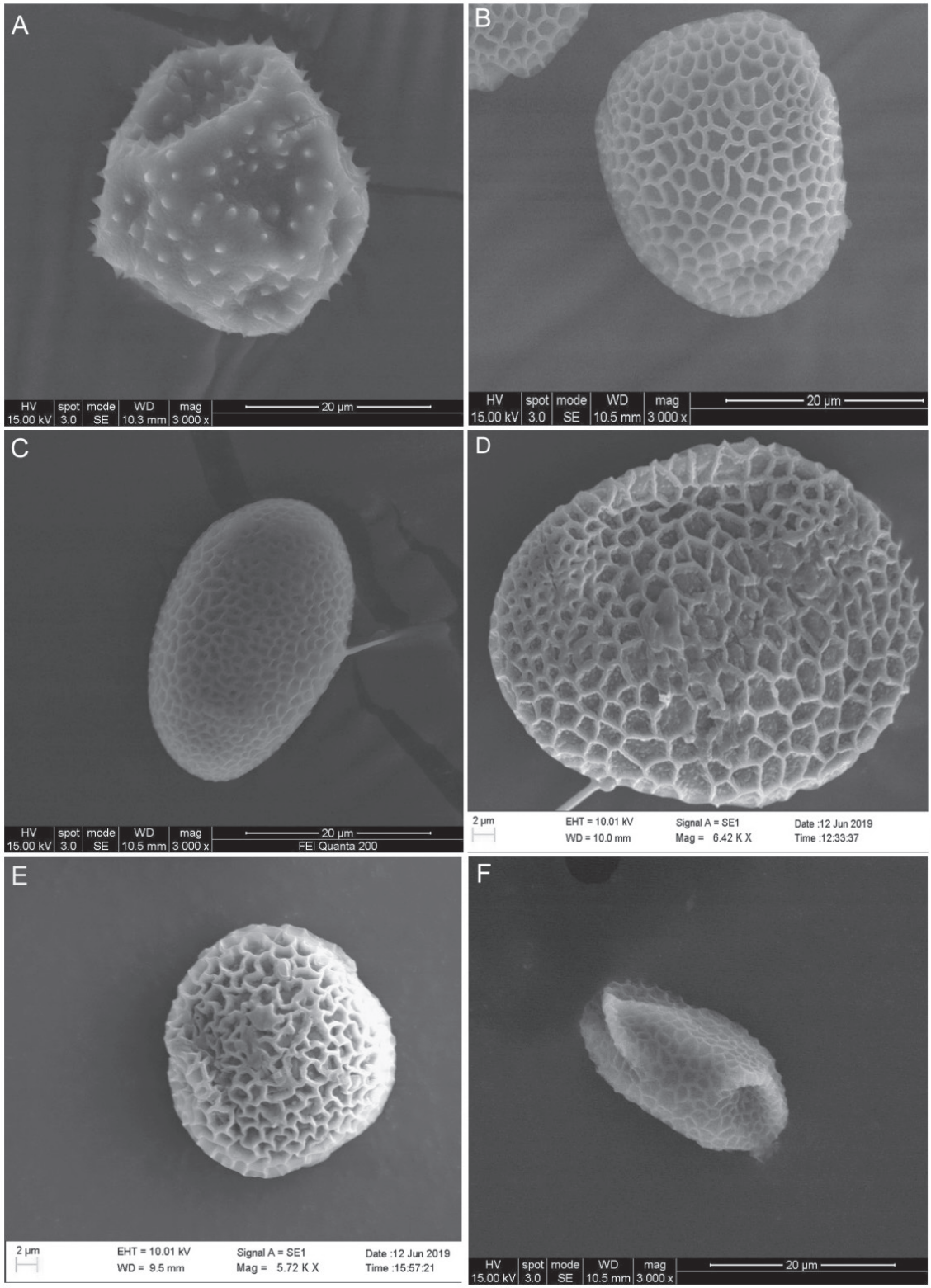

Figure 5. **A**: *Impatiens fruticosa* Lesch. *ex* DC.; **B**: *Impatiens levingei* Gamble *ex* Hook. f.; **C**: *Impatiens scabriuscula* Heyne; **D**: *Impatiens latifolia* Wight.; **E**: *Impatiens modesta* Wight; **F**: *Impatiens balsamina* L.

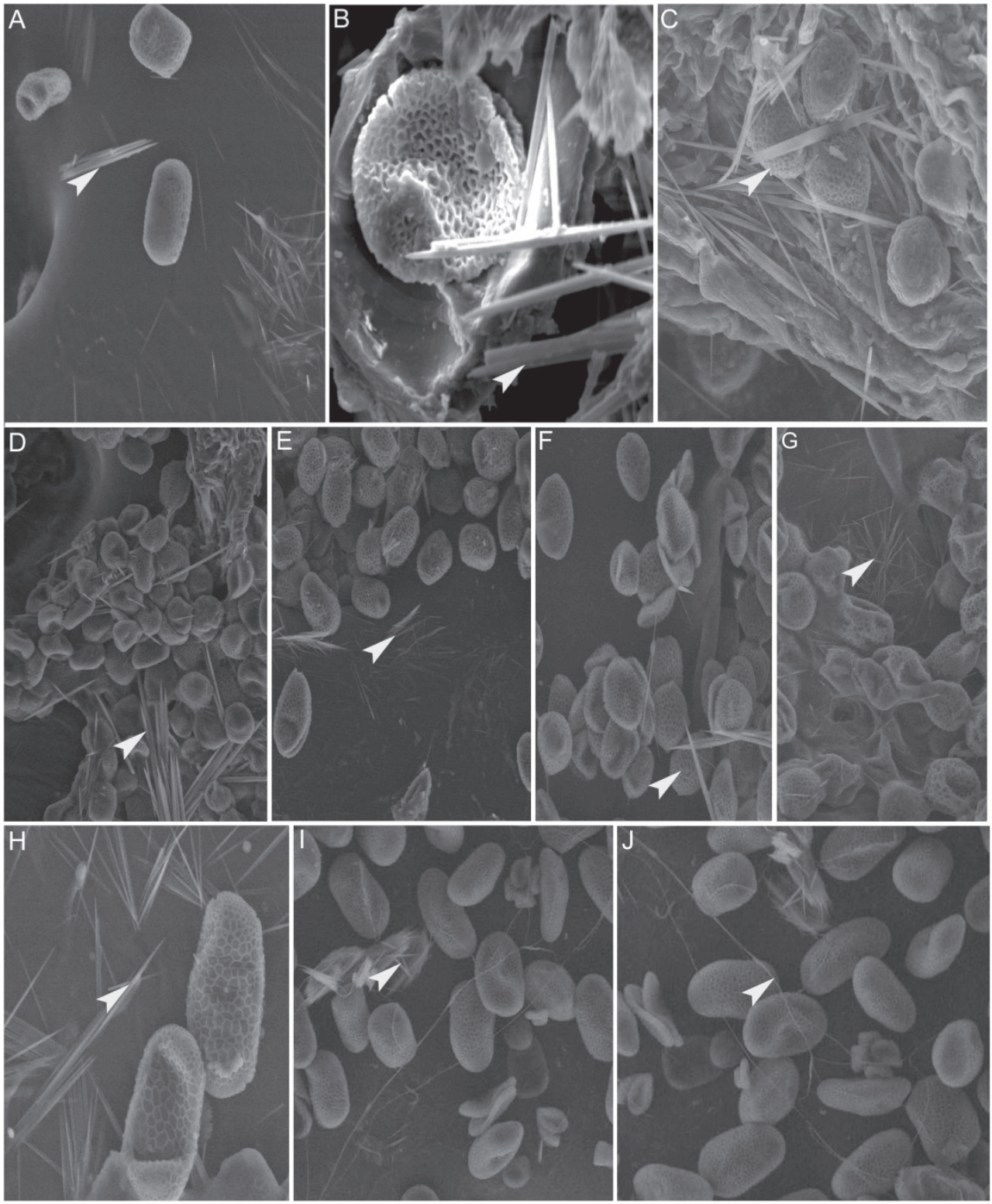

Figure 6. A-I Shows the rapids in pollen grains. **A**: *Impatiens tenella* B. Heyne *ex* Wight & Arn.; **B**: *Impatiens rufescens* Benth. *ex* Wight & Arn.; **C**: *Impatiens pendula* Heyne *ex* Wight & Arn.; **D**: *Impatiens minor* (DC.) Bennet; **E**: *Impatiens leschenaultii* (DC.) Wall. *ex* Wight & Arn.; **F**: *Impatiens grandis* Heyne; **G**: *Impatiens gardneriana* Wight; **H**: *Impatiens walleriana* Hook. f. **I**: *Impatiens scabriuscula* Heyne. **J:** pollen thread in *Impatiens scabriuscula*.

(1.09 μm). Most of the examined pollen shape is prolate (10 spp.) or subprolate (5 spp.) and prolate-spheroidal (3 spp.), respectively (Table 2).

Shape in polar view

The present study observed a wide range of pollen shape within the Nilgiris *Impatiens* species, varying from rectangular, circular, elliptic, triangular, elliptic-circular and quadrangular of all the studied *Impatiens*. The shape of majority of the pollen grains (6 spp.) of genus *Impatiens* are rectangular. Some others are elliptic (4 spp.) and about 2 species are elliptic-circular. Alternatively, quadrangular, triangular, quinquangular shapes have also been observed from negligible number (1) of species. Erdtman (1952) stated that the shape of the pollen grains determines the ratio of polar axis and equatorial diameter. The present study recorded the highest P/E ratio in *I. walleriana* (1.78) and the lowest was observed in *I. modesta* (1.09) (Table 1).

Exine ornamentation

The reticulate exines ornamentation was observed in most of the *Impatiens* species except for *I. fruticosa* which showed a rather distinct echinate type of ornamentation. The highest lumen diameter was recorded in *I. clavicornu* (2.86 μm) and lowest was observed in *I. scabriuscula* (1.12 μm).

Aperture characters

The apertures observed within *Impatiens* are simple and mostly monocolpate, dicolpate, tricolpate and tetracolpate. The colpate aperature is monocolpate with four taxa (*I. scabriuscula, I. rufescens, I. latifolia* and *I.cuspidata*), dicolpate with one taxa (*I. balsamina*), tricolpate with 2 taxa (*I. levingei* and *I. clavicornu,*) and tetracolpate is single taxa (*I. walleriana*), respectively. It is clear from our data that the aperture condition greatly defines pollen shape; the number of aperture and polar view also should be considered as dependent characters (Janssens et al. 2012).

Raphides

In all *Impatiens* species examined, there are some polynological features that are rare in the species, especially in case of *I. scabriuscula, I. walleriana, I. tenella, I. rufescens, I. pendula, I. minor, I. leschenaultii, I. grandis* and *I. gardneriana*. They could easily be distinguished from other species by the presence of raphides.

Pollen threads were observed in only mature anthers of *I. scabriuscula* shown in Figure 6 as white arrowheads in photo J but are present in the majority of the Asian *Impatiens* (Vogel and Cocucci 1988). These fine cellulose fibers form a dense network covering the anther slits. Most of the grains have granules in the foot layer in the lumina at the inside of the lumina. Granules can be solitary or interconnected and fused with neighboring muri. Although, rarely present in *Impatiens* a few south Indian species with a reticulate ornamentation pattern are characterized by a microreticulate margo in *I. cuspidata*.

Discussion

Palynology of genus *Impatiens* as described in Table 3. are generally prepared for observing the characteristic feature of *Impatiens* species under the SEM without disturbing the characteristic morphological features. For such characterization, the following features of pollen grains, pollen shape and exine ornamentation were observed which might greatly help in the identification of the genus *Impatiens* under study. It is apparent from other related studies that routine morphological feature assessment does not always give complete proof or identity of species.

Presence or absence of raphides was also differed from one another thus they might appear differently to view under SEM technique. Kubilzki (2004a, b); Lens et al. (2005) considered all subclades of balsaminoids were found to have the features of raphides, grouped under the Ericales. Pollen threads were observed in only mature anthers of *I. scabriuscula* but are present in the majority of the Asian *Impatiens* (Vogel and Cocucci 1988).

Categorizing genus *Impatiens* into different groups based on colporate alone does not however reflect their complete variation. It also adds that pollen grains are microscopically versatile requiring wide range of variables at polarity, symmetry, sexine ornamentation, shape and polar view as differentiating factors. These features have been observed for the monocolpate to biological characteristics which can be an aid to identification of species of *Impatiens*. In number of apertures, pollen grains of genus *Impatiens* are monocolpate to tetracolpate. Certain species are however no colpate.

The size of the pollen grains facilitated the differentiation of pollen grain with small as well as medium under SEM. Because of only small and medium size variations involved in the size for the differentiation of pollen grains, attention has been focused on the study of equatorial axis of pollen grains. The equatorial axis less than 14.66 (μm) has not been observed in Asian *Impatiens* under SEM. Majority of pollen grains of *Impatiens* species are smaller than 28.52 μm. The mean average E-axis of Asian *Impatiens* was about 16.522 μm.

Because of the variation on the polar axis, they are being classified as rectangular, quadrangular, elliptic, circular, triangular, etc. Majority of the large sized pollen grains are rectangular and elliptic circular type. The heterogeneity in the shape of pollen grain in genus Impatiens implies that distinct shapes of prolate, subprolate, prolate spheroidal are evident. The pollen grains of *I. gardneriana*

Wight exhibited the highest equatorial axis with the elliptical circular polar axis and prolate spheroidal shape. The pollen grains of African genus *Impatiens* on the other hand possess no prolate pollen (Janssens et al. 2012). The results of the present study are not in accordance with the findings of Janssens et al. (2012). They reported the pollen grains of genus *I. leschenaultii* were quadrangular in shape. But the present study revealed the shape was rectangular.

Pollen grains of Asian *Impatiens* are generally monocolpate. Bi-, tri- and tetracolpate are also present in Asian *Impatiens*. Perveen and Qaiser (2001) recognized tetracolpate, rectangular and reticulate from Pakistan. Grey-Wilson (1980a) was the first to stress the possible value of pollen characters to tackle taxonomical questions in *Impatiens* as he used pollen morphological data to detect possible hybrids and to optimize his species aggregation hypothesis on African *Impatiens*.

The pollen grains of Asian *Impatiens* are aporus and the pollen grains of African *Impatiens* on the other hand possessed frequently distributed pori. This is supportive in agreement to the results observed by Huynh (1968); Grey-Wilson (1980b). The sexine ornamentation of the Asian *Impatiens* shows reticulate type and plesiomorphic. The lumen size of Asian *Impatiens* varies considerably among clades or even between closely related species. One species was Echinate (*I. fruticosa* Lesch. *ex* DC). Similarly, different species of Asian *Impatiens* such as *I. cyclocoma, I. javensis, I. hirsuta* and *I. fruticosa*) were found to have echinate sexine ornamentation.

Ruchisansakun et al. (2015) stated that the combination of molecular phylogenetic and morphological character has facilitated the delimitation of natural infrageneric lineage within the complex genus *Impatiens* and suggested that even though molecular species demonstrated the critical nature of previous *Impatiens* classification, new monophyletic and clearly diagnosable lineages can be found in *via* extended character state research. Yu et al. (2015) analyzed the pollen, seed morphology and phylogeny of *Impatiens* using the three molecular markers such as ITS, *atpB* and *trnL-F*.

Pollen grains are generally four-aperturate. Tri-aperturate pollen is also present in African balsams but less frequent compared to four-aperturate pollen (Janssens et al. 2012). Balsaminaceae that shows a distinct variation is the granule density within the lumina or they can be fused with each other forming a dense mass. Another pollen character within Balsaminaceae shows a distinct variation as the granule density in the lumina (Janssens et al. 2005). Granules can either be absent or very sparse or they can be fused with each other and with neighboring muri. In some cases, granules fill nearly the entire lumina (Janssens et al. 2018). According to recent analysis (Janssens 2006, 2007, 2009b) these species are closely related thereby suggesting that the presence or absence of a margo might be a taxonomically useful character within Asian *Impatiens*.

Key to species based on pollen morphology

1a. Sexine echinate	**6. *I. fruticosa***
b. Sexine reticulate	2.
2a. Shape prolate	3.
b. Shape subprolate	12.
3a. Radial symmetry	**9. *I. levingei***
b. Bilateral symmetry	4.
4a. Heteropolar	**4. *I. latifolia***
b. Isopolar	5.
5a. Pollen size small	**1. *I. balsamina***
b. Pollen size medium	6.
6a. Polar axis < 35 µm	**18. *I. walleriana***
b. Polar axis > 35 µm	7.
7a. Aperturate	**16. *I. scabriuscula***
b. Non aperturate	8.
8a. Lumen diameter <1.85 µm	**10. *I. leschenaultii***
b. Lumen diameter >1.85 µm	9.
9a. P/E ratio >1.8 µm	**13. *I. oppositifolia***
b. P/E ratio <1.8 µm	10.
10a. Polar view elliptic	**5. *I. fasciculata***
b. Polar view rectangular	11.
11a. Equatorial view <17µm	**17. *I. tenella***
b. Equatorial view >17 µm	**12. *I. minor***
12a. Polar view quinquangular	**15. *I. rufescens***
b. Polar view not quinquangular	13.
13a. Heteropolar	**2. *I. clavicornu***
b. Isopolar	14.
14a. Pollen size small	**14. *I. pendula***
b. Pollen size medium	15.
15a. Colpate- 1	**3. *I. cuspidata***
b. Colpate-2	16.
16a. Prolate-spheroidal	17.
b. Other than prolate-spheroidal	**7. *I. grandis***
17a. Radial symmetry	**8. *I. gardneriana***
b. Bilateral symmetry	**11. *I. modesta***

Conclusion

The result concluded that the peculiar characteristics of *Impatiens* pollen are medium sized, quadrangular, reticulate and exine ornamentation. The palynological features may appear as tough to differentiate species but in reality, they are fascinating and quite useful for classification and identification of closely related species in a genus. The lack of simplified, illustrated SEM analysis is the major constrain experienced by several

systematic researchers. Palynological feature through SEM differentiation is the best procedure to justify the species and phylogenetic relationship. The present study, in addition with the reference from the previous literature confirmed the pollen morphological character through SEM is inevitable for the taxonomic identification of the species and it will be the base line information resolving many taxonomical problems on evolutionary relationship of plant species grouped under respective families. Therefore, SEM analysis is a valuable tool for studying the pollen morphological features for the species identification of genus *Impatiens*.

Acknowledgements

I would like to acknowledge Dr. Kadirvelu, Director, Life Science, DRDO, Bharathiar University (Coimbatore, Tamilnadu, India) for permitting to use SEM study and thankful to the Department of Botany, Bharathiar University for providing necessary facilities to carry out the study.

References

Bigazzi M, Selvi F (1998) Pollen morphology in the Boragineae (Boraginaceae) in relation to the taxonomy of the tribe. Pl Syst Evol 213:121-151.

Bhaskar V (2012) Taxonomic monograph on *Impatiens* L. (Balsaminaceae) of Western Ghats, South India: the key genus for endemism. Centre for Plant Taxonomic Studies, Bangalore, India.

Caris PL, Geuten KP, Janssens SB, Smets EF (2006) Floral development in three species of *Impatiens*. Amer J Bot 93:1-14.

Durdana Y, Nair PKK (1988) Pollen Morphology of Indian Geraniales. Vol. XI-XVI. New Delhi.

Erdtman G (1952) Pollen Morphology and Plant Taxonomy: Angiosperms. Chronica Botanica Co., Waltham, Massachusetts.

Erdtman G (1971) Pollen Morphology and Plant Taxonomy: Angiosperms. Corr. reprint of 1952. Hafner, New York.

Erdtman G. 1986. Pollen morphology and plant taxonomy: angiosperms (Vol. 1). Brill Archive.

Gamble, J.S. and Fischer, C.E.C., 1915. Flora of the Presidency of Madras (Vol. 1, pp. 134-145). London, UK:: West, Newman and Adlard.

Gamble, J.S., 1921. Flora of the Presidency of Madras: Rubiaceae to Ebenaceae/JS Gamble. Adlard & Son.

Gamble, J.S., 1934. Flora of the Presidency of Madras, vol. III. Bot. Survey of India.

Gamble JS (1915-1936) Flora of the Presidency of Madras. Vol. I-III. Adlard & Sons Ltd., London.

Grey-Wilson C (1980a) *Impatiens* of Africa. Balkema AA, Rotterdam.

Grey-Wilson C (1980b) *Impatiens* in Papuasia. Studies in Balsaminaceae: I. Kew Bull 34:661-688.

Huynh KL (1968) Morphologie du pollen des Tropaeolacées et des Balsaminacées. I. Morphologie du pollen des Tropaeolacées. Grana 8:88-184.

Janssens S, Lens F, Dressler S, Geuten K, Smets E, Vinckier S (2005) Palynological variation in balsaminoid Ericales. II. Balsaminaceae, Tetrameristaceae, Pellicieraceae and general conclusions. Ann Bot 96:1061-1073.

Janssens S, Geuten K, Yuan YM, Song Y, Küpfer P, Smets E (2006) Phylogenetics of *Impatiens* and *Hydrocera* (Balsaminaceae) using chloroplast *atpB-rbcL* spacer sequences. Syst Bot 31:171-180.

Janssens SB, Wilson YS, Yuan YM, Nagels A, Smets EF, Huysmans S (2012) A total evidence approach using palynological characters to infer the complex evolutionary history of the Asian *Impatiens* (Balsaminaceae). Taxon 61:355-367.

Janssens SB, Vinckier S, Bosselaers K, Smets EF, Huysmans S (2018) Palynology of African *Impatiens* (Balsaminaceae). Palynol 43:621-630.

Janssens S, Geuten K, Viaene T, Yuan YM, Song Y, Smets E (2007) Phylogenetic utility of the AP3/DEF K-domain and its molecular evolution in *Impatiens* (Balsaminaceae). Mol Phylogenet Evol 43:225-239.

Janssens SB, Knox EB, Huysmans S, Smets EF, Merckx VS (2009b) Rapid radiation of *Impatiens* (Balsaminaceae) during Pliocene and Pleistocene: Result of a global climate change. Mol Phylogenet Evol 52:806-824.

Kubitzki K (2004a) Pellicieraceae. In Kubitzki K, Ed. Families and Genera of Vascular Plants. Vol. 6. Springer-Verlag, Berlin. 297-299.

Kubitzki K (2004b) Tetrameristaceae. In Kubitzki K, Ed. Families and Genera of Vascular Plants. Vol. 6. Springer-Verlag, Berlin. 461-462.

Kremp G (1965) Encyclopedia of Pollen Morphology. University of Arizona Press, Tucson.

Matthew KM (1983) The Flora of the Tamilnadu Carnatic. Parts (1-3). Rapinat Herbarium, Tiruchirapalli, India.

Nair NC, Henry AN, Kumari GR, Chithra V (1983) Flora of Tamil Nadu, India. Coimbatore: Botanical Survey of India, Southern circle. Vol. I.

Lens F, Dressler S, Vinckier S, Janssens S, Dessein S, Van Evelghem L, Smets E (2005) Palynological variation in balsaminoid Ericales. I. Marcgraviaceae. Ann Bot 96:1047-1060.

Lens F, Dressler S, Jansen S, Van Evelghem L, Smets E. 2005a. Relationships within balsaminoid Ericales: a wood anatomical approach. Americ J Bot 92: 941–953.

Perveen A, Qaiser M (2001) Pollen flora of Pakistan - XXVI. Balsaminaceae. Turkish J Bot 25:35-38.

Punt W, Hoen PP, Blackmore S, Nilsson S, Le Thomas A (2007) Glossary of pollen and spore terminology. Rev Palaeobot Palynol 143:1-81.

Reitsma T (1970) Suggestions towards unification of descriptive terminology of angiosperm pollen grains. Rev Palaeobot Palynol 10:39-60.

Ruchisansakun S, Van Der Niet T, Janssens SB, Triboun P, Techaprasan J, Jenjittikul T, Suksathan P (2015) Phylogenetic analyses of molecular data and reconstruction of morphological character evolution in Asian *Impatiens* section *Semeiocardium* (Balsaminaceae). Syst Bot 40:1063-1074.

Shajitha PP, Dhanesh NR, Ebin PJ, Joseph L, Devassy A, John R, Mathew L (2016) Molecular phylogeny of Balsams (Genus *Impatiens*) based on ITS regions of nuclear ribosomal DNA implies two colonization events in south India. J App Biol Biotech 4(6):001-009.

Vogel S, Cocucci A (1988) Pollen threads in Impatiens, their nature and function. Beitr Biol Pflanzen 63:271-287.

Yu SX, Janssens SB, Zhu XY, Lidén M, Gao TG, Wang W (2015) Phylogeny of *Impatiens* (Balsaminaceae): integrating molecular and morphological evidence into a new classification. Cladistics 32:179-197.

Acta Biologica Szegediensis

Volume 64(2):221-232, 2020
Acta Biologica Szegediensis
http://abs.bibl.u-szeged.hu/index.php/abs
DOI:10.14232/abs.2020.2.221-232

ARTICLE

Effect of phospho-compost and phosphate laundered sludge combined or not with endomycorrhizal inoculum on the growth and yield of tomato plants under greenhouse conditions

EL Gabardi Soumaya[1], Mouden Najoua[1], Chliyeh Mohamed[1], Selmaoui Karima[1], Ouazzani Touhami Amina[1], Filali-Maltouf Abdelkarim[2], Ibnsouda Koraichi Saad[3], Amir Soumia[4], Benkirane Rachid[1], EL Modafar Cherkaoui[5], Douira Allal[1]*

[1]Laboratoire des Productions Végétales, Animales et Agro-industrie, Equipe de Botanique, Biotechnologie et Protection des Plantes, Faculté des Sciences, Université-Ibn Tofail- Kénitra-Maroc
[2]Laboratoire de Microbiologie et Biologie Moléculaire, Faculté des Sciences, Université Mohammed V, Rabat, Maroc
[3]Laboratoire de Biotechnologie Microbienne, Faculté des Sciences et Techniques, Université Sidi Mohamed Ben Abdellah, Fès, Maroc
[4]Laboratoire Polyvalent en Recherche et Développement, Université Sultan Moulay Slimane, Beni Mellal, Maroc
[5]Laboratoire d'Agrobiotechnologie et Bioingénierie Molécularie, Faculté des Sciences et Techniques, Université Cadi Ayyad, Marrakech, Morocco

ABSTRACT The study aims to evaluate the effect of endomycorrhizal inoculum (arbuscular mycorrhizal fungi), phospho-compost and phosphate sludge in single (M, PC, PS) or dual combinations (PC+M, PS+M, PS+PC) compared to agricultural and Mamora soils (A and S) on the growth, flowering, and yield of tomato plants. Among the studied treatments, the substrates containing 5% of phospho-compost combined with endomycorrhizal inoculum (PC+M) gave the most positive effect followed by phospho-compost (PC) and endomycorrhizal inoculum (M). In response to PC+M substrate, tomato plant height, the number of leaves and flowers attained 90 cm, 30, and 25, respectively. In substrates PC and M, tomato plants showed a height of 85 and 75 cm, leaves number of 30 and 19 leave/plant and number of flowers of 21, and 19 flower/plant. An optimal yield with (12 fruits/plant) was recorded in tomato plants grown on the substrate amended with bio-inoculant (AMF) and phospho-compost at a rate of 5%. In terms of qualitative parameters, the highest fresh and dry weight of aerial plant parts and root system were recorded in tomato plants grown in culture substrate incorporating 10 g of endomycorrhizal inoculum and 5% of phospho-compost reaching respectively103.4 g, 34 g 90.1 g, 28.9 g as compared to 87, 51, 23 and 24.1 g noted by tomato plants on the substrate with phospho-compost (5%) (PC). The highest mycorrhization parameters (frequency (F), intensity of mycorrhization (M), average arbuscular content (A), average vesicular content (V), average intraradicular spore content (S)) were found in the roots of tomato plants growing on substrates amended with 5% phospho-compost plus 10 g of endomycorrhizal inoculum, with percentages of 100% F, 61% M, 40.67% A, 18.36% V, and 56.9% S.

KEY WORDS
endomycorrhizal inoculum
growth parameters
phospho-compost
sludge
tomato
yield

ARTICLE INFORMATION
Submitted
21 November 2020.
Accepted
31 January 2021.
***Corresponding author**
E-mail: douiraallal@hotmail.com

Introduction

Composting has always been one of the most effective strategies for organic waste recycling (Santos et al. 2011) and is also a beneficial practice to improve soil structure (Celik et al. 2004) and its restoration (Scotti et al. 2016). Generally, soil with compost amendments had a positive effect on crop lands fertility and productivity (Celik et al. 2004; Pérez-Piqueres et al. 2006). Indeed, compost, a product of the composting process, is considered an important source of nutrients for cultivated plants (Duong et al. 2012) by enhancing plant yields and protecting them from numerous soil-borne pathogens (Pane et al. 2013).

Composting phosphate laundered sludge to produce phospho-compost biofertilizer is an important way to be explored to valorize these sludges, which still contains a significant amount of phosphorus, stored at phosphate mine sites (Hakkou et al. 2009; Ouakibi et al. 2013). In this sense, very satisfactory results were noted in bean plants: culture substrates containing 2.5 and 7.5% of phospho-compost showed a significant impact on growth and yield parameters (El Gabardi et al. 2019b).

The efficiency of phosphate sludges, as an essential

component of phospho-compost, is due to its richness of infectious propagules of arbuscular mycorrhizal fungi (El Gabardi et al. 2019c, d). These microorganisms have the potential to solubilize the phosphate and can convert insoluble phosphate into soluble forms available to plants (Pradhan and Sukla 2006; Sharma et al. 2007), thus increasing the tolerance of plants to soil pathogens and abiotic stresses (Smith and Read 2008). They are also like better microorganisms capable of improving the yield and quality of crops (Hijri 2016).

Other studies have shown that incorporation of compost into the soil represents a reservoir of nutrients to plants (Scotti et al. 2016; Yang et al. 2017) which may be useful and beneficial for the formation and functioning of arbuscular mycorrhizal fungi. Several studies have reported that compost addition improved AM root colonization, spore production, and development of AM extraradical hyphae (Labidi et al. 2007; Valarini et al. 2009; Tanwar et al. 2013; Cavagnaro 2015). Also, some research has reported that AM fungi can directly take advantage of organic matter (Hodge et al. 2001; Govindarajulu et al. 2005; Jin et al. 2005) which may promote plant growth and enhance carbon allocation to soil fungi (Lee et al. 2004; Donn et al. 2014).

The aim of this work was to investigate *in vivo* the effect of phospho-compost, phosphate laundered sludge alone, and in combination with endomycorrhizal inocula on the growth and yield of tomato plants.

Materials and Methods

Plant material

Tomato seeds belonging to the Campbell 33 variety were superficially disinfected with sodium hypochlorite diluted to 1% for 10 min, rinsed thoroughly with sterile distilled water, dried and set to pre-germinate in plastic seedling trays, filled with wet peat, and covered with a 20-micron thick plastic film for two days. After the various treatments, the planting was carried out when the seedlings reached 2 true well-spreading leaves (Woo et al. 1996) in 17 cm × 14 cm plastic pots and perforated at the base.

Mycorrhizal inoculum

A composite endomycorrhizal inoculum was prepared from phosphate sludge and rhizospheric soils of plant species grown there and it was used to inoculate mycotrophic species (e.g., maize, leek, barley, sorghum). The inoculum contained multiple endomycorrhizal species, 31 of which were identified morphologically (El Gabardi et al. 2019b): *Acaulospora scrobiculata, Acaulospora laevis, Acaulospora colossica, Acaulospora gedanensis, Acaulospora morrowiae, Acaulospora excavate, Acaulospora* sp.1, *Acaulospora* sp.2, *Acaulospora* sp.3, *Entrophospora schenckii, Entrophospora kentinensis, Entrophospora infrequens, Glomus intraradices, Glomus deserticola, Glomus etunicatum, Glomus caesaris, Glomus aggregatum, Glomus aureum, Glomus macrocarpum, Glomus mossae, Glomus claroideum, Glomus globiferum, Glomus fasciculatum, Glomus versiforme, Glomus pansihalos, Glomus manihoti, Glomus verruculosum, Glomus* sp., *Scutellospora nigra, Scutellospora biornata*, and *Scutellespora castenea*. Barley (*Hordeum vulgare* L.) was used as a host plant to multiply the composite mycorrhizal inoculum. Barley seeds were disinfected with 5% sodium hypochlorite for 2 min, then germinated in plastic pots filled with a mixture of sterile sand and endomycorrhizal inoculum. After 4 weeks of culture, the barley roots were excised, rinsed 3 times with distilled water, and cut into 1 - 2-mm long fragments. These root fragments were used as the endomycorrhizal inoculum.

Culture substrate

Two culture substrates were used: Mamora soil (S) and agricultural soil (A). Mamora soil is a loose structured very sandy soil (91.1% sand) with a slightly basic pH of 7.5. It is characterized by a low cation exchange capacity (7 meq/100 g), a very low salinity, and an organic matter content of not more than 0.7%. This soil was deficient in total phosphorus (0.239%), total potassium 0.15 (meq/100 g) and total nitrogen (0.05%). The soil was autoclaved three times for one hour at 121 °C.

The phospho-compost incorporated into the substrate 'soil of Mamora' was obtained after composting mining waste from phosphate laundered sludge and household waste (30% of phosphate sludge and 70% of household waste) by the Polyvalent Laboratory in Research and Development, Sultan Moulay Slimane University (Beni-Mellal). The dose of phospho-compost used in this study was 5%.

Experiments in tomato was conducted in randomized block design with 8 treatment combinations (with ten repetitions per treatment and each pot containing only one plant), viz,

S: 100% low phosphorus soil (Mamora soil)
A: 100% agricultural soil
NPK: 100% S amended after 20 days, following transplantation, by NPK (14/28/14) at a rate of 50 mg/kg of soil.
PC+S: phospho-compost (5%) + S (95%)
S+PS: phosphate sludge (5%) + S (95%)
S+M: S (100%), inoculated with 10 g of AMF (M).
PC+S+M: phospho-compost (5%) + S (95%), inoculated with 10 g of AMF (M).
S+S+PS: S (95%) + phosphate sludge (5%), inoculated with 10 g of AMF (M).

Tomato seedlings inoculation technique

Tomato plants were transferred separately to plastic pots filled with sterile Mamora sand. The inoculation of the plants consisted of placing near each root system approximately 10 g of inoculum used in the form of the infected barley roots, containing propagules of endomycorrhizal fungi. Plastic pots were filled with sterile substrate and they were placed in a plastic greenhouse. Watering was done with tap water every two days.

Experimental design

The experimental protocol was designed in random blocks with ten repetitions per treatment. Each pot contained only one plant.

Extraction and identification of spores from growing media in pots

Extraction of endomycorrhizal fungi spores from the substrate was performed according to the method of Gerdemann and Nicolson (1963). The number of spores in 100 g of soil was estimated by binocular direct counting (magnification × 10).They were then mounted on glass microscope slideswith polyvinyl alcohol lacto-glycerol (PVLG), observed under a microscope (× 40) and classified according to their color, size, hypha of attachment and their consistency in order to identify their genus (Ferrer and Herrera 1981; Schenck and Smith 1981; Walker and Mize 1982; Hall 1984; Schenck and Perez 1987; Morton and Benny 1990; Dalpé et al. 1992).

Root staining for the evaluation of AMF root colonization

The roots of the tomato plants which develop on the different substrates were colored, according to the technique of brightening and coloring of the roots of Phillips and Haymann (1970), to observe the different structures of endomycorrhizal fungi. The roots were washed with tap water and the finer roots were cut into fragments approximately 1 cm long. These fragments were bleached with a solution of potassium hydroxide: KOH (10%) for 45 min at 90 °C in the water bath. And then serially whitened them for 5 min by adding four drops of 33% H_2O_2. Then fragments were rinsed with distilled water and stained with a solution of cresyl blue for 15 min at 90 °C in water bath. They were finally rinsed with distilled water and observed using a microscope. The mycorrhizal roots proportion was identified for each sample.

Evaluation of the mycorrhization rate

The mycorrhization parameters were evaluated by the overall assessment of 30 fragments and described as Trouvelot et al. (1986), and Amir and Renard (2003). Root fragments were observed at the magnifications of 100 and 400. The arbuscules and vesicles of AMF frequency and levels were measured by assigning an index of mycorrhization of 0-5 (0: None; 1: trace; 2: less than 10%; 3: 11 to 50%; 4: 51 to 90%; 5: more than 91%).

Frequency of mycorrhization (F%)

The frequency of mycorrhization (F%) was calculated by the percentage of colonization of the host plant roots in arbuscular fungi.

$$F\% = 100 \times (N - N_0)/ N$$

N: the number of observed root fragments; N_0: the number of non-mycorrhizal fragments

Intensity of mycorrhization (M%)

Intensity of AM infection in the root cortex was determined by the five-class classification system following the method described by Trouvelot et al. (1986). This measurement is based on the infection (M%) in each root segment using values from 0 to 5. Numbers indicate the proportion of root cortex colonized by the fungus (0 = without colonization; 1 = colonization trace; 2 = less than 10%; 3 = from 11 to 50%; 4 = from 51 to 90%; and 5 = more than 90% of the volume of root segment occupied by the fungus). M% was estimated by the following equation:

$$M\% = (95n5 + 70n4 + 30n3 + 5n2 + n1) / N$$

where n5, n4, n3, n2, and n1 are the number of fragments in the respective categories 5, 4, 3, 2, and 1 (Alarcón and Cuenca 2005).

Arbuscular content (A%)

$$A\% = (100\ mA3 + 50\ mA2 + 10\ mA1)/100$$

where, mA3, mA2, mA1 are the percentages (%), respectively, assigned to the notes A3, A2, A1, with, mA3 = (95 n5A3 + 70 n4A3 + 30 n3A3 + 5 n2A3 + n1A3)/N. The same for A1 and A2.

In this formula, n5A3 represents the number of fragments noted 5 with A3; n4A3 is the number of fragments noted 4 with A3; A0: no arbuscules; A1: some (10%) arbuscules; A2: moderately abundant (50%) arbuscules; A3: very abundant (100%) arbuscules.

Vesicle content (V%)

$$V\% = (100\ mV3 + 50\ mV2 + 10\ mV1)/100;$$

Where, mV3, mV2, mV1 are the percentages (%), respectively, assigned to the notes V3, V2, V1, with, mV3 = (95 n5V3 + 70 n4A3 + 30 n3A3 + 5 n2A3 + n1A3) /N, The

Table 1. Averaged quantitative parameters (plant height, number of leaves, flowers, and fruits) of tomato plants as a function of different soil substrates.

Treatment	Plant height (cm)	Number of leaves	Number of flowers	Number of fruits
A	50^{e}	10^{d}	13^{c}	4^{d}
S	55^{e}	11^{d}	11^{d}	4^{d}
S+NPK	65^{d}	15^{c}	10^{d}	5^{d}
S+PS	57^{e}	14^{c}	12^{cd}	4^{d}
S+PS+M	60^{d}	12^{d}	13^{c}	6^{cd}
S+M	75^{c}	18^{b}	19^{b}	7^{c}
S+PC	85^{b}	19^{b}	21^{b}	9^{b}
S+PC+M	90^{a}	30^{a}	25^{a}	12^{a}

Two values in the same column followed by the same letter do not differ significantly at the level 5%.
A: 100% agricultural soil; S: 100 % soil; S+NPK: soil+NPK; S+PS: soil + 5% phosphate sludges; S+M: soil + 10 g of endomyrrhizal inoculum; S+PS+M: soil + 5% sludges + 10 g of endomycorrhizal inoculum; S+PC: soil + 5% phospho-compost; S+PC+M: soil + 5% phospho-compost + 10 g of endomycorrhizal inoculum.

same for V1 and V2;
In this formula, n5V3 represents the number of fragments noted 5 with V3; n4V3 is the number of fragments noted 4 with V3;
V0: no vesicles; V1: some (10%) vesicles; V2: moderately abundant (50%) vesicles; V3: very abundant (100%) vesicles.

Quantitative parameters

The growth parameters, the length of the aerial part, the number of leaves, the weights of the aerial and root parts of the plants which develop on the different used substrates, were noted at the end of the experiment.

Qualitative parameters

The biomass of the aerial part and the fruits fresh weight were measured using a precision balance on the same day while the root biomass was measured after one night so that the rinsing water does not distort the results. The dry weights of the aerial and root parts were determined after drying at 80 °C for 72 h.

Statistical analysis

The data processing focused on the analysis of variance and the PPDS test at the 5% threshold.

Results

The obtained results showed a significant effect of compost amendment when combined with endomycorrhizal inoculums on the growth of tomato plants which exhibited a higher value of different parameters. In the culture substrate containing compost amendement at a rate of 5% and 10 g of the endomycorrhizal inoculums, the average plant height reached 90 cm, with 30 leaves, 25 flowers, and 12 fruits per plant. These outcomes differed significantly from those recorded in tomato plant grown in substrate amended with phospho-compost at a rate of 5% alone showing an average height of 85 cm, with 19 leaves, 21 flowers, and only 9 fruits per plant. While in the presence of the third treatment composed by endomycorrhizal inoculums, the average height of plants was 75 cm with a mean number of 18 leaves, 19 flowers, and 7 fruits per plant.

At the opposite, lowest values were observed in plants growing on agricultural soil and Mamora soil where the average plant height was 55 cm and 50 cm, with 11 and 10 leaves, 13 and 11 flowers, and 4 fruits per plant, respectively (Table 1; Fig. 1 and 2). The data regarding plant growth characteristics including fresh weight, dry weight of both aerial and root parts represented in Table 2, showed significant differences among the tested treatments.

The better result was observed in tomato plants grown

Figure 1. Tomato plant development on the different culture substrates tested. S+PC+M: soil + 5% phospho-compost + 10 g of endomycorrhizal inoculum; S+PC: soil + 5% phospho-compost; S+M: 10 g of endomycorrhizal inoculum; S+PS: soil + 5% phosphate sludges; S: 100 % soil.

Table 2. Effect of different culture substrates on the averaged growth and yield parameters of tomato plants.

Culture substrates	FWA (g)	DWA (g)	FWR (g)	DWR (g)	WF (g)
A	20.9^{e}	10.2^{f}	12^{f}	4.7^{e}	32.5^{e}
S	14.4^{f}	4.5^{d}	10.2^{f}	2.1^{f}	27.3^{f}
S+NPK	43.6^{c}	16.7^{c}	24^{e}	7.4^{d}	36.4^{e}
S+PS	34.5^{d}	14.9^{d}	14^{f}	5.1^{e}	29.6^{f}
S+M	45^{c}	12^{e}	42^{c}	13.8^{c}	50.7^{c}
S+PS+M	37.7^{d}	9,9^{f}	32^{d}	11.1^{c}	43.6^{d}
S+PC	87^{b}	23^{b}	51^{b}	24.1^{b}	63.6^{b}
S+PC+M	103.4^{a}	34^{a}	90.1^{a}	28.9^{a}	70.7^{a}

Two values in the same column followed by the same letter do not differ significantly at the level 5%.
FWA: fresh weight of aerial part; DWA: dry weight of aerial part; FWR: fresh weight of root part; DWR: dry weight of root; WF: weight of fruits.
A: 100% agricultural soil; S: 100 % soil; S+NPK: soil+NPK; S+PS: soil + 5% phosphate sludges; S+M: soil + 10 g of endomyrrhizal inoculum; S+PS+M: soil + 5% phosphate sludges + 10 g of endomycorrhizal inoculum; S+PC: soil + 5% phospho-compost; S+PC+M: soil + 5% phospho-compost + 10 g of endomycorrhizal inoculum.

in substrate supplemented with compost amendment and 10 g of endomycorrhizal inoculum with 104 g and 34 g for fresh weight and dry weight of aerial parts respectively exceeding those noted for the fresh weight (90.1 g) and dry weight (28.9 g) of root parts. Whilst, in the Mamora soil and agricultural soil, the fresh/dry weight of the aerial part was the lowest in the order of 14.4 g / 4.5 g, 20.9 g / 10.2 g, respectively, compared with the respective values 10.2 g / 2.1 g and 12 g / 4.7 g for the root parts.

The same trends were observed in the weight of tomatoes which was higher in plant developed on substrate amended with phospho-compost at rate of 5% and 10 g of endomycorrhizal inoculum (70.7 g) followed by those noted in substrate supplemented with a rate 5% of phospho-compost (63.6 g) and the substrate that only contains endomycorrhizal inoculum giving a weight of 50.7 g. Whereas, the lowest fruit weight was noted in tomato plants from agricultural soil and Mamora soil with 32.5 g and 27.3 g, respectively (Table 2, Fig. 2 and 3).

Microscopic observations of tomato roots stained with trypan blue after having been taken off from the studied culture substrates revealed that all of them were mycorrhized (Table 3). They had all structures of AMF (arbuscules, vesicles, spores, intra and extra-radicular hyphae (Fig. 4).

The maximal mycorrhizal frequency (100%) was noted in roots of tomato plants grown in three substrates. The frequency of mycorrhization is maximum (100%) in the roots of tomato plants growing on the substrate amended with phospho-compost (5%) + 10 g of endomycorrhizal inoculum, as well as in those of plants in the substrates amended with 10 g of endomycorrhizal inoculum alone and with 5% of mud plus 10 g of endomycorrhizal inoculum. In addition, the substrates amended with 5% phospho-compost alone, 5% mud alone and agricultural soil, presented mycorrhization frequencies of 96%, 89% and 73%, respectively. However, no significant difference was observed between the different treatments at the 5% threshold (Table 3).

The intensity of mycorrhization of the roots of tomato plants is medium (61%) at the level of the substrate amended with 5% of phospho-compost + 10 g of endomycorrhizal inoculum and low at the level of the substrates amended with 10 g of endomycorrhizal inoculum alone, phospho-compost alone, 5% mud plus 10 g of endomycorrhizal inoculum, 5% mud alone and agricultural soil, the

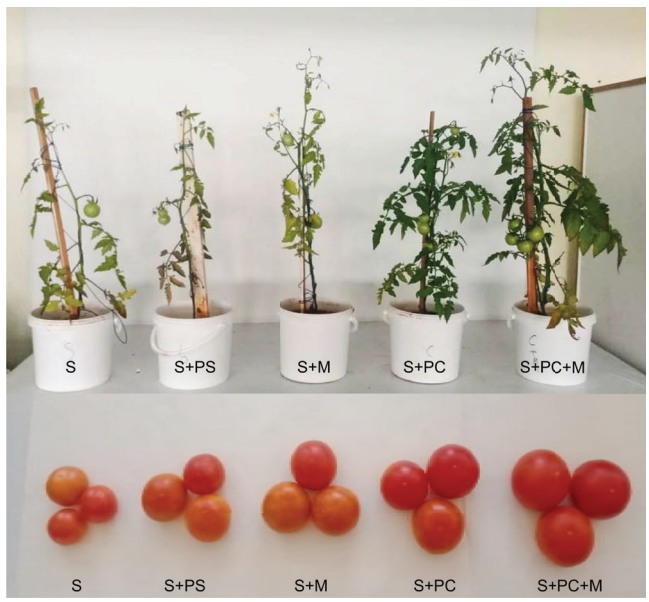

Figure 2. Tomato plant development as regarding plant height (A) and fruit caliber produced by tomato plants (B) grown on different culture substrates. S: 100 % soil; S+PS: soil + 5% phosphate sludges; S+M: soil + 10 g of endomycorrhizal inoculum; S+PC: soil + 5% phospho-compost; S+PC+M: soil + 5% phospho-compost + 10 g of endomycorrhizal inoculum.

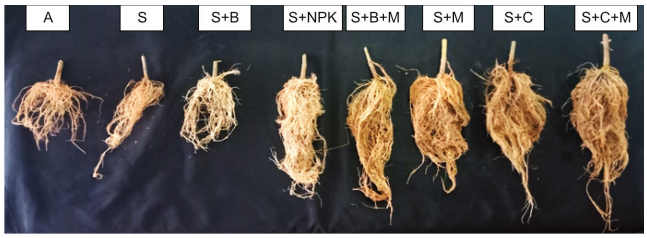

Figure 3. Root system growth of tomato plants in the response of different soil substrates. A: 100% agricultural soil; S: 100 % soil; S+PS: soil + 5% phosphate sludges; S+NPK: soil+NPK; S+PS+M: soil + 5% phosphate sludges + 10 g of endomycorrhizal inoculum; S+M: soil + 10 g of endomycorrhizal inoculum; S+PC: soil + 5% phospho-compost; S+PC+M: soil + 5% phospho-compost + 10 g of endomycorrhizal inoculum.

percentages of which are 38%, 35%, 27%, 19% and 12%, respectively.

The average arbuscular content was higher in tomato plants grown on the soil which was amended with endomycorrhizal fungi (10 g) and phospho-compost (5%) or only with the endomycorrhizal fungi alone registering respectively percentages of 40.67% and 39.23%. The lowest rates of colonization were found on those grown on soil adding with sludge (5%) and 10 g of endomycorrhizal inoculum (29.56%), 5 g of sludge (16%), phospho-compost-amended soil (15.81%) as compared to the agricultural soil (10%).

As stated above, combining the endomycorrhizal inoculum (10 g) and phospho-compost (5%) in culture substrate of tomato plants was more favorable showing an average content in vesicles of 18.36%, followed by those recorded in substrates containing 10 g of endomycorrhizal inoculum alone (11.23%), 5% of phospho-compost (10.14%), and 5% of mud added with endomycorrhizal inoculum (8.45%).

The highest intra-radicular spore content of tomato plants (56.9%) was noted in the roots of plants grown on the amended substrate with 5% phospho-compost + 10 g endomycorrhizal inoculum reaching (56.9%) while in the substrate supplemented with 10 g endomycorrhizal inoculum alone, the content was 33.21% (Table 3). By the contrary, the lowest content (13.2%) was recorded in the root cortex of tomato plants grown on the substrate containing 5% of the phosphate laundered sludge.

The extracted spores had a lower density in all tested substrates; 14 and 10 spores / 100 g soil were found in the rhizosphere of plants grown in substrate incorporating 5% of phospho-compost with 10 g of endomycorrhizal fungi and that containing endomycorrhizal inoculum alone, respectively. The lowest spore numbers, 3 and of 2 spores / 100 g soil, were detected in the rhizosphere of plants developed on substrate enriched with 5% phosphate laundered sludge alone and on agricultural soil, respectively.

The morphological study of spores revealed the presence of 12 different morphotypes represented by the following species *Acaulospora sporocarpia, Acaulospora delicata, Rhizophagus clarus, Acaulospora* sp., *Rhizophagus aggregatus, Funneliformis smoseae, Rhizophagus intraradices, Glomus* sp., *Funneliformis constrictum, Gigaspora gigantia, Diversispora trimurales, Acaulospora foveate* (Fig. 5). These species belonged to the three families (*Glomaceae, Acaulosporaceae* and *Gigasporaceae*), 2 orders (Glomerales and Diversisporales).

Discussion

The supply of 5% phospho-compost to the cultivation substrate combined with an endomycorrhizal inoculum had positively affected all growth and yield parameters of tomato plants. Indeed, plant height, their leaves, flowers, and fruits number were far greater than those noted in plants grown in substrates without supplements. In this context, recent study results had revealed that phospho-compost at a rate 2.5% and 5% increased both growth

Table 3. Parameters of root mycorrhization of tomato plants grown on different soil substrates.

Culture substrates	F%	M%	A%	V%	S%
A	73^{b}	12^{f}	10^{e}	-	-
S	-	-	-	-	-
S+PS	89^{ab}	19^{e}	16^{d}	-	13,2^{d}
S+M	100^{a}	38^{b}	39.23 ^{b}	11.23^{b}	33,21^{b}
S+PS+M	100^{a}	27 ^{d}	29,56^{c}	8.45^{c}	29,91^{c}
S+PC	96^{a}	35^{c}	15.81^{d}	10.14^{b}	31,45^{bc}
S+PC+M	100^{a}	61^{a}	44.67^{a}	18.36^{a}	56,9^{a}

Two values in the same column followed by the same letter do not differ significantly at the level 5%.
A: 100% agricultural soil; S: 100 % soil; S+PS: soil + 5% phosphate sludges; S+M: soil + 10 g of endomyrrhizal inoculum; S+PS+M: soil + 5% phosphate sludges + 10 g of endomycorrhizal inoculum; S+PC: soil + 5% phospho-compost; S+PC+M: soil + 5% phospho-compost + 10 g of endomycorrhizal inoculum.

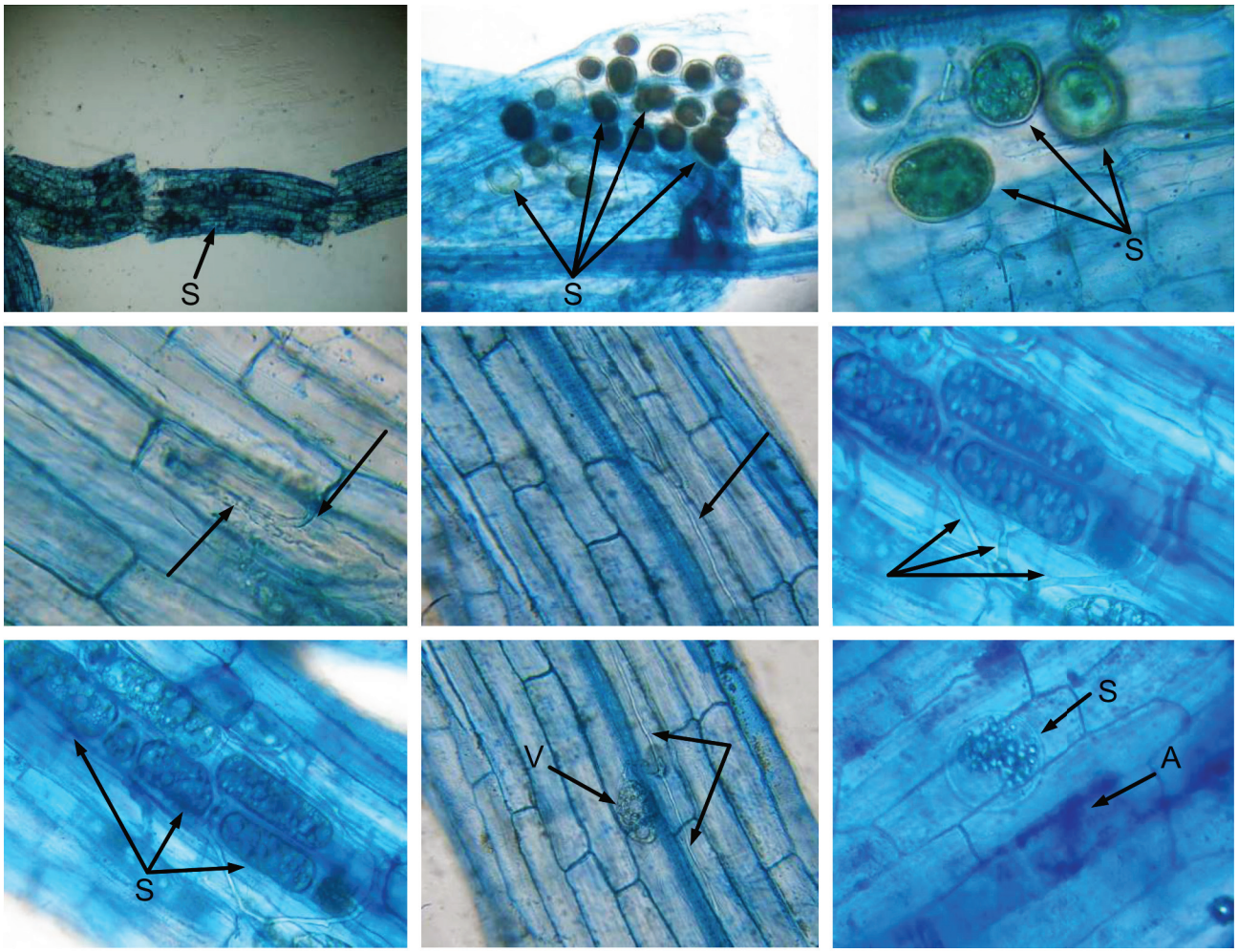

Figure 4. Endomycorrhizal fungi structures observed in root samples of tomato plants grown in the tested culture substrates: arbuscules (a), vesicles (v), spores (s), and intracellular hyphae (hi) (G×400).

parameters and yield of bean plants (El Gabardi et al. 2019e).

In accordance with our findings, many other studies have shown that the application of organic manure in combination with arbuscular mycorrhizal fungi (AMF) enhanced crop yield under greenhouse conditions (Gapasin and Ronayre 2003; Diongzon and Gapasin 2000; Serfoji et al. 2010) and in the field (Germani and Plenchette 2005). Akhter et al. (2015) reported a significant effect of compost and AMF complex on the growth of tomato (*Solanum lycopersicum* L.) plants reflected by an improvement of root and shoot dry weight of tomato plants as well as AMF colonization of the roots. Similarly, El Kinany et al. (2019), have demonstrated the beneficial effect of compost application and inoculation with a commercial strain of the arbuscular mycorrhizal fungi (AMF), *Glomus iranicum*, on the growth of micropropagated date palm

Table 4. Spores number counted in the rhizosphere of tomato plants growing on different soil substrates.

Culture substrates	Number of spores / 100 g of soil
S	-
A	2^{d}
S+NPK	-
S+PS	3^{d}
S+PS+M	5^{c}
S+PC	6^{c}
S+M	10^{b}
S+PC+M	14^{a}

Two values in the same column followed by the same letter do not differ significantly at the 5% threshold.
S: 100 % soil; A: 100% agricultural soil; S+NPK: soil+NPK; S+PC: soil + 5% phospho-compost; S+PS: soil + 5% phosphate sludges; Soil+M: 10 g of endomycorrhizal inoculum; S+PC+M: soil + 5% phospho-compost + 10 g of endomycorrhizal inoculum; S+PS+M: soil + 5% phosphate sludges + 10 g of endomycorrhizal inoculum.

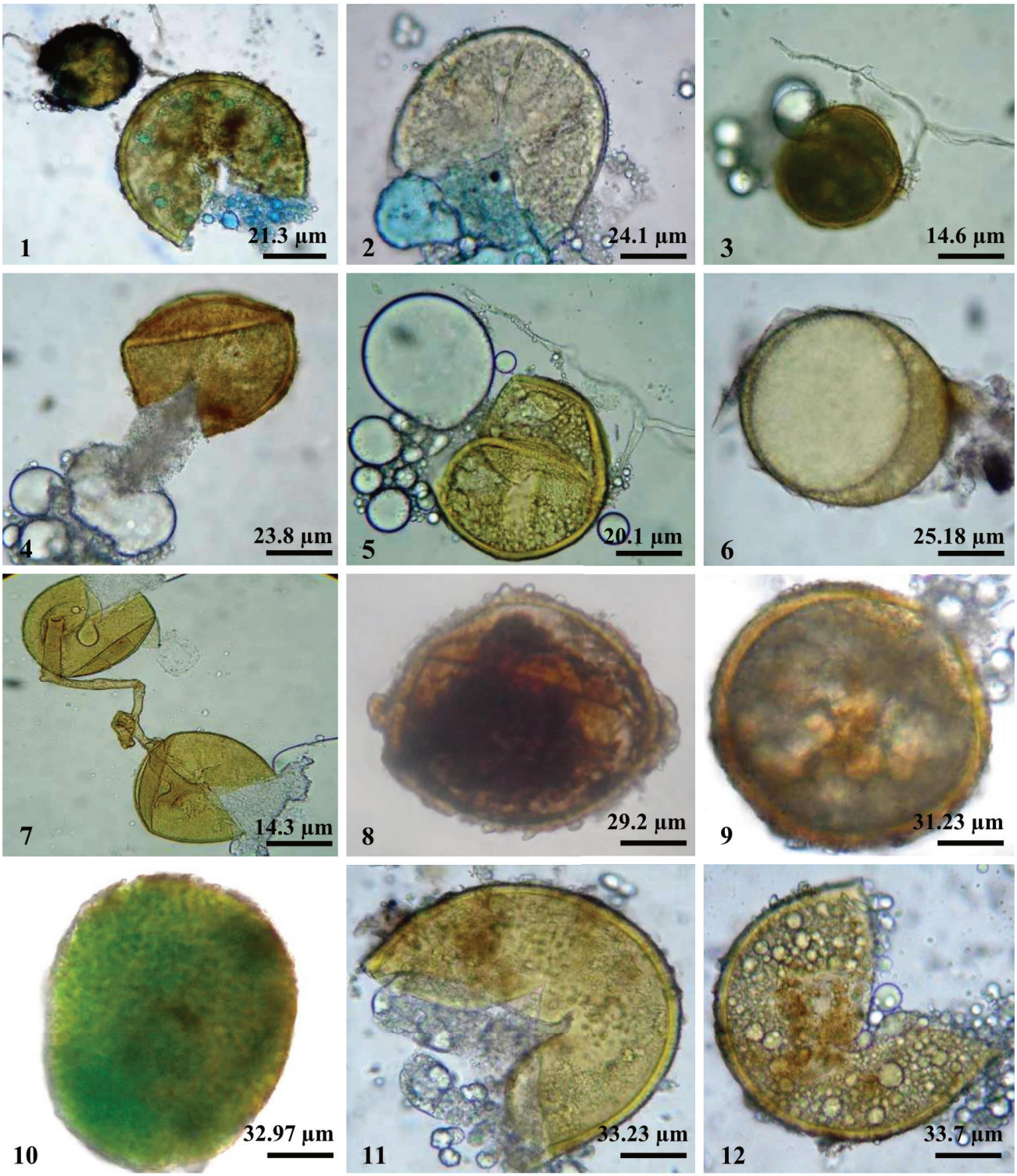

Figure 5. Spores of endomycorrhizal fungal species isolated from the rhizosphere of tomato plants grown on different culture substrates. 1: *Acaulospora sporocarpia*; 2: *Acaulospora delicata*; 3: *Rhizophagus clarum*; 4: *Acaulospora* sp.; 5: *Rhizophagus aggregatus*; 6: *Funneliformis moseae*; 7: *Rhizophagus intraradices*; 8: *Glomus* sp; 9: *Funneliformis constrictum*; 10: *Gigaspora gigantea*; 11: *Diversispora trimurales*; 12: *Acaulospora foveata*.

plantlets. These authors have signed the important contribution of AMF inoculation to micronutrient uptakes like iron and zinc. Also, the mixture of compost and AMF had contributed to the uptake of another micro-element such as Bor (El Kinany et al. 2019).

The incorporation of only 5% of the phospho-compost or 10 g mycorrhizal roots by mycorrhizal fungi to the substrate also has a positive effect on growth and yield parameters (90 cm, 12 fruits/plant). De Bertoldi et al. (1983) and Pommel and Lasserre (1982) noted that soil amendment with composts is an agricultural practice that can correct plant nutrient deficiencies, ensure adequate nutrition, help plants to tolerate stressful situations, maintain optimal soil fertility and improve crop quality. Vanai (1995) reported that the growth of maize (*Zea mays* L.) was enhanced after the incorporation of urban compost into crop plots. The study conducted on tomato cultivation has revealed that the production and profitability were optimal with the addition of compost rate of 30 t/ha (Kitabala et al. 2016). Mouria et al. (2010) found that solid waste compost and its extracts increased plant growth parameters and yields of tomato crops. Charland et al. (2001) indicated that a good compost, even when applied at a low rate, ensured yield improvement of cultivated plants with respect to those planted in unfertilized soils. Lee et al. (2004) have demonstrated that different concentrations of commercial compost promote lettuce (*Lactuca sativa*) growth. In addition, under soil stress conditions, it has been found that two commercial composts incorporated into the soil at a 4% rate of application tended to the growth, nodulation and nitrogen fixationof soybean plants (*Glycine max* L.) (Lawson et al. 1995). El Kadiri Boutchich (2016) claimed the efficiency of composts based on sewage sludge, and wastewater alone or mixed with organic substrates on the growth of wheat shoot and roots.

In agreement with our results, Salvioli et al. (2008) suggested that AMF application provides numerous benefits on both the quantity and quality of tomato productivity. Those of El Amerany et al. (2019) reported that tomato growth parameters significantly improved in mycorrhized plants compared to non-mycorrhized plants. Jochems-Tanguay (2014) reported that inoculation with endomycorrhizal fungi increased average crop yields by 0.079 t/ha (2.4%) for soybeans and 3.3 t/ha (8.7%) for potatoes. According to (Koomen et al. 1987), the use of mixed (multiple) inoculums was equally or more effective than inoculum with only a single species in promoting plant growth in a low-phosphate soil at pH 4.8 and pH 6.8.

Cosme et al. (2018) showed that the roots of more than 71% of vascular plant species, such as tomato, can get in symbiosis with AMF. Nevertheless, its ultimate effect on plant growth may vary upon fungal species involved in the association (Koomen et al. 1987; Duponnois et al. 2013; Chen et al. 2017).

Regarding the impact of different tested substrates on the mycorrhizal statuts of tomato plants, it revealed that combination of 5% of phospho-compost and 10 g of endomycorrhizal inoculum in substrate had the greatest benefits as evidenced by increased rates of root colonization and mycorrhizal intensity, arbuscular and vesicular contents and densities of spores encountered in rhizospheric soil of tomato plants.

Thereby, our findings indicated that AM fungal spore density, AM root colonization and extraradicular hyphae density were improved by this substrate. These results were consistent with previous studies which suggest that compost addition most often had a positive effect on AM growth, and sporulation (Labidi et al. 2007; Tanwar et al. 2013; Cavagnaro 2015). According to Gryndler et al. (2009), this beneficial effect can be attributed to the richness of compost with humic acid capable to stimulate arbuscular mycorrhizal hyphal growth and sporulation. For Yang et al. (2017), N, P-rich compost can also stimulate them. Indeed, AM fungi will grow more when the soil available phosphorus concentration is sufficient for AM growth (Treseder and Allen 2002). According to Yang et al. (2018), compost provides a sustained release of P and thus maintained a moderate level of soil available phosphorus. Valarini et al. (2009) have reported significant increases in root colonization of wheat and bean as the dose of compost added to culture substrate increases. However, Copetta et al. (2011) observed that AM root colonization in *S. lycopersicum* decreased along with increasing compost addition gradient. In view of these inconsistent results, AM fungi responses to compost may be influenced by compost type (Copetta et al. 2011; Cavagnaro, 2014), plant species (Copetta et al. 2011; Cavagnaro 2014), and dosage of compost (Copetta et al. 2011).

In the same manner, the spore density of AMF was differently affected by studied substrates where the most efficient containing 5% of phospho-compost amendment and 10g of endomycorrhizal inoculum which hosted 14 spores/100 g of soil followed by that incorporating 10 g of endomycorrhizal inoculum singly hosting 10 spores/100 g of soil. Variables densities were reported in sludge soil of different sites (El Gabardi et al. 2019d), and in rhizospheric soil of bean as a function of different compost doses addition (El Gabardi et al. 2019) or of three crops bean, wheat, and grass land receiving compost amendment (Valerini et al. 2009).

Morphological identification of AMF spores collected from different growing substrates showed the presence of 12 species, and the predominance of the genus *Glomus* which was also encountered in the rhizospheric zone of Citrus (Artib et al. 2016), Carob tree (Talbi et al. 2015), oleaster (Sghir et al. 2013), date palm tree (Sghir et al.

2014), beans (El Gabardi et al. 2019e), phosphate laundered sludge (El Gabardi et al. 2019b), and from soil sites adjacent to Khouribga phosphate mine (El Gabardi et al. 2019a).

Conclusion

The combination of phospho-compost produced from phosphate-laundered sludge and endomycorrhizal inoculum in culture substrate has significantly contributed to plant growth improvement. This association seems to confer a synergetic effect increasing both plant growth and root colonization compared to the single application of each amendment. The concomitant presence of these biofertilizers has probably facilitated more exchanges between the plants and the growing area and will have to offer potential protection of the roots against soil borne pathogens.

Acknowledgements

The Authors would like to acknowledge the support through the R & D Initiative – Appel à projets autour des phosphates APPHOS – sponsored by OCP (OCP Foundation, R&D OCP, Mohammed VI PolytechnicUniversity, National Center of Scientific and technicalResearch CNRST, Ministry of Higher Education, Scientific Research and Professional Training of Morocco MESRSFC) under the project entitled 'Procédés biotechnologiques pour la valorisation des boues et des déchets miniers de phosphate : Formulation d'un Phosphocompostbiofertilisant pour application directeen agriculture productive et respectueuse de l'environnement » (Réf. BIO-MOD-01/2017).

References

Akhter A, Hage-Ahmed K, Soja G, Steinkellner S (2015) Compost and biochar alter mycorrhization, tomato root exudation, and development of *Fusarium oxysporum* f. sp. *lycopersici*. Front Plant Sci 6:529.

Alarcón C, Cuenca G (2005) Arbuscular mycorrhizas in coastal sand dunes of the Paraguanä Peninsula, Venezuela. Mycorrhiza 16(1):1-9.

Amir H, Renard A (2003) Etude microbiologique générale de quelques sols de forêts sclérophylles de Nouvelle-Calédonies: Statuts des mycorhizes à arbuscules. PCF-SUNC N° 54/2003/CP.22.

Artib M, Chliyeh M, Touati J, Talbi Z, Selmaoui K, Ouazzani Touhami A, Benkirane R, Douira A (2016) Study of arbuscular mycorrhizal fungi diversity in the rhizosphere of citrus grown in Morocco. IJAPBS 5(3):2277-4688.

Cavagnaro TR (2014) Impacts of compost application on the formation and functioning of arbuscular mycorrhizas. Soil Biol Biochem 78:38-44.

Cavagnaro TR (2015) Biologically regulated nutrient supply systems: compost and arbuscular mycorrhizas-a review. Adv Agron 129:293-321.

Celik I, Ortas I, Kilic S (2004) Effects of compost, mycorrhiza, manure and fertilizer on some physical properties of a Chromoxerert soil. Soil Tillage Res l78:59-67.

Charland M, Cantin S, St Pierre MA, Côté L (2001) Recherche sur les avantages à utiliser le compost. Dossier CRIQ 640- PE27158 (R1), Rapport final. Recyc-Quebec p. 35.

Chen S, Zhao H, Zou C, Li Y, Chen Y, Wang Z, Jiang Y, Liu P, Wang M, Ahammed GJ (2017) Combined inoculation with multiple arbuscular mycorrhizal fungi improves growth, nutrient uptake and photosynthesis in cucumber seedlings. Front Microbiol 8:2516.

Cosme M, Fernández I, Van der Heijden MG, Pieterse CM (2018) Non-mycorrhizal plants: the exceptions that prove the rule. Trends Plant Sci 23:577-587.

Copetta A, Bardi L, Bertolone E, Berta G (2011) Fruit production and quality of tomato plants (*Solanum lycopersicum* L.) are affected by green compost and arbuscular mycorrhizal fungi. Plant Biosyst 145:106-115.

Dalpé R, Debresson C, Xiaoping H (1992) The public sector as first user of innovations. Res Policy 21(3):251-263.

De Bertoldi M, Vallini G, Pera (1983) The biology of composting: A review. Waste Manag Res 1(2):157-176.

Diongzon MLD, Gapasin RM (2000) Animal manure and mycorriza applied singly and in combination for the control of the rice root-knot nematode (*Meloidogyne graminicola* Golden and Birchfield) in green onion (*Allium fistulosum* L.). Philipp J Crop Sci 25:26-30.

Donn S, Wheatley REBM, Loades KW, Hallett PD (2014) Improved soil fertility from compost amendment increases root growth and reinforcement of surface soil on slopes. Ecol Eng 1:458-465.

Duong TTT, Penfold C, Marschner P (2012) Differential effects of composts on properties of soils with different textures. Biol Fertil Soils 48:699-707.

Duponnois R, Hafidi M, Ndoye I, Ramanankierana H, Bà AM (2013) Des Champignons Symbiotiques Contre La Désertification : Écosystèmes Méditerranéens, Tropicaux Et Insulaires. Third edition. Marseille, pp. 511.

El Amerany F, Rhazi M, Wahbi S, Taourirte M, Meddich A (2019) The effect of chitosan, arbuscular mycorrhizal fungi, and compost applied individually or in combination on growth, nutrient uptake, and stem anatomy of tomato. Sci Hortic 261:1-12.

El Gabardi S, Chliyeh M, Selmaoui K, Ouazzani Touhami A, El Modafar C, Filali Maltouf A, Elabed S, Ibnsouda

Koraichi S, Amir S, Moukhli A, Benkirane R, Douira A (2019a) Diversity of endomycorrhizal fungi isolated from soil sites adjacent to Khouribga phosphate mines (Morocco). Interciencia J 44(4):60-83.

El Gabardi S, Chliyeh M, Ouazzani Touhami A, El Modafar C, Filali Maltouf A, Elabed S, Ibnsouda Koraichi S, Amir S, Moukhli A, Benkirane R, Douira A (2019b) Diversity of mycorrhizal fungi arbuscular at phosphates sludge, Khouribga region (Morocco). Plant Arch 19(2):2233-2241.

El Gabardi S, Chliyeh M, Mouden N, Ouazzani Touhami A, El Modafar C, Filali Maltouf A, Elabed S, Ibnsouda Koraichi S, Amir S, Moukhli A, Benkirane R, Douira A (2019c) Determination of the endomycorrhizogenic potential of phosphate laundered sludge by using the mycorrhizal infectious method (PIM). Plant Cell Biotechnol Mol Biol 20(11&12):501-510.

El Gabardi S, Chliyeh M, Selmaoui K, Ouazzani Touhami A, El Modafar C, Filali Maltouf A, Elabed S, Ibnsouda Koraichi S, Amir S, Moukhli A, Benkirane R, Douira A (2019d) Study of the endomycorrhizogenic potential of phosphate laundered sludge. Wulfenia 26(5):1-20.

El Gabardi S, Chliyeh M, Mouden N, Selmaoui K, Ouazzani Touhami A, El Modafar C, Filali Maltouf A, Elabed S, Ibnsouda Koraichi S, Amir S, Moukhli A, Benkirane R, Douira A (2019e) Study of the effect of different phosphocompost doses on the growth and development of bean plants. Plant Cell Biotechnol Mol Biol 20(15&16):710-725.

El Kadiri Boutchich G, Tahiri S, Mahi M, Sisouane M, Kabil EM, El Krati M (2016) Effets de différents composts matures à base de boues d'épuration et des substrats organiques sur les propriétés morphologiques et physiologiques de deux variétés de blé. J Mater Environ Sci 7(12):5810-5827.

El Kinany S, Achbani E, Faggroud M, Ouahmane L, El Hilali R, Haggoud A, Bouamri R (2019) Effect of organic fertilizer and commercial arbuscular mycorrhizal fungi on the growth of micropropagated date palm cv. Feggouss. J Saudi Soc Agric Sci 18(4):411-417.

Ferrer R L, Herrera R A (1981) El género Gigaspora Gerdemann et Trappe (Endogonaceae) en Cuba. Rev Jardín Bot Nacional Habana 1:43-66.

Gapasin RM, Ronayre DK (2003) Effect of VAM [Vesicular arbuscular mycorrhizae] applied singly or in combination with selected organic materials on the rice root-knot nematode *Meloidogyne*. J Trop Plant Pathol 122:81-82.

Gerdemann JW, Nicolson TH (1963) Spores of mycorrhizal endogone species extracted from soil by wet sieving and decanting. Trans Br Mycol 46(2):235-244.

Germani G, Christian Plenchette Ch (2005) Potential of Crotalaria species as green manure crops for the management of pathogenic nematodes and beneficial mycorrhizal fungi. Plant Soil 266:333-342.

Govindarajulu M, Pfeffer PE, Jin HR, Abubaker J, Douds DD, Allen JW (2005) Nitrogen transfer in the arbuscular mycorrhizal symbiosis. Nature 435:819-823.

Gryndler M, Hrselova H, Cajthaml T, Havrankova M, Rezacova V, Gryndlerova H (2009) Influence of soil organic matter decomposition on arbuscular mycorrhizal fungi in terms of asymbiotic hyphal growth and root colonization. Mycorrhiza 19(4):255-266.

Hakkou R, Benzaazoua M, Bussière B (2009) Laboratory evaluation of the use of alkaline phosphate wastes for the control of acidic mine drainage. Mine Water Environ 28(3):206-218.

Hall I R (1984) Taxonomy of VA mycorrhizal fungi. In Powell CL and Bagyraj DJ, Eds, VA Mycorrhiza. CRC Press, Boca Raton, Florida, USA. 57-94.

Hijri M (2016) Analysis of a large dataset of mycorrhiza inoculation field trials on potato shows highly significant increases in yield. Mycorrhiza 26(3):209-214.

Hodge A, Campbell CD, Fitter AH (2001) An arbuscular mycorrhizal fungus accelerates decomposition and acquires nitrogen directly from organic material. Nature 413:297-299.

Jochems-Tanguay L (2014) Les inoculants mycorhiziens pour une agriculture Québécoise plus productive et moins dépendante aux engrais phosphatés. Université de Sherbrooke, PhD Thesis. pp. 1-87.

Jin H, Pfeffer PE, Douds DD, Piotrowski E, Lammers PJ, Shachar-Hill Y (2005) The uptake, metabolism, transport and transfer of nitrogen in an arbuscular mycorrhizal symbiosis. New Phytol 168:687-696.

Keoomen I, Grace C, Hayman DS (1987) Effectiveness of single and multiple mycorrhizal inocula on growth of clover and strawberry plants at two soil pHs. Soil Biol Biochem 19(5):539-544.

Kitabala MA, Tshala UJ, Kalenda MA, Tshijika IM, Mufind KM (2016) Effets de différentes doses de compost sur la production et la rentabilité de la tomate (*Lycopersicon esculentum* Mill) dans la ville de Kolwezi, Province du Lualaba, Congo. J Appl Biosci 102:9669-9679.

Labidi S, Nasr H, Zouaghi M, Wallander H (2007) Effects of compost addition on extra-radical growth of arbuscular mycorrhizal fungi in *Acacia tortilis* sp. raddiana savanna in a pre-Saharan area. Appl Soil Ecol 35:184-192.

Lawson IYD, Muramatsu K, Nioh I (1995) Effects of organic matter on the growth, nodulation and nitrogen fixation of soyabean grown under acid and saline conditions. Soil science and plant nutrition 41(4):721-728.

Lee JJ, Park RD, Kim YW, Shim JH, Chae DH, Rim YS (2004) Effect of food waste compost on microbial population, soil enzyme activity and lettuce growth. Bioresour Technol 93:21-28.

Mouria B, Ouazzani Touhami A, Douira A (2010) Valorisation agronomique du compost et de ses extraits sur la culture de la tomate. Rev Ivoir Sci Technol 16:165-190.

Morton J B, and Benny J (1990) Revised classification of arbuscular mycorrhizal fungi (Zygomycetes): a new order, Glomales, two new suborders, Glominae and Gigasporinae, and two new families, Acaulosporaceae and Gigasporaceae, with an amendation of Glomaceae. Mycotaxon 37:471-491.

Ouakibi O, Loqman S, Hakkou R, Benzaazoua M (2013) The potential use of phosphatic limestone wastes in the passive treatment of AMD: A laboratory study. Mine Water Environ 32(4):266-277.

Pane C, Piccolo A, Spaccini R, Celano G, Villecco D, Zaccardelli M (2013) Agricultural waste-based composts exhibiting suppressivity to diseases caused by the phytopathogenic soil-borne fungi *Rhizoctonia solani* and *Sclerotinia minor*. Appl Soil Ecol 65:43-51.

Pérez-Piqueres A, Edel-Hermann W, Alabouvette C, Steinberg C (2006) Response of soil microbial communities to compost amendments. *Soil Biol Biochem* 38:460-470.

Phillips JM, Hayman DS (1970) Improved procedures for clearing root and staining parasitic and vesicular-arbuscular mycorrhizal fungi for rapid assessment of infection. Trans. Br Mycol Soc 55:158-161.

Pommel B, Lasserre M (1982) Aptitude de plusieurs déchets urbains à fournir du phosphore aux cultures. Agronomie 2(9):851-857.

Pradhan N, Sukla LB (2006) Solubilization of inorganic phosphate by fungi isolated from agriculture soil. Afr J Biotechnol 5:850-854.

Salvioli A, Novero M, Lacourt Bonfante P (2008) The impact of mycorrhizal symbiosis on tomato fruit quality. 16th IFOAM Organic World Congress, Modena, Italy, June 16-20.

Santos JA, Nunes LAPL, Melo WJ, Araujo ASF (2011) Tannery sludge compost amendment rates on soil microbial biomass of two different soils. Eur J Soil Biol 47:146-151.

Sghir F, Chliyeh M, Kachkouch W, Khouader M, Ouazzani Touhami A, Benkirane R, Douira A (2013) Mycorrhizal status of *Olea europaea* spp. oleaster in Morocco. J Appl Biosci 61:4478-4489.

Sghir F, Touati J, Chliyeh M, Ouazzani Touhami A, Filali-Maltouf A, El Modafar C, Moukhli A, Oukabli A, Benkirane R, Douira A (2014) Diversity of arbuscular mycorrhizal fungi in the rhizosphere of date palm tree (*Phoenix dactylifera*) in Tafilalt and Zagora regions (Morocco). Int J Pure Appl Biosci 2(6):1-11.

Scotti R, Pane C, Spaccini R, Palese AM, Piccolo A, Celano G (2016) On-farm compost: a useful tool to improve soil quality under intensive farming systems. Appl Soil Ecol 107:13-23.

Serfoji P, Rajeshkumar S, Selvaraj T (2010) Management of root-knot nematode *Meloidogyne incognita* on tomato cv Pusa Ruby. by using vermicompost, AM fungus, *Glomus aggregatum* and mycorrhiza helper bacterium, *Bacillus coagulans*. J Agric Technol 6:37-45.

Schenck N C, Smith G S (1981) Additional new and unreported species of mycorrhizal fungi (Endogonaceae) from Florida. Mycologia 74(1):77-92.

Schenck NC, Perez Y (1987) Manual for the Identification of VA Mycorrhizal Fungi. First Edition, Synergistic Pub, Gainesville. 286 p.

Smith SE, Read DJ (2008) Mycorrhizal Symbiosis. Academic Press, London.

Talbi Z, El Asri A, Touati J, Chliyeh M, Ait aguil F, Selmaoui K, Sghir F, Ouazzani Touhami A, Benkirane R, Douira A (2015) Morphological characterization and diversity of endomycorrhizae in the rhizosphere of Carob tree (*Ceratonia siliqua*) in Morocco. Biolife 3(1):196-211.

Tanwar A, Aggarwal A, Yadav A, Parkash V (2013) Screening and selection of efficient host and sugarcane bagasse as substrate for mass multiplication of *Funneliformis mosseae*. Biol Agric Hortic 29:107-117.

Treseder K, Allen F (2002) Direct nitrogen and phosphorus limitation of arbuscular mycorrhizal fungi: a model and field test. New Phytol 155:507-515.

Trouvelot A, Kough JL (1986) Mesure du taux de mycorhization VA d'un système radiculaire. Recherche de méthodes d'estimation ayant une signification fonctionnelle. In Physiological and genetical aspects of mycorrhizae. In Gianinazzi-Pearson V. and Gianinazzi S, Eds, INRA Ed. Paris. pp. 217-221.

Valarini PJ, Curaqueo G, Seguel A, Manzano K, Rubio R, Cornejo P (2009) Effect of compost application on some properties of a volcanic soil from central South Chile. Chil J Agr Res 69:416-425.

Vanai P (1995) Valorisation agronomique d'un compost urbain produit par méthanisation : Étude en milieu tropical, Thèse présentée pour l'obtention du titre de Docteur en Sciences de l'Université Française du Pacifique (UFP), Spécialité Chimie, pp. 172.

Woo SL, Zoina A, Del Sorbo G, Lorito M, Nanni B, Scala F, Noveiello C (1996) Characterization of *Fusarium oxysporum* f. sp. *phaseoli* by pathogenic races, VCGs, RFLPs, and RAPD. Phytopathology 86:966-972.

Walker C, Mize C (1982) Population of endogonaceous fungi at two locations in central Iowa. Can J Bot 60:2518-2529.

Yang W, Guo Y, Wang X, Chen C, Hu Y, Cheng L (2017) Temporal variations of soil microbial community under compost addition in black soil of Northeast China. Appl. Soil Ecol 121:214-222.

Yang W, Gu S, Xin Y, Bello A, Sun W, Xu X (2018) Compost addition enhanced hyphal growth and sporulation of arbuscular mycorrhizal fungi without affecting their community composition in the soil. Front Microbiol 9:169.

Acta Biologica Szegediensis

Volume 64(2):233-237, 2020
Acta Biologica Szegediensis
http://abs.bibl.u-szeged.hu/index.php/abs

DOI:10.14232/abs.2020.2.233-237

ARTICLE

Wastes after distillation of *Helichrysum italicum* – biological active compounds and free radical scavenging activity

Milena Nikolova[1]* Ana Dobreva[2] Strahil Berkov[1]

[1]Institute of Biodiversity and Ecosystem Research, Bulgarian Academy of Sciences, Sofia, Bulgaria
[2]Institute of Roses, Essential and Medicinal Cultures, Kazanluk, Bulgaria

ABSTRACT Distillation wastewater, by-products from steam and water distillation as well as raw material used as control of flower heads of *Helichrysum italicum* were comparative analyzed for content of the biologically active compounds by GC/MS. Acetone exudates, methanol extracts and ethyl acetate fractions obtained after alkaline hydrolyze of the studied materials were received. The three types of extraction products as well as the distillation wastewater were examined for free radical scavenging activity by DPPH assay. Phenol, fatty- and organic acids, sterols, triterpenes, sugars and sugar alcohols were identified. Succinic acid and myo-inositol were identified as main components of distillation wastewater. Hydroxycinnamic acid, caffeic acid and 4(p)-hydroxybenzoic acid were dominant compounds of the ethyl acetate fractions. Triterpenes and fatty acids, sterols and flavonoids are among the main biologically active substances in the methanolic extracts and acetone exudates. The ethyl acetate fractions were found to possess the highest free radical scavenging activity (IC_{50} < 50 μg/mL). Significant differences in the activity between wastes and raw materials were not found. The results showed that the waste products after distillation of *H. italicum* contain important biologically active substances and the extracts with high antioxidant activity can be obtained from them.
Acta Biol Szeged 64(2):233-237 (2020)

KEY WORDS
GC/MS
flavonoids
phenolic acids
triterpenes
sterols

ARTICLE INFORMATION
Submitted
03 June 2020.
Accepted
19 August 2020.
***Corresponding author**
E-mail: mtihomirova@gmil.com

Introduction

Helichrysum italicum (Roth) G. Don. is an endemic Mediterranean plant, widely used in medicine and perfumery because of anti-inflammatory, analgesic, antibacterial, antistress, anti-depressant sedative properties of its essential oil (Saint-Lary et al. 2018; Staver et al. 2018; Ninčević et al. 2019). An inescapable pressure on this wild resource in the last decade resulted in a shift from wild harvest to cultivation. Its plantation farming experienced a huge expansion in Eastern European Mediterranean countries. In Bulgaria the cultivation and processing of *Helichrysum* has been done for several years. As a result of the intensive use of the species for extraction of essential oil a large amount of agro-industrial residues and by-products remain. The content of bioactive compounds in these wastes and their potential for application has not been investigated so far. Utilization of these wastes would be important for the conservation of natural resources and also from the point of view for the global concept of agro-waste usage (Otles et al. 2015; Saha et al. 2019). Two major types of waste are generated: wastewater and solid waste biomass. The main approaches to biomass conversion are combustion, composting, conventional and advanced extraction process, chemical and/or enzymatic reactions and development of bioprocess (Kalra et al. 2002; Santana-Méridas et al. 2012; Slavov et al. 2017). Two common types of substances are mostly recovered as by-products (besides the aroma compounds): polyphenols and polysaccharides. Most of the applications of these chemical-based products have been addressed to exploit their antioxidant, cosmeceutical and/or pharmacological properties (Fierascu et al. 2019; Makris et al. 2019; Matos et al. 2019; Pandey et al. 2010; Slavov et al. 2019). The residual distillation water of some aromatic plant may influence monoterpene synthesis and accumulation in plants and hence may be used for targeted modification of its essential oil composition (Zheljazkov and Astatkie 2012; Zheljazkov et al. 2010). Another investigation reveals potential to recovery of polyphenols (Rusanov et al. 2014).

The purpose of the present study was to determine the bioactive compounds composition and the free radical scavenging activity of various waste products from the distillation of *H. italicum*, with a view to guidelines for their valorization and application.

Materials and Methods

Plant material

Helichrysum italicum was from the plantation in Institute for Roses and Essential and Medicinal Cultures, Kazanlak, Bulgaria. The plants originated from Bosnia. They were two years old at the time of the investigation. The biomass was obtained after vapor and water distillation in the semi-industrial installation with 100 dm^3 vessel. The wastewater was collected after water distillation.

Extractions of plant materials

Acetone exudates were prepared from air-dried, not grounded aerial parts of the samples (raw material and waste from distillation) by rinsed with acetone for 5 min to dissolve the material accumulated on the surfaces. Methanolic extracts were prepared from air-dried, ground plant parts of studied samples by classical maceration with methanol for 24 h. Ethyl acetate fractions were obtained by alkaline hydrolyze of the plant material of the studied samples by 2 M NaOH, for 4 h at room temperature. After acidification to pH 1-2 with cc. HCl, the phenolic compounds were extracted with EtOAc two times and after that evaporated to obtain fraction rich on alkaline hydrolysable phenolic acids. Distillation wastewater was evaporated to dryness. The obtained extractions, fractions and dry residue from the distillation water were silylated with 50 μL of N,O-bis-(trimethylsilyl)trifluoro-acetamide (BSTFA) in 50 μL of pyridine for 2 h at 50 °C.

Gas chromatography mass spectrometry (GC–MS) analysis.

The GC-MS spectra were recorded on a Thermo Scientific Focus gas chromatograph coupled with Thermo Scientific dual stage quadrupole (DSQ) mass detector operating in electron ionization (EI) mode at 70 eV. A DB-5MS column (30 m x 0.25 mm x 0.25 μm) was used. Chromatographic conditions were described by Nikolova et al. (2016). The metabolites were identified as TMSi derivatives comparing their mass spectra and Kovats Indexes (RI) with those of an on-line available plant specific database (Golm Metabolome Database). The amounts of the metabolites (μg/mL) are expressed relative to the internal standard (3,4 dichloro-4-hidroxybenzoic acid) using the calculated areas for both components.

Free radical scavenging activity

The effect of methanolic extracts, acetone exudates and ethyl acetate fractions as well as distillation wastewater on DPPH radicals was estimated according to Stanojević et al. (2009). The results were calculated by GraphPad Prism ver. 3.00. All experiments were carried out in triplicate.

Results

Methanolic extracts, acetone exudates and ethyl acetate fractions were obtained in search for biologically active substances in the waste products from the distillation of the flower heads of *H. italicum*. Thirty-two compounds were identified. Acetone exudates contain lipophilic compounds accumulated on the surface areas of the plant material whereas methanolic extracts contain polar and lipophilic compounds. The identified compounds are presented at Table 1. In the acetone exudates the main components were identified as triterpene acids (11,12). Stigmasterol (8), β-sitosterol (9) and β-amyrin (10) were established also. Flavonoid aglycones - quercetin (24) and methyl derivatives of apigenin (22,23) and luteolin (25) were detected. A variety of phenolic acids – caffeic (32), 4(p)-hydroxybenzoic (26), vanillic, (27) protocatechuic (28), hydroxycinnamic (30) were found. Fatty acids and alcohols were also determined. Chlorogenic (33) and quinic (29) acids, kaempferol 4-methyl ether (21) and tocopherol (6) were found only in the acetone exudate of raw material.

In the methanolic extracts monosaccharides – fructose (18), glycose (19) and sugar derivatives - myo-inositol (20) as well as triterpene acids were found in the significant amounts. Free phenolic acids, fatty- and organic acids as well as flavonoids were also found.

Ethyl acetate fractions comprise mainly alkaline hydrolysable phenolic acids. Caffeic (32) and hydroxycinnamic (30) acids were determined as main phenolic acids. Protocatechuic acid (28) was also abundant in the fraction of untreated flower heads moreover, gallic acid (31) was found only in this sample. The detailed information is presented at Table 2.

In the distillation wastewater the main component was identified as myo-inositol (sugar alcohol) (20) around

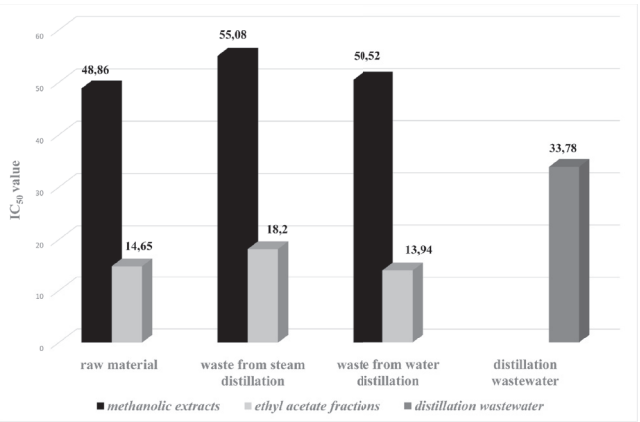

Figure 1. Free radical scavenging activity of the wastes after distillation and raw material of *H. italicum*.

Table 1. Compounds identified of acetone exudates and methanolic extracts of the wastes after distillation and raw material of *H. italicum.*

Compounds	RI	Acetone exudates*			Methanolic extracts*			DWW
		RM	SD	WD	RM	SD	WD	
Fatty alcohols and acids								
Tetradecanol (1)	1757	36.4	8.1	0.4	0.1		2.8	
Hexadecanol (2)	1955	8.2	7.4	5.95	14.5	5.5	13.4	
Hexadecanoic acid (3)	2041	292.7	28.5	28.5	519.3	686.2	741.8	
Octadecanoic acid (4)	2124	222	10.4	62	56.8	3.6	4.3	
Hexacosanol (5)	2938	99.3	0.1	0.8	176.2	0.1	73.4	
Sterols and triterpenes								
Tocopherol (6)	3122	6.9			12.2			
Campesterol (7)	3265		16.4	9	0.1		1.5	
Stigmasterol (8)	3319	33.25	61.05	47.6	37.8	2.4	12.7	
β-Sitosterol (9)	3335	16	138.4	27.1	33	8.2	13.7	
β-Amyrin (10)	3415	9.13	8.1	9.1	0.2	0.2		
Triterpene acid 1 (11)	3733	46.45	122	55.95	153.7	77.2	580	
Triterpene acid 2 (12)	3778	156.2	386	122.7	463.4	1268.5	5117.9	
Organic acids, sugars and sugar derivatives								
Phosphoric acid (13)	1120	14.9	0.2	2.2	33	5.4	11.4	0.2
Succinic acid (14)	1310	14.9	0.9	6.25	26.5	23.6	67.3	26.9
Malic acid (15)	1488	16.1	1.7	2.2	28.5	43.9	184.1	
Meso-erythritol (16)	1493				31.3	5.3	4.2	0.5
Pyroglutamic acid (17)	1512			9.75	10.1		31.8	1
Fructose (18)	1805	88.1	8.65	8.7	410.3	326.2	230.7	
Glucose (19)	1882	176.4	3.85	3.8	157.2	227.4	195.6	
Myo-Inositol (20)	2093	6.6	10.6	1.4	42.4	497.4	749.6	66.5
Flavonoid aglycones								
Kaempferol 4-Me (21)	3001	0.45			0.08			
Apigenin 4□-Me (22)	3040	5.2	2.8	2.05		0.4	1.5	
Scutellarein 6,4□-Me (23)	3108	6.9	7.8	3.7		0.9		
Quercetin (24)	3192	0.2		0.5	0.6			
Luteolin 7,4□-Me (25)	3240	1	0.5	1.4	0.05	0.6	2.2	
Free phenolic acids								
4(p)-hydroxybenzoic acid (26)	1635	2.75	4.3	3.4	15	6.4	2.2	
Vanillic acid (27)	1776	0.5	1.55	4.55	1.4	10.9	11.10	0.3
Protocatechuic acid (28)	1813	0.1	3.95	4.3	34.3	2.5	27.2	
Quinic acid (29)	1863	38	0.6		98.1	170.2	30.4	
Hydroxycinnamic acid (30)	1932		2.6	1.5	5.8	0.9	4	
Gallic acid (31)	1960				1.6	2.7		
Caffeic acid (32)	2131	13.65	1.4	0.5	9.1	5.6	19.6	
Chlorogenic acid (33)	3110	3.8			16.2	1.4	28.2	

RM – raw material; SD - waste after steam distillation; WD - waste after water distillation; DWW- distillation waste water; Me - methyl ether *data were expressed for each analyte relative to the internal standard (3,4 dichloro-4-hidroxybenzoic acid) using the calculated areas for both components

66% of all identified compounds. Succinic acid (14) was the second component presented also in large amount. The results are presented at Table 1.

Methanolic extracts, acetone exudates and ethyl acetate fractions as well as distillation wastewater were evaluated for free radical scavenging activity against DPPH radicals. The results are presented as IC_{50} values - extract concentration providing 50% inhibition of the DPPH solution (Fig.1). With exception of acetone exudates, the methanolic extracts, ethyl acetate fractions and distillation wastewater showed significant activity with IC_{50} values less than 50 $\mu g\,mL^{-1}$. The ethyl acetate fractions displayed

Table 2. Phenolic acids identified of ethyl acetate fractions of the wastes after distillation and raw of *H. italicum*.

Phenolic acids	RI	RM	SD	WD
Salicylic acid (34)	1210	1.9	0.7	
Cinnamic acid trans (35)	1376	2.6		
4(p)-hydroxybenzoic acid (26)	1635	39.2	22.1	4.2
Vanillic acid (27)	1776	20.4	7.4	2.2
Hydroxycinnamic acid cis (36)	1789	43.7	5.7	2
Protocatechuic acid (28)	1813	173.9	38.4	6.6
Syringic acid (36)	1884	10.8	0.9	
Hydroxycinnamic acid trans (30)	1948	168.5	110.3	85
Gallic acid (31)	1960	5.7		
Ferulic acid trans (37)	2103	7.4	7.7	1
Caffeic acid trans (32)	2142	260.8	881.5	159.5

RM: raw material; SD: waste after steam distillation; WD: waste after water distillation.
*Data were expressed for each analyte relative to the internal standard (3,4 dichloro-4-hidroxybenzoic acid) using the calculated areas for both components

the most significant activity whereas the acetone exudates the lowest upper 200 μg mL^{-1}. Significant difference in the antiradical properties between extracts and fractions of different waste products was not found.

Discussion

The results presented show that the waste products from the distillation of essential oil of *H. italicum* contain important bioactive compounds. Triterpenes and sterols are bioactive substances that have been shown to possess anti-inflammatory, antimicrobial, antiallergic, antiviral, hepatoprotective, cytotoxic and other important biological activities (Holanda et al. 2008; Sultana and Ata 2008; Vázquez et al. 2012). The presence of triterpenes in *H. italicum* has already been reported in the literature (Mezzetti et al. 1970; Nostro et al. 2000; Guinoiseau et al. 2013). The occurrence of triterpene acids in significant amounts in the extracts from by-products after steam and water distillation was found in the present study. Significant free radical scavenging activity has been reported for *H. italicum* (Molnar et al. 2017) that is consistent with received data of DPPH assay in the present work. Phenolic acids have been determined as main contributors of antioxidant properties (Sato et al. 2011). A variety of this class compounds were established in the methanolic extracts and ethyl acetate fractions of the waste products and raw materials. The high antiradical activity of the extracts and fractions is suggested to be due precisely to the high content of phenolic acids in them. Myo-inositol and succinic acid were established as dominant components in the distillation wastewater. Antitumor properties, beneficial effect on diseases such as diabetes, obesity and neurodegenerative disorders have been reported for myo-inositol and its derivatives (Bizzarri et al. 2016; Chhetri, 2019). Antibacterial action and use in the treatment of acne has been reported for succinic acid (Wang et al. 2014). Later research outlined succinic acid as a promising compound for use in cosmetics (Theunissen and Courbes 2018). These data indicate that distillation wastewater could find application in cosmetic products.

Conclusion

The results presented here indicate that the waste products from the distillation of *H. italicum* contain important bioactive compounds - triterpene acids, sterols, phenolic acids, sugar alcohols - substances with important biological activities. These data outline the possibility from the waste materials of *H. italicum* to be recovered fractions or pure compounds with valuable properties. Finding application of these waste products will allow a fuller use of the plant material of the species.

References

Akaberi M, Sahebkar A, Azizi N, Emami SA (2019) Everlasting flowers: phytochemistry and pharmacology of the genus *Helichrysum*. Ind Crops Prod 138:111471.

Bizzarri M, Dinicola S, Bevilacqua A, Cucina A (2016) Broad spectrum anticancer activity of myo-inositol and inositol hexakisphosphate. Int J Endocrinol 2016:5616807.

Chhetri DR (2019) Myo-inositol and its derivatives: Their emerging role in the treatment of human diseases. Front Pharmacol 10:11-72.

Facino M, Carini M, Franzoi L, Pirola O, Bosisio E (1990) Phytochemical characterization and radical scavenger activity of flavonoids from *Helichrysum italicum* G. Don (Compositae). Pharmacol Res 22:709-720.

Fierascu R, Fierascu I, Avramescu S, Sieniawska E (2019) Recovery of natural antioxidants from agro-industrial side streams through advanced extraction techniques. Molecules 24(23):4212.

Guinoiseau E, Lorenzi V, Luciani A, Muselli A, Costa JP, Casanova JG, Berti L (2013) Biological properties and resistance reversal effect of *Helichrysum italicum* (Roth) G. Don. In Méndez-Vilas A, Ed., Formatex Research Center, Spain, 1073-1080.

Holanda Pinto SA, Pinto LM, Cunha GM, Chaves MH, Santos FA, Rao VS (2008) Anti-inflammatory effect of alpha, beta-amyrin, a pentacyclic triterpene from

Protium heptaphyllum in rat model of acute periodontitis. Inflammopharmacology 16(1):48-52.

Kalra A, Kumar S, Katiyar N, Bahl JR, Bansal RP, Chauhan HS, Prasad A, Pandey R, Dhawan OP, Krishna A, Srivastava R (2002) Method for the faster multiplication of earthworms, and production of vermicompost from the distillation waste of industrial aromatic crops. Patent No: US 6,488,733 B2.

Makris D, Sahin S (2019) Polyphenolic antioxidants from agri-food waste biomass. Antioxidants 8(12):624.

Matos MS, Romero-Díez R, Álvarez A, Bronze MR, Rodríguez-Rojo S, Mato RB, Cocero MJ, Matias AA (2019) Polyphenol-rich extracts obtained from winemaking waste streams as natural ingredients with cosmeceutical potential. Antioxidants 8(9):355.

Mezzetti T, Orzalesi G, Rossi C, Bellavita V (1970) A new triterpenoid lactone, alpha-amyrin and uvaol from *Helichrysum italicum*. Planta Med 18(4):326-331.

Molnar M, Jerković I, Suknović D, Bilić Rajs B, Aladić K, Šubarić D, Jokić S (2017) Screening of six medicinal plant extracts obtained by two conventional methods and supercritical CO_2 extraction targeted on coumarin content, 2,2-diphenyl-1-picrylhydrazyl radical scavenging capacity and total phenols content. Molecules *22*:348.

Nikolova M, Aneva I, Berkov S (2016) GC-MS metabolic profiling and free radical scavenging activity of *Micromeria dalmatica*. Biol Nyssana 7(2):159-165.

Ninčević T, Grdiša M, Šatović Z, Jug-Dujaković M (2019) *Helichrysum italicum* (Roth) G. Don: Taxonomy, biological activity, biochemical and genetic diversity. Ind Crops Prod 138:111487.

Nostro A, Germanò MP, D'angelo V, Marino A, Cannatelli MA (2000) Extraction methods and bioautography for evaluation of medicinal plant antimicrobial activity. Lett Appl Microbiol 30(5):379-384.

Otles S, Despoudi S, Bucatariu C, Kartal C (2015) Food waste management, valorization, and sustainability in the food industry. In Galanakis CM, Ed., Academic Press, Cambridge, 3-23.

Pandey R, Kalra A (2010) Inhibitory effects of vermicompost produced from agro-waste of medicinal and aromatic plants on egg hatching in *Meloidogyne incognita* (Kofoid and White) chitwood. Curr Sci 98(6):833-835.

Rusanov K, Garo E, Rusanova M, Fertig O, Hamburger M, Atanassov I, Butterweck V (2014) Recovery of polyphenols from rose oil distillation wastewater using adsorption resins – a pilot study. Planta Med 80:1657-1664.

Theunissen L, Courbes F (2018) Succinic acid: a promising multi-functional ingredient for cosmetic and personal-care applications**.** H&PC Today 13(2):42-44.

Saha A, Basak BB (2020) Scope of value addition and utilization of residual biomass from medicinal and aromatic plants. Ind Crops Prod 145:111979.

Saint-Lary L, Minagloub FH, Escrivac C, Beylsa AS, Badie F (2018) *Helichrysum italicum* D.C. essential oil from Balkans. Perfum Flavor 43:52-66.

Santana-Méridas O, González-Coloma A, Sánchez-Vioque R (2012) Agricultural residues as a source of bioactive natural products. Phytochem Rev 11(4):447-466.

Slavov A, Vasileva I, Stefanov L, Stoyanova A (2017) Valorization of wastes from the rose oil industry. Rev Environ Sci Biotechnol 16**:**309-325.

Slavov A, Yantcheva N, Vasileva I (2019) Chamomile wastes (*Matricaria chamomilla*): New source of polysaccharides. Waste Biomass Valor 10(9):2583-2594.

Staver M, Gobin I, Ratkaj I, Petrovic M, Vulinovic A, Dinarina-Sablic M, Broznic D (2018) In vitro antiproliferative and antimicrobial activity of the essential oil from the flowers and leaves of *Helichrysum italicum* (Roth) G. Don growing in central Dalmatia (Croatia). J Essent Oil-Bear Plants 21(1):77-91.

Stanojević L, Stanković M, Nikolić V, Nikolić L, Ristić D, Canadanovic-Brunet J, Tumbas V (2009) Antioxidant activity and total phenolic and flavonoid contents of *Hieracium pilosella* L. extracts. Sensors 9:5702-5714.

Sultana N, Ata A (2008) Oleanolic acid and related derivatives as medicinally important compounds. J Enzyme Inhib Med Chem 23:739-756.

Zeljković S, Šolić ME, Maksimović M (2015) Volatiles of *Helichrysum italicum* (Roth) G. Don from Croatia. Nat Prod Res 29(19):1874-1877.

Zheljazkov V, Astatkie T (2012) Distillation waste water can modify peppermint (*Mentha* × *piperita* L.) oil composition. Ind Crops Prod 36(1):420-426.

Zheljazkov VD, Astatkie T, Horgan T, Rogers S (2010) Effect of plant hormones and distillation water on mints. HortScience 45(9):1338-1340.

Vázquez LH, Palazon J, Navarro-Ocaña A (2012) The pentacyclic triterpenes α-β-amyrins: a review of sources and biological activities. In Venketeshwer R, Ed., Phytochemicals - A Global Perspective of Their Role in Nutrition and Health. IntechOpen, Rijeka, Croatia.

Wang Y, Kuo S, Shu M, Yu J, Huang S, Dai A, Two A, Gallo RL, Huang CM (2014) *Staphylococcus epidermidis* in the human skin microbiome mediates fermentation to inhibit the growth of *Propionibacterium acnes*: implications of probiotics in acne vulgaris. Appl Microbiol Biotechnol 98(1):411-424.

Acta Biologica Szegediensis

Volume 64(2):239-249, 2020
Acta Biologica Szegediensis
http://abs.bibl.u-szeged.hu/index.php/abs

DOI:10.14232/abs.2020.2.239-249

ARTICLE

Potentials of synthesised *Lessertia montana* zinc oxide nanoparticles on free radicals-mediated oxidative stress and carbohydrate-hydrolysing enzymes

Fatai O. Balogun, Anofi O.T. Ashafa*

Phytomedicine and Phytopharmacology Research Group, Department of Plant Sciences, University of the Free State, Phuthadijthaba 9866, Qwaqwa, Free State, South Africa

ABSTRACT The study evaluated the effects of green absorbed zinc oxide nanostructures on oxidative stress-mediated free radicals and carbohydrate-hydrolysing enzymes. The synthesised *Lessertia montana* zinc oxide nanoparticles were characterised using different spectroscopic, microscopic, and diffraction techniques. The activity of *L. montana* ZnONPs against 1,1-diphenyl-2-picrylhydrazyl (DPPH), 2,2'-azino-bis(3-ethylbenzothiazoline-6-sulfonic acid (ABTS), metal chelating assay, alpha-amylase and alpha-glucosidase were determined using standard methods. *L. montana* ZnONPs were stable nanoparticles (NPs), appeared cubical (predominantly) in shape, and in nanometre range sizes. The synthesised NPs are very active ($p < 0.05$) against DPPH and alpha-glucosidase (0.120 and 0.037 g/L, respectively) when compared with other samples and controls, quercetin (0.349 g/L) and acarbose (0.065 g/L). However, their interaction with quercetin revealed a good ABTS (0.093 g/L) scavenging and an excellent metal chelating (0.027 g/L) effect compared to other samples. The mode of inhibition of alpha-amylase and alpha-glucosidase enzymes by *L. montana* ZnONPs was competitive and non-competitive, respectively. The study outcomes revealed that the synthesised ZnONPs possessed the potential to mitigate oxidative stress and diabetes *in vitro*.

Acta Biol Szeged 64(2):239-249 (2020)

KEY WORDS
antidiabetics
FTIR
green synthesis
Lessertia montana
nanoparticles
zinc oxide

ARTICLE INFORMATION
Submitted
18 October 2020.
Accepted
02 November 2020.
***Corresponding author**
E-mail: ashafaaot@ufs.ac.za

INTRODUCTION

Nanoparticles (NPs) owing to excellent features have continued to find relevance in different scientific domains such as medicine, food, cosmetics, textiles, etc. based on their size, distribution, and morphology (Sorescu et al. 2016). They are very important because of the atom-like characteristics resulting from a large surface area to volume ratio among many others (Nithya and Kalyanasundharam 2019). Nanostructures, (NS) be it metallic (gold, silver, platinum, zinc, etc.) or their corresponding oxides such as zinc oxide are synthesised via physical, chemical, and biological methods. However, due to side effects resulting from chemical synthesis involving the use of dangerous chemicals leading to the release or production of environmentally unfriendly by-products, interest in an eco-friendly method found in biological procedures becomes germane (Ogunyemi et al. 2019).

The use of medicinal plants in the biosynthesis of NPs is a laudable and/ or better alternative aimed or embraced for the production of safe NS devoid of toxic substances. The reason for the medicinal plant usage or exploration has been attributed to the presence of functional groups arising from the inherent phytoconstituents such as phenols, flavonoids, alkaloids, amide, amine, terpenoids, etc. (Rai and Ingle 2012; Ogunyemi et al. 2019)

Zinc oxide, a metallic oxide NP, classed with the likes of Au, C, and graphene is regarded as a superior NS as a result of its wide and numerous applications in electronics, biology, medicine, communication, etc. In fact, immense progress on the use or application of this NP has continued to be felt particularly in the area of gene delivery, biological identification/labelling, drug development/delivery, biological sensor, nanomedicine, optical/ chemical properties and so on. Additionally, the recent trend in the use of natural products in the synthesis of NPs had also been explored with ZnO. It is therefore interesting to note that quite a number of plants including but not limited to *Aloe barbadensis*, *Abutilon indicum*, *Solanum torvum*, *Laurus nobilis*, *Olea europaea*, *Hibiscus subdariffa*, *C. halicabum*, *Costus igneus*, etc. have found their relevance as used in the ZnONPs synthesis (Sangeetha et al. 2011; Bala et al. 2015; Nithya and Kalyanasundharam 2019; Prashanth et al. 2018; Ezealisiji et al. 2019; Fakhari et al. 2019; Ogunyemi et al. 2019; Vinotha et al. 2019) with

established antibacterial, antioxidant and antidiabetic effects. Additionally, in the review compiled by Vishnukumar and others (2018), it was evident that the part of plants mostly studied for ZnONPs applications is their leaves. Notwithstanding the afore-mentioned, very few reports are available in the literature on the antioxidative and antidiabetic effects of plant synthesised ZnONPs (Vishnukumar et al. 2018).

It is interesting to state that quite a number of studies centred on modifying the processes involved in the synthesis of zinc oxide nanoparticles have been reported by various authors as cited in the work of Vishnukumar et al. (2018), these modifications were in an effort to establish methods with better potentials of the NPs. While some reports studied the impact of varying concentrations, different solvents (during synthesis), temperature, etc. on the crystallite size of the synthesised nanoparticles, others investigated the need to maintain the pH using NaOH to enhance the precipitation kinetics. To a very large extent, high concentration and temperature are opined to bring about a reduction in the (crystallite) size of the NPs while a NaOH mediated synthesis presented a larger size NS as witnessed in a study using *Coriandrum sativum* leaf extract.

In terms of application and/ or biomedical advancement of phyto-synthesised ZnONPs, efforts on a number of plants had culminated into huge successes in diseases management (against free radical, cancer, bacterial and fungal infections, etc.), drug development, cosmetics, optical devices, solar cells, etc. (Vishnukumar et al. 2018).

Lessertia montana (previously *Sutherlandia montana*), a member of the Fabaceae family is a South African indigenous plant whose ethnobotanical attributes and indigenous uses were well reported in the work of Ashafa et al. (2019). The pharmacological potentials of the leaf and whole plant as an anticancer, anti-stress, antidepressant, anti-HIV, antioxidant and antidiabetic are adequately submitted in the different reports and/ or reviews (van Wyk and Albrecht 2008; Aboyade et al. 2014). In fact, the phytochemical determination, antioxidative and antidiabetic properties of the seeds, pods and leaf extracts of the plant were evaluated in our laboratory (Alimi and Ashafa, 2018; Ashafa et al. 2019) and these studies revealed the superior pharmacological benefits of the leaves than other parts. Hence, this study was designed to investigate the antioxidant and antidiabetic potentials (*in vitro*) of zinc oxide nanoparticles synthesised from *L. montana*.

MATERIALS AND METHODS

Chemicals

Acarbose, quercetin, p-nitrophenyl-α-D-glucopyranoside (pNPG), porcine pancreatic α-amylase, rat intestinal α-glucosidase, 1, 1-diphenyl-2-picrylhydrazyl (DPPH) and 2, 2′-Azino-bis(3-ethylbenzothiazoline-6-sulfonic acid (ABTS) were purchased from Sigma-Aldrich (South Africa) while zinc oxide was obtained from Merck Chemicals (South Africa). The water used was glass distilled while other chemicals/reagents used were of analytical grade.

Preparation of plant extracts

The whole plant of *Lessertia montana* was collected in Kestell, eastern Free State, South Africa. It was identified and authenticated by Prof Ashafa of the Plant Sciences Department at the University of the Free State and the voucher specimen (Alimed/01/2016/QHb) was deposited in the University herbarium. The IUCN policy statement on research concerning plant species at risk of extinction was adhered to and the plant was confirmed not to be near extinction as it was listed as a plant of the least concern according to the red list of plants by South Africa National Biodiversity Institute (SANBI) (*http://redlist.sanbi.org/genus.php?genus=3050*). The leaves were separated from the whole plant, washed under running water, and air-dried at room temperature until the attainment of uniform weight after 4 days. The dried leaf materials were afterward ground into powder using a laboratory blender (Warring Instrument, USA). The acquisition of the *L. montana* aqueous leaf extract according to Ogunyemi et al. (2019) with slight modification was achieved by weighing 2 g of the samples in a 250 mL conical flask and extracted with 200 mL distilled water. The flask containing the mixture was suspended on a heater with a magnetic stirrer (MSH 10, Labcon Consumables, South Africa) (6 *g*) exposed to heat at 65 °C for 4 hours. The cooled mixture was filtered using adsorbent cotton wool followed by Whatman filter paper No 1 and thereafter centrifuged (BHG Roto Uni II, Germany) (650 *g*) for 5 min to collect the supernatant used for the synthesis of ZnONPs.

Synthesis of ZnONPs

One hundred millilitres (100 mL) of zinc oxide (1 M) and freshly generated *L. montana* aqueous leaf extract (ratio 1:1) was mixed in a 200 mL conical flask, subjected to continuous agitation (10 *g*) at 70 °C for 4 hours to obtain NPs solution. The mixture was cooled at room temperature and centrifuged at 10000 *g* for 20 minutes and the residue, NPs pellets were washed four times with distilled water, dried at 50 °C and kept at -80 °C pending further characterisation and analysis (Ogunyemi et al. 2019) while the supernatant was discarded.

Characterisation of NPs

UV-Vis spectrum analysis

The synthesised *Lessertia montana* zinc oxide nanoparticles (LmZnONPs) was characterised (first of all) by measuring and noting the point of optimum absorption using ultra-violet visible (UV) 5 Bio spectrophotometer (Metler Toledo, Switzerland) in the 100 – 800 nm range with aim of evaluating the optical property of the ZnONPs.

Scanning electron microscope (SEM) / energy-dispersive x-ray spectroscopy (EDS)

The synthesised ZnONPs' structural morphology and elemental composition were analysed with the use of SEM combined with energy dispersive spectrum (EDS) using Tescan Vega 3 SEM Oxford X-Max^N EDS equipment. A small quantity of synthesised *L. montana* ZnONPs powder was sparingly sprinkled on the carbon-coated copper grid and thereafter dried under mercury lamp for 10 minutes.

Fourier transform infrared spectroscopy (FT-IR)

Lessertia montana ZnONPs were subjected to the Fourier transform infrared (FTIR) machine, to have an insight about the functional biomolecules embedded in the synthesised NPs and this, was achieved with the aid of Spectrum 100 series FTIR spectrometer (Perkin Elmer, Waltham, Massachusetts, United States). The sample was scanned (4 cm^{-1} resolution) in the spectra or wavelength range of 650-4000 cm^{-1} at room temperature.

X-ray diffraction (XRD)

The D8 advance diffractometer (Bruker AXS, Germany) using a LynxEye detector was used. The voltage set at 40 kV, tube current 40 mA and Cu-Kα radiation ($\lambda K\alpha_1$ = 1.5406Å) was employed providing information about the morphology of the NPs. The recorded range of 2Θ was 20-100 with a 0.5-second/step, equivalent to an effective time of 92 second/step for a scintillation counter. The Debye-Scherrer's formula was used to estimate the crystallite particle sizes.

Antioxidant assays

The free radicals scavenging activities of the synthesised NPs were assessed using DPPH, ABTS, and metal chelating assays.

DPPH radical scavenging activity

The method of Braca et al. (2001) was adopted to determine the reduction of 1, 1-diphenyl-2-picrylhydrazyl (DPPH) radical by *L. montana* ZnONPs and other samples (extract, ZnO and quercetin) at various concentrations (0.125 – 1.000 g/L) prepared in 10% dimethyl sulfoxide (DMSO). Briefly, 0.1 mL of the samples were exposed to 0.1 mL methanolic solution (0.004%) DPPH radical in a 96-well microtiter plate. Subsequently, the inhibition of the DPPH radical by the samples was viewed by the changes in colour from pink to yellow and golden following 30 minutes incubation in the dark. The absorbance was measured at 517 nm. The percentage inhibition of the sample that scavenged DPPH radical was calculated using the expression $[(A_0–A_1)/A_0]\ x\ 100$, where A_0 is the absorbance of the control, and A_1 is the absorbance of the sample. The half-maximal inhibitory concentration (IC_{50}) values of the samples were calculated graphically and accordingly (Balogun and Ashafa 2016a).

ABTS radical determination

The ability of the samples to scavenge $ABTS^+$ chromophore resulting from the reaction of ABTS solution with potassium persulfate was determined based on Re et al. (1999) method. 50 mL of 7 mM aq. ABTS and 2.45 mM $K_2S_2O_7$ (50 mL) were prepared, reacted in the dark for 16 hours to produce an ABTS-$K_2S_2O_7$ solution. Approximately 0.2 mL of the solution was exposed to 0.02 mL aliquot of the sample and absorbance measured after 15 minutes of incubation at 734 nm using a BIO-RAD microplate reader (model 650, Japan).

Metal chelating activity

Dinis et al. (1994) protocol for determining the chelating capacity of a substance was used. One hundred µL *L. montana* ZnONPs and other samples at the tested concentrations were mixed with 0.5 mL 2 mM $FeCl_2$ solution and the reaction began with the addition of 0.2 mL (5 mmol/L) ferrozine, shook vigorously and thereafter allowed to stand at room temperature for 600 seconds. The spectrophotometric measurement of the mixture was taken at 562 nm. The percentage inhibition of ferrozine–Fe^{2+} complex formation was determined from the expression $[(A_0–A_1)/A_0]\ x\ 100$ as described above.

In vitro antidiabetic potentials

The alpha-amylase (α-AML) and alpha-glucosidase (α-GCD) assays were used to assess the antidiabetic activity (*in vitro*) of the green synthesised ZnONPs as presented in the reports of various authors below.

α-Amylase inhibitory assay

McCue and Shetty (2004) modified procedure was adopted in determining the inhibitory effect of α-AML by the *L. montana* zinc oxide nanoparticles. In brief, 50 µL of the samples (ZnONPs, extract, ZnO and acarbose) at ranging concentrations of 0.125 – 1.000 g/L were reacted with the same volume of α-AML prepared in sodium phosphate buffer (SPB; 0.02 M, pH 6.9) at a concentration of 0.5 g/L and pre-incubated at 25 °C for 10 minutes. Subsequently,

the addition of 50 µL of the 1% starch solution into the sample wells followed by 0.1 mL of di-nitro salicylic acid (DNS) reagent to stop the reaction and incubated at 25 °C for another 10 minutes. The mixture was suspended in boiling water for 5 minutes, thereafter cooled, diluted with 1 mL distilled water (DW), and measured the absorbance at 540 nm. Distilled water replaced the extract to represent the control using the same protocol. The α-amylase inhibitory activity was calculated as percentage inhibition following the above expression $[(A_0–A_1)/A_0] \times 100$ and the IC_{50} calculated graphically as defined in the report of Balogun and Ashafa (2016a).

Kinetics of α-amylase inhibition

The mode of α-AML inhibition by *L. montana* ZnONPs was evaluated according to Ali et al. (2006) method. The reaction mixture contained 0.25 mL synthesised ZnONPs (5 mg/mL) pre-incubated with 0.25 mL α- AML solution for 10 minutes at 25 °C in a set of 5 test tubes and 0.25 mL phosphate buffer (PB) pre-incubated with 0.25 mL α-AML in another set of 5 test tubes. Thereafter, 0.25 mL starch solution in increasing concentrations (0.30 – 5.00 gL^{-1}) was dispensed in all test tubes to set the reaction in motion, followed by the introduction of DNS (0.02 mL) to bring the reaction to an end. The protocol continued as described above in the α-amylase inhibitory assay. Moreover, in an effort to determine the amount of reducing sugars released and converted to reaction velocities, a maltose standard curve was plotted, where the kinetics of inhibition of α-AML activity by synthesised ZnONPs was determined using Lineweaver and Burk (1934).

α-Glucosidase inhibitory assay

The antidiabetic effect of the *L. montana* ZnONPs was also assessed on the α-glucosidase enzyme using the procedural description of Kim et al. (2005) where the substrate, p-nitrophenyl glucopyranoside (*p*NPG) (5 mM) used was prepared in 0.02 M phosphate buffer (pH 6.9). Fifty µL of the varying concentrations of the samples (0.125 – 1.000 g/L) pre-incubated with 0.1 mL α-glucosidase (0.5 g/L) were mixed in a test tube. Fifty µL *p*NPG was afterward introduced into the reaction mixture to begin the reaction while 2 mL Na_2CO_3 (0.1 M) was finally dispensed to stop the process followed by incubation at 37 °C for 30 min. The α-glucosidase activity was determined by measuring the yellow-coloured para-nitrophenol (*p*NP) released from *p*NPG at 405 nm as the percentage inhibition determined by adopting the expression $[(A_0–A_1)/A_0] \times 100$ and the IC_{50} obtained as explained in the work of Balogun and Ashafa (2016a).

Mode of α-glucosidase inhibition

Ali et al. (2006) modified method was used to explore the kinetics of inhibition of the enzyme by synthesised ZnONPs. In summary, 0.05 mL (5 g/L) sample was diluted with 0.1 mL of α-GCD solution pre-incubated for 10 minutes at 25 °C in a set of five vials and concurrently, α-GCD solution reacted with 0.05 mL phosphate buffer (pH 6.9) in another set of 5 vials. Subsequently, fifty microliters *p*NPG in ascending concentrations (0.125 – 2.000 g/L) was introduced to the two sets of test vials to kick-start the reaction process and the mixture allowed to incubate at 25 °C for 10 minutes. Finally, the reaction was terminated with 0.5 mL of Na_2CO_3. A para-nitrophenol (*p*-NP) standard was used to depict spectrophotometrically the amount of reducing sugars released and kinetics of *L. montana* ZnONPs on the α-glucosidase activity determined using Michaelis-Menten kinetics.

Statistical analysis

Data analyses were carried out by one-way analysis of variance (ANOVA), followed by Bonferroni's multiple comparison test. Results expressed as mean ± standard error of mean (SEM) using Graph pad Prism version 3.0 for Windows, Graph Pad Software, SanDiego, California, USA.

RESULTS AND DISCUSSION

The simplicity, stability, affordability, and eco-friendliness of the synthesised NPs from medicinal plants afford great relevance to the biological methods in nanotechnology, hence the acceptability in drug discovery and development (Sun et al. 2019). The antioxidant and antihyperglycaemic potentials of the aqueous leaf extract of *Lessertia montana* (Alimi and Ashafa 2017) propelled undertaking the study to evaluate the effect of the synthesised nanoparticle (*Lessertia montana* ZnONPs) on these disease conditions. In the work of Alimi and Ashafa (2017), various phytochemicals such as alkaloids, flavonoids, phenols, saponins, etc. are detected in the aqueous extract of the leaf and in fact, these phytoconstituents are regarded as polyphenols (Ezealisiji et al. 2019) and also depicted by the various functional groups on the FTIR spectrum. Therefore, the probable mechanism of ZnONPs synthesis from *L. montana* entails the reaction of Zn^{2+} in the solution with the polyphenols (flavonoids, alkaloids, phenols) in the extract resulting in the reduction of the Zn^{2+} to ZnO, which on complexation will (at the end of the reaction) form ZnONPs (Basneth et al. 2018; Ogunyemi et al. 2019; Ezealisiji et al. 2019).

The zinc oxide nanoparticles synthesised using *L. montana* leaves extract was observed to give a light-yellow precipitate, dried to obtain ZnO nanopowder used in the characterisation processes (CP). The CP was initiated with a UV-Vis spectrophotometer to determine

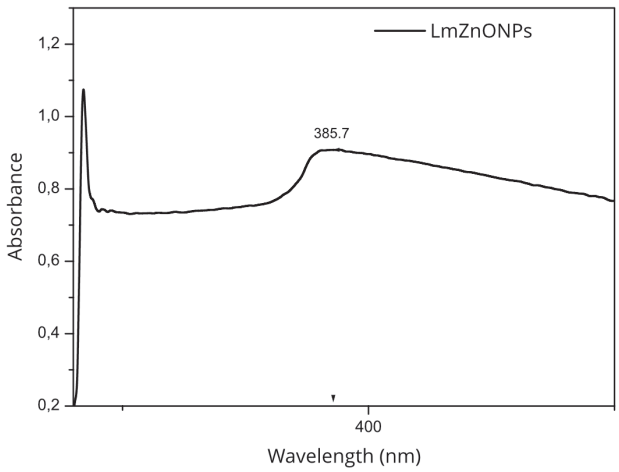

Figure 1. UV-Vis spectra of synthesised *L. montana* ZnONPs showing the maximum absorbance at 387.5 nm.

the region of optimum absorption of the ZnONPs (Fig. 1) observed at a wavelength range of 387.5 nm (Fig. 1) after being monitored on the spectra range between 100 - 800 nm. The observed absorbance value aligned with the reports of previous authors who submitted the maximum absorption of ZnO to be in 380-387 range (Nithya and Kalyanasundharam 2018; Mohammadian et al. 2018; Ogunyemi et al. 2019). However, it must be noted that the differences in the absorption of a substance and in this case, ZnO nanoparticle is dependent on several factors including synthesis procedure, particle size, shape, contamination, and so on. Intriguingly, the observed absorption of *L. montana* ZnONPs at 387 nm was in line with the submission of Nithya and Kalyanasundharam (2019) for *C. halicacabum* leaf. Additionally, the energy of the bandgap was calculated from the expression $E = h\nu = hf = hc/\lambda$ since $f = c/\lambda$

Where 'h' denotes the Plank's constant, 'c' signify the speed of light while 'λ' connotes the wavelength

The optical band gap energy for *L. montana* ZnONPs was calculated to be 3.2 eV. It is worthy of mention that different studies have reported different values for ZnONPs. In a study, it is submitted at 3.88 eV (Ogunyemi et al. 2019), whereas other reports maintained that it varies between 3.1 to 3.3 eV (Srikant and Clarke, 1998) and 3.16 - 3.22 eV (Ramesh et al. 2014; Rehana et al. 2017) while others (Vishnukumar et al. 2018; Kalpana and Devi Rajeswari 2018) established it at 3.3 eV and 3.37 eV, respectively. However, variation in band gap energy has been suggested to be due to valence band-donor transition overpowering the optical absorption (Srikant and Clarke 1998). The obtained value for the study was in agreement with the report of Ramesh et al. (2014).

Fourier transform infrared spectroscopy was performed on the synthesised ZnONPs with the view to depict the likely functional groups or the phytochemicals acting as capping and stabilizing agents. FTIR was similarly undertaking to express the vibrational and rotational motion of the concerned molecule. Thus, the FTIR spectrum for *L. montana* ZnONPs revealed a peak at 3365 cm^{-1} corresponding to the O-H stretching of hydroxyl groups. Bayrami et al. (2020) citing from the work of Sundrarajan et al. (2015) submitted that peaks in the region of 3700 to 3300 are due to O-H stretching vibration. Peaks at 2945 cm^{-1}, 1412 cm^{-1} 1046 cm^{-1} corresponded to broad bands of medium C-H (Bayrami et al. 2020), strong C-C and strong, broad CO-O-CO stretching due to alkanes, aromatic group (Elumalai et al. 2015; Rehana et al. 2017), and anhydride respectively. The peak at 1596 cm^{-1} corresponds to medium N-H bending due to amine region, 892 cm^{-1} corresponded to strong C=C bending due to alkene (vinylidene) and 699 cm^{-1} due to strong C=C bending due to alkene (cis disubstituted) (Fig. 2). The reports of Alimi and Ashafa (2017), as well as Ashafa et al. (2019), reported various phytochemicals such as alkaloids, flavonoids, phenolics, tannins, triterpenes, phytosterols, and cardiac glycosides. Interestingly, most of these functional groups observed in the FTIR spectra underlie these phytochemicals. Typically, alkaloids contain nitrogen groups such as amide; phenols and flavonol (a class of flavonoids) bear OH groups attached to the aromatic ring structures. In line with the aforementioned, the presence of these functional groups in the spectrum is indicative that these secondary metabolites bond strongly to ZnONPs despite several washing, hence, the possible association between the phytoconstituents and surface of the Zn resulting in the potential conversion of ZnO

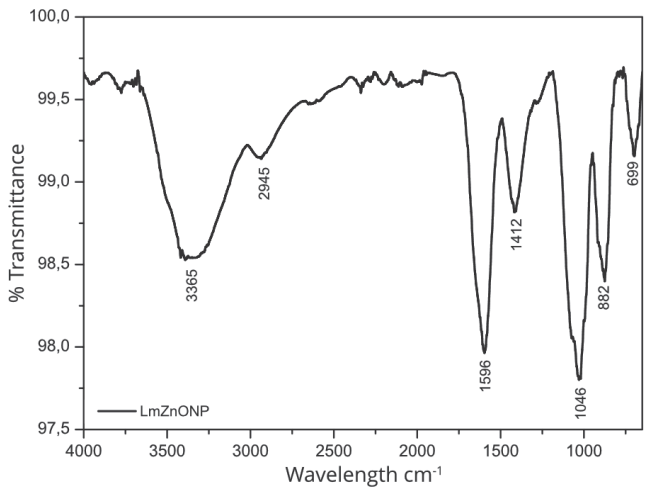

Figure 2. Fourier transform infrared (FTIR) spectra of *L. montana* ZnONPs showing various prominent peaks.

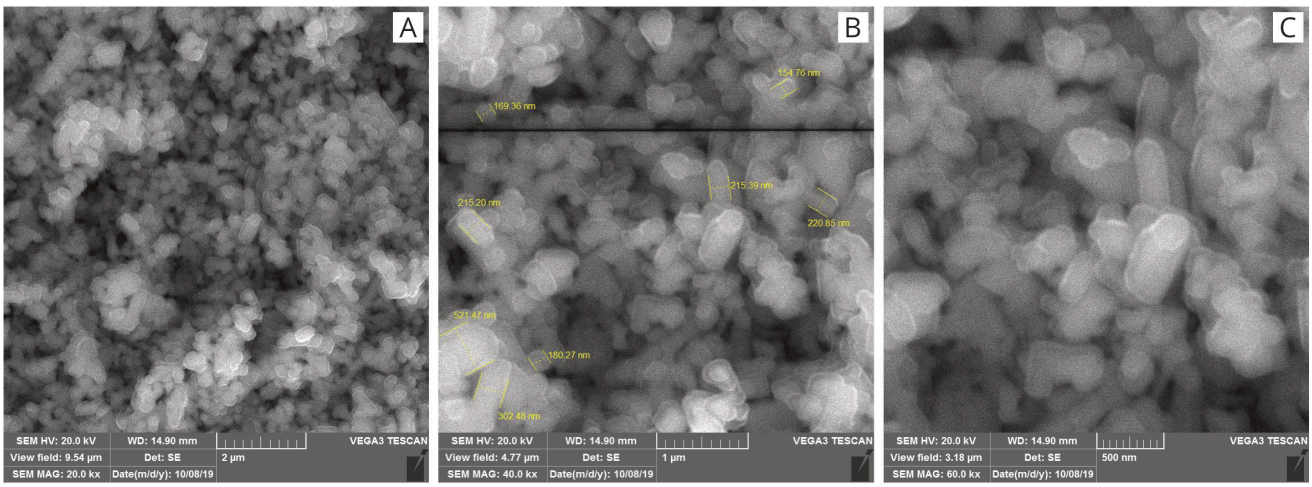

Figure 3. A, B and C are SEM pictures of synthesised *L. montana* ZnONPs at 2 µm, 1 µm and 500 nm, respectively.

to ZnONPs while maintaining the stability of ZnONPs (Rajakumar et al. 2018).

The use of the SEM technique on a substance accords information on the morphology of the substance and in our case, the synthesised ZnO nanostructures. In the present study, a critical view of the NPs morphology indicated a mixture of cubical and spherical structures which was in agreement with the work of Rajakumar et al. (2018) though the presence of the cubic-like structures were more (Fig. 3A, 3B and 3C) with varying size ranging from 154.78 to 521.47 nm (Fig. 3B). The energy dispersive spectra (EDS) provided details on the composition of the elements, i.e. zinc and oxygen involved in the compound ZnO or the stoichiometric ratio, found to be 82.6 and 17.4 proportion respectively in this study (Fig. 4). The observed revelation is indicative of the usage of an analytical grade of zinc oxide (chemical) powder (Kumar et al. 2013; Ogunyemi et al. 2019) for the *L. montana* ZnONPs synthesis. Interestingly, the EDS spectrum showed the presence of other elements including nitrogen and carbon, which could be attributed to the endowed bioactive constituents available in *L. montana* plant and responsible for the stabilization of ZnONPs as established in the report of Bala et al. (2015).

Fig. 5 showed prominent peaks (arising from ZnO) positioned at various 2Θ values 31.8, 34.4, 36.3, 47.5, 56.6, 62.9, 66.4, 68.0, 69.1, 72.6, 77.0 and 81.4 degrees which correspond to 'hkl'(miller indices) crystal planes of 100, 002, 101, 102,110, 103, 200, 112, 201, 004, 202 and 104, respectively. The Scherer equation adopted to evaluate the green synthesised ZnONPs crystallite size as shown in the expression below:

$$D = K\lambda/\beta Cos\Theta$$

Where D represent the crystallite size, K is the shape factor (constant) and equals 0.94, λ is the x-ray wavelength (1.5406Å) and β is the full width at half maximum of the dominant or peak of interest. Thus, the D values for the *L. montana* ZnONPs visible peaks are 27.3, 24.8, 23.3, 14.7, 11.6, 8.6, 7.3, 11.0, 9.6, 11.3, 7.9 and 8.6 nm, respectively. These values (sizes) are smaller as compared to the SEM (larger size) report, attributed to the agglomeration of the smaller size particles (Ogunyemi et al. 2019) particularly if the synthesis occurs in an aqueous medium (Rajakumar et al. 2018) as achieved in this study. The crystallite sizes ranged between 7.3 to 27.3 nm with an average size of

Table 1. Free radicals potentials and metal chelating effect of synthesised *L. montana* ZnONPs.

Parameters	IC_{50} (g/L)			
	L. montana ZnONPs	*L. montana*	ZnO	Quercetin
DPPH	$0.120 \pm 1.42^{a*}$	0.261 ± 1.55^{b}	1.165 ± 5.60^{c}	0.349 ± 4.27^{d}
ABTS	0.711 ± 8.07^{a}	0.964 ± 7.27^{b}	1.166 ± 9.45^{c}	0.093 ± 3.77^{d}
Metal chelating	0.184 ± 5.94^{a}	0.554 ± 3.00^{b}	0.591 ± 3.15^{c}	0.027 ± 9.87^{d}

ZnONPs: zinc oxide nanoparticles; DPPH: 1,1-diphenyl-2-picrylhydrazyl; ABTS: 2,2-azino benzothiazolidine(-6-sulphonic) acid; ZnO: zinc oxide
*Values with different superscript letters along the same column for each parameter are significantly different ($p < 0.05$) from each other

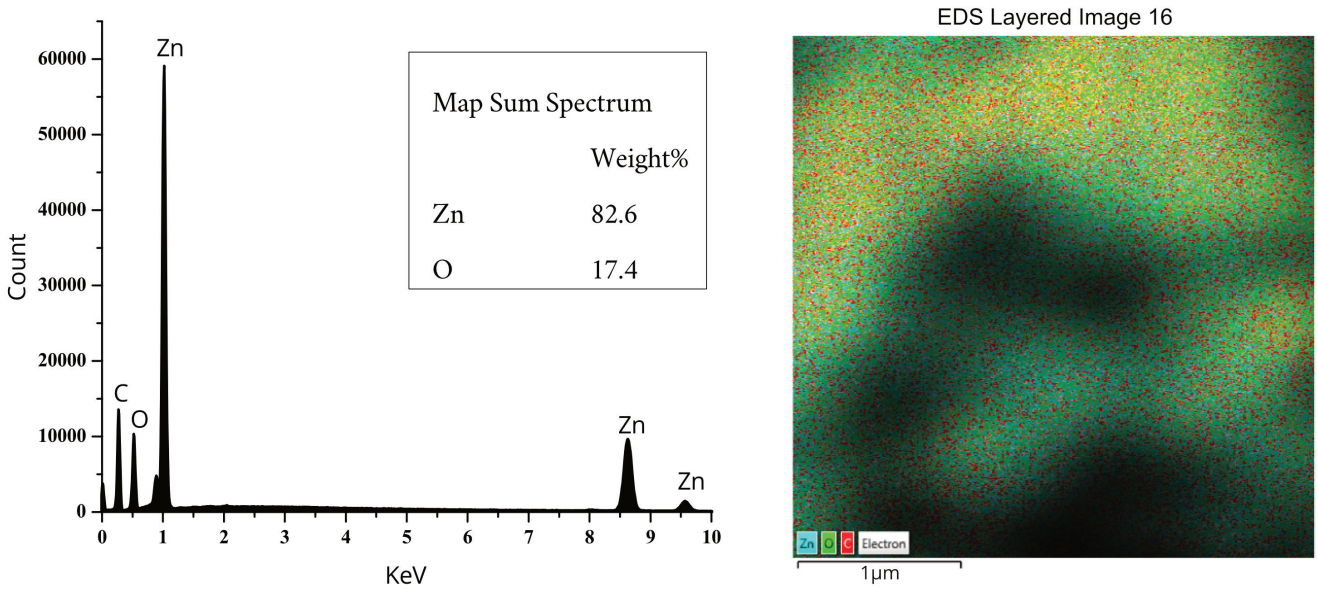

Figure 4. Energy dispersive spectra (EDS) of the synthesised *L. montana* ZnONP showing the elemental composition of ZnO in the nanostructures (left) and the corresponding image (right).

13.8 nm. Interestingly, very few studies on ZnO using medicinal plants have this type of very small nano-sized particles. Smaller-sized nanoparticles are endowed with larger surface area to volume ratio, which enhances their binding to cell's surface, according them a great deal of preference in biological applications (Rehana et al. 2017; Vishnukumar et al. 2019).

The negative consequences of free radicals have necessitated research into this field (free radical chemistry). Free radicals (FRs) are reactive oxygen or nitrogen species produced by the body on exposure to diseased state (Lobo et al. 2010). It must be noted that FRs are not necessarily bad but excessive production in the body system is what must be guided against. Hence, equilibrium between FRs and the body's antioxidant defence mechanism must be maintained for the proper functioning of the cells, otherwise, it results in a state of oxidative stress, which means the defence mechanism of the body is overpowered or compromised and ultimately result into cell death. Thus, prompt intervention with the use of antioxidants (synthetic or natural) is necessary (Balogun and Ashafa 2016b). In an effort to study the effect of antioxidative substances on free radicals, various *in vitro* (DPPH, ABTS, hydroxyl radicals, superoxide anions, etc.) and *in vivo* methods are adopted by researchers. In this study, the antioxidative potential of the synthesised NPs was evaluated on DPPH and ABTS as well as metal chelating. It was observed that going by half-maximal inhibitory concentration results, *L. montana* ZnONPs performed exceedingly well ($p < 0.05$) in all the assays including DPPH (120.31 µg/mL), ABTS (711.45 µg/mL) and metal chelating (184.16 µg/mL) when compared with other samples (extract, ZnO and quercetin) except with ABTS and metal chelating where the control, quercetin displayed better ($p < 0.05$) activity (93.94, 27.81 µg/mL, respectively) which is expected (Table 1). The excellent activity observed by synthesised ZnONPs against DPPH as reflected in the colour change from pink to yellow is an indication of its potential in reducing stable DPPH with its hydrogen ion donating-ability. DPPH method is the most important assay for the determination of the antioxidant potential of a substance or compound (followed by ABTS assay) (Sanchez-Moreno et al. 1999; Sagar and Ashok 2012). The mechanism of action is that the antioxidant substance donates hydrogen atom to the radical (DPPH) with an

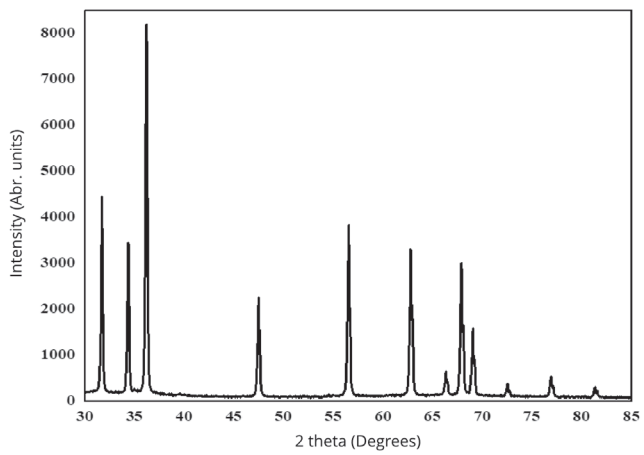

Figure 5. XRD spectrum of synthesised *L. montana* ZnONPs.

Table 2. Inhibitory activities of synthesised *L. montana* ZnONPs on hydrolysing enzymes of carbohydrates.

Parameters	IC_{50} (g/L)			
	L. montana ZnONPs	*L. montana*	ZnO	Acarbose
α-amylase	0.620 ± 3.35[a]*	0.196 ± 3.39[b]	0.300 ± 5.37[c]	0.594 ± 1.48[d]
α-glucosidase	0.037 ± 7.48[a]	0.095 ± 7.38[b]	0.119 ± 4.23[c]	0.065 ± 5.38[d]

ZnONPs: Zinc oxide nanoparticles; ZnO: Zinc oxide.
*Values with different superscript letters along the same column for each parameter are significantly different ($p<0.05$) from each other

unbalanced shell electron, resulting in the reduction or reduced form of the radical, and when this is achieved, the pink colour of the radical changes to yellow. Summarily, since the introduction of antioxidant substance cushions or fortifies the weakened defence mechanism preventing cell death (Lewinski et al. 2008; Lobo et al. 2010), *L. montana* ZnONPs may be suggested to exhibit a similar role. Interestingly, these findings corroborate the reports of similar studies where synthesised ZnONPs from medicinal plants inhibits the activities of the studied radicals. Typically, the activity of *Costus igneus* aqueous leaf (20-100 μg/mL) extracts was compared with Ci-ZnO (nanoparticle) against DPPH and was found to depict 75% inhibition as compared with extract alone having 55% (Vinotha et al. 2019). Additionally, in a study by Rehana et al. (2017), where the free radical scavenging potentials of five plants (*A. indica*, *H. rosa-sinensis*, *M. koenigi*, *M. oleifera*, and *T. indica*) used in the synthesis of ZnONPs were tested against ABTS, DPPH, hydroxyl radical, superoxide radical and hydrogen peroxide revealed significant activities better than standards (ascorbic acids and rutin) (Rehana et al. 2017). A similar trend was also reported in the work of Rajakumar et al. (2018) with *Andrographis paniculata* leaf ZnONPs curbing the activities of DPPH, reducing power and nitric oxide.

Diabetes mellitus is a chronic metabolic disease characterised by hyperglycaemia due to abnormalities in protein, carbohydrate, and lipids metabolism resulting from ineffective insulin or insulin-resistant or both (Krentz and Bailey 2005; Rehana et al. 2017). During postprandial hyperglycaemia, the utmost management approach of the ailment is to inhibit the constant production of glucose (available in the blood) aided by hydrolysing enzymes such as alpha-amylase (found in the pancreas) and alpha-glucosidase (found in the brush border of the intestine) (Balogun and Ashafa 2017). Notable inhibitors of these enzymes are acarbose, miglitol, and so on, which act by slowing down the persistent hydrolysis of starch to produce glucose. Sadly, these inhibitors come with side effects such as gastrointestinal (GIT) discomfort, bloating, etc., hence, looking for an alternative inhibitor from natural products without side effects becomes germane (Sathya and Siddhuraju 2012; Rehana et al. 2017). Moreover, it is important to state that any inhibitor with this feature must be able to inhibit alpha-amylase mildly while inhibiting alpha-glucosidase strongly. A view of the antidiabetic result from the study showed that the *L. montana* aqueous extract (0.197 g/L) and synthesised ZnONPs (0.037 g/L) revealed the best potential at significantly ($p < 0.05$) inhibiting the activities of α-amylase and α-glucosidase respectively when compared with other samples and standard, acarbose (0.594 and 0.065 g/L, respectively). Intriguingly, as reiterated above, *L. montana* ZnONPs showed a character depicted of a good antihyperglycaemic agent with the lowest IC_{50} value (0.037 g/L) against alpha-glucosidase (strongest inhibition) and highest IC_{50} value (0.620 g/L) against alpha-amylase (mildest inhibition) (Table 2). The result is in tandem with the revelation from Rehana et al. (2017) where *T. indica* ZnONPs exhibited the highest inhibitory concentration against alpha-amylase and alpha-glucosidase enzymes as compared with other four plants, whose inhibitions are better than ZnONPs synthesised by chemical method. Moreover, too, ZnONPs synthesised by *A. paniculata* revealed a moderate alpha-amylase activity, which was better than the extract counterpart (Rajakumar et al. 2018).

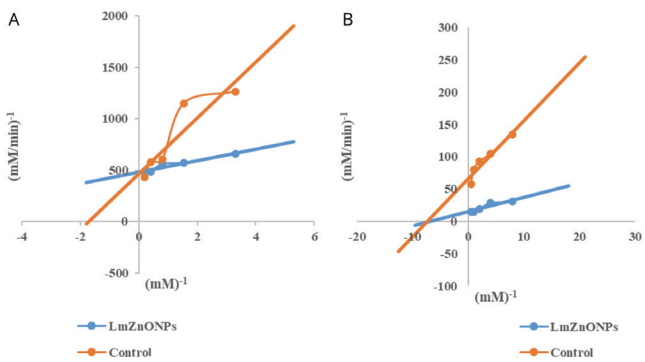

Figure 6. A competitive inhibition of alpha-amylase (A) and non-competitive inhibition of alpha-glucosidase (B) by *L. montana* ZnONPs.

In this study, the likely mode of inhibition for α-amylase by *L. montana* ZnONPs established a constant Vmax value

(0.0021 mM/min) between the control and NPs with a decreased Km values from 0.579 mM^{-1} (control) to 0.116 mM^{-1} (*L. montana* ZnONPs) signifying a competitive inhibition (Fig. 6A). The implication of this is that synthesised *L. montana* ZnONPs competed with the substrate at binding at the active site of the enzyme, thus slowing down the conversion of carbohydrate to disaccharides. On the other hand, a constant Km value (0.14 mM^{-1}) and a decreased Vmax values from 0.066 mM/min to 0.015 mM/min for alpha-glucosidase thus, depicting a non-competitive inhibition (Fig. 6B). This thus indicates that *L. montana* ZnONPs possibly binds to a site apart from the active site of the enzyme thereby binding with either free enzyme or enzyme-substrate complex interfering with the action of both (Mayur et al. 2010).

CONCLUSION

The *Lessertia montana* synthesised zinc oxide nanoparticles, no doubt, revealed good antioxidative and antidiabetic potentials which could be attributed to the presence of phytonutrients. Hence, the need to embrace plant-derived nanoparticles becomes vital, not only because of its low cost of synthesis, environment friendliness etc. but owing to the enhanced activity as compared with the bulk extract (as depicted in this study). Furthermore, the relatively small size of NPs, which would aid effective absorption or penetration into cells, including possible interaction with the cell surface of biomolecules in order to elicit adequate cellular responses would be preferable for biological applications.

ACKNOWLEDGMENTS

The authors acknowledge the support from Directorate Research and Development, University of the Free State (UFS), Free State for the postdoctoral fellowship awarded to Dr. FO Balogun (2-459-B3425) tenable at Phytomedicine and Phytopharmacology Research Group, Department of Plant Sciences, UFS, Qwaqwa Campus, Free State. The authors also acknowledge the intellectual input of Dr. Obi of Physics Department, UFS, Qwaqwa, Free State in the interpretation of some of the results as well as National Research Foundation (NRF) for the usage of Tescan Vega 3 SEM Oxford X-Max^N EDS equipment (provided to Chemistry Department, UFS, Qwaqwa) for paid SEM-EDS analyses.

REFERENCES

Aboyade OM, Styger G, Gibson D, Hughes G (2014) *Sutherlandia frutescens*: the meeting of science and traditional knowledge. J Altern Complement Med 20(2):71-76.

Ali H, Houghton PJ, Soumyanath A (2006) Alpha-amylase inhibitory activity of some Malaysian plants used to treat diabetes; with particular reference to *Phyllanthus amarus.* J Ethnopharmacol 107(3):449-455.

Alimi AA, Ashafa AOT (2017) An *in vitro* evaluation of the antioxidant and antidiabetic potential of *Sutherlandia montana* E. Phillips & R.A. Dyer leaf extracts. Asian Pac J Trop Biomed 7(9):765-772.

Ashafa AOT, Balogun FO, Adegbegi JA (2019) *In vitro* kinetics of inhibition of the endogenous hyperglycaemia antagonists of alpha-amylase and alpha-glucosidase in the pod and seed extracts of *Lessertia montana*. J Appl Pharm Sci 9(01):42-50.

Bala N, Saha S, Chakraborty M, Maiti M, Das S, Basu R, Nandy P (2015) Green synthesis of zinc oxide nanoparticles using *Hibiscus subdariffa* leaf extract: effect of temperature on synthesis, anti-bacterial activity and anti-diabetic activity. RSC Adv 5:4993–5003.

Balogun FO, Ashafa AOT (2017) Aqueous roots extract of *Dicoma anomala* (Sond.) extenuates postprandial hyperglycaemia *in vitro* and its modulation against on the activities of carbohydrate-metabolizing enzymes in streptozotocin-induced diabetic Wistar Rats. S Afr J Bot 112:102-111.

Balogun FO, Ashafa AOT (2016a) Antioxidants, hepatoprotective and ameliorative potentials of aqueous leaf extract of *Gazania krebsiana* (Less.) against carbon tetrachloride –induced liver injury in rats. Trans Royal Soc S Afr 71(2):145-156.

Balogun FO, Ashafa AOT (2016b) Antioxidant and hepatoprotective activities of aqueous root extracts of *Dicoma anomala* (Sond.) against carbon tetrachloride induced liver damage in rats. J Trad Chin Med 36:505-513.

Basnet P, Chanu TI, Samanta D, Chatterjee S (2018) A review on bio-synthesized zinc oxide nanoparticles using plant extracts as reductants and stabilising agents. J Photochem Photobiol B Biol 183:201-221.

Bayrami A, Haghgooie S, Pouran SR, Arvanag FM, Habibi-Yangjeh A (2020). Synergistic antidiabetic activity of ZnO nanoparticle encompassed by *Urtica dioica* extract. Adv Powder Technol 31:2110-2118.

Braca A, Tommasi ND, Bari LD, Pizza C, Politi M, Morelli I (2001) Antioxidant principles from *Bauhinia terapotensis.* J Nat Prod 64(7):892-895.

Dinis TCP, Madeira VMC, Almeida LM (1994) Action of phenolic derivatives (acetoaminophen, salycilate and 5-aminosalycilate) as inhibitors of membrane lipid

peroxidation and as peroxyl radical scavengers. Arch Biochem Biophys 315(1):161-169.
Elumalai K, Velmurugan S, Ravi S, Kathiravan V, Ashokkumar S (2015) Bio-fabrication of zinc oxide nanoparticles using leaf extract of curry leaf (*Murraya koenigii*) and its antimicrobial activities. Mat Sci Semicon Process 34:365-372.
Ezealisiji KM, Siwe-Noundou X, Maduelosi B, Nwachukwu N, Krause RWM (2019) Green synthesis of zinc oxide nanoparticles using *Solanum torvum* (L.) leaf extract and evaluation of the toxicological profile of the ZnO nanoparticles-hydrogel composite in Wistar albino rats. Int Nano Let 9:99-107
Fakhari S, Jamzad M, Fard HK (2019) Green synthesis of zinc oxide nanoparticles: a comparison. Green Chem Lett Rev 12(1):19-24.
Kalpana VN, Devi Rajeswari V (2018) A review on green synthesis, biomedical applications and toxicity studies of ZnONPs. Bioinorganic Chem Appl 18:3569758.
Kim YM, Jeong YK, Wang MH, Lee WY, Rhee HI (2005) Inhibitory effects of pine bark extract on alpha-glucosidase activity and postprandial hyperglycemia. Nutr 21(6):756-761.
Krentz AJ, Bailey CJ (2005) Oral antidiabetic agents: current role in type 2 diabetes mellitus. Drugs 65(3):385-411.
Kumar SS, Venkateswarlu P, Rao VR, Gollapalli NR (2013) Synthesis, characterization and optical properties of zinc oxide nanoparticles. Int Nano Lett 3:30-36.
Lewinski N, Colvin V, Drezek R (2008) Cytotoxicity of nanoparticles. Small 4:26-49
Lineweaver H, Burk D (1934) The determination of enzyme dissociation constants. J Am Chem Soc 56(3):658-666.
Lobo V, Patil A, Phatak A, Chandra N (2010) Free radicals, antioxidants, and functional foods: Impact on human health. Pharmacog Rev 4(8):118-126.
Mayur B, Sandesh S, Shruti S, Sung-Yum S (2010) Antioxidant and α- glucosidase inhibitory properties of *Carpesium abrotanoides* L. J Med Plant Res 4:1547-1553.
Mccue P, Shetty K (2004) Inhibitory effects of rosmarinic acid extracts on porcine pancreatic amylase *in-vitro*. Asia Pac J Clin Nutr 13(1):101-106.
Mohammadian M, Es'haghi Z, Hooshmand S (2018) Green and chemical synthesis of zinc oxide nanoparticles and size evaluation by UV-vis spectroscopy. J Nanomed Res 1:7.
Nithya K, Kalyanasundharam S (2019) Effect of chemically synthesis compared to biosynthesized ZnO nanoparticles using aqueous extract of *C. halicacabum* and their antibacterial activity. OpenNano 4:100024.
Ogunyemi SO, Abdallah Y, Zhang M, Fouad H, Hong X, Ibrahim E, Islam Masum MdM, Hossain A, Mo J, Li B (2019) Green synthesis of zinc oxide nanoparticles using different plant extracts and their antibacterial activity against *Xanthomonas oryzae* pv oryzae. Artif Cells Nanomed Biotechnol 47(1):341-352
Prashanth GK, Prashanth PA, Nagabhushana BM, Ananda S, Krishnaiah GM, Nagenda HG, Sathyananda HM, Rajendra Singh C, Yogisha S, Anand S, Tejabhiram Y (2018) Comparison of anticancer activity of biocompatible ZnO nanoparticles prepared by solution combustion synthesis using aqueous leaf extracts of *Abutilon indicum*, *Melia azedarach* and *Indigofera tinctoria* as biofuels. Artif Cells Nanomed Biotechnol 46:968-979.
Rai M, Ingle A (2012) Role of nanotechnology in agriculture with special reference to management of insect pests. Appl Microbiol Biotechnol 94:287-293.
Rajakumar G, Thiruvengadam M, Mydhili G, Gomathi T, Chung I (2018) Green approach for synthesis of zinc oxide nanoparticles from *Andrographis paniculata* leaf extract and evaluation of their antioxidant, anti-diabetic, and anti-inflammatory activities. Bioprocess Biosyst Eng 41:21-30.
Ramesh M, Anbuvannan M, Viruthagiri G (2014) Green synthesis of ZnO nanoparticles using Solanum nigrum leaf extract and their antibacterial activity. Spectrochim Acta A 136:864-870.
Re R, Pellegrini N, Proteggente A (1999) Antioxidant activity applying an improved ABTS radical cation decolorisation assay. Free Rad Bio Med 26(9-10):1231-1237.
Rehana D, Mahendiran D, Kumar RS, Rahiman AK (2017) *In vitro* antioxidant and antidiabetic activities of zinc oxide nanoparticles synthesized using different plant extracts. Bioprocess Biosyst Eng 40:943-957.
Sagar G, Ashok B (2012) Green synthesis of silver nanoparticles using *Aspergillus niger* and its efficacy against human pathogens. Eur J Expt Biol 2(5):1654-1658.
Sanchez-Moreno C, Larrauri JA, Saura-Calixto F (1999) Free radical scavenging capacity and inhibition of wines, grape juices and related polyphenolic constituents. Food Res Int 32:407-412.
Sangeetha G, Rajeshwari S, Venckatesh R (2011) Green synthesis of zinc oxide nanoparticles by *Aloe barbadensis* Miller leaf extract: structure and optical properties. Mat Res Bull 46:2560-2566.
Sathya A, Siddhuraju P (2012) Role of phenolics as antioxidants, biomolecule protectors and as antidiabetic factors—evaluation on bark and empty pods of *Acacia auriculiformis*. Asian Pac J Trop 5:757-765.
Sorescu A, Alexandrina N, Rodica-Mariana I, Ioana-Raluca S (2016) Green synthesis of silver nanoparticles using plant extracts. Proceed 4th Int Virtual Confer Adv Sci Res; 2016 June 6-10; Chem Sci; Royal Society of Chemistry, Cambridge, UK, 188-193.
Srikant V, Clarke DR (1998) On the optical band gap of zinc oxide. J Appl Phys 83(10):5447-5451.
Sun B, Hu N, Han L, Pi Y, Gao Y, Chen K (2019) Antican-

cer activity of green synthesised gold nanoparticles from *Marsdenia tenacissima* inhibits A549 cell proliferation through the apoptotic pathway. Artif Cells Nanomed Biotechnol 47(1):4012-4019.

van Wyk BE, Albrecht C (2008) A review of the taxonomy, ethnobotany, chemistry and pharmacology of *Sutherlandia frutescens* (Fabaceae). J Ethnopharmacol 119:620-629.

Vinotha V, Iswarya A, Thaya R, Govindarajan M, Alharbi NS, Kadaikunnan S, Khaled JM, Al-Anbr MN, Vaseeharan B (2019) Synthesis of ZnO nanoparticles using insulin-rich leaf extract: Antidiabetic, antibiofilm and antioxidant properties. J Photochem Photobiol 197:111541.

Vishnukumar P, Vivekanandhan S, Misra M, Mohanty AK (2019) Recent advances and emerging opportunities in phytochemical synthesis of ZnO nanostructures. Mat Sci Semicon Proc 80:143-161.

Acta Biologica Szegediensis

Volume 64(2):251-259, 2020
Acta Biologica Szegediensis
http://abs.bibl.u-szeged.hu/index.php/abs

DOI:10.14232/abs.2020.2.251-259

ARTICLE

Determination and uncertainty analysis of inorganic arsenic in rice by UHPLC-ICPMS

Rajesh Rangasamy[1]*, Praveen Kumar Malekadi[1], D. Peer Mohamed[1], Dheeraj Kumar Tyagi[1], Rahul Raveendran[1], Ananda Gupta[2]

[1]Export Inspection Agency-Kolkata (Laboratory), Kolkata-700107, India
[2]Export Inspection Agency-Kolkata, Kolkata-700001, India

ABSTRACT The present study arose from the need of to determine inorganic arsenic (iAs) at low levels in rice. Ultra-high performance liquid chromatography coupled with inductively coupled plasma mass spectrometry (UHPLC-ICPMS) using Kinetic Energy Discrimination (KED) mode to eliminate spectral interferences was used for analysis of iAs. Sample preparation involves extraction of inorganic arsenic (sum of As^{3+} and As^{5+}) with water by heating at 90 °C for 5 min in water bath. Separation is accomplished with a reversed-phase ion pack column using a gradient chromatographic method followed by ICPMS analysis within 5 min. The method was validated in accordance with Commission Regulation (EU) No 836/2011 and performance characteristics were verified. Acceptable values were obtained for specificity, repeatability ($HorRat_r$ < 0.6), within-lab reproducibility ($HorRat_R$ < 0.3) with recovery 80-90%, limit of quantification (0.02 mg/kg), fitness-for-purpose and trueness (using CRM); thus, the method can be considered for official control purposes.
Acta Biol Szeged 64(2):251-259 (2020)

KEY WORDS
inorganic arsenic
measurement uncertainty
method validation
UHPLC-ICPMS
rice

ARTICLE INFORMATION
Submitted
3 December 2020.
Accepted
13 December 2020.
***Corresponding author**
E-mail: govtrajeshrangasamy@gmail.com

Introduction

Arsenic (As) is a naturally occurring element in the Earth's crust. It is a metal element that is naturally present in water, air and soil, and is absorbed by some food crops as they grow (Hughes et al. 2011). It is not an additive or ingredient in foods and cannot be eliminated from the food we eat or the water we drink. The main sources of arsenic pollution include certain pesticides and herbicides, wood preservatives, phosphate fertilizers, industrial waste, mining activities, coal burning and smelting (Manjarrez-Domínguez et al. 2019). There are two general types of arsenic compounds. It is present in two general forms: inorganic and organic. These classifications are based on their carbon chemistry and are strictly not classified by the method of farming - as arsenic is in soil and water, both organically- and conventionally grown crops will contain arsenic. The inorganic arsenic is widely considered as detrimental to health (Sanchez et al. 2016). Studies have found alarming levels of arsenic in rice. For many people, rice is a simple and comforting food. In Asia rice is an ancient symbol of wealth, success, fertility, and good health. More than half the world's population, it is a staple food and makes up a large portion of people's diets. Millions of people around the world are exposed to drinking water that contains high amounts of inorganic arsenic mainly south America and Asia (Choi et al. 2010). Fish, shrimp, shellfish, and other seafood may contain significant amounts of organic arsenic, the less toxic form. Rice absorbs more arsenic from water and soil compared to other common food crops. Moreover, studies show that arsenic exposure is more critical in rice than in any other food stuff (Saifullah et al. 2018) and the arsenic level in rice is 10 times higher than in wheat and barley. In addition to direct ingestion, using rice straw for cattle feed increases the risk of arsenic exposure, which is the single biggest food source of inorganic arsenic toxic form. Arsenic may accumulate in the soil of paddy fields, worsening the problem. Paddy rice is particularly susceptible to arsenic contamination, due to the reasons of grown in flooded paddy fields that require high quantities of irrigation water, but in many areas the irrigation water is contaminated with arsenic (Seyfferth et al. 2014).

Brown rice especially might contain high levels of arsenic, particularly in its inorganic forms. Using contaminated water for cooking is another concern because rice grains easily absorb arsenic from cooking water when they are boiled. Young children are also at risk if rice-based products make up a large part of their diet. Studies showed that children who were exposed to arsenic in drinking water scored significantly lower on standardized tests (Wang et al. 2007). Also, pregnant

women who consumed even very low levels of arsenic from food products went on to have children who were much more likely to develop respiratory problems in the first four months of their lives. Arsenic consumption has also been linked to liver, kidney, and prostate damage (Das et al. 2018). The toxicity of arsenic depends not only on the total concentration, but also its chemical forms as these differ in terms of mobility, toxicity, and bioavailability. The inorganic trivalent arsenic (As^{3+}) and pentavalent arsenic (As^{5+}) are the most toxic forms, whereas other common forms including the organic monomethyl arsenic (MMA) and dimethyl arsenic (DMA) have significantly reduced toxicities. It is known that the majority of arsenic in marine organisms is in the form of arsenobetaine, which is non-toxic (Avula et al. 2008).

European Food Safety Authority (EFSA) included rice among the foods that most contribute to iAs exposure and pointed out the need to produce speciation data for different food commodities to estimate the health risk associated with dietary arsenic exposure (Llorente-Mirandes et al. 2012). The European Committee for Standardization (CEN) published in 2008 a standardized method, EN 15517:2008, for the determination of iAs in seaweed. The WHO classifies arsenic as carcinogenic and EFSA's latest risk assessment of arsenic found that exposure to arsenic in Europe is close to the limit that can be considered as not safe (Usydus et al. 2009). EFSA is therefore encouraging member states to reduce arsenic exposure as much as possible. According to the World Health Organization guidelines, the permissible level for total arsenic in drinking water is 10 ng/ml (WHO 2011). The country that has regulated the level of iAs in rice is China, where the maximum contaminant level permitted is 0.20 mg/kg (Chen et al. 2018). Although no such limit exists for food products, the Food and Agriculture Organization / World Health Organization (FAO/WHO) recommend an intake no greater than 15 μg/kg body weight per week. The Federal Institute for Risk Assessment (BfR) has assessed the proposed maximum levels in 2014 for rice and rice products from a health point of view and comes to the conclusion that the maximum level of 0.2 mg of inorganic arsenic per kilogram recommended for white rice is only suitable to avoid particularly high levels in rice. Recently, the limit for iAs in rice has been fixed as 0.20 and 0.25 mg/kg by Codex Alimentarius Commission in 2016 and the European Commission as per Regulation No. 2015/1006/EU in 2015. Exposure to inorganic arsenic is primarily of concern because of its cancer-causing properties (Ooki et al. 2018). Arsenic has been classified by the International Agency for Research into Cancer (IARC) as a human carcinogen on the basis of increased incidence of cancers at several sites in people exposed to arsenic at work, in the environment or through their diet. However, arsenic is also more acutely toxic than other metallic compounds and it was used in earlier times as a rodenticide, while continual low-level exposure to arsenic is associated with skin, vascular and nervous system disorders (Flora et al. 2007). Many methods have been published for the determination of iAs using Hydride Generation-Atomic Absorption Spectrometry. There is a problem in doing the analysis of arsenic speciation due to high pH which leads to additional deprotonation of the arsenate anion (Adrian 2011). In recent years, to measure different forms of arsenic using High-performance liquid chromatography coupled with inductively coupled plasma mass spectrometry (HPLC- ICPMS) is used. In this, UHPLC separates the forms and ICP-MS detects them as they elute from the column. The advantage of ICP-MS is very sensitive and can measure trace levels, as demonstrated by its use to measure impurities in a wide range of environmental samples. Further, this method is applicable to meet the performance criteria considering the maximum levels fixed for iAs in rice as set by the codex and EC. In this article, we describe a fully validated method as per European Union Commission Regulation No. 882/2004/EC.

Materials and methods

Chemicals and consumables

Ammonium carbonate (EMSURE, ACS) were supplied by Merck (Germany) High purity water (18.2 MΩ.cm, 0.22 μm filtered) were from a water purufucation system (Evoqua Water Technologies, Germany). Standard reference material of arsenite (As^{3+}) and arsenate (As^{5+}), 1000 mg/l solution, traceability to NIST were purchased from Sigma Aldrich (Switzerland). Prepared working standards (10 mg/l) from 1000 mg/l standard by diluting 1 ml to 100 ml with water and used for preparation of linearity standards, 0.5, 1.0, 5.0, 10, 15 and 20 μg/l mix. Syringe filters (0.22 μm, 25 mm) was purchased from Agilent Technologies (India)

Equipment

Equipment used for sample preparation: analytical balance (Sartorius, Switzerland), refrigerated centrifuge (Sorvall Legend XIR, Thermo Scientific), water bath (Equitron, India), and vortex (Spinax, Tarsons, India).

The chromatographic analysis was performed using ultra-high performance liquid chromatograph (Ultimate 3000, Dionex, Thermo Scientific, Germany) comprising pump, autosampler and column compartment. Mass spectrometric analysis was performed using iCAP Q equipment (Thermo Scientific, Germany). The optimized LC-ICPMS conditions are summarized in Table 1.

Table 1. Optimized UHPLC and ICPMS conditions for inorganic arsenic

HPLC Experimental Conditions	
HPLC column	Dionex IonPac AS7, RFIC, Analytical 4 X 250 mm.
Mobile phase	A) 150 mM ammonium carbonate; B) water
HPLC elution program	0.0 - 2.0 min: 70% A, 30% B 2.2 -3.0 min: 100% A 4.0 - 6.0 min: 70% A, 30% B
Flow rate (ml/min)	1.0
Column temperature (˚C)	40
Injection volume (µl)	20
ICP-MS Experimental Condition	
Plasma power (W)	1550
RF generator supply voltage (V)	38.70
Plasma cooling water flow (l/min.)	0.73
Plasma gas slow (l/min)	14
Auxiliary flow (l/min)	0.80
Collision gas flow, CCT-1 (l/min)	4.83
Nebulizer gas flow (l/min)	1.0550
Spray chamber temperature (˚C)	2.7
Operation mode	Kinetic Energy Discrimination (KED)
Peristaltic pump speed (rpm)	40

Sample preparation

Homogenized sample (0.5 g) was made up to 10 ml with water in a 15 ml centrifuge tube, vortexed for at least one minute and kept in a water bath at 90 °C for 5 min. Then vortexed again and centrifuged for 10 min (8000 rpm, 5 °C) and filtered through 0.22 µm syringe filter and transfer to HPLC sample vial. Adopted the same technique for both sample and sample blank. For preparation of spike recovery sample added known volume of $As^{3+}$and As^{5+} standard, adopted the same procedure as sample preparation.

Method validation

The method validation was performed according to Commission Regulation (EU) No 836/2011 amending Regulation of (EC) No 333/2007 and verified performance criteria for applicability, specificity, repeatability (RSD_r), reproducibility (RSD_R), recovery, limit of detection (LOD), limit of quantitation (LOQ) and fitness for purpose.

The validation was performed at four concentration levels with 6 replicates in rice sample. The concentration levels were 0.02, 0.2, 0.5 and 1 mg/kg of inorganic arsenic and a total of 24 samples were spiked and analysed along with blank samples. The experiments were performed on three different occasions to evaluate repeatability and within laboratory reproducibility. As the rice sample contains arsenic naturally and difficult to get blank sample, hence the rice sample was soaked in water overnight and cleaned three times with water then dried in oven at 105 °C for 4 h to reduce the levels of iAs in rice, which was reported in earlier studies carried out by Raab et al. (2009) and EFSA Journal 2014. The dried sample is grinded to fine powder and used as blank material. The same was used for spike recovery study. Specificity was checked by analysing representative blank samples six replicates per day. It was observed that free from matrix or spectral interferences in the region of interest. The spectral interference was eliminated by selecting Kinetic Energy Discrimination (KED) as there is no another isotope for arsenic. Linearity was tested from the calibration curves at 1, 5, 10, 15, 20 µg/l including blank was checked by least-squares linear regression. The calibration curves were best fitted to a linear curve and correlation coefficients (r2) were higher or equal to 0.99.

Results and discussion

Optimization of extraction

Weighted (0.5 g) of homogenized rice is extracted with water using heated water bath technique to determine the best extraction efficiency. Earlier studies show that the methanol method has been widely used for arsenic speciation in plants (Singh and Ma 2006; Mathews et al. 2010). Though As extraction efficiency in the fronds was satisfactory at 80-90%, the efficiency for the roots was low at ~60% (Zhao et al. 2015). This is consistent with Zhang et al. (2002) who reported ~60% for the roots and 85-100% for the fronds. Further, methanol is lethal during extraction process in addition to generating harmful waste. In consequence, it is essential to develop a new method with satisfactory extraction efficiency and less toxic waste. Also, the problem of deprotonation of arsenate anion, due to high pH using acidic extraction method, was eliminated by extracting with water applying heat treatment. However in the present study, the extraction with water typically provided high extraction recoveries. The method was optimized by using less quantity of sample (0.5 ± 0.05 g) to reduce the matrix effect and minimize the ion suppression and ion enhancement.

Specificity

A blank sample (water) was analysed by LC-ICP-MS in each batch, and no signal was observed at the retention times of the As^{3+} and As^{5+}. Therefore, reagents in the blank did not provoke interferences in the chromatograms. The presence of a high content of chloride (Cl^-) in the matrices could lead to the misidentification of arsenic with ICP-MS detection (Story et al. 1992; Pretty et al. 1993). A blank

sample (water) spiked at 50 mg/l with Cl standard solution was analysed to check the possible interference with As^{3+} and As^{5+}, and no signal was observed at the retention time of As^{3+} and As^{5+} at 1.5 min (90 sec) and 3.4 min (205 sec), respectively. The ion intensity at m/z 75 (^{75}As) was monitored and additionally, the ion intensities at m/z 77 ($^{40}Ar^{37}Cl$ and ^{77}Se) and m/z 35 (^{35}Cl) were monitored to detect possible argon chloride ($^{40}Ar^{35}Cl$) interference at m/z 75. However, no possible interferences were occurred, possibly due to the operation of the ICP-MS using KED mode, which was reported to eliminate poly atomic and isobaric interference from co-eluting chloride species (Juskelis et al. 2013; Day et al. 2002; Maher 2015). The selectivity of the method regarding the ($^{40}Ar^{35}Cl$) interference for the arsenic species studied was verified.

Establishment of LOD and LOQ

As per Corley (2003), for most modern analytical methods, the detection limit may be divided into two components, instrumental detection limit (IDL) and method detection limit (MDL). In the validation study, IDL and instrumental quantification limit (IQL) were calculated for As^{3+} and As^{5+} on the standard deviation of y-intercepts of regression analysis (σ) and the slope (S) of the standard curves, using the following equation, IDL = 3 σ/S. IQLs were calculated from the equation IQL = 10 σ/S. Limit of detection (LOD) has been determined analysing a solution fortified with concentration similar to predicted LOD, which is 0.002 mg/kg (0.001 mg/kg As^{3+} and 0.001 mg/kg As^{5+}). Limit of quantitation (LOQ) is set as one tenth of maximum limit (0.2 mg/kg) which is verified by fortifying sample at 0.02 mg/kg (0.01 mg/kg As^{3+} and 0.01 mg/kg As^{5+}). The linearity of As^{3+}, As^{5+} and chromatographic separation of inorganic arsenic is given in Figure 1.

Repeatability and within laboratory reproducibility

Precision was assessed as within-day repeatability and as between-day intermediate precision (Menditto et al. 2007). In both cases, spiking experiments were carried out by adding As^{3+} and As^{5+} standards to rice samples and homogenized. The mixtures were then extracted as stated in sample preparation. Unspiked samples were also analysed in order to calculate the spike recovery. Precision, expressed in terms of relative standard deviation (% RSD) of iAs recovery, was assessed by analyzing spiked rice samples at 0.02 mg/kg (LOQ), 0.2 mg/kg, 0.5 mg/kg, and 1 mg/kg levels. For evaluate the between-day precision, three different analysis days and different analysts for spiking were taken into consideration. For within-day repeatability, six samples for each spiking level were analysed within a day. The precision acceptance criterion (Deventor et al. 2005; Frys et al. 2011) matches the 2/3 Horwitz function (Horwitz 1982). Satisfactory precision

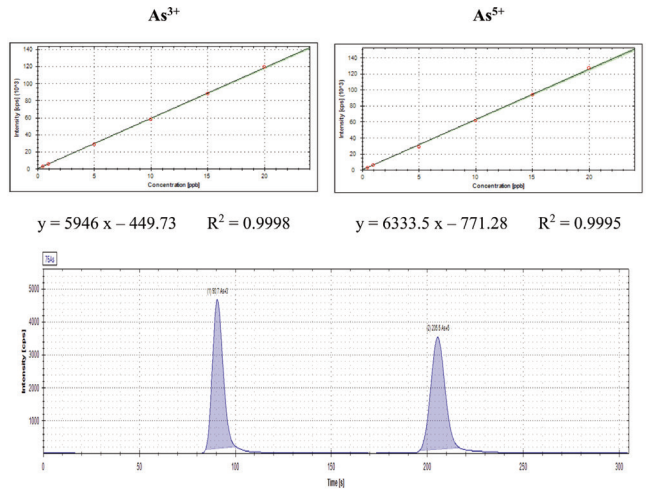

Figure 1: Linearity of As3+and As5+ and standard chromatogram (5 µg/l)

was obtained in all cases, and the results obtained are consistent with the precision acceptance criteria.

As precision often varies with analyte concentration, precision repeatability was calculated for inorganic arsenic (sum of $As^{3+}$and As^{5+}) at four spiking levels 0.02, 0.2, 0.5 and 1 mg/kg (individual concentration of $As^{3+}$and As^{5+} at 0.01, 0.1, 0.25 and 0.5 mg/kg (each concentration 6 times). The repeatability was calculated as relative standard deviation (RSD_r) of measurements for the sample, done by the same analyst, on the same instrument within a short period of time. The % RSD_r, and $HorRat_r$ (Horwitz and Albert 2006; Thomson 2000) ranged was tabulated in Table 2.

The reproducibility was determined through the analysis of blank rice samples fortified in six replicates at four spiking levels 0.02, 0.2, 0.5 and 1 mg/kg (each concentration 6 times). Six replicate test portions at each of the four fortification levels (n = 18) were analysed on three separate days. Repeatability $HorRat_R$ (Horwitz and Albert 2006; Thomson 2000) and within lab reproducibility data were tabulated in Table 2.

The average recovery for inorganic arsenic was around 89% with $HorRat_r$ ranged from 0.05 to 0.16 and $HorRat_R$ ranged from 0.04 to 0.08 which is less than 2 as per criteria in line with EU 836/2011.

The intra- and interday data were used for the respective determination of the repeatability (r) and within-laboratory reproducibility (R). Precision (intra- and interday) was established through the estimation of $HorRat_r$ and $HorRat_R$. The Horwitz equation (Horwitz et al. 1980) was used for estimation of precision at 0.20, 0.50 and 1.0 mg/kg, and the modified equation (Thompson 2000) was used for precision at 0.02 mg/kg using the following equations as per EU No. 836/2011:

Table 2. Recovery, repeatability and within lab reproducibility of inorganic arsenic in rice.

Element	Spiked at (mg/kg)	Repeatability				Within laboratory reproducibility			
		Average recovery (%)	RSD_r (%)	HorwitzRSD_r	$HorRat_r$	Average recovery (%)	RSD_R (%)	Horwitz RSD_R	$HorRat_R$
As^{3+}	0.01	94.35	2.11	14.52	0.15	90.76	1.53	22.00	0.07
	0.1	95.09	0.47	14.52	0.03	90.80	0.93	22.00	0.04
	0.25	94.27	1.27	12.91	0.10	89.87	1.18	19.56	0.06
	0.5	97.26	0.79	11.63	0.07	92.53	1.57	17.63	0.09
As^{5+}	0.01	84.33	8.19	14.52	0.56	80.15	4.51	22.00	0.21
	0.1	83.30	1.18	14.52	0.08	80.12	1.22	22.00	0.06
	0.25	80.32	0.83	12.91	0.06	80.86	1.02	19.56	0.05
	0.5	81.75	0.58	11.63	0.05	80.59	0.86	17.63	0.05
Inorganic As (sum of As^{3+} + As^{5+})	0.02	89.34	2.35	14.52	0.16	85.46	1.68	22.00	0.08
	0.2	89.20	0.63	13.35	0.05	85.46	0.93	22.00	0.04
	0.5	87.29	0.60	11.63	0.05	83.87	0.78	17.63	0.04
	1.0	89.51	0.58	10.49	0.06	85.06	0.99	15.89	0.06

$HorRat_r$ = observed RSDr/calculated RSD_R using (modified) Horwitz equation; and

$HorRat_R$ = the observed RSD_R/calculated RSD_R using (modified) Horwitz equation.

RSD_R was calculated by using the Horwitz equation $2C^{(-0.15)}$.

Where, C = the concentration ratio $1.2 \times 10^{-7} \leq C \leq 0.138$); and by using the modified Horwitz equation (22%) for the concentrations less than 1.2×10^{-7}.

Recovery and ruggedness

Since certified reference materials were used for the analytes and matrices of interest, the recovery from spiked blank samples was measured as an alternative to trueness. The recoveries were calculated for iAs by spiking at four levels viz. at 0.02 mg/kg (LOQ), 0.2 mg/kg, 0.5 mg/kg, and 1 mg/kg which are tabulated in Table 2. Also, to check the trueness, certified reference (ERM-BC211) material was used and achieved 125.03 µg/kg (100.8% recovery) against certified value 124 ± 11 µg/kg. The reproducibility (RSD_R) achieved 6.0% and $HorRat_R$ 0.28 which was within acceptance criteria (less than 2) and found satisfactory.

The analytical method is tested with a fortified sample under different experimental conditions and the different analyst to check the ruggedness. The recovery was 80% with RSDr 3.53% and $HorRat_r$ is 0.24 which is within the acceptance criteria (EU No. 836/2011).

Measurement uncertainty and fitness for purpose approach

The measurement uncertainty in estimation of iAs in rice corresponds to various sources like weighing balance, water bath, volume, centrifuge, temperature, standard purity, dilutions, calibration curve, repeatability. The type A source was the repeatability obtained through the method, and the type B sources included the calibration graph, standard stock solution preparation, sample weight, make-up volume, and water bath temperature. The standard uncertainty due to type A source was calculated as

$$U_{Rep} = \sigma/\sqrt{p}, \text{ where p = the number of readings}$$

The standard uncertainty due to the calibration graph was calculated as

$$U(Co) = u(C_0) = \frac{SD_{xy}}{b} \times \sqrt{\frac{1}{p} + \frac{1}{n} + \frac{(C_0 + C_m)^2}{S_{xx}}}$$

where C_0 = mean concentration of readings (µg/kg); SD_{xy} = the residual SD; b = slope; p = number of readings; n = the number of calibration concentrations; C_m = the mean value of calibration standards; $S_{xx} = \Sigma(Ci - Cm)2$ where Ci = concentration of calibration standard at level i.

The standard uncertainty due to the standard stock solution was calculated as
where U1 to U5 are the relative standard uncertainties

$$U_{STD} = STD_{Conc.} \times \sqrt{(U_1^2 + U_2^2 + U_3^2 + U_4^2 + U_5^2)}$$

due to purity and dilution of standards.

The standard uncertainty due to the weight of the sample was calculated as
where USM = the uncertainty of the balance.

$$U_{Sample\ mass} = \sqrt{2 \times (U_{SM}/2)^2}$$

The standard uncertainty due to volume was calculated as

$$U_{Pipette\text{-}vol.} = \sqrt{2 \times (U_{micropipette}/2)^2}$$

Table 3. Measurement uncertainty and fitness-for-purpose for inorganic arsenic in rice.

Element	At level of concentration (mg/kg)	Combined measurement uncertainty (u_c) (mg/kg)	Maximum standard measurement uncertainty (Uf) (mg/kg)	Criteria for fitness-for-purpose (u_c<Uf) as per EU No. 836/2011
As3+	0.01	0.001	0.002	Complies
	0.1	0.008	0.018	
	0.25	0.020	0.045	
	0.5	0.040	0.090	
As5+	0.01	0.001	0.002	Complies
	0.1	0.007	0.018	
	0.25	0.016	0.045	
	0.5	0.031	0.090	
Inorganic As (sum of As^{3+} + As^{5+})	0.02	0.002	0.004	Complies
	0.2	0.010	0.036	
	0.5	0.051	0.090	
	1.0	0.101	0.150	

The standard uncertainty due to make-up volume was calculated as

$$U_{\text{Flask-vol.}} = \sqrt{2 \times (U_{\text{Flask-vol.}}/2)^2}$$

The standard uncertainty due to water bath temperature was calculated as

$$U_{\text{Water bath temp}} = \sqrt{2 \times (U_{\text{Water bath temp.}}/2)^2}$$

The standard uncertainty due to centrifuge temperature was calculated as

$$U_{\text{Centrifuge temp}} = \sqrt{2 \times (U_{\text{Centrifuge temp.}}/2)^2}$$

The standard uncertainty due to centrifuge rpm was calculated as

$$U_{\text{Centrifuge rpm}} = \sqrt{2 \times (U_{\text{Centrifuge rpm}}/2)^2}$$

The combined uncertainty was calculated as

$$u_{\text{combined}} = C_0 \times \sqrt{(U_{x1}^2 + U_{x2}^2 + U_{x3}^2 + U_{x4}^2 + U_{x5}^2 + U_{x6}^2)}$$

The expanded uncertainty was calculated at the 95% confidence level using a coverage factor of k = 2. Measurement uncertainty was estimated by following the EURACHEM/CITAC Guide CG4. It adopted the approach of grouping the uncertainty components into two categories based on their method of evaluation, i.e. type

Table 4. Summary of method performance characteristics for inorganic arsenic in rice

Parameter	As^{3+}	As^{5+}	Inorganic As(sum of As^{3+} + As^{5+})	Criteria as per EU No. 836/2011
Applicability	Rice and cereal products			Foods specified in Regulation (EC) No. 1881/2006
Specificity	Free from matrix or spectral interferences			Free from matrix or spectral interferences
Repeatability* (RSD_r)	0.15	0.56	0.16	$HorRat_r$ less than 2
Reproducibility* (RSD_R)	0.07	0.21	0.08	$HorRat_R$ less than 2
Recovery* (%)	86-95	75-84	80-90	-
LOD (mg/kg)	0.001	0.001	0.002	0.012 (3/10th of LOQ)
LOQ (mg/kg)	0.01	0.01	0.02	0.040
Fitness-for-purpose*	0.001 u_c<Uf 0.002 Complies	0.001 u_c<Uf 0.002 Complies	0.001 u_c<Uf 0.004 Complies	Combined standard Uncertainty(u_c) less than Maximum standard uncertainty (Uf)
Trueness (using CRM ERM-BC211)# (µg/kg)	-	-	125.03 ± 7.50	124 ± 11 (Certified value)

A and type B. In this case, the type A uncertainty was the repeatability and the type B corresponded to the calibration graph, standard stock solution, sample weight, and make-up volume. The observation was made under the same conditions of measurement at ambient temperature, and the sample temperature was maintained at 25 ± 2 °C. The standard uncertainty due to type A was 0.00044 based on the iAs in rice from ten different trials was measured. In the case of type B, the standard uncertainty due to the calibration graph was estimated as 0.056 and 0.109 for As^{3+} and As^{5+}, respectively; the standard uncertainty due to standard stock solution was 0.013; the standard uncertainty due to sample weight was 0.00014; and the standard uncertainty due to make-up volume was 0.086, the standard uncertainty due to temperature of water bath was 0.64, the standard uncertainty due to temperature and rpm of centrifuge were 0.37 and 19.2, respectively. The combined uncertainty was 0.002 and the expanded uncertainty was 0.004 mg/kg. The final result of iAs was 0.02 ± 0.004 mg/kg. Similarly, uncertainty at 0.2, 0.5 and 1.0 mg/kg was calculated, and the expanded uncertainty for 0.010, 0.051, and 0.101 mg/kg, respectively.

Fitness for purpose

The measurement of uncertainty was calculated at a confidence level of 95% found to be less than the maximum standard measurement uncertainty calculated using formulae below as per EU 836/2011 (C3.3.1 and C 3.3.2) and tabulated in Table 3.

The fitness-for-purpose approach was used to assess the suitability of using the method for official control purposes. Fitness-for-purpose was calculated using the following formula:

where *Uf* = the maximum standard measurement uncertainty`(mg/kg); C = the concentration of interest (mg/kg); and α = the numeric factor to be used depending on the value of C (i.e., 0.2 for concentrations ≤0.05 mg/kg, 0.18 for concentrations 0.051-0.500 mg/kg and 0.15 for concentrations 0.500 - 1.0 mg/kg).

This method is applicable for determination of inorganic arsenic (Sum of $As^{3+}$and As^{5+}) in rice and cereal products by LC-ICPMS at a range of 0.020 - 1.0 mg/kg. The summary of method performance characteristics for inorganic arsenic in rice as per EC 333/2007 amending regulation EC 836/2011 mentioned in Table 4.

Conclusion

One of the main advantages of this method is that it allows quantification of inorganic arsenic in routine analysis in easy and fast sample preparation technique. Using this simple extraction method using water achieves good repeatability and reproducibility with this method. Further, the trueness of the method is satisfactory with regard to the validation data as well as the results from CRM comparisons. The recoveries between 80-90%, LOD at 0.002 mg/kg, LOQ at 0.02 mg/kg with repeatability of 0.16 ($HorRat_r$) and reproducibility of 0.08 ($HorRat_R$) were obtained. The overall analysis time is less because the extraction time is very short and sample preparation is fast and robust. The method takes a full advantage of specificity and no interfering signals to the As^{3+} and As^{5+} compounds used was detected in rice. From the validation study, it can be concluded that trueness (% recovery) and precision (repeatability and within lab reproducibility) of method were satisfactory. The LOQ achieved is low enough and suitable for determining the arsenic species at the low levels found in the samples. The results on CRM shows good agreement with the certified values, as well as with the results on arsenic species reported in the literature. The criteria for acceptance as per validation were met and hence confirming that the method adopted is fit for the intended purpose (quantitative analysis of inorganic arsenic in rice). Based on the above satisfactory validation of methods of inorganic arsenic in rice with respect to method performance criteria as per Commission Regulation (EU) No 836/2011, the method was fit for the purpose and deemed suitable for regulatory analysis of inorganic arsenic in rice by UHPLC-ICPMS at the stated range.

Acknowledgments

The authors gratefully acknowledge the support given by Export Inspection Council, New Delhi, India and Export Inspection Agency-Kolkata for completion of the work.

References

Adrian AA (2011) Arsenic speciation analysis by ion chromatography - A critical review of principles and applications. Am J Analyt Chem 2:27-45.

Avula B, Wang YH, Khan IA (2015) Arsenic speciation and fucoxanthin analysis from seaweed dietary supplements using LC-MS. J AOAC Int. 98(2):321-329.

Chen H, Tang Z, Wang P, Zhao FJ (2018) Geographical variations of cadmium and arsenic concentrations and arsenic speciation in Chinese rice. Environ Pollut 238:482-490.

Choi BS, Choi SJ, Kim DW, Huang M, Kim NY, Park KS, Kim CY, Lee HM, Yum YN, Han ES, Kang TS, Yu IJ, Park JD (2010) Effects of repeated seafood consumption on urinary excretion of arsenic species by volunteers. Arch Environ Contam Toxicol 58(1):222-229.

Commission Regulation (EU) No 836/2011 of 19 August 2011 amending Regulation (EC) No 333/2007 laying down the methods of sampling and analysis for the official control of the levels of lead, cadmium, mercury, in foodstuffs.

Corley J (2003) Handbook of Residue Analytical Methods for Agrochemicals. Vol. 1. John Wiley.

Das S, Langthasa P, Barhoi D, Upadhaya P, Giri S (2018) Effect of nutritional status on arsenic and smokeless tobacco induced genotoxicity, sperm abnormality and oxidative stress in mice in vivo. Environ Mol Mutagen 59(5):386-400.

Day JA, Montes-Bayón M, Vonderheide AP, Caruso JA (2002) A study of method robustness for arsenic speciation in drinking water samples by anion exchange HPLC-ICP-MS. Anal Bioanal Chem 373(7):664-668.

Deventer K, Van Eenoo P, Mikulcíková P, Van Thuyne W, Delbeke FT (2005) Quantitative analysis of androst-4-ene-3,6,17-trione and metabolites in human urine after the administration of a food supplement by liquid chromatography/ion trap-mass spectrometry. J Chromatogr B Analyt Technol Biomed Life Sci 15828(1-2):21-26.

Zhao D, Li H-B, Xu J-Y, Luo J, Ma LQ (2015) Arsenic extraction and speciation in plants: Method comparison and development. Sci Total Environ 523:138-145.

Ellison SLR, Williams A (Eds) (2012) EURACHEM/CITAC Guide CG 4, Quantifying Uncertainty in Analytical Measurement. 3rd Ed., Developed by the Joint EURACHEM/CITAC Working Group. http://www.citac.cc/QUAM2012_P1.pdf

European Committee for Standardization (2008) EN 15517:2008. Foodstuffs. Determination of trace elements. Determination of inorganic arsenic in seaweed by hydride generation atomic absorption spectrometry (HGAAS) after acid digestion.

European Food Safety Authority (2014) Dietary exposure to inorganic arsenic in the European population. EFSA J 12(3):3597.

Flora SJ, Bhadauria S, Kannan GM, Singh N (2007) Arsenic induced oxidative stress and the role of antioxidant supplementation during chelation: a review. J Environ Biol 28(2):333-347.

Fryš O, Bajerová P, Eisner A, Mudruňková M, Ventura K (2011) Method validation for the determination of propellant components by Soxhlet extraction and gas chromatography/mass spectrometry. J Sep Sci 34:2405-2410.

Horwitz W, Albert R (2006) The Horwitz Ratio (HorRat): A useful index of method performance with respect to precision. J AOAC Int 89:1095-1109.

Horwitz W (1982) Evaluation of analytical methods used for regulation of foods and drugs. Anal Chem 54(1):67-76.

Horwitz W, Kamps LR, Boyer KW (1980) Quality assurance in the analysis of foods and trace constituents. J Assoc Off Anal Chem 63:1344-1354.

Hughes MF, Beck BD, Chen Y, Lewis AS, Thomas DJ (2011) Arsenic exposure and toxicology: a historical perspective. Toxicol Sci 123(2):305-332.

Juskelis R, Li W, Nelson J, Cappozzo JC (2013) Arsenic speciation in rice cereals for infants. J Agric Food Chem 61(45):10670-10676.

Kunito T, Kubota R, Fujihara J, Agusa T, Tanabe S (2008) Arsenic in marine mammals, seabirds, and sea turtles. Rev Environ Contam Toxicol 195:31-69.

Maher WA, Ellwood MJ, Krikowa F, Raberc G, Fostera S (2015) Measurement of arsenic species in environmental, biological fluids and food samples by HPLC-ICPMS and HPLC-HG-AFS. J Anal At Spectrom 30(10):2129-2183

Manjarrez-Domínguez CB, Prieto-Amparán JA, Valles-Aragón MC, Delgado-Caballero MDR, Alarcón-Herrera MT, Nevarez-Rodríguez MC, Vázquez-Quintero G, Berzoza-Gaytan CA (2019) Arsenic distribution assessment in a residential area polluted with mining residues. Int J Environ Res Public Health 16(3):375.

Mathews S, Ma LQ, Rathinasabapathi B, Natarajan S, Saha UK (2010) Arsenic transformation in the growth media and biomass of hyperaccumulator *Pteris vittata* L. Bioresour Technol 101:8024-8030.

Menditto A, Patriarca M, Magnusson B (2007) Understanding the meaning of accuracy, trueness and precision. Accred Qual Assur 12:45.

Ooki A, Begum A, Marchionni L, Vanden Bussche CJ, Mao S, Kates M, Hoque MO (2018) Arsenic promotes the COX2/PGE2-SOX2 axis to increase the malignant stemness properties of urothelial cells. Int J Cancer 143(1):113-126.

Pretty JR, Blubaugh EA, Caruso JA (1993) Determination of arsenic(III) and selenium(IV) using an on-line anodic stripping voltammetry flow cell with detection by inductively coupled plasma atomic emission spectrometry and inductively coupled plasma mass spectrometry. Anal Chem 65(23):3396-3403.

Raab A, Baskaran C, Feldmann J, Meharg AA (2009) Cooking rice in a high water to rice ratio reduces inorganic arsenic content. J Environ Monitor 11(1):41-44.

Saifullah, Dahlawi S, Naeem A, Iqbal M, Farooq MA, Bibi S, Rengel Z (2018) Opportunities and challenges in the use of mineral nutrition for minimizing arsenic toxicity and accumulation in rice: A critical review. Chemosphere 194:171-188.

Sanchez TR, Perzanowski M, Graziano JH (2016) Inorganic arsenic and respiratory health, from early life exposure to sex-specific effects: A systematic review. Environ Res 147:537-555.

Seyfferth AL, McCurdy, S, Schaefer MV, Fendorf S (2014) Arsenic concentrations in paddy soil and rice and health implications for major rice-growing regions of Cambodia. Environ Sci Technol 48(9):4699-4706.

Singh N, Ma LQ (2006) Arsenic speciation, and arsenic and phosphate distribution in arsenic hyperaccumulator *Pteris vittata* L. and non-hyperaccumulator *Pteris ensiformis* L. Environ Pollut 141(2):238-246.

Story WC, Caruso JA, Heitkemper DT, Perkins L (1992) Elimination of the chloride interference on the determination of arsenic using hydride generation inductively coupled plasma mass spectrometry. J Chromatogr Sci 30(11):427-432.

Thompson M (2000) Recent trends in inter-laboratory precision at ppb and sub-ppb concentrations in relation to fitness for purpose criteria in proficiency testing. The Analyst 125(3):385-386.

Llorente-Mirandes T, Calderón J, López-Sánchez JF, Centrich F, Rubio R (2012) A fully validated method for the determination of arsenic species in rice and infant cereal products. Pure Appl Chem 84(2):225-238.

Usydus Z, Szlinder-Richert J, Polak-Juszczak L, Komar K, Adamczyk M, Malesa-Ciecwierz M, Ruczynska W (2009) Fish products available in Polish market-assessment of the nutritive value and human exposure to dioxins and other contaminants. Chemosphere 74(11):1420-1428.

Wang SX, Wang ZH, Cheng XT, Li J, Sang ZP, Zhang XD, Han LL, Qiao XY, Wu ZM, Wang ZQ (2007) Arsenic and fluoride exposure in drinking water: children's IQ and growth in Shanyin county, Shanxi province, China. Environ Health Perspect 115(4):643-647.

World Health Organization (2011) Arsenic in Drinking-water. Background Document for Development of WHO Guidelines for Drinking-water Quality (WHO/SDE/WSH/ 03.04/75/Rev/1). http://www.who.int/water_sanitation_health/dwq/chemicals/ arsenic.pdf.

Zhang W, Cai Y, Tu C, Ma LQ (2002) Arsenic speciation and distribution in an arsenic hyperaccumulating plant. Sci Total Environ 300:167-177.